

LA-12906-PR
Progress Report

*The Manuel Lujan Jr.
Neutron Scattering Center
Experiment Reports
1993 Run Cycle*



LANSCÉ

Los Alamos
NATIONAL LABORATORY

Los Alamos National Laboratory is operated by the University of California for the United States Department of Energy under contract W-7405-ENG-36.

Prepared by Roger Farrer, Group CIC-1 and
Amy Longshore, Group CIC-1
Design by Gail Flower, Group CIC-1

Photography by John Flower, Group CIC-9

Previous reports in this series, unclassified,
are LA-11933-PR, LA-12194-PR,
LA-12407-PR, and LA-12647-PR.

This work was supported by
the U.S. Department of Energy,
Office of Energy Research.

An Affirmative Action/Equal Opportunity Employer

This report was prepared as an account of work sponsored by an agency of the United States Government. Neither The Regents of the University of California, the United States Government nor any agency thereof, nor any of their employees, makes any warranty, express or implied, or assumes any legal liability or responsibility for the accuracy, completeness, or usefulness of any information, apparatus, product, or process disclosed, or represents that its use would not infringe privately owned rights. Reference herein to any specific commercial product, process, or service by trade name, trademark, manufacturer, or otherwise, does not necessarily constitute or imply its endorsement, recommendation, or favoring by The Regents of the University of California, the United States Government, or any agency thereof. The views and opinions of authors expressed herein do not necessarily state or reflect those of The Regents of the University of California, the United States Government, or any agency thereof.

DISCLAIMER

Portions of this document may be illegible in electronic image products. Images are produced from the best available original document.

LA-12906-PR
Progress Report

UC-414
Issued: June 1995

*The Manuel Lujan Jr.
Neutron Scattering Center (LANSCE)
Experiment Reports
1993 Run Cycle*

*Compiled by
Roger Farrer
Amy Longshore*

RECEIVED
AUG 10 1995
OSTI

Los Alamos
NATIONAL LABORATORY

Los Alamos, New Mexico 87545

DISTRIBUTION OF THIS DOCUMENT IS UNLIMITED

MASTER

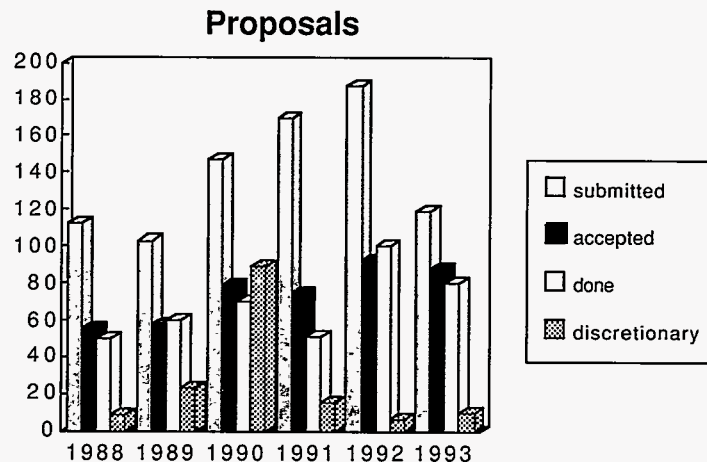
Contents

<i>Abstract</i>	<i>vii</i>
<i>LANSCe Highlights</i>	<i>1</i>
<i>User Program</i>	<i>7</i>
<i>Users visiting LANSCe during 1993</i>	<i>11</i>
<i>Filter Difference Spectrometer</i>	<i>13</i>
<i>(FDS) Experiment Reports</i>	<i>16</i>
<i>High Intensity Powder Diffractometer</i>	<i>37</i>
<i>(HIPD) Experiment Reports</i>	<i>40</i>
<i>Low-Q Diffractometer</i>	<i>67</i>
<i>(LQD) Experiment Reports</i>	<i>70</i>
<i>Neutron Powder Diffractometer</i>	<i>103</i>
<i>(NPD) Experiment Reports</i>	<i>106</i>
<i>Neutron Transmission Flight Path</i>	<i>139</i>
<i>(NTFP) Experiment Reports</i>	<i>141</i>
<i>PHAROS</i>	<i>147</i>
<i>(PHAROS) Experiment Reports</i>	<i>150</i>
<i>Single Crystal Diffractometer</i>	<i>155</i>
<i>(SCD) Experiment Reports</i>	<i>158</i>
<i>Surface Profile Analysis Reflectometer</i>	<i>177</i>
<i>(SPEAR) Experiment Reports</i>	<i>180</i>
<i>Appendices</i>	<i>201</i>
<i>Publication List</i>	<i>202</i>
<i>Author Index</i>	<i>213</i>
<i>Subject Index</i>	<i>216</i>

Abstract

This year the Manuel Lujan Jr. Neutron Scattering Center (LANSCE) ran an informal user program because the U.S. Department of Energy planned to close LANSCE in FY1994. As a result, an advisory committee recommended that LANSCE scientists and their collaborators complete work in progress:

At LANSCE, neutrons are produced by spallation when a pulsed, 800-MeV proton beam impinges on a tungsten target. The proton pulses are provided by the Clinton P. Anderson Meson Physics Facility (LAMPF) accelerator and an associated Proton Storage Ring (PSR), which can alter the intensity, time structure, and repetition rate of the pulses. The LAMPF protons of Line D are shared between the LANSCE target and the Weapons Neutron Research (WNR) facility, which results in LANSCE spectrometers being available to external users for unclassified research about 80% of each annual LAMPF run cycle. Measurements of interest to the Los Alamos National Laboratory (LANL) may also be performed and may occupy up to an additional 20% of the available beam time. These experiments are reviewed by an internal program advisory committee. This year, a total of 127 proposals were submitted. The proposed experiments involved 229 scientists, 57 of whom visited LANSCE to participate in measurements. In addition, 3 (nuclear physics) participating research teams, comprising 44 scientists, carried out experiments at LANSCE. Instrument beam time was again oversubscribed, with 552 total days requested and 473 available for allocation.



LANSCE
Highlights



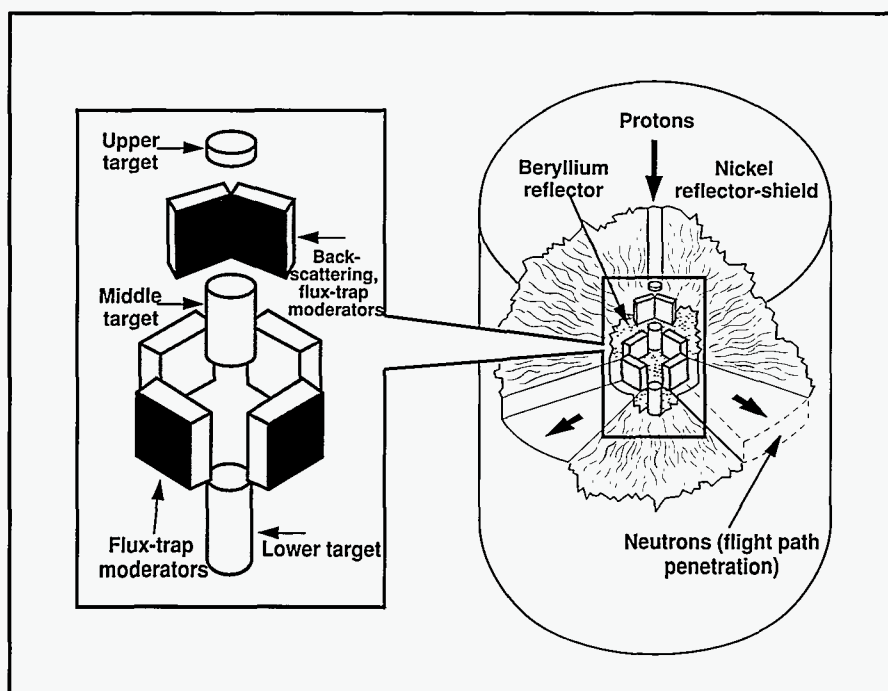
Overview

The Manuel Lujan Jr. Neutron Scattering Center (LANSCE) is a pulsed-spallation neutron source equipped with time-of-flight spectrometers for condensed-matter research. Neutron scattering is a powerful technique for probing the microscopic structure of condensed matter. Both the energies and wavelengths of thermal neutrons closely match typical excitation energies and interatomic distance in solids and liquids. Because neutrons have no charge, they penetrate bulk samples of material to give precise information on the position and motions of individual atoms. The magnetic moment of a neutron interacts with unpaired electrons, making neutrons ideal for probing microscopic magnetic properties. Because neutron-scattering cross sections do not vary in a systematic manner with the atomic number of the scattering nucleus, neutrons and x-rays can provide complementary structural information. This technique is particularly effective for structural problems in biological studies; both hydrogen and deuterium scatter neutrons strongly but with different cross sections.

LANSCE offers a range of instruments for determining the atomic and magnetic structure and dynamics of polycrystalline and crystalline materials, such as high-temperature superconductors, pharmaceuticals, and polymers; and the structure of molecular coatings of solid and liquid surfaces.

One instrument at LANSCE—a powder diffractometer—has a higher resolution than any other instrument of its type in the United States. Important industrial uses of the facility include the measurement of residual stress in metals, ceramics, and composites; the determination of texture in metals and alloys; the characterization of void and precipitate sizes in alloys and ceramics; and the examination of layer structure of protective surface coatings.

At LANSCE, spallation neutrons are produced when pulses of high-energy protons (800-MeV) impinge on a tungsten target. The Clinton P. Anderson Meson Physics Facility (LAMPF) provides the pulses, and the Proton Storage Ring (PSR) can alter the intensity, time structure, and repetition rate of the pulses. Spallation produces neutrons of relatively high energy, so moderators adjacent to the target must be used to reduce the energies to those required for condensed-matter research. Because of the unique flux-trap design of the target/moderator/reflector shield, LANSCE produces neutrons more efficiently than any other spallation neutron source used for condensed-matter research. This capability means that scientists can perform experiments more quickly, more accurately, and with smaller samples at LANSCE than at any other similar facility.



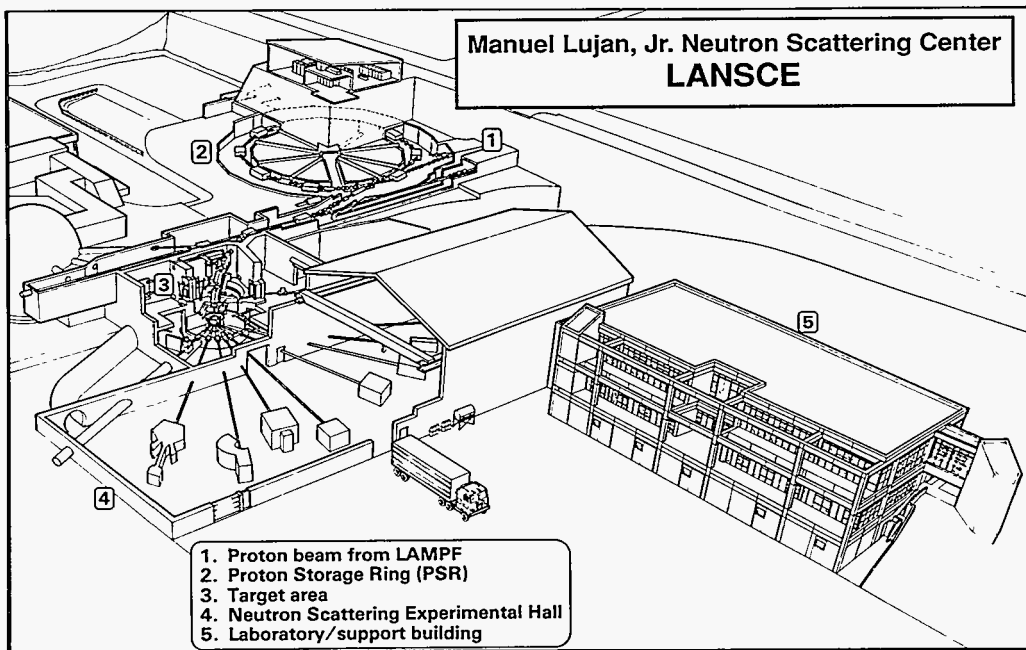
Target design with flux-trap moderators and shielding for the LANSCE upgrade design of the spallation neutron source.

Mission

LANSCE is a pulsed-spallation neutron source for neutron-scattering investigations in physics, chemistry, biology, and materials science. A DOE-sponsored facility, LANSCE has two main missions: it serves as a national user facility with peer-reviewed access for scientists from academia, federal laboratories, and industry; and it is a resource for condensed-matter researchers at Los Alamos.

To support its primary missions, LANSCE

- designs and builds new and powerful neutron-scattering spectrometers,
- designs and builds targets/moderator systems for optimal production of neutrons,
- designs and builds electronic and computer hardware and software for data acquisition and analysis,
- performs forefront research in neutron scattering,
- assists users of the facility during data collection and analysis,
- promotes the application of neutron-scattering techniques to new areas of science and technology, and
- provides an educational resource for undergraduate and graduate students.



An artist's conception of the proton beam from LAMPF (1) feeding into the PSR (2), which then sends it to the LANSCE neutron production target (3). Several of the spectrometers are contained in Experiment Hall 1 (4), and additional resources are contained in the support building (5).

Student Programs

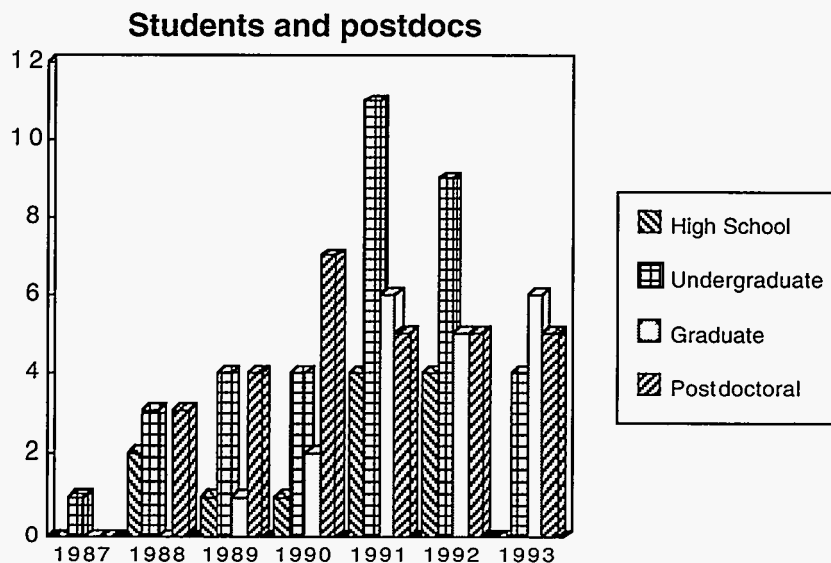
Students are an active part of the operational and organizational elements of LANSCE. Students from local high schools and undergraduate and graduate programs from around the world have the opportunity to learn aspects of experimental design and instrumentation; computer simulation; computer programming; data and numerical analysis; and administrative office operation, which includes office management, technical design and illustration, writing and editing, and organizational development. Student appointments range from 90 days to 1 year (with possible extensions depending on funding and programmatic impact). LANSCE encourages students to work independently and to develop their ideas to fruition.

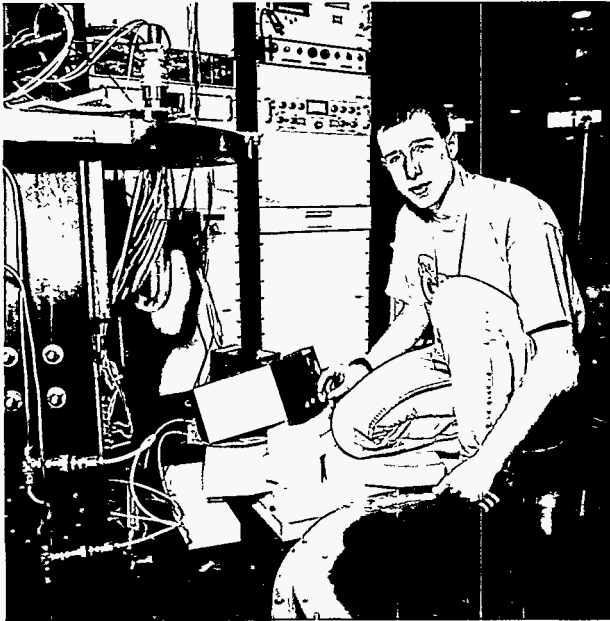
Student employment is coordinated through the Human Resources Division, Staffing—Special Programs and Services, and Science Education and Outreach. Programs at the Laboratory include

- Science and Technology Alliance (STA)
- Service Academies Research Associates (SARA)

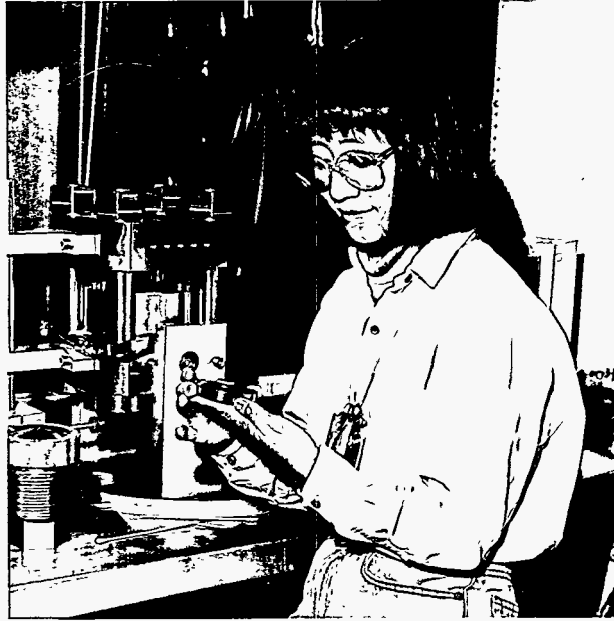
- Science and Engineering Research Semester (SERS)
- Historically Black Colleges and Universities Program (HBCU)
- High School Cooperative Program
- Undergraduate Student Program
- Graduate Student Program
- University Internship/Co-op Programs

In addition, LANSCE participates in the Laboratory's Postgraduate Programs. Postdoctoral candidates must have received their doctoral degree less than 3 years before the appointment at LANSCE. Candidates are nominated by LANSCE scientists and reviewed by a Laboratory-wide committee before the awards are given. Each appointment is for a period of 2 years, with a discretionary third year for researchers with good potential. The Postgraduate Program is active; the Laboratory views it as a means of attracting new scientific talent. LANSCE supplements this program by paying part or all of the overhead for suitably qualified candidates.





RB94 026 03



RB94 026 11



RB94 026 04



RB94 026 07

Upper left: David Knaul, a SERS student from Clarkson University, installs infrared heaters on the stress rig for the NPD. Upper right: Jiaming Morgan, a graduate student from New Mexico State University, places an anvil into the high-pressure cell, which is used in HIPD. Lower left: A doctoral candidate at New Mexico State University, Agus Purwanto, sets up an experiment to observe the structural distortion of a sample on NPD. Lower right: Stephen Wages, who came as both an undergraduate and graduate student from Rochester Institute of Technology, analyzes reflectivity data after an experiment on SPEAR.

User Program



User Program

Research programs at LANSCE cover a broad range: solid-state physics, chemistry, metallurgy, crystallography, structural biology, materials science, and nuclear physics. About 80% of the available beam time is intended for unclassified, nonproprietary research, and the remaining 20% is for support of the Laboratory's programmatic mission. Of the time available for condensed-matter research, three-quarters is distributed to an

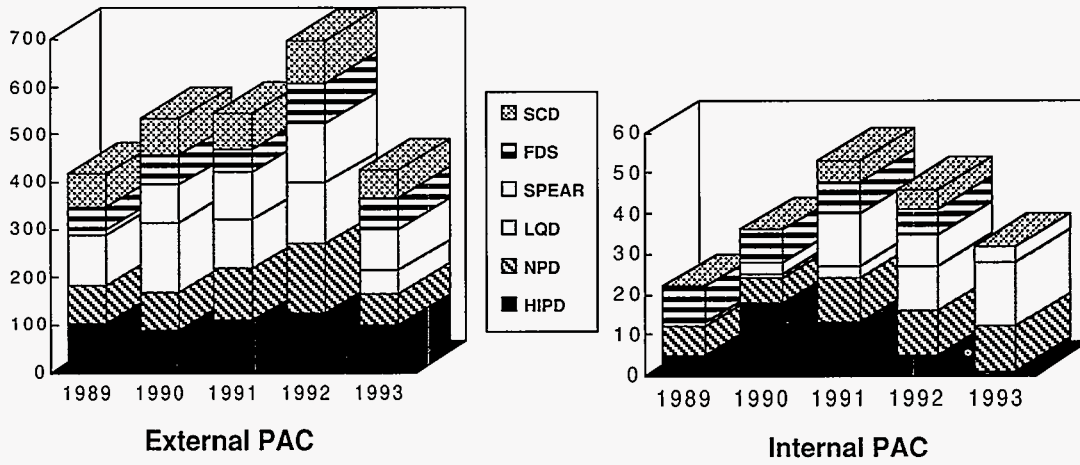
informal user program. Advice on experiments to be performed in this category is provided by the LANSCE advisory committee. DOE cost-recovery rules apply to proprietary experiments. LANSCE sponsors participating research teams (PRTs), which are guaranteed access to a beam line for a negotiated period in exchange for financial participation in constructing a neutron spectrometer or ancillary equipment.



RB93 071 014

Dick Visser, left, of Loughborough University of Technology and Allen Larson of LANSCE examine SCD data.

Instrument days requested



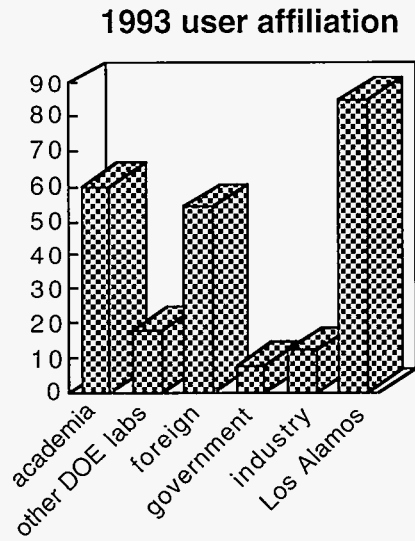
RB93 071 007

Sergei Stishov, right, Director of the Institute for High-Pressure Physics, Russian Academy of Sciences, and Bob Von Dreele of LANSCE look at a high-pressure assembly.

Users visiting LANSCE during 1993

Last name	First	Affiliation	Country
<i>Benmore</i>	<i>Christopher</i>	<i>University of Guelph</i>	<i>Canada</i>
<i>Butler</i>	<i>Paul</i>	<i>University of Tennessee–Knoxville</i>	<i>USA</i>
<i>Havela</i>	<i>Ladislav</i>	<i>Charles University</i>	<i>Czech Republic</i>
<i>Sechovský</i>	<i>Vladimir</i>	<i>Charles University</i>	<i>Czech Republic</i>
<i>Dotson</i>	<i>Lori</i>	<i>Arizona State University</i>	<i>USA</i>
<i>James</i>	<i>Mike</i>	<i>Rockwell International Science Center</i>	<i>USA</i>
<i>Hasegawa</i>	<i>Tai</i>	<i>Stanford University</i>	<i>USA</i>
<i>Stride</i>	<i>John</i>	<i>University of East Anglia</i>	<i>United Kingdom</i>
<i>Egami</i>	<i>Takeshi</i>	<i>University of Pennsylvania</i>	<i>USA</i>
<i>Allison</i>	<i>John</i>	<i>Ford Motor Company</i>	<i>USA</i>
<i>Hellstrom</i>	<i>Eric</i>	<i>University of Wisconsin–Madison</i>	<i>USA</i>
<i>Roll</i>	<i>Armin</i>	<i>Ludwig-Maximilians–Universität München</i>	<i>Germany</i>
<i>Hellman</i>	<i>Frances</i>	<i>University of California–San Diego</i>	<i>USA</i>
<i>Swope</i>	<i>R. Jeffrey</i>	<i>University of Colorado</i>	<i>USA</i>
<i>Forsman</i>	<i>W</i>	<i>University of Pennsylvania</i>	<i>USA</i>
<i>Dunand</i>	<i>David</i>	<i>MIT</i>	<i>USA</i>
<i>Weidner</i>	<i>Donald</i>	<i>State University of New York</i>	<i>USA</i>
<i>Rakovan</i>	<i>John</i>	<i>State University of New York–Stony Brook</i>	<i>USA</i>
<i>Zocco</i>	<i>Thomas</i>	<i>Los Alamos National Laboratory</i>	<i>USA</i>
<i>Wilcoxon</i>	<i>Jess</i>	<i>Sandia National Laboratories</i>	<i>USA</i>
<i>Visser</i>	<i>Dirk</i>	<i>Loughborough University of Technology</i>	<i>United Kingdom</i>
<i>Toprakcioglu</i>	<i>Christopher</i>	<i>Cavendish Laboratory</i>	<i>United Kingdom</i>
<i>Thiyagarajan</i>	<i>Pappannan</i>	<i>Argonne National Laboratory</i>	<i>USA</i>
<i>Craft</i>	<i>Sharon</i>	<i>Sandia National Laboratories</i>	<i>USA</i>
<i>Suck</i>	<i>Jens-Boie</i>	<i>Institut Laue Langevin</i>	<i>France</i>
<i>Smyth</i>	<i>Joseph</i>	<i>University of Colorado</i>	<i>USA</i>
<i>Kergil</i>	<i>Deanna</i>	<i>Los Alamos National Laboratory</i>	<i>USA</i>
<i>Russell</i>	<i>Thomas</i>	<i>IBM</i>	<i>USA</i>
<i>Vradis</i>	<i>Alexandros</i>	<i>University of Patras</i>	<i>Greece</i>
<i>Rhyne</i>	<i>James</i>	<i>University of Missouri–Columbia</i>	<i>USA</i>
<i>Parise</i>	<i>John</i>	<i>State University of New York</i>	<i>USA</i>
<i>Osborn</i>	<i>Raymond</i>	<i>Argonne National Laboratory</i>	<i>USA</i>
<i>Browning</i>	<i>James</i>	<i>Martin Marietta</i>	<i>USA</i>
<i>Mari</i>	<i>Danièle</i>	<i>Institut de Genie Atomique</i>	<i>France</i>
<i>Lager</i>	<i>George</i>	<i>University of Louisville</i>	<i>USA</i>
<i>Leinenweber</i>	<i>Kurt</i>	<i>State University of New York</i>	<i>USA</i>
<i>Jayasooriya</i>	<i>Upali</i>	<i>University of East Anglia</i>	<i>United Kingdom</i>
<i>Ikeda</i>	<i>Susumu</i>	<i>KEK National Lab. for High Energy Physics</i>	<i>Japan</i>
<i>Hoffer</i>	<i>James</i>	<i>Los Alamos National Laboratory</i>	<i>USA</i>
<i>Hamilton</i>	<i>William</i>	<i>Oak Ridge National Laboratory</i>	<i>USA</i>
<i>Gray</i>	<i>George</i>	<i>Los Alamos National Laboratory</i>	<i>USA</i>
<i>Egelstaff</i>	<i>Peter</i>	<i>University of Guelph</i>	<i>Canada</i>
<i>Albinati</i>	<i>Alberto</i>	<i>Università di Milano</i>	<i>Italy</i>
<i>Mattes</i>	<i>B.</i>	<i>Los Alamos National Laboratory</i>	<i>USA</i>
<i>Ezeilo</i>	<i>Andrew</i>	<i>Imperial College</i>	<i>United Kingdom</i>
<i>Stishov</i>	<i>Sergei</i>	<i>Institute for High-Pressure Physics</i>	<i>Russia</i>
<i>Kent</i>	<i>Michael</i>	<i>Sandia National Laboratories</i>	<i>USA</i>
<i>Dreux</i>	<i>Peter</i>	<i>University of Pennsylvania</i>	<i>USA</i>

Last name	First	Affiliation	Country
Chaiko	David	Argonne National Laboratory	USA
Shapiro	Alex	University of California–San Diego	USA
Watson	Susan	University of California–San Diego	USA
Todd	Richard	University of Oxford	United Kingdom

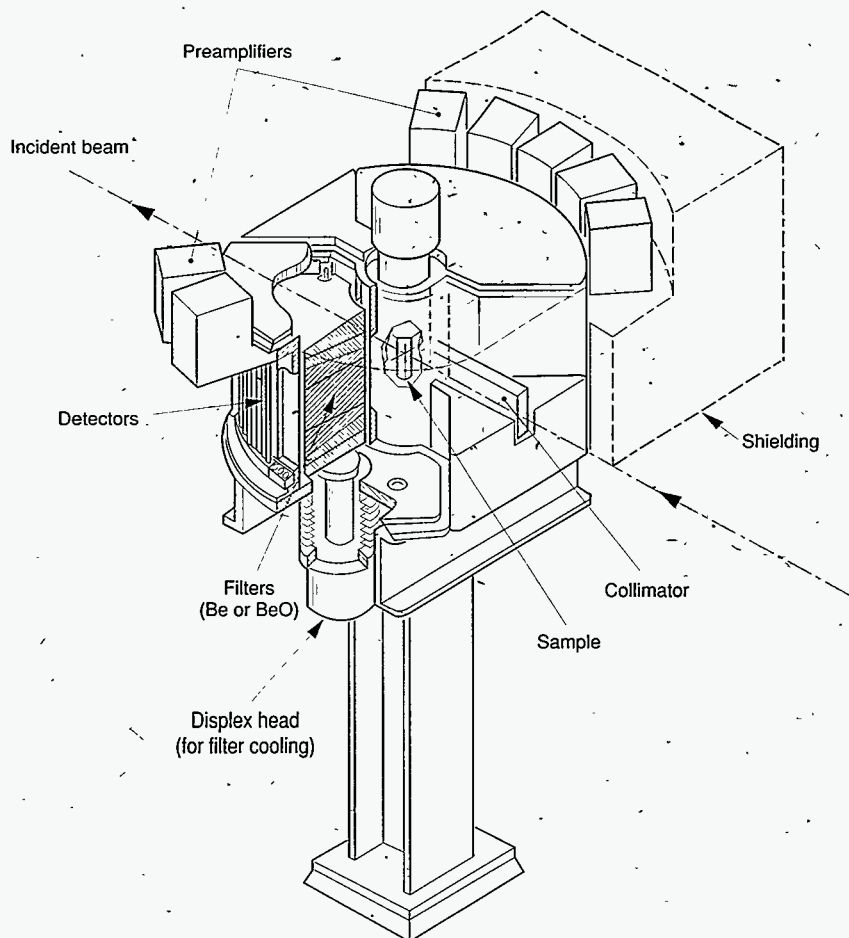


*Filter Difference
Spectrometer (FDS)*

Filter Difference Spectrometer (FDS)

The Filter Difference Spectrometer (FDS) is designed to determine the energy transferred to a sample by measuring changes in the energies of neutrons scattered by the sample in the beam. Because it detects neutrons over a very large solid angle, the FDS is most useful for measurements requiring high sensitivity, such as dilute systems and the vibrations of molecules adsorbed on surfaces. Scattered neutrons reach the detectors through polycrystalline Be or BeO filters, which will only pass neutrons that fall within the energy bandwidth of the filters. This pass through the filters determines the final energy of the scattered neutrons. Energy transfers can then be calculated

from the time of flight of the neutron from the source to the detector. The use of both Be and BeO filters allows different spectra to be taken, which results in much improved resolution. Data can also be corrected using a model filter-response function using either a numerical filter-difference-method or maximum-entropy-method deconvolution. Energy resolution can thereby be improved to a range of 1.5 to 2% of the energy transfer over most of the range of the spectrometer. Because the energy transfer varies in a fixed way with momentum transfer, FDS is best used to observe excitations with little or no dispersion.



Instrument Details

Energy-transfer range	100–5000 cm ⁻¹ (13–620 meV)*
Q range	1.5–17 Å ⁻¹
Energy-transfer resolution	1.5–6.5%, depending on data treatment
Beam size at sample	2.5 cm wide x 10 cm high
Detectors	60 ³ He (1.3 cm in diameter)
Filter analyzers	5 Be, 5 BeO, each subtending a scattering angle of 18°; refrigerated
Moderator	Chilled water at 283 K
Sample environment	10–300 K; closed-cycle refrigerator; furnace temperature limit 673 K; Be-Cu pressure cell to 20 kbar
Sample size	0.5–100 g
Experiment duration	2 hours to 2 days

**In certain cases the range can be extended to elastic scattering.*

Juergen Eckert, instrument scientist

FDS Experiment Reports

6025	<i>Vibrational Spectroscopy of Oxocentered Trinuclear Metal Complexes</i>	17
6026	<i>Cluster Surface Analogy</i>	19
6084	<i>Highly Elongated H-H Bonds in Dihydrogen Complexes of Osmium</i>	21
6085	<i>Dynamics of Doped Polyaniline Films</i>	23
6086	<i>The Temperature Dependence of the Vibrational Modes of Acetanilide-F₃</i>	25
6087	<i>A Platinum-Ethylene Complex with a Highly Activated C=C Bond</i>	27
6089	<i>Application of Zirconium Disulfide as Catalyst in Preparation of Amines</i>	29
6091	<i>Ligand Effects on Dihydrogen Binding</i>	31
6092	<i>Active Sites in Zeolites</i>	33
6107	<i>Hydrogen Bond Dynamics in Quinolinic Acid</i>	34

Instrument used: <i>(please type)</i>	Local contact: Juergen Eckert	Proposal number: <i>(for LANSCE use only)</i> 6025
---------------------------------------	--------------------------------------	---

Title: VIBRATIONAL SPECTROSCOPY OF OXOCENTERED TRINUCLEAR METAL COMPLEXES	Report received: <i>(for LANSCE use only)</i> 6/23/94
---	--

Authors and affiliations:

Upali A. Jayasooriya and John A. Stride
School of Chemical Sciences
University of East Anglia
Norwich NR4 7TJ
UK

Experiment report:

VIBRATIONAL SPECTROSCOPY OF OXOCENTERED
TRINUCLEAR METAL COMPLEXES

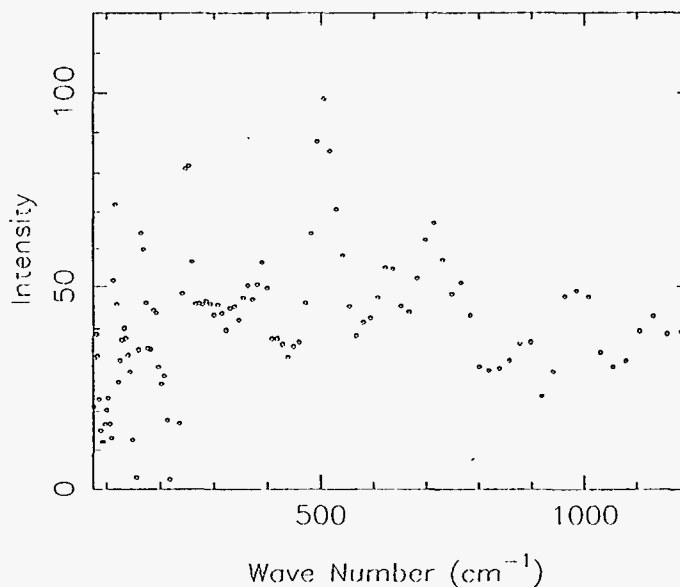
Vibrational spectra of complexes of the general type $[M_3M'O(OOCR)_6L_3]$, have been reported in detail in a series of papers beginning in 1981 [1]. The complexes include homonuclear trivalent metal clusters ($M=Cr, Mn, Fe, Rh$ and Ru), mixed-metal M_2M' and mixed-valence $M_2^{III}M^{II}$ systems. They are important metal model systems for the study of magnetic and electronic interactions between metal ions and we have already found that for a proper understanding of such phenomena a detailed knowledge of the vibrational characteristics of these compounds is essential. One point of major importance has been the characterisation of the mixed-valence compounds as 'localised' or 'delocalised' relative to the time-scale of molecular vibrations. Our approach to this problem has been to assign the normal modes and hence the symmetry, of the metal ion triangle, by comparing suitable examples of mixed-valence and mixed-metal clusters. In particular, the in-plane vibration $\nu_{as}(M_3O)$ of the central oxygen atom has been used to show that (in the case of $M=Fe$ and Mn), the electron transfer process $M^{II} - M^{III}$ is slow on the vibrational time scale [1c, e]. To proceed further, we plan to obtain data on the curvature of the relevant adiabatic potential surfaces, rather than relying on simple theoretical models which are all we have at present [1c], and for this a thorough knowledge of the vibrational modes is required. Infrared and Raman spectroscopies were the main techniques used in the past with a single inelastic neutron scattering (INS) study [1g], which gave an

Experiment report (continued):

assignment of the 'illusivive' vibrations of the ligated water and those of water molecules of crystallisation to a broad spectral feature stretching from *ca* 400 to 800 cm^{-1} . The present investigation is to further explore the unique strengths of INS coupled with partial isotopic substitutions to get a better vibrational assignment for this important molecular system.

The INS spectra of the compounds $[\text{Cr}_3\text{O}(\text{OOCCH}_3)_6(\text{H}_2\text{O})_3]\text{Cl} \cdot 5\text{H}_2\text{O}$ and $[\text{Fe}_2\text{MnO}(\text{OOCCH}_3)_6(\text{H}_2\text{O})_3] \cdot 3\text{H}_2\text{O}$ were run together with deuterated analogues with either only (OOCCD_3) or only D_2O substituted. Spectra of fully deuterated samples were also run. All spectra obtained were of good quality and detailed assignments are in progress. Of particular interest is the observation of INS bands assignable to isolated water molecules, present as either ligands or as molecules of crystallisation. This was done by making use of the isotopic dilution of the protons in the almost fully deuterated sample. The chromium compounds with different isotopic substitutions are shown in the following figures. The relatively sharp band at *ca* 500 cm^{-1} and the broader ones at *ca* 620 and 700 cm^{-1} in the fully deuterated sample spectrum are due to the few percent of protons left over in this sample. The vibrations of these isotopically diluted species are expected to be decoupled from the rest of the system and therefore one expects to see sharp features as observed. The band at 500 cm^{-1} is assigned to the stretching mode of the Cr-OH₂ bond while the others are assignable to the librational motions of the water molecules of crystallisation.

$\text{Cr}_3\text{O}(\text{CD}_3\text{COO})_6(\text{D}_2\text{O})_3\text{Cl} \cdot 5\text{D}_2\text{O}$, mezei

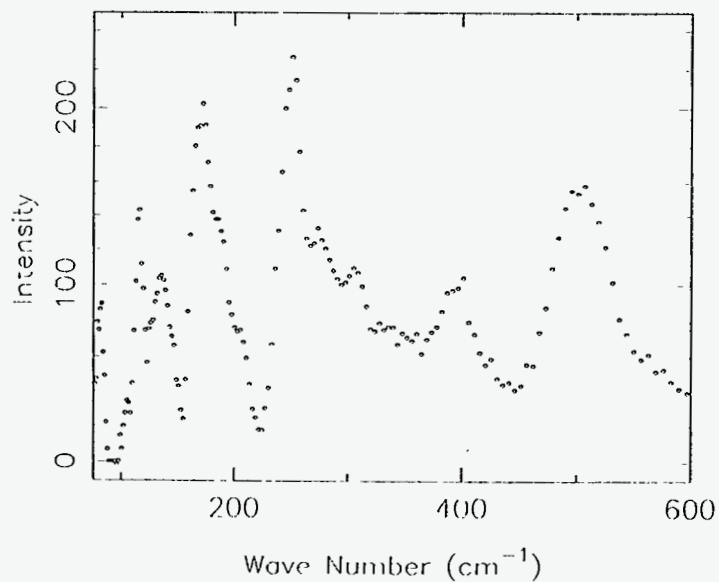


References:

- 1(a) M.K.Johnson, D.B.Powell, R.D.Cannon, *Spectrochim. Acta* **37A** (1981) 995;
- (b) M.K.Johnson, D.B.Powell, R.D.Cannon, *Spectrochim. Acta* **38A** (1982) 307;
- (c) R.D.Cannon L.Montri, D.B.Brown, K.M.Marshall, C.M.Elliott, *J.Am.Chem.Soc.* **106** (1984) 2591; (d) L.Montri, R.D.Cannon, *Spectrochim. Acta* **41A** (1985) 643; (e) L.Meesuk, U.A.Jayasooriya, R.D.Cannon, *J.Am.Chem.Soc.* **109** (1987) 2009; (f) L.Meesuk, U.A.Jayasooriya, R.D.Cannon, *Spectrochim. Acta* **43A** (1987) 687; (g) R.P.White, N.Chai Sa-ard, S.K.Bollen, R.D.Cannon, U.A.Jayasooriya *Spectrochim. Acta* **46A** (1990) 903.

Instrument used: <i>(please type)</i> FDS	Local contact: Juergen Eckert	Proposal number: <i>(for LANSCE use only)</i> 6026
Title: CLUSTER SURFACE ANALOGY		Report received: <i>(for LANSCE use only)</i> 7/5/94
<p>Authors and affiliations:</p> <p style="text-align: center;">Upali A. Jayasooriya and John A. Stride School of Chemical Sciences University of East Anglia Norwich NR4 7TJ UK</p>		
<p>Experiment report:</p> <p>Small organic groups attached to metal cluster cores in metal cluster compounds are providing an essential link in the understanding of vibrational data from surfaces of catalytic importance [1]. Alkoxy groups on metal surfaces, methoxy groups in particular, are of current interest because of the industrially important methanol synthesis using copper catalysts. The structural assignments for the methoxy species on metal surfaces is still controversial with spectroscopic data apparently disagreeing with interpretations of diffraction data [2].</p> <p>A cluster compound used for some initial interpretations of reflection absorption infrared spectroscopic data of methoxy on copper surfaces was $\text{Os}_3(\text{CO})_{10}(\mu_2\text{-H})(\mu\text{-OCH}_3)$. For successful use of model compounds for any assignment problem, it is imperative to have an unambiguous assignment of the vibrational modes of the model. We therefore planned to investigate the above cluster compound using inelastic neutron scattering, which should highlight the vibrations of interest, those of the hydrogenous ligand.</p> <p>However at the time of the experiment, we were only able to synthesis the ethoxy analogue, $\text{Os}_3(\text{CO})_{10}(\mu_2\text{-H})(\mu\text{-OCH}_2\text{CH}_3)$, and therefore the experiment was carried out on this compound. Good spectra were obtained (Figure). A tentative assignment is given (Table). A confirmation of this assignment will require spectra of partially deuterium substituted compounds. This experiment illustrates the main advantages of using INS for these studies. First the absence of the forest of carbonyl deformation modes around 500 cm^{-1} which tend to obscure the ligand bands of interest when IR and Raman spectroscopy is used. Second, the high intensities of the low frequency deformation and torsional modes of the ligand of interest.</p>		

Experiment report (continued):



WAVENUMBER/CM ⁻¹	ASSIGNMENT
125	$\tau(\text{O-Et})$
147	$\omega(\text{Os}_2\text{-OEt})$
177	$\delta(\text{O-C-C})$
255	$\tau(\text{CH}_3)$
275	$\rho(\text{Os}_2\text{-OEt})$
300 to 400	$\nu(\text{Os-CO})\text{'s}$
500	$\nu(\text{Os}_2\text{-O})$ & $\gamma(\text{Os}_2\text{-H})$
705	$\rho(\text{CH}_3)$ & $\rho(\text{CH}_2)$
980	$\nu(\text{C-C})$
1140	$\nu(\text{C-O})$
1250	$\omega(\text{CH}_2)$
1330	$\delta^s(\text{CH}_3)$
1525	$\delta^s(\text{CH}_2)$ & $\delta^{\text{as}}(\text{CH}_3)$

References:

- [1] N.Sheppard, Ann. Rev. Phys. Chem., **39** (1988) 589;
- [2] U.A.Jayasooriya, C.E.Anson, O.Al-Jowder, G.D'Alfonso. P.L.Stanghellini, R.Rossetti, Surface Science **294** (1993) 131.

Instrument Used: (please type) FDS	Local Contact Juergen Eckert	Proposal Number: (for LANSCE Use Only) 6084
--	--	--

Title: Highly elongated H-H bonds in dihydrogen complexes of osmium.	Report received: (for LANSCE Use Only) 4/12/94
--	---

Authors and affiliations:

Tai Hasegawa, Stanford University
 Juergen Eckert, LANSCE, LANL
 Henry Taube, Stanford University

The osmium dihydrogen complexes *trans*-Os(en)₂(η²-H₂)L, **1**, (Fig. 1), where en = ethylenediamine, are highly unusual among the growing class of dihydrogen complexes in that these compounds are stable for a large variety of *trans* ligands L, ranging from Cl⁻ to biomolecules¹, such as inosine 5'-monophosphate. In fact, the ¹H NMR signal from the dihydrogen ligand can be utilized as a molecular recognition probe for the *trans* ligand L. The reason for this is that the electronic properties of L have a pronounced effect on the binding of dihydrogen ("trans effect"). We have previously² shown that the barrier to rotation of the dihydrogen ligand may be taken as a relative measure of the degree of backbonding from metal d - orbitals to the antibonding σ* orbital of the H₂ ligand. It is therefore of great interest to determine the barrier to rotation of H₂ for a number of complexes **1** with different L in order

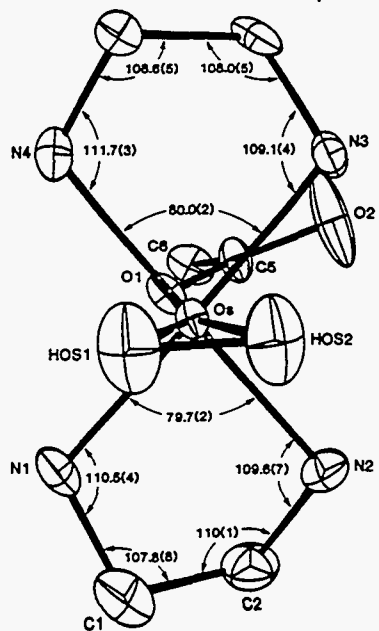


Fig. 1 Neutron Diffraction structure³ of [Os(en)₂(η²-H₂)L]PF₆ with L = CH₃CO₂

Experiment report (continued):

to ascertain how the nature of L influences backdonation to and binding of dihydrogen and the attendant varying NMR properties. However, complexes **1** appear to have large values for the H-H distance, as indicated by the neutron diffraction result³ ($d = 1.34 \text{ \AA}$) and low values of $J(\text{H,D})$. The rotational tunnel splitting for H_2 would therefore be small, and perhaps unobservable. The higher librational transitions of the dihydrogen ligand, on the other hand, are always measurable, and we have therefore collected vibrational data on FDS of an such an Os- H_2 complex with $\text{L} = \text{CH}_3\text{CN}$ utilizing the spectral difference method. This compound has a value of $J(\text{H,D})$ of 17.7 Hz which is much larger than that of **1**, i.e. 9.04 Hz so that we may expect $d(\text{HH})$ to be shorter in the acetonitrile compound. The resulting spectral difference $[\text{Os}(\text{en})_2\{\text{H}_2 - \text{D}_2\}\text{CH}_3\text{CN}]$ is shown in Fig. 2. Librational transitions are evident at 80 and 175 cm^{-1} . Additional features may be attributed to incomplete subtraction of skeletal modes because of the strong Os-H interactions and to Os- H_2 wagging and rocking modes.

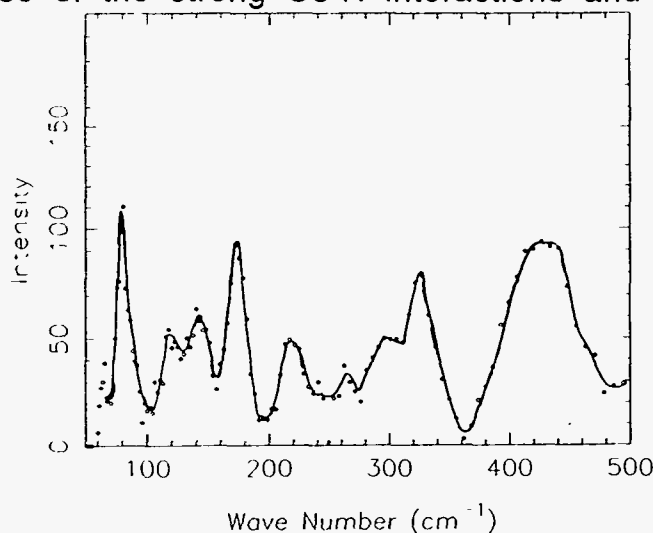


Fig. 2. FDS spectral difference $[\text{Os}(\text{en})_2\{\text{H}_2 - \text{D}_2\}\text{CH}_3\text{CN}] \text{PF}_6$ at $T = 15\text{K}$.

Shortly after the FDS experiment we were able to collect low frequency INS data on the MIBEMOL spectrometer at the Laboratoire Leon Brillouin of the CE Saclay, France. These data revealed a surprisingly large rotational tunnel splitting of about 17 cm^{-1} . Preliminary analysis of all the observed rotational transitions suggests that the rotational potential is predominantly of four-fold symmetry, most likely because of the highly symmetric coordination of the N ligands about the metal. Because of this backdonation may not vary much as the dihydrogen ligand rotates and so that the barrier to rotation is surprisingly low.

References:

1. Z.-W. Li and H. Taube, *Science* **256**, 210 (1992).
2. J. Eckert and G. J. Kubas, *J. Phys. Chem.* **97**, 2378 (1993).
3. T. Hasegawa, Z.-W. Li, S. Parkin, H. Hope, R. K. McMullan, T. F. Koetzle and H. Taube, *J. Am. Chem. Soc.* (to be published).

Instrument Used: <i>(please type)</i> FDS	Local Contact Juergen Eckert	Proposal Number: <i>(for LANSCE Use Only)</i> 6085
Title: Dynamics of doped polyaniline films		Report received: <i>(for LANSCE Use Only)</i> 4/11/94
Authors and affiliations: Ben Mattes, MST-11, LANL Juergen Eckert, LANSCE, LANL Simon Billinge, LANSCE, LANL		
Experiment report: <p>Since the original observation of their exceptional electronic transport properties by Shirakawa and coworkers¹ in 1977, conducting polymers have undergone a remarkable evolution in terms of synthesis, processing, and materials properties. As a direct result of this focused effort there are now a wealth of new possibilities (e.g., highly selective separation membranes,²⁻⁴ biosensors,⁵ corrosion resistant coatings,⁶ light emitting diodes⁷) in addition to the many "conventional" applications originally envisioned.^{8,9} Still many basic questions remain concerning the fundamental nature of electrical charge storage and mass transport in these unusual compounds. Moreover these properties are known to be inextricably linked to both synthesis and processing procedures which can impart structural modifications on a multitude of length scales.</p> <p>The aim of the present experiment was to assess the use of vibrational spectroscopy by incoherent inelastic neutron scattering (IINS) as a tool for obtaining local structural information on the changes in polyaniline films that result from acid doping. These changes have a dramatic effect on the selective gas permeability of the polyaniline membrane² when used for gas separation. Polyaniline films have, of course, been extensively studied by optical spectroscopies. IINS spectroscopy has the advantage that spectra can readily be obtained on metallic polymers, and that it is most sensitive to low frequency motions involving protons, such as the important ring torsional modes, and the bending of the N-H groups along the polymer backbone.</p> <p>We have collected the IINS spectra of three polyaniline samples at 15K, as-cast, doped in HCl and doped in DCl. The three spectra are shown in Fig. 1 over the range 300 - 2000 cm⁻¹. Most of the features in this range arise from the ring modes and the in- and out-of-plane bending modes of the CH groups. Differential spectra do reveal noticeable intensity changes which are the result of different numbers of NH groups and quinoid rings. On this basis we</p>		

Experiment report (continued):

may assign the N-H bending mode in the vicinity of 850 cm^{-1} . This value for $\gamma(\text{NH})$ also indicates that the intermolecular H-bond is fairly strong. Other differences occur in the C-N and C=N stretching region. Other spectral changes upon doping are masked by the presence of a relatively large amount of water in the doped sample. Further analysis of the data is in progress, but future experiments will utilize fully dried films as well as oriented films to differentiate between in-plane and out-of-plane modes. Our data do represent a substantial improvement over an earlier experiment¹⁰, and it is clear that INS can provide important information on these systems especially since it can be used on metallic samples as well.

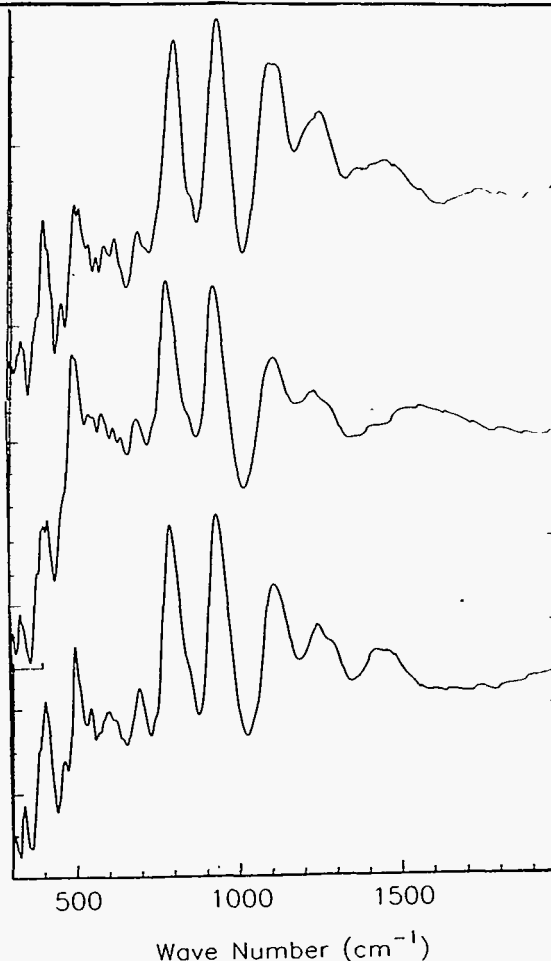


Fig. 1 INS spectra (Maximum Entropy Reconstruction) of polyaniline films: as cast (top); doped in HCl (center) and doped in DCI (bottom).

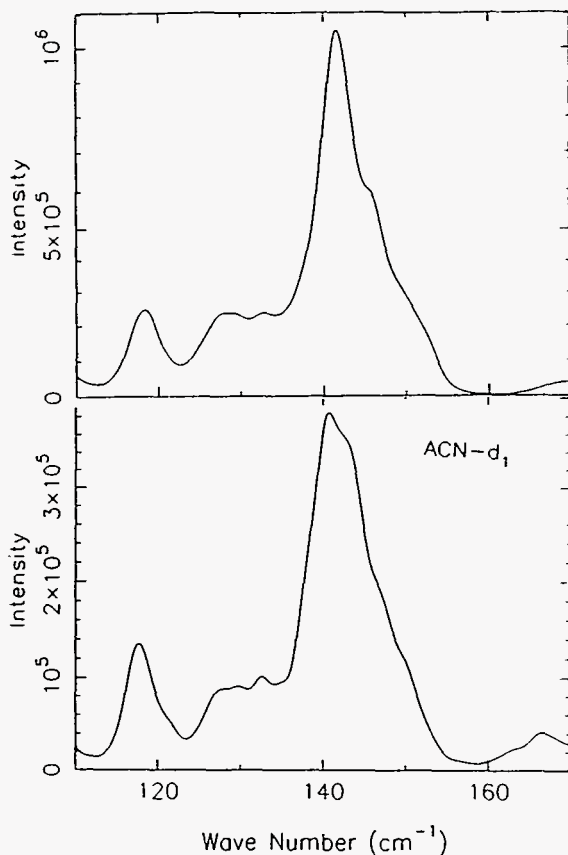
References:

1. H. Shirakawa, E. Louis, A. MacDiarmid, C. Chiang, and A. Heeger, *J. Chem. Soc. Chem. Commun.* 578 (1977).
2. R. Kaner, H. Reiss, B. Mattes, and M. Anderson, *Science* **252**, 1412 (1991).
3. D. Feldheim and C. Elliot, *J. Membrane Sci.* **70**, 9 (1992).
4. W. Liang and C. Martin, *Chem. Mat.* **3**, 390 (1991).
5. D. Hoa, T. Kumar, N. Punekar, R. Srinivasa, R. Lal, and A. Contractor, *Anal. Chem.* **64**, 2645 (1992).
6. S. Sathiyarayanan, S. Dhawan, D. Trivedi, and K. Balakrishnan, *Corrosion Sci.* **33**, 1831 (1992).
7. J. Burroughes *et al.*, *Nature* **347**, 539 (1990).
8. *Science and Applications of Conducting Polymers*, edited by W. Salaneck, D. Clark, and E. Samuelsen (Adam Hilger, Bristol, 1991).
9. K. F. Schoch *et al.*, *IEEE Trans. on Power Delivery* **7**, 1681 (1992).
10. J. L. Sauvajol, D. Djurado, A. J. Dianoux, J. E. Fischer, E. M. Scherr and A. G. McDiarmid. *Phys. Rev.* **B47**, 4959 (1993).

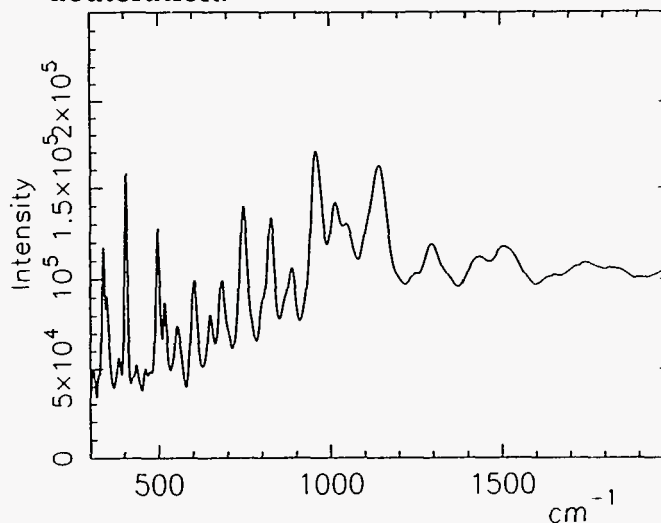
Instrument Used: <i>(please type)</i> FDS	Local Contact Juergen Eckert	Proposal Number: <i>(for LANSCE Use Only)</i> 6086
Title: The temperature dependence of the vibrational modes of acetanilide-F3.		Report received: <i>(for LANSCE Use Only)</i> 4/18/94
Authors and affiliations: Juergen Eckert, LANSCE, LANL Mariette Barthes, Université Montpellier II, France		
<p>The anomalous temperature dependence of the amide 1 mode and other vibrational anomalies in acetanilide ($C_6H_5NHCOCH_3$ or ACN) have been the subject of a large amount of attention because of their potential relevance to such important issues as the energy transport in biological systems. A large number of explanations have been proposed for these observations, including solitons or self-trapped states. Localization of vibrational energy has been predicted but not observed for lattices of pure systems and is also invoked to model some biological processes in polypeptides such as conformational changes in DNA. A full understanding the dynamics of the amide group in the model system ACN is therefore of importance as a contribution to both of these issues.</p> <p>We have recently shown by single crystal neutron diffraction¹ that a previous suggestion by W. Fann et al.² that the unconventional amide-1 mode³ in acetanilide has its origin in two slightly non-degenerate configurations of the amide proton is incorrect. This suggestion had contradicted previous theories of the excess intensity in this mode at low temperature that involve Davydov-like solitons^{4,5}, "polaronic" localized modes^{6,7}, coupled oscillators⁸, or the temperature tuning of a Fermi resonance⁹.</p> <p>In order to make progress in resolving these issues we have been carrying out a series of spectroscopic studies on ACN and its isotopomers¹⁰⁻¹² and had demonstrated¹² that the vibrational dynamics of the amide proton are largely decoupled from those of the rest of the molecule, i.e. that it has local mode character.</p> <p>In this series of experiments on FDS we had planned to study the temperature dependence of the vibrational spectra of methyl-fluorinated ACN. The reason for this is that we found the amide dynamics to be strongly influenced by the methyl group: the vibrational anomalies disappear when the methyl group is deuterated; methyl-flourinated ACN, however does show the vibrational anomalies. Moreover, in recent ab-initio calculations Gao and Karplus¹³ demonstrated the interaction between the amide proton and adjacent methyl group in the related system N-methylacetamide.</p> <p>We were not, however, able to carry out successfully most of our intended work because the INS spectra we collected on our samples were contaminated by noisy detectors to the point where reliable identification of vibrational modes could not be made.</p>		

Additional time was made available later in the cycle and we were able to collect a good spectrum of amide-deuterated acetanilide. This was necessary because we have begun analyzing all our INS data by normal coordinate analysis and INS spectral lineshape fitting. Isotopic data is crucial for reliable assignments as well as identification of vibrational interactions.

ACN 12K



Three spectra are shown below: on the left we compare the methyl torsional band in normal ACN with that of amide-deuterated ACN. On the right the high frequency part of amide-deuterated ACN is shown. The influence of amide proton deuteration on the torsional band of the methyl group is very pronounced, and similar to what we previously observed¹¹ for phenyl ring deuteration.



References:

1. S. W. Johnson, M. Barthes, J. Eckert, R. K. McMullan and M. Muller (to be published).
2. W. Fann, L. Rothberg, M. Roberson, S. Benson, J. Madey, S. Etemad and R. Austin, *Phys. Rev. Lett.* **64**, 607, 1990
3. G. Careri, U. Buontempo, F. Galluzi, A. C. Scott, E. Gratton and E. Shyamsunder, *Phys. Rev. B* **30**, 4689, 1984.
4. J. C. Eilbeck, P. S. Lomdahl and A. C. Scott, *Phys. Rev. B* **30**, 4703, 1984.
5. S. Takeno, *Prog. Theor. Phys.* **75**, 1, 1986.
6. D. M. Alexander and J. A. Krumhansl, *Phys. Rev. B* **33**, 7172, 1986.
7. A. C. Scott, I. J. Bigio and C. T. Johnston, *Phys. Rev. B* **39**, 12883, 1989
8. A. Campa, A. Giansanti and A. Tenenbaum, *Phys. Rev. B* **36**, 4394, 1987
9. C. T. Johnston, B. J. Swanson, *Chem. Phys. Lett.* **114**, 547, 1985.
10. M. Barthes, R. Almairac, J. L. Sauvajol, J. Moret, R. Currat, J. Dianoux, *Phys. Rev. B* **43**, 5223, 1991
11. M. Barthes, J. Eckert, S. W. Johnson, B. I. Swanson, C. J. Unkefer and J. Moret, *J. Phys. (France)* **2**, 1929 (1992).
12. M. Barthes, H. Kellouai, G. Page, J. Moret, S. W. Johnson and J. Eckert, *Physica D* **68**, 45, 1993
13. H. Gao and M. Karplus, *J. Phys. Chem.* **96**, 7273 (1992).

Instrument Used: <i>(please type)</i> FDS	Local Contact Juergen Eckert	Proposal Number: <i>(for LANSCE Use Only)</i> 6087
Title: A platinum-ethylene complex with a highly activated C=C bond.		Report received: <i>(for LANSCE Use Only)</i> 5/9/94

Authors and affiliations:

Alberto Albinati, Università di Milano, Italy
 Juergen Eckert, LANSCE, LANL
 Peter Hoffman, Technische Universität München, Germany

The ethylene ligand in the complex $\text{Pt}(\text{C}_2\text{H}_4)(\text{tBu}_2\text{P-CH}_2\text{-Pt}^t\text{Bu}_2)$ was recently found by us to have a highly activated C=C bond as shown by a bond distance of 1.443(7) Å. This may be compared with that for the well known Zeise's Salt, $\text{K}[\text{PtCl}_3(\text{C}_2\text{H}_4)]$ where $d(\text{C}=\text{C}) = 1.375$ Å. Normal bond distances for a single and double carbon-carbon bond are 1.541 and 1.337 Å, respectively. Pt-C carbon distances reflect the stronger Pt-C interactions which accompanies the weakened C=C interactions in olefin binding: these are 2.089 Å (ave.) for the complex in our study compared with an average distance of 2.131 Å in Zeise's salt. The molecular structure of $\text{Pt}(\text{C}_2\text{H}_4)(\text{tBu}_2\text{P-CH}_2\text{-Pt}^t\text{Bu}_2)$ determined by single crystal X-ray diffraction is shown in Fig. 1 below.

Quantitative indication of these interactions can be obtained by vibrational spectroscopy. For example, weakening of the C=C bond of the C_2H_4 ligand

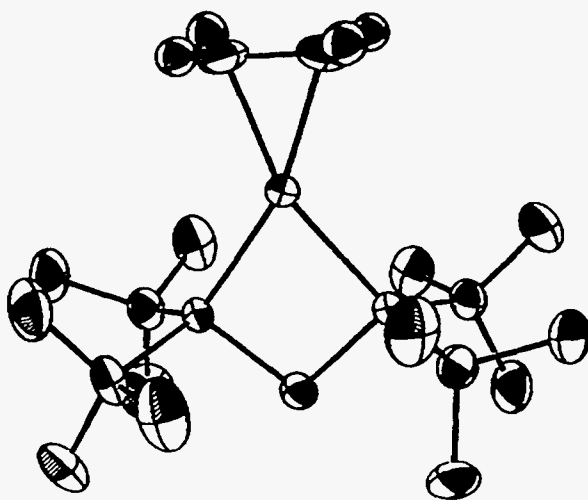


Fig. 1. Structure of $\text{Pt}(\text{C}_2\text{H}_4)(\text{tBu}_2\text{P-CH}_2\text{-Pt}^t\text{Bu}_2)$.

Experiment report (continued):

should result in the lowering of some of the internal mode frequencies of C_2H_4 relative to those of free C_2H_4 , whereas $Pt-(C_2H_4)$ deformation modes should have higher frequencies than those of the less strongly bound C_2H_4 ligand in Zeise's salt. Since particularly the latter modes are most easily identified by INS we have collected INS spectra of the title compound and a "blank" sample with two chloride ligands instead of the C_2H_4 . The spectral difference of the two samples is shown below in Fig.2. Tentative assignments are based on previous INS studies¹ and normal coordinate analyses². The expected trends are indeed observed. For example, the $Pt-C_2$ rock, wag and twist are assigned at 212, 123 and 185 cm^{-1} in Zeise's salt whereas we find these at 262, 198 and 235 cm^{-1} , respectively, for the more strongly bound C_2H_4 in the title compound. The weakening of the carbon - carbon bond in turn is reflected, for example, by the $C=C$ stretching mode at 1425 cm^{-1} in this compound compared with 1515 cm^{-1} for Zeise's salt and 1614 cm^{-1} in solid ethylene.

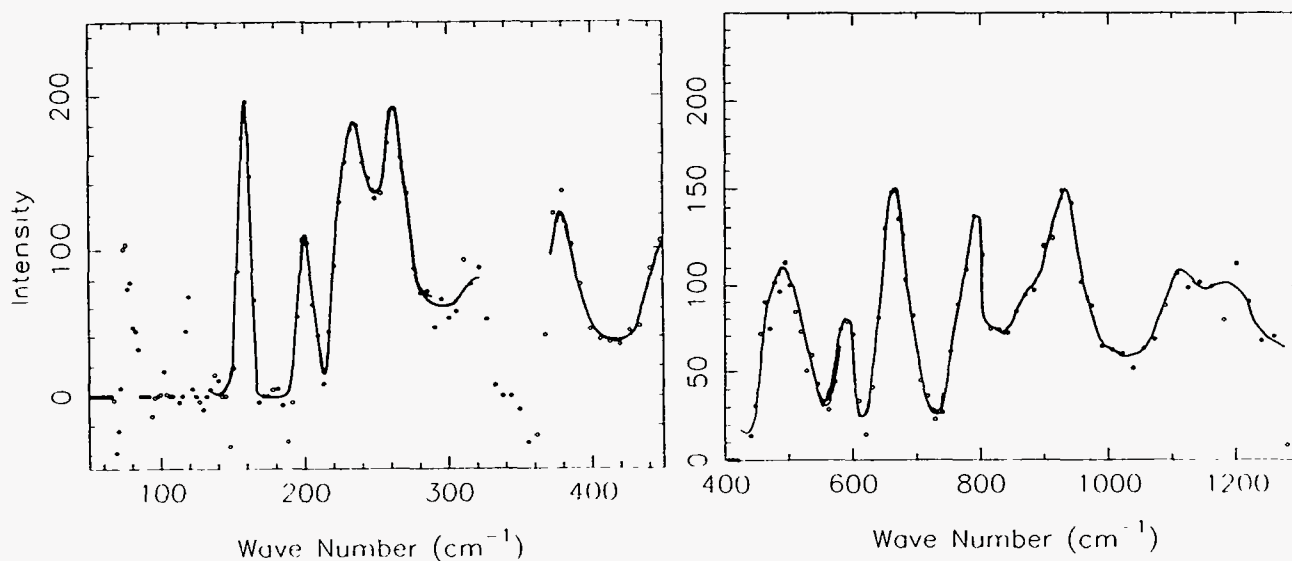


Fig. 2 Sample difference spectra $Pt\{(C_2H_4)-Cl_2\}(tBu_2P-CH_2-PtBu_2)$ showing primarily $Pt-(C_2H_4)$ modes.

References:

1. J. Howard, K. Robson and T. C. Waddington, *Spec. Acta* **38A**, 903 (1982).
2. J. Pradilla-Sorzano and J. Fackler, *J. Mol. Spectroscopy* **22**, 80 (1967).

Instrument Used: <i>(please type)</i> FDS	Local Contact Juergen Eckert	Proposal Number: <i>(for LANSCE Use Only)</i> 6089
---	--	---

Title:
Application of zirconium disulfide as catalyst in preparation of amines.

Report received:
(for LANSCE Use Only)
4/13/94

Authors and affiliations:

Lori Dotson, Arizona State University
 Juergen Eckert, LANSCE, LANL
 Eddie Ong, LANSCE, LANL
 W. S. Glaunsinger, Arizona State University

Unlike the amphoteric host graphite, transition metal disulfides (TMD) intercalate only electron donors, such as alkali metals and Lewis bases. Ammonia is the simplest Lewis base that intercalates into the TMDs. Hence, it can be considered a prototypical molecule for studying intercalation, reaction mechanisms and the nature of guest-guest and guest-host interactions in these materials. A redox-rearrangement scheme is now generally accepted to explain NH₃ intercalation into TMDs

The driving force for intercalation is thought to be the transfer of electrons from the guest to the lowest unoccupied energy levels of the host which are either empty or partially empty transition metal d bands. In the case of a completely filled metal d_{z²} band, charge transfer cannot occur. There are two classic examples which illustrate this behavior.

The first is NH₃ intercalation into TiS₂ which is representative of redox-rearrangement reactions. NH₃ and NH₄⁺ are co-intercalated into TiS₂ with a concomitant charge transfer of 1 mol e⁻/mol NH₄⁺ to the host conduction band. The resulting compound is best described as (NH₄⁺)_y(NH₃)_y"TiS₂^{y'}-, where y'=0.25 for the equilibrated material

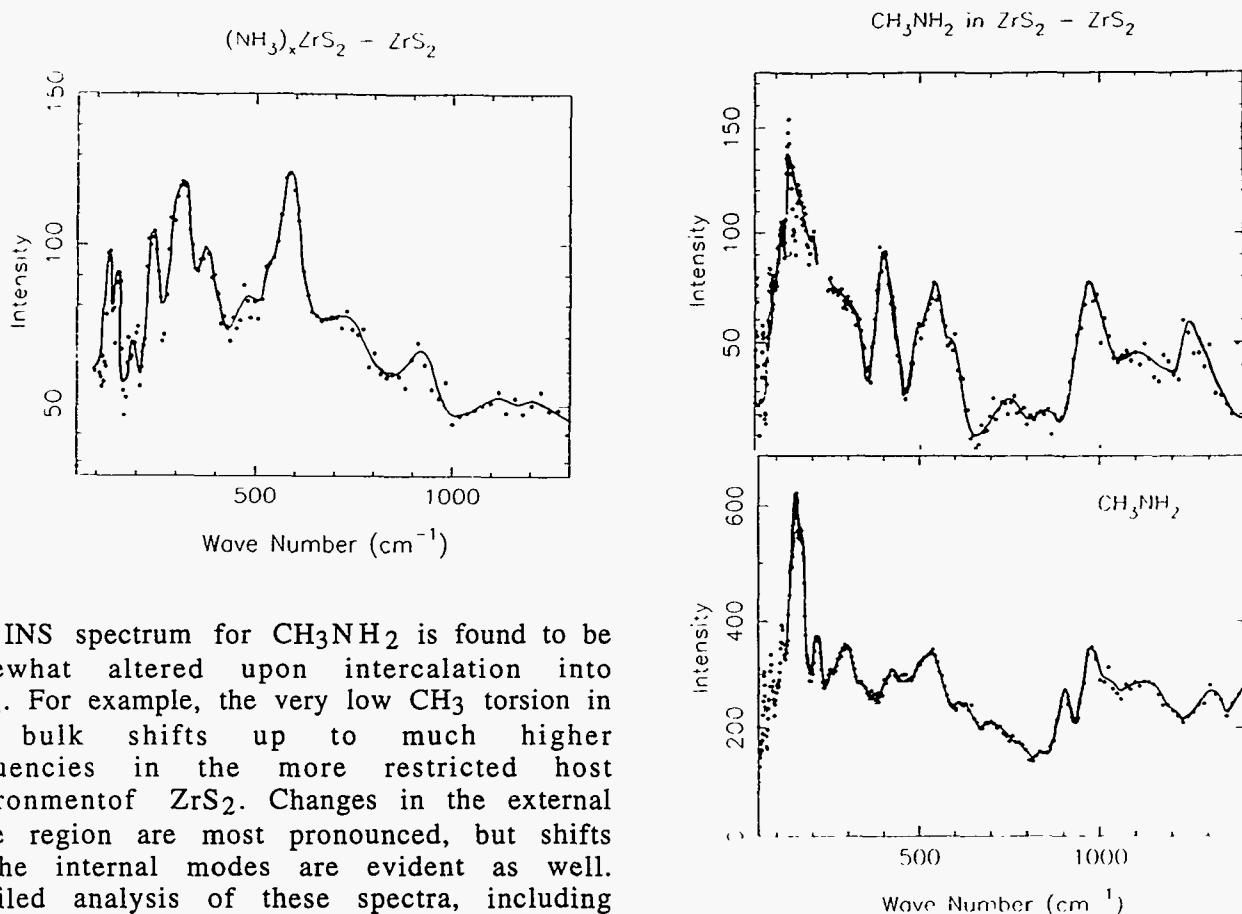
In contrast, MoS₂ is an example of a host with a completely filled d_{z²} band and does not intercalate ammonia. The transition metal d_{z²} band in MoS₂ is completely filled and the next available states are much higher in energy. Assuming that the electronic ground state for NH₃ is lower than this band, the charge transfer reaction is not favorable.

In order to further explore the role of redox chemistry in stabilizing intercalation compounds, we are investigating the intercalation of NH₃ and CH₃NH₂ into ZrS₂. It is known to intercalate NH₃, is isostructural and isoelectronic with TiS₂, yet it has a larger band gap (1.6 eV) than TiS₂ (0.32 eV). Since the valence band is comprised primarily of sulfur p orbitals, to the first approximation the energy levels are comparable for TiS₂ and ZrS₂. In any case, the top of the valence band for ZrS₂ is expected to be somewhat higher in energy because the d orbitals for Zr are higher than those of Ti. This results in a higher level for the available states in ZrS₂. This is expected to reduce the degree of charge transfer to ZrS₂.

We have been investigating^{1,2} intercalation compounds of TMD's by inelastic neutron scattering. This technique provides unique information on guest-host and guest-guest

Experiment report (continued):

interactions as well as some insight into the structural arrangement of the guest molecules within the host. We have therefore collected INS spectra of NH_3 and CH_3NH_2 intercalated in ZrS_2 . In order to assess the relative strengths of guest-host interactions in various TMD's it is necessary to have INS spectra of bulk samples of the intercalants for comparison. Such data does exist for NH_3 , but not for CH_3NH_2 . We have therefore also collected INS spectra of CH_3NH_2 and CD_3NH_2 , as well as other methylamines and/or their HCl salts. Data on di- and trimethylamines was taken in order to determine if these species are formed upon intercalation of methylamine. INS spectra obtained on FDS are shown below for NH_3/ZrS_2 (left), $\text{CH}_3\text{NH}_2/\text{ZrS}_2$ (right, top) and bulk CH_3NH_2 (right, bottom).



The INS spectrum for CH_3NH_2 is found to be somewhat altered upon intercalation into ZrS_2 . For example, the very low CH_3 torsion in the bulk shifts up to much higher frequencies in the more restricted host environment of ZrS_2 . Changes in the external mode region are most pronounced, but shifts in the internal modes are evident as well. Detailed analysis of these spectra, including normal coordinate analysis³ of the bulk spectra is in progress. We do not, however, find any evidence for di- or trimethylamines in the spectrum of $\text{CH}_3\text{NH}_2/\text{ZrS}_2$.

Apart from the strong peak at 600 cm^{-1} the spectrum of NH_3/ZrS_2 shows few changes relative to that of bulk NH_3 . This is in strong contrast to the case of NH_3/TiS_2 , and supports the conclusion that there is no electron exchange to ZrS_2 upon NH_3 intercalation

References:

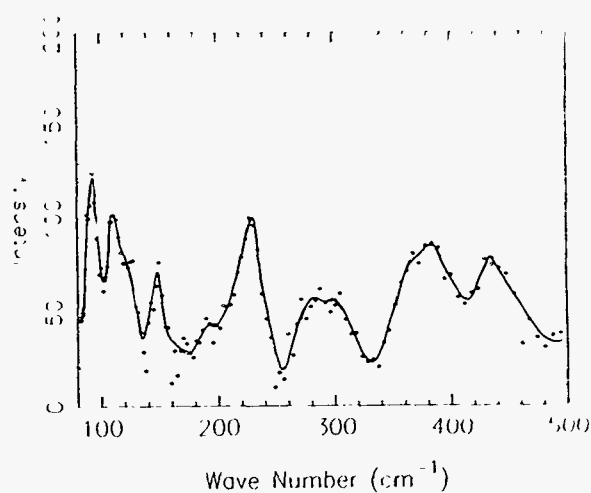
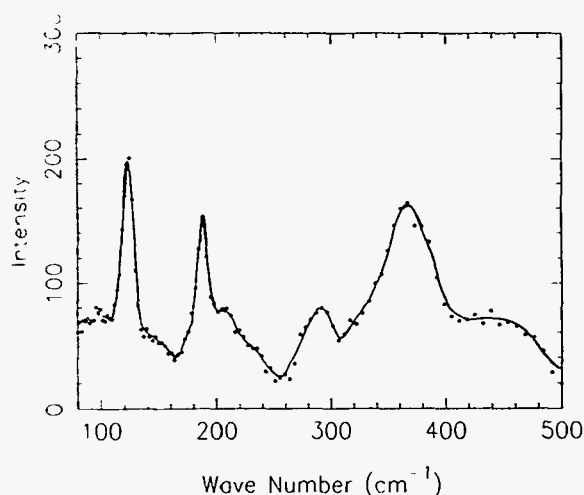
1. W. S. Glaunsinger, M. J. McKelvey, E. M. Larson, R. B. von Dreele, J. Eckert and N. L. Ross, *Solid State Ionics* 34, 281 (1989).
2. E. W. Ong, J. Eckert, L. A. Dotson and W. S. Glaunsinger, *Chem. Mat.* (in press, 1994).
3. A. Martin, J. Eckert, and R. K. McMullan (to be published).

Instrument Used: <i>(please type)</i> FDS	Local Contact Juergen Eckert	Proposal Number: <i>(for LANSCE Use Only)</i> 6091
Title: Ligand effects on dihydrogen binding.		Report received: <i>(for LANSCE Use Only)</i> 4/27/94
Authors and affiliations: Juergen Eckert, LANSCE, LANL Julienne Guilbeault Rabor, University of Hawaii Greg Kubas, CST-3, LANL Xiao-Liang Luo, CST-3, LANL		
<p>The direct electronic interaction between the dihydrogen ligand and the metal center also reflects the effect of the co-ligands of dihydrogen. The reason for this is that the electronic state of the metal is strongly affected by these other ligands. For example, the more basic these ligands are the more electron density is shifted to the metal. This in turn raises the energy of the highest occupied d-orbital in the complex and thereby increases the interaction with $\sigma^*(H_2)$. Backdonation from the metal to the dihydrogen ligand may then become strong enough to result in cleavage of the H-H bond, which is the accepted mechanism for oxidative addition to form a dihydride. A ligand that is a strong σ-donor, on the other hand, may impede the σ-donation from the dihydrogen to the metal and thus prevent dihydrogen binding, especially when it is located in the <i>trans</i> position to the dihydrogen. Ligands that are π-acceptors, such as CO, may compete with the backdonation to $\sigma^*(H_2)$, and can therefore stabilize dihydrogen binding towards cleavage to hydride in the earlier, more π-basic transition metals (e.g. group 6) or in the presence of other electron-rich ligands .</p> <p>It is apparent from the foregoing considerations that a careful analysis of these ligand effects in relation to measured barriers to dihydrogen rotation could provide detailed information on the origin and strength of the all important $d_{\pi}(M) - \sigma^*(H_2)$ interaction. Morris has recently applied the concept of ligand additivity effects to derive generalizations of the acidity and stability of dihydrogen complexes of octahedral d^6 transition metal complexes. In this approach electrochemical parameters E_L for each type of ligand are added and a value for the electrochemical potential $E_{1/2}(d^5/d^6)$ calculated by empirical formulas derived by Lever that differ for each metal. This quantity gives an overall measure of the electron-donating ability of the ligand set. Morris obtained ranges of the parameter $E_{1/2}$ for which stable dihydrogen complexes may be expected. No obvious correlation was found¹, however, between the overall electron donating ability of the metal fragment as derived from the ligand additivity method and the measured barrier to rotation.</p> <p>One of the problems in comparing the effects of different sets of ligands arises from the fact that the barrier to rotation measures essentially a difference in backbonding for the dihydrogen ligand between its orientation at the maximum and minimum of the rotational potential function. Nonetheless, if changes are made to the ligands that are</p>		

Experiment report (continued):

not as drastic as going from $\text{FeH}(\text{dppe})_2$ to $\text{FeH}(\text{PP}_3)$, for example, then the barrier should be a good relative measure of the degree of backbonding as it should be for comparisons of the effect of the metal center when the ligands are the same.

We have therefore collected INS data on two Mo dihydrogen complexes in which only minor changes have been made to the ligands. These are of the form $\text{Mo}(\text{CO})(\text{H}_2)(\text{R}_2\text{PCH}_2\text{CH}_2\text{PR}_2)_2$ where $\text{R} = -\text{CH}_2-\text{C}_6\text{H}_5$ (1) and $-\text{CH}_2-m-\text{C}_6\text{H}_4\text{CH}_3$ (2), and are closely related to the compound with $\text{R} = \text{Ph}$ (3) which we have previously studied². Both of these ligand sets would be expected to be slightly more electron-donating than 3 and therefore lead to marginally higher barriers to H_2 rotation. The INS differential spectra (complex with H_2 ligand minus complex with D_2 ligand) for 1 and 2 are shown below (left and right, respectively).



While the spectrum of 1 can be readily assigned (torsional transitions at 122, 187 and 293 cm^{-1} yield¹ a rotational potential with $V_2 = .48$, $V_4 = .72$ kcal/mol), the data for 2 are more complex. This is confirmed by low frequency data collected by us on the MIBEMOL instrument at the Laboratoire Léon Brillouin, which shows considerable structure in the rotational tunneling peaks. In the absence of a structure determination for 2 we can only suggest that either disorder in the molecular structure or steric interaction between the H_2 ligand and the methyl group in the nearby *m*-position could be responsible. A preliminary analysis of the rotational data for 2 yields a barrier that is intermediate between those previously obtained for two forms of 3 that were crystallized with different solvent molecules.

References:

1. J. Eckert and G. J. Kubas, *J. Phys. Chem.* **97**, 2378 (1993).
2. G. J. Kubas, C. J. Burns, J. Eckert, S. W. Johnson, A. C. Larson, P. J. Vergamini, C. J. Unkefer, G. K. R. Khalsa, S. A. Jackson and O. Eisenstein, *J. Am. Chem. Soc.* **115**, 569 (1993).

Instrument Used: (please type) FDS	Local Contact Juergen Eckert	Proposal Number: <i>(for LANSCE Use Only)</i> 6092
---	---	--

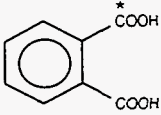
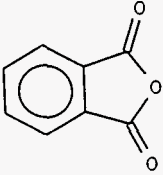
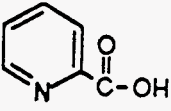
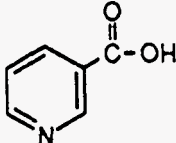
Title: Active sites in zeolites	Report received: <i>(for LANSCE Use Only)</i> 4/14/94
--	---

Authors and affiliations:

Amy Martin, LANSCE, LANL
 Juergen Eckert, LANSCE, LANL

We had intended to study the adsorption of ethylene and cyclopropane in zeolite-L. However, the INS spectra we collected on these samples were contaminated by noisy detectors to the point where reliable identification of adsorbate vibrational modes cannot be made.

Upgrade of the FDS detector electronics is urgently needed before this experiment can be repeated.

Instrument Used: <i>(please type)</i> FDS	Local Contact Juergen Eckert	Proposal Number: <i>(for LANSCE Use Only)</i> 6107
Title: Hydrogen bond dynamics in quinolinic acid		Report received: <i>(for LANSCE Use Only)</i> 4/26/94
Authors and affiliations: Horst Küppers, Universität Kiel, Germany Juergen Eckert, LANSCE		
Experiment report: <p>As part of our ongoing program to study the dynamics and geometries of extremely short hydrogen bonds ($R(\text{OO}) \sim 2.4 \text{ \AA}$) we have been collecting extensive vibrational spectra on single crystals of lithium hydrogen succinate, lithium hydrogen phthalate dihydrate¹ and most recently, quinolinic acid² (QNA; 2,3-pyridinedicarboxylic acid; $\text{C}_7\text{H}_3\text{H}_2\text{NO}_4$). In a prior experiment on FDS we obtained data on two polycrystalline samples with the H-bond either protonated or deuterated. Assignments of the vibrational modes of these systems is greatly facilitated by the use of oriented single crystals (as well as the selectively deuterated compounds) since in all three of these systems the H-bond is macroscopically oriented in a single direction, which can be aligned either parallel or perpendicular to the Q vector of the neutron. There are, of course, two different perpendicular orientations, one in-plane (relative to the ring system of these molecules), the other out-of-plane. Thus it is, for example, a relatively simple matter to distinguish between the out-of-plane and in-plane deformation modes of the C-H groups on the ring, or the in- and out-of-plane bends of the H-bond proton. Nonetheless, we found that some ambiguities in the assignments remained, and have therefore collected INS powder spectra of four compounds that are structurally closely related to the two H-bonded systems of interest. These are phthalic acid 1 and phthalic anhydride 2 (related to Li-H-Phthalate) as well as picolinic acid 3 and nicotinic acid 4 (related to quinolinic acid).</p> <div style="display: flex; justify-content: space-around; align-items: center;"> <div style="text-align: center;">  <p>1</p> </div> <div style="text-align: center;">  <p>2</p> </div> <div style="text-align: center;">  <p>3</p> </div> <div style="text-align: center;">  <p>4</p> </div> </div>		

Experiment report (continued):

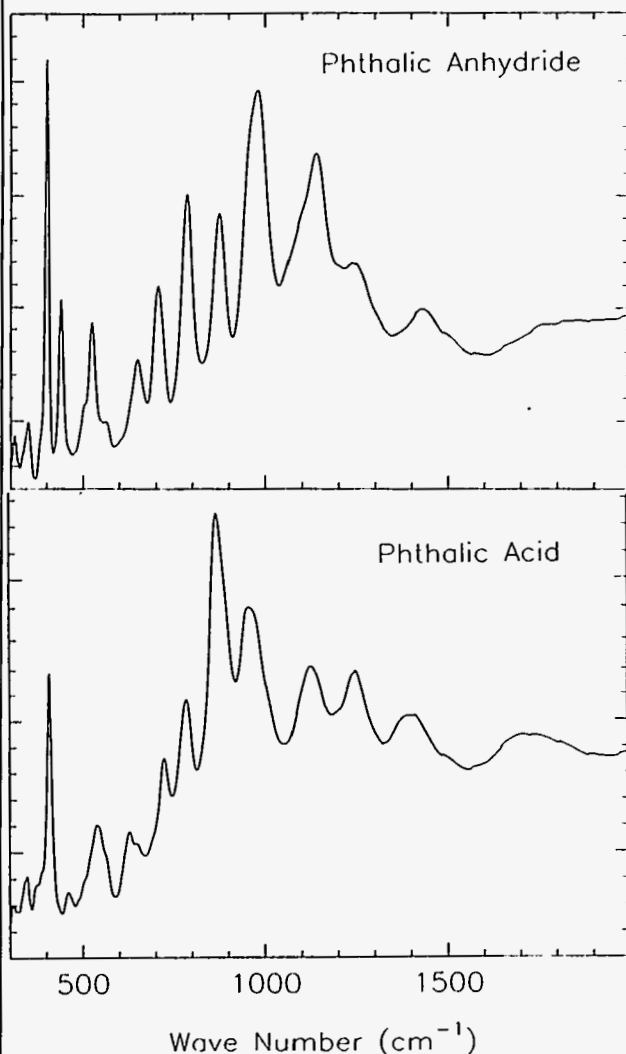


Fig. 1 INS spectra of Phthalic Anhydride (top) and Phthalic Acid

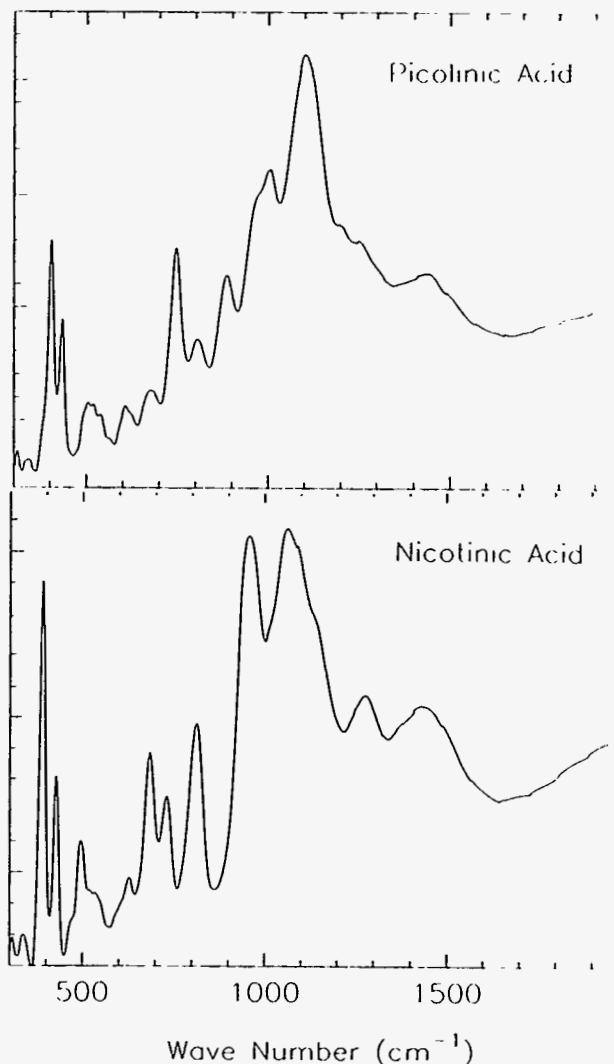


Fig. 2 INS spectra of Picolinic Acid (top) and Nicotinic Acid.

The above spectra are an important aid in our ongoing effort to perform full normal coordinate analyses and INS intensity calculations with the program CLIMAX³. This should enable us to obtain the most detailed dynamical information yet on very short hydrogen bonds.

References:

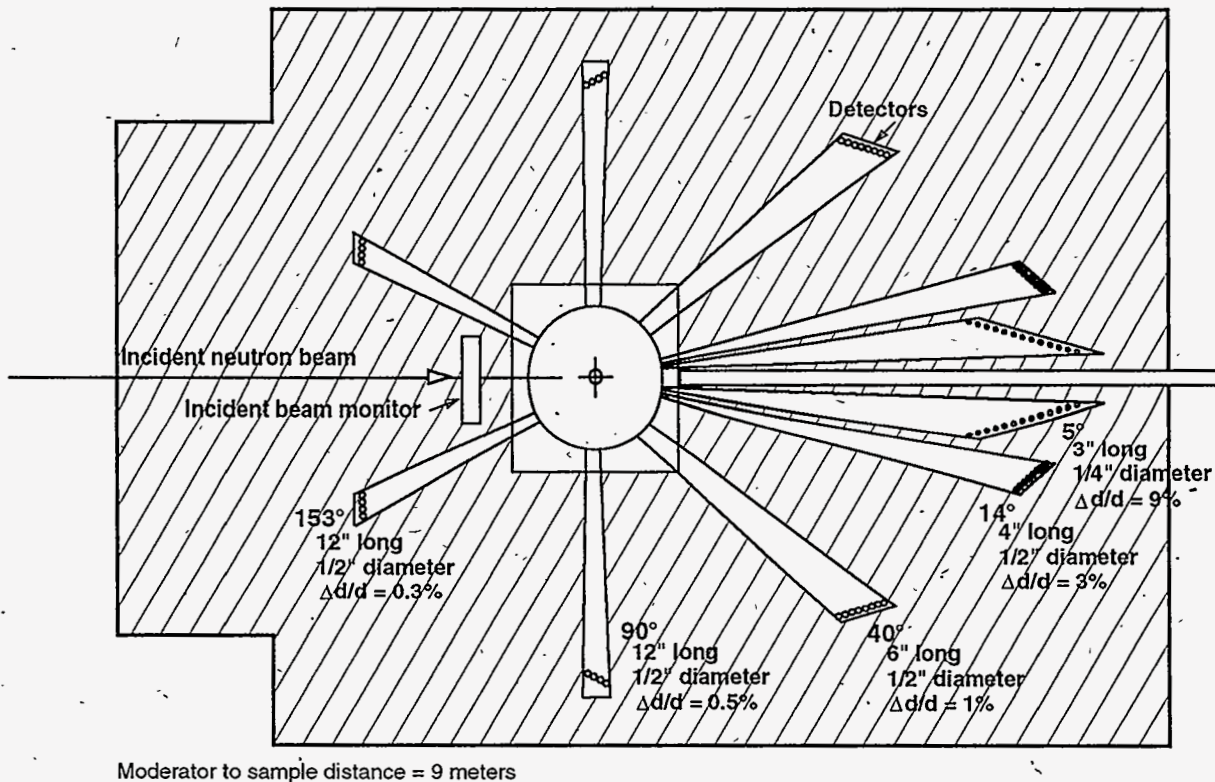
1. H. Küppers and J. Eckert, 15th European Crystallographic Meeting, Dresden, Germany 8/28 - 9/2, 1994.
2. H. Küppers and J. Eckert, *Acta Cryst. A* **49**, C173 (1993).
3. G. J. Kearley, *Spec. Acta* **48A**, 349 (1992).

*High Intensity Powder
Diffractometer (HIPD)*

High Intensity Powder Diffractometer (HIPD)

The High Intensity Powder Diffractometer (HIPD) is designed to study the atomic structures of materials that are available only in polycrystalline or noncrystalline form. In the HIPD, a collimator directs the pulsed neutron beam onto a cylindrical or flat plate sample supported in a vacuum chamber. Banks of detectors located at various angles to the incident beam detect the neutrons. A VAX computer collects the data from each detector as a function of time of flight (TOF) and stores the data in a FASTBUS memory module. Because the neutron TOF is directly proportional to the neutron wavelength, the measured diffraction pattern yields exact information on the atomic arrange-

ment in the sample. The HIPD offers exceptionally high data rates with nearly three decades of range in momentum transfer or d-spacing. An ambient-temperature, high-intensity water moderator provides a usable neutron flux at wavelengths out to 10 Å. Low backgrounds permit the routine use of wavelengths down to 0.2 Å. The HIPD is intended primarily for studies of liquids and amorphous solids, for magnetic diffraction studies, and for crystallographic studies of samples that are either very small or are in extreme environments of temperature, pressure, or magnetic fields. This instrument is also useful for experiments that require time-resolved diffraction measurements.



Instrument Details

Wavelength range	0.2–10.0 Å		
Beam width	0.3–1.0 cm, variable		
Beam height	0.3–5.0 cm, variable		
Q range	0.2–60 Å ⁻¹		
Detector banks, d-spacing range (approximate), and resolution:			
	±14°	2.0–33.6 Å	3.0%
	±40°	0.84–13.7 Å	1.0%
	±90°	0.40–6.65 Å	0.5%
	±153°	0.25–4.75 Å	0.3%
Range of scattering angle	14°–153°		
Moderator	Chilled water at 283 K		
Sample environment	13–300 K; closed-cycle refrigerator; 10-GPa high-pressure cell; vacuum furnace, limit 1000 K		
Sample size	0.005–4 cm ³		
Experiment duration	5 minutes to 1 day, depending on sample size		

Robert Von Dreele, instrument scientist
Eric Larson, instrument technician

HIPD Experiment Reports

5061	<i>Certification of NIST Standard Reference Material (SRM) 656 - Si₃N₄</i>	41
6000	<i>Magnetic and Crystallographic Properties of UCuSn</i>	42
6003	<i>Magnetic and Crystallographic Properties of the Heusler Alloy UPtSn</i>	44
6010	<i>Compressibility of Hydrous Garnets</i>	46
6012	<i>Studies of the Magnetic Structures and Strain Content of Nanocrystalline Antiferromagnets</i>	48
6030	<i>A High-Pressure Neutron Powder Diffraction Study of Pb(Zr_{0.7}Ti_{0.3})O₃</i>	49
6032	<i>Magnetic Ordering in U₂Pd₂In and U₂Pd₂Sn</i>	52
6054	<i>Pressure Dependence of the Structure of Nitromethane</i>	54
6055	<i>High-Pressure Structure of Acetic Acid: Does it Dimerize?</i>	56
6056	<i>Phase Transitions in Cristobalite at High Pressure</i>	58
6072	<i>Structural Properties of α- and β-UD₃</i>	60
6073	<i>Structure of Mixed Electrodes, Bi₃M₂SbO₁₁, M=Ir, Ru</i>	62
6083	<i>Local Structure of La_{1.875}Sr_{0.125}CuO₄: Differential Pair Distribution Function Study</i>	63
6499	<i>Magnetic Ground State of UCoGa</i>	65

Instrument Used: <i>(please type)</i> HIPD	Local Contact R.B. Von Dreele	Proposal Number: <i>(for LANSCE Use Only)</i> 5061
Title: Certification of NIST Standard Reference Material (SRM) 656 - Si ₃ N ₄		Report received: <i>(for LANSCE Use Only)</i> 5/6/94
Authors and affiliations: Robert B. Von Dreele, LANSCE, Los Alamos National Laboratory James Cline, Ceramics Division, NIST		
Experiment report: <p>The two NIST Standard Reference Materials, SRM 676 (alumina powder) and SRM 640b (silicon powder) have been demonstrated to exhibit no preferred orientation or extinction. Four samples, individually made up as 50/50 by weight, were examined on HIPD to determine the accuracy and precision of quantitative phase analysis by Rietveld refinement of neutron TOF data. Recent improvements in the TOF background functions have resulted in accurate (to <0.1%) and precise (<0.02%) quantitative analysis of these mixtures demonstrating that either one is suitable as a spiking material for certification of a new quantitative analysis SRM for the amorphous content of silicon nitride. Moreover, the power of a properly formulated Rietveld refinement procedure for quantitative phase analysis was also demonstrated. Parallel Rietveld analysis of x-ray powder diffraction data resulted in less accurate but equally precise analysis. It would appear that for the latter analyses, the accuracy of the method is limited by the ability of the model functions, particularly those for the peak profiles, used by the Rietveld code to correctly fit observed data.</p> <p>Certification of SRM 656 for amorphous silicon nitride content and a/b ratio was effected by parallel examination of x-ray and TOF powder diffraction data from a suite of samples in which the chosen silicon nitride material was spiked with SRM676 alumina. Ten individually prepared mixtures of SRM656 and SRM 676 were examined by TOF neutron diffraction on HIPD and 40 samples were examined by monochromatized Cu Kα x-ray diffraction at NIST to provide the certification data. As noted above the results from the X-ray data and neutron TOF data are of similar precision but the x-ray results display a small offset from the TOF results.</p>		

Instrument Used: <i>(please type)</i> HIPD	Local Contact: R. A. Robinson	Proposal Number: <i>(for LANSCE Use Only)</i> 6000
Title: Magnetic and Crystallographic Properties of UCuSn		Report received: <i>(for LANSCE Use Only)</i> 4/12/94
Authors and affiliations: A. Purwanto*, R. A. Robinson ; LANSCE, LANL L. Havela, V. Sechovský ; Charles University, Prague, Czech Republic H. Nakotte ; University of Amsterdam, The Netherlands *and NMSU		
Experiment report: It was thought[1,2] that UCuSn crystallizes in the hexagonal symmetry, together with UAuSn and UPdSn. Since the atomic size of Cu is significantly smaller than that of Sn, the atomic radius argument[3] suggests that UCuSn should be ordered crystallographically. This is, in fact, the case for UPdSn[4] which crystallizes in the GaGeLi structure type (P6 ₃ mc space group). Magnetically, UCuSn would then be expected to exhibit a bizarre noncollinear magnetic order as in UPdSn[4]. However, we were surprised by the fact that the neutron data taken at LANSCE indicating UCuSn does not crystallize in hexagonal symmetry with the lattice parameter $a = 4.5 \text{ \AA}$ and $b = 7.2 \text{ \AA}$ as reported elsewhere[2]. Peaks with significant intensities at 5.31 \AA , 2.75 \AA and 2.30 \AA are unindexed. A weaker unindexed peak also appear at about 2.45 \AA . Note that a higher order of 5.31 \AA peak situates at 2.66 \AA having the strongest intensity. The unindexed peaks can all be indexed assuming an orthorhombic structure. Preliminary analysis indicates that the possible crystallographic space groups are either P2 ₁ cn or Pnma. The choice of lattice parameters for the former are $a = 4.54 \text{ \AA}$, $b = 7.84 \text{ \AA}$, $c = 7.22 \text{ \AA}$ while the latter are $a = 7.22 \text{ \AA}$, $b = 4.54 \text{ \AA}$, $c = 7.84 \text{ \AA}$. We obtained the best fit for P2 ₁ cn with the reduced χ^2 , wRp and Rp, respectively, about 20.8%, 11.0% and 8.3% lower than those of Pnma. We also checked whether UCuSn is crystallographically ordered. Note that there is only one site symmetry in P2 ₁ cn, i.e; the general site. The atomic fraction refinement dropped the Cu occupancy by 4.8% and raised the Sn occupancy by 2.7% with the reduced χ^2 , wRp and Rp lowered by 2.2%, 1.2% and 1.0% respectively. This indicates that the compound is in 1:1:1 stoichiometry with small deviation, i.e; it is crystallographically ordered . Below the ordering temperature $T_N = 60 \text{ K}$, four extra peaks appear at about 7.81 \AA , 4.53 \AA , 3.83 \AA , 2.96 \AA . Magnetic contributions to nuclear reflections appear at about 5.28 \AA , 3.26 \AA , 2.82 \AA . Preliminary analysis indicates that they are indexable in orthorhombic symmetry, respectively, as 010, 100, 101, 120, 011, 012, and 102. Further analysis is in progress.		

Experiment report (continued):

Fig. 1. Plot of a portion of the time-of-flight spectra, along with Rietveld fits, reflection markers and residual, from one 153° bank of HIPD at room temperature with P2₁cn space group. The intensities have been divided by the incident spectrum.

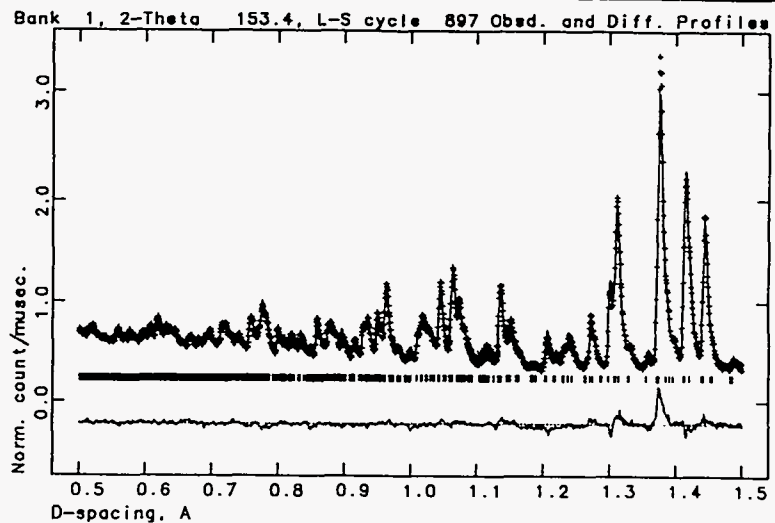
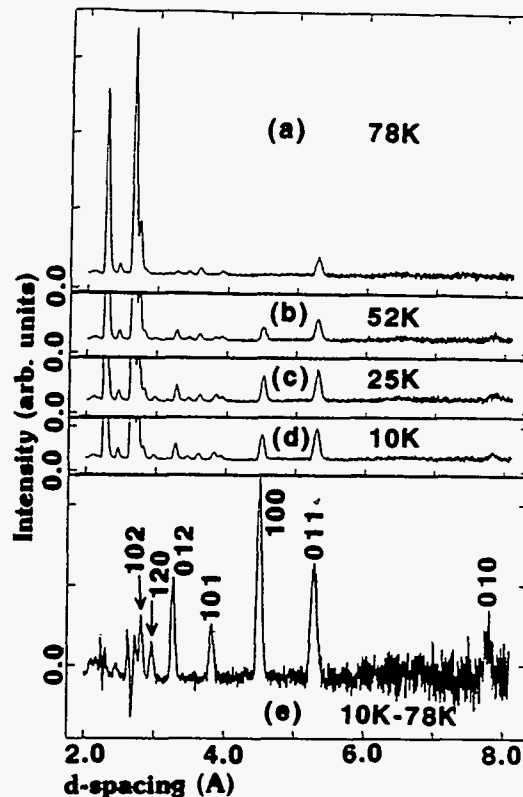


Fig. 2. Plot of a portion of the UCuSn raw data taken in one 40° bank of HIPD at four different temperatures. As the temperature is lowered, four extra peak appear at about 7.81 Å, 4.53 Å, 3.83 Å, 2.96 Å. The bottom plot (e) is the 10 K - 78 K difference curve. The indices are preliminary in the orthorhombic symmetry. The intensities have been divided by the incident spectrum.



References:

- [1] R. A. Robinson, J. W. Lynn, V. Nunez, K. H. J. Buschow, H. Nakotte, A. C. Lawson, Phys. Rev. B 47, 5090 (1993).
- [2] H. Fujii, H. Kawanaka, T. Takabatake, E. Sugiura, K. Sugiyama, M. Date, Jour. of Mag. & Mag. Mat. 87, 237 (1990).
- [3] W. Hume-Rothery, Atomic Theory for Students of Metallurgy (The Institute of Metals, London, 1962), p. 126.
- [4] R. A. Robinson, A. C. Lawson, J. A. Goldstone, K. H. J. Buschow, Jour. of Mag. & Mag. Mat. 126, (1993).

Instrument Used: <i>(please type)</i> HIPD	Local Contact: R. A. Robinson	Proposal Number: <i>(for LANSCE Use Only)</i> 6003															
Title: Magnetic and Crystallographic properties of the Heusler Alloy UPtSn		Report received: <i>(for LANSCE Use Only)</i> 4/12/94															
Authors and affiliations: <p>A. Purwanto*, R. A. Robinson, A. C. Lawson ; LANSCE, LANL</p> <p>H. Nakotte ; Univ. of Amsterdam, The Netherlands</p> <p>K. H. J. Buschow ; Philips Research Laboratories, The Netherlands</p> <p>*and NMSU</p>																	
Experiment report: <p>For some time, we have been working on magnetism in UTX (T=transition-metal element and $X=p$-electron metal) compounds, with the intent of understanding the effect of $5f-d$ hybridization on U magnetic moment formation and, in particular, the very large magnetic anisotropies in U-compounds. UTX compounds order in a variety of structures [1], from the cubic MgAgAs (or "half-Heusler") structure type, through CaIn_2 and Fe_2P hexagonal structure types to the orthorhombic CeCu_2 structure type. We have measured magnetic structures in U-compounds with each of the 4 structure types, but the simplest is clearly the cubic MgAgAs structure type, in which U-atoms lie on a simple FCC lattice. Also, there has been considerable interest in the cubic structure because of its "half-metallic magnetic" behavior in UNiSn [2].</p> <p>In this experiment, we concentrated on another cubic compound, namely UPtSn. Based on the bulk measurements, UPtSn exhibits fairly strong antiferromagnetic interaction in the paramagnetic phase and appears to order antiferromagnetically at about $T_N=75$ K, though the variation of the magnetic susceptibility with temperature is by no means normal - there is no clear maximum at T_N.</p> <p>The powder diffraction data were taken at 85 K, 50 K and 10 K. The crystallographic refinement confirms the MgAgAs structure type. The structural parameters are :</p> <p>Space Group $F\bar{4}3m$</p> <table border="0"> <tr> <td>U</td> <td>(4b)</td> <td>1/2</td> <td>1/2</td> <td>1/2</td> </tr> <tr> <td>Pt</td> <td>(4d)</td> <td>3/4</td> <td>3/4</td> <td>3/4</td> </tr> <tr> <td>Sn</td> <td>(4a)</td> <td>0</td> <td>0</td> <td>0</td> </tr> </table> <p>Lattice parameter at 85 K $a(\text{\AA})=6.60234 \pm 0.00015$</p> <p>The data obtained showed no detectable magnetic signal. Our data indicates that any ordered moment at low temperature must be less than $0.4 \mu_B$.</p>			U	(4b)	1/2	1/2	1/2	Pt	(4d)	3/4	3/4	3/4	Sn	(4a)	0	0	0
U	(4b)	1/2	1/2	1/2													
Pt	(4d)	3/4	3/4	3/4													
Sn	(4a)	0	0	0													

Experiment report (continued):

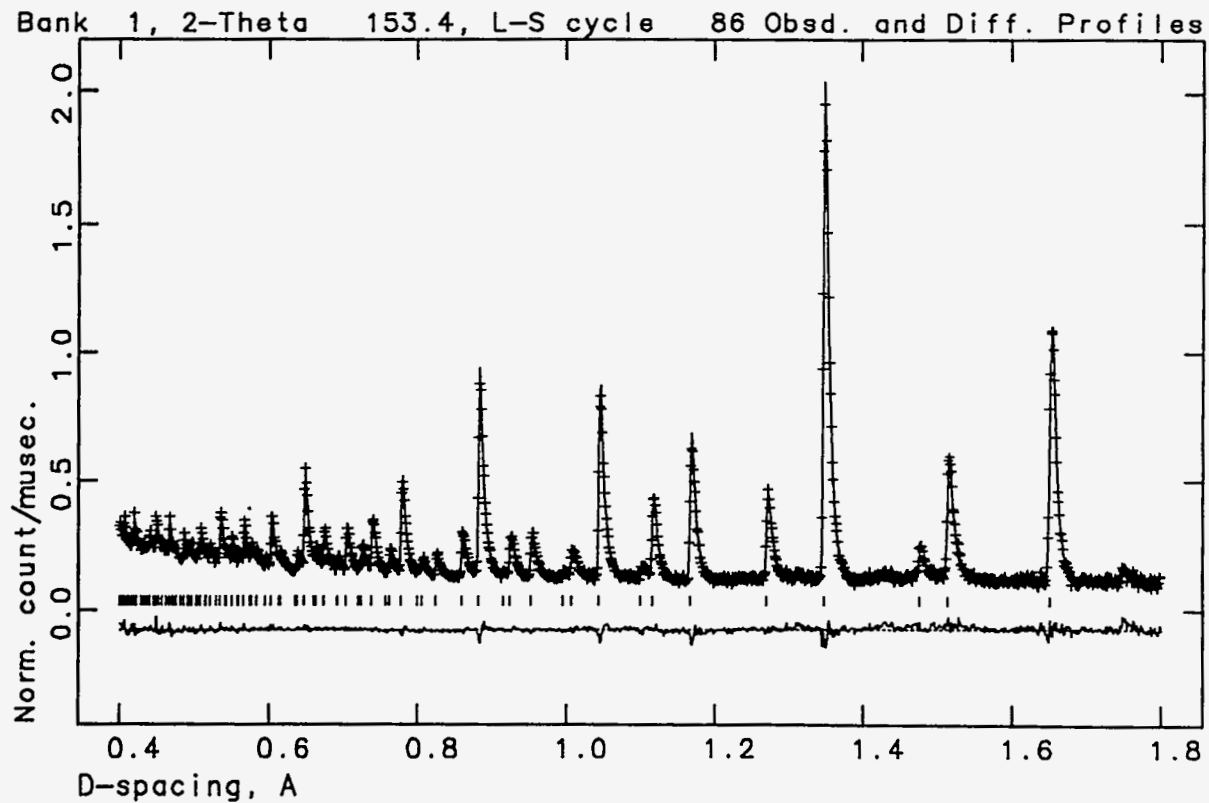


Fig. 1. Plot of a portion of the diffraction pattern along with Rietveld fits, reflection markers and residual, from one 153° bank of HIPD at 85 K. The intensities have been divided by the incident spectrum.

References:

- [1] T. T. M. Palstra et al., *J. Magn. Magn. Mater.* 67, 331 (1987)
- [2] M. Yethiraj, R. A. Robinson, J.J. Rhyne, J. A. Gotaas and K. H. J. Buschow, *J. Magn. Magn. Mater.*, 79, 355 (1989)

Instrument used: <i>(please type)</i> HIPD	Local contact: Robert Von Dreele	Proposal number: <i>(for LANSCE use only)</i> 6010
Title: Compressibility of Hydrous Garnets		Report received: <i>(for LANSCE use only)</i> 3/15/94
Authors and affiliations: George A. Lager, Department of Geography and Geosciences, University of Louisville, Louisville, Kentucky 40292		
Experiment report: <p style="text-align: center;"> Powder data were collected on HIPD for one hydrogarnet sample $(Ca_3Al_2(O_4H_4)_3)$; space group $la3d$; $a=12.00 \text{ \AA}$ loaded in the Nelmes-Besson pressure cell. The objective of the experiment was to determine the effect of OH^- substitution on the compressibility of the garnet structure. The substitution of even small amounts of OH^- ion in the garnet structure can have a large effect on physical properties. To test current geophysical models of the Earth's interior, high-pressure, in-situ data must be obtained for these minerals. Neutron-diffraction methods were used in order to evaluate whether changes in hydrogen-bond geometry at pressure were an important element of the compression mechanism. </p> <p> Unfortunately, the diffraction data were unusable. No well-defined diffraction peaks were observed in either of two data sets collected at low pressure ($\sim 2 \text{ GPa}$) for 24-36 hours. The sample was well-crystallized, fully-deuterated, and an excellent neutron scatterer, based on previous experiments at IPNS (Lager <i>et al.</i>, 1987). It is possible that hydrogen-deuterium exchange occurred during loading; however, the structure of $Mg(OD)_2$ was successfully refined in a previous high-pressure experiment on HIPD in which the same cell and loading procedures were used. In addition, given the short exposure time (30 minutes) to the atmosphere, and the low relative humidity at LANSCE (5%), one would expect the exchange to be minimal. This particular sample has been recently investigated by X-ray powder methods (Olijnyk <i>et al.</i>, 1991) at pressures up to 42 GPa. In the entire pressure range, the X-ray pattern was of sufficient quality to determine the unit-cell parameter. Therefore, the poor quality of the neutron pattern was not due to amorphization of the sample. X-ray examination of the sample after removal from the pressure cell revealed no observable changes in the diffraction pattern. </p>		

Experiment report (continued):

References:

Lager, G.A., Armbruster, Th., and Faber, J. (1987) Neutron and X-ray diffraction study of hydrogarnet $\text{Ca}_3\text{Al}_2(\text{O}_4\text{H}_4)_3$. *American Mineralogist*, 72, 756-765.

Olijnyk, H., Paris, E., Geiger, C.A., and Lager, G.A. (1991) Compressional study of katoite ($\text{Ca}_3\text{Al}_2(\text{O}_4\text{H}_4)_3$) and grossular garnet. *Journal of Geophysical Research*, 96, 14313-14318.

Instrument Used: <i>(please type)</i> HIPD	Local Contact M.R. Fitzsimmons	Proposal Number: <i>(for LANSCE Use Only)</i> 6012
Title: Studies of the Magnetic Structures and Strain Content of Nanocrystalline Antiferromagnets		Report received: <i>(for LANSCE Use Only)</i> 3/7/94
Authors and affiliations: M.R. Fitzsimmons, LANSCE, LANL J.A. Eastman, Materials Science Division, ANL		
Experiment report: <p style="text-align: center;">The Roles of Grain Size and Strain on Antiferromagnetic Order in Nanocrystalline Chromium</p> <p style="text-align: center;">M. R. Fitzsimmons[§], J. A. Eastman[*], R. B. Von Dreele[§], and L. J. Thompson[*]</p> <p style="text-align: center;">[§] Manuel Lujan Jr., Neutron Scattering Center, Los Alamos National Laboratory, Los Alamos, NM 87545</p> <p style="text-align: center;">[*]Materials Science Division, Argonne National Laboratory, Argonne, IL 60439</p> <p>Abstract- Neutron diffraction investigations of powder and consolidated ultra-fine-grain-sized chromium samples indicate that antiferromagnetic order in the body-centered-cubic phase of this material is suppressed to well below the Néel temperature of coarse-grained and single crystal chromium. The suppression is correlated strongly with decreasing grain size. Antiferromagnetic order was not observed in powder nor consolidated samples with grain sizes less than 16nm, indicating that free surfaces and grain boundaries play the same role in preventing antiferromagnetic order. Antiferromagnetic order was observed in nanocrystalline samples with grain sizes greater than 19 nm at 20 K. No correlation is seen between the Néel temperature and the degree of long-ranged microstrain, nor with contents of light-element impurities in the samples. Even in cases where antiferromagnetic order is detected, the transversely-polarized AF₁ spin density wave magnetic phase is never seen. While this may suggest that spin density wave phases do not occur in nanocrystalline chromium, the presence of the longitudinally-polarized AF₂ spin density wave phase can not be ruled out unambiguously.</p> <p>submitted to Phys. Rev. B, 1994.</p>		

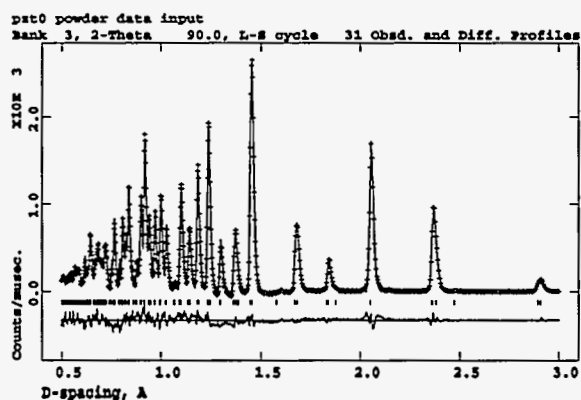
Experiment report (continued):

$$P = \frac{3}{2} K_0 \left[\left(\frac{V}{V_0} \right)^{-\frac{7}{3}} - \left(\frac{V}{V_0} \right)^{-\frac{5}{3}} \right] \left\{ 1 - \frac{3}{4} (4 - K_0') \left[\left(\frac{V}{V_0} \right)^{-\frac{3}{2}} - 1 \right] \right\}.$$

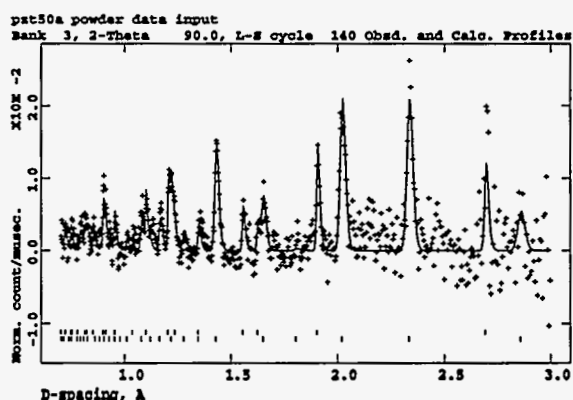
Here we set $K_0' = 4$ for simplification, so the equation reduces to

$$P = \frac{3}{2} K_0 \left[\left(\frac{V}{V_0} \right)^{-\frac{7}{3}} - \left(\frac{V}{V_0} \right)^{-\frac{5}{3}} \right].$$

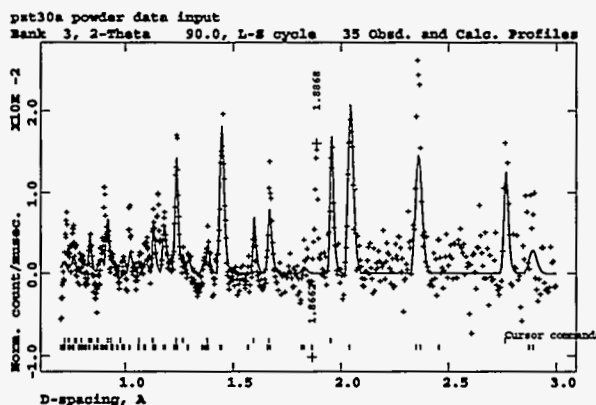
The fit of the data points to this formulation gives the values for the bulk modulus $K_0 = 99 \pm 8$ GPa, and initial volume $V_0 = 68.75 \pm 0.22 \text{ \AA}^3$ for cubic phase. The curve fit is shown in Fig. 2. The large uncertainty for K_0 may be caused by insufficient experimental data points as well as the assumption $K_0' = 4$.



(a)



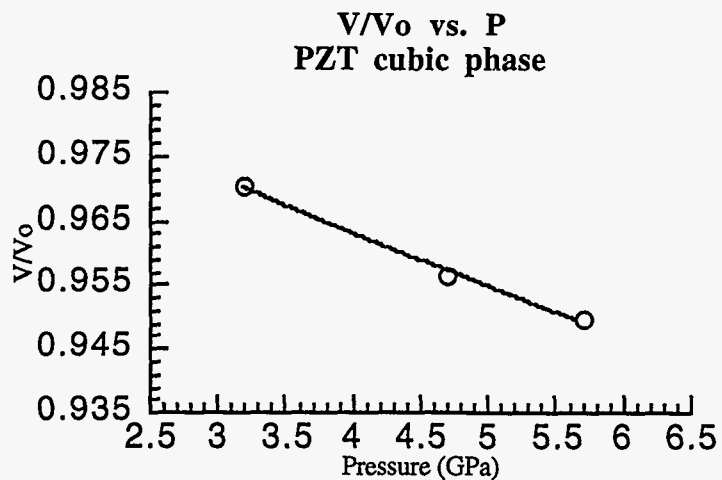
(b)



(c)

Figure 1. Observed and calculated (full line) neutron intensity profiles for $\text{PbTi}_{0.3}\text{Zr}_{0.7}\text{O}_3$. (a) rhombohedral phase at ambient temperature and pressure. (b) cubic phase at 4.7 GPa. (c) unknown phase at 1.8 GPa with R3c fit.

Experiment report (continued):



(c)

Figure 2. experiment data fit to Birch equation

References:

1. Decker D.L., J. Appl. Phys., vol.36, No.1, 157-162, Jan, 1965.
2. Glazer A.M., Mabod S.A., Clarke R. *Acta Cryst.*, B34, 1060-1065, 1978.
3. Liu L., Bassett W.A., *J. Geophys. Res.*, vol.77, No.26, 4934-4937, 1972.

Instrument Used: <i>(please type)</i> HIPD	Local Contact: Robert A. Robinson	Proposal Number: <i>(for LANSCE Use Only)</i> 6032
Title: Magnetic Ordering in U₂Pd₂In and U₂Pd₂Sn		Report received: <i>(for LANSCE Use Only)</i> 4/12/94
Authors and affiliations: L. Havela, V. Sechovský ; Charles University, Prague, Czech Republic F. R. de Boer, H. Nakotte and K. Prokeš ; Univ. of Amsterdam, The Netherlands A. Purwanto*, R. A. Robinson ; LANSCE, LANL * and NMSU		
Experiment report: A large number of UTX compounds where <i>T</i> is a transition metal element and <i>X</i> is a <i>p</i> -electron metal has been studied in order to see the role of <i>5f</i> -ligand hybridisation on the magnetic ordering[1]. In almost all ternary (1:1:1) U-intermetallic compounds, it has been found that the U-moments are highly anisotropic and are systematically aligned perpendicular to the directions of nearest-neighbor U-U links. Recently, a large number of U ₂ T ₂ X compounds crystallizing in tetragonal U ₃ Si ₂ structure with P4/mbm space group has been studied by means of bulk measurements and x-ray diffractions at room temperature[2]. For most of them, the nearest U-U distance is along the <i>c</i> -axis denoted by <i>d</i> _⊥ (see Fig. 1(a)), except for U ₂ Ni ₂ Sn and U ₂ Pd ₂ Sn which have the nearest U-U distance in the basal plane denoted by <i>d</i> _∥ (see Fig. 1(b)). Based on the simple picture obtained for UTX compound, we expect for most of U ₂ T ₂ X compounds studied elsewhere[2] that the U-moments to lie in the tetragonal basal plane. That is, most of them have in-plane anisotropy. In this work, we concentrate on the magnetic ordering of U ₂ Pd ₂ In and U ₂ Pd ₂ Sn. At room temperature, the nearest U-U link of the former is definitely <i>d</i> _⊥ , while the latter is marginally <i>d</i> _∥ [2]. However, at low temperatures, we observed that the nearest U-U link for U ₂ Pd ₂ Sn is <i>d</i> _⊥ . We have shown that the crossover which occurs at about 225 K is due to a change in U-positions within the cell and not to anisotropic thermal contraction[3]. For both compounds, a pure magnetic peak appears at 101 reflection in tetragonal symmetry. Other magnetic contributions appear at 111, 210, 200 for both compounds and in addition 201,211 for U ₂ Pd ₂ Sn (see Fig. 2). Using GSAS and fitting the individual peak, we obtained the same magnetic structure for both compounds. U-moments lie in the tetragonal basal plane in a noncollinear arrangement shown in Fig. 3, with moment magnitudes of 1.57 and 1.95 μ _B per U-atom for U ₂ Pd ₂ In and U ₂ Pd ₂ Sn respectively. These compounds obey the same picture as that of the UTX compounds, namely; U-moments are systematically aligned perpendicular to the directions of nearest-neighbor U-U links. This work has been submitted for publication[3].		

Experiment report (continued):

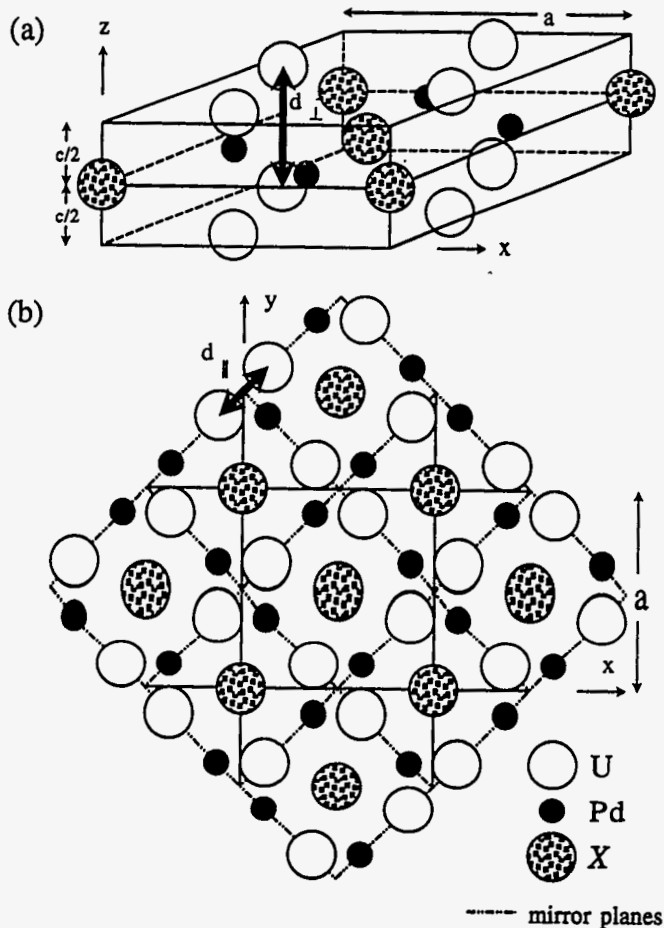


Fig. 1 : The crystallographic structure of U_2Pd_2X , with $X=In$ and Sn : a) schematic view, showing one of the nearest U-U distance in c -direction d_{\perp} and b) projected onto a basal plane, showing one of the nearest U-U distance in tetragonal basal plane d_{\parallel} . The atom sizes are not drawn to scale, but the atom coordinates within the cell are

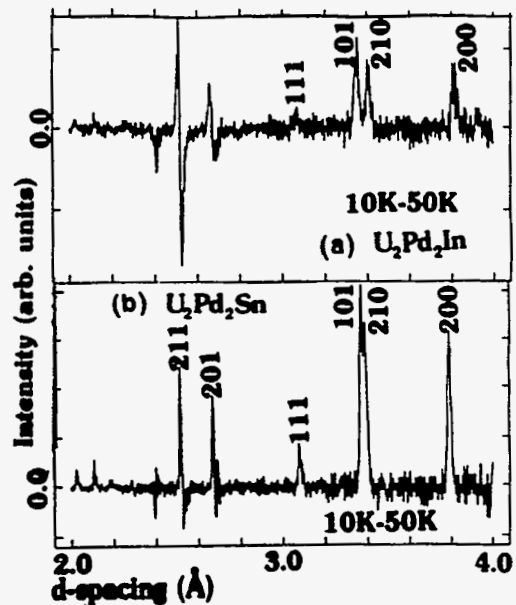


Fig. 2 : Plot of a portion of a difference curve 10 K- 50 K for (a) U_2Pd_2In and (b) U_2Pd_2Sn raw data taken in the $\pm 90^\circ$ and $\pm 153^\circ$ bank respectively. An extra peak appears at about 3.35 Å, indexed as 101 in tetragonal symmetry. The intensities have been divided by the incident spectrum.

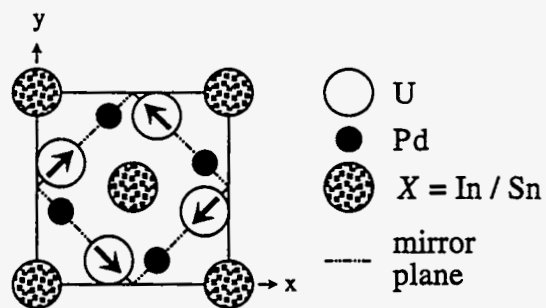


Fig. 3 : The magnetic structure of U_2Pd_2X , where $X=In$ and Sn , projected onto tetragonal basal plane. The atom sizes are not drawn to scale, but the atom coordinates within the cell are drawn to scale

References:

- ¹R. A. Robinson, A. C. Lawson, V. Sechovský, L. Havela, Y. Kergadallan, H. Nakotte and F. R. de Boer, submitted to Actinides '93, Conference, Santa Fe 19-24 Sept. 1993, accepted for publication in J. Alloys and Compounds.
- ²H. Nakotte, K. Prokeš, E. Brück, N. Tang and F. R. de Boer, P. Svoboda, V. Sechovský, L. Havela, J. M. Winand, A. Seret, J. Rebizant and J. C. Spirlet, submitted to Physica B
- ³A. Purwanto, R. A. Robinson, L. Havela, V. Sechovský, P. Svoboda, H. Nakotte, K. Prokeš, F. R. de Boer, A. Seret, J. M. Winand, J. Rebizant, J. C. Spirlet, submitted to Phys. Rev. B.

Instrument Used: <i>(please type)</i>	Local Contact	Proposal Number: <i>(for LANSCE Use Only)</i>
HIPD	R.B. Von Dreele	6054
Title: Pressure Dependence of the Structure of Nitromethane		Report received: <i>(for LANSCE Use Only)</i> 5/6/94

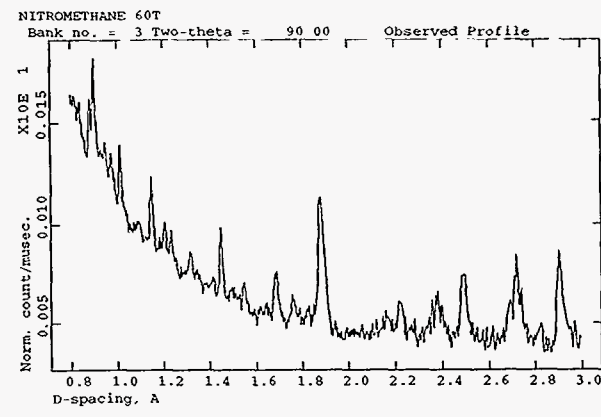
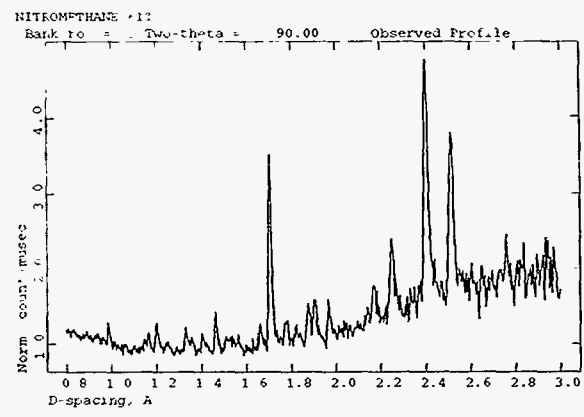
Authors and affiliations:

R.B. Von Dreele, LANSCE, Los Alamos National Laboratory

D. Schiferl, M-6, Los Alamos National Laboratory

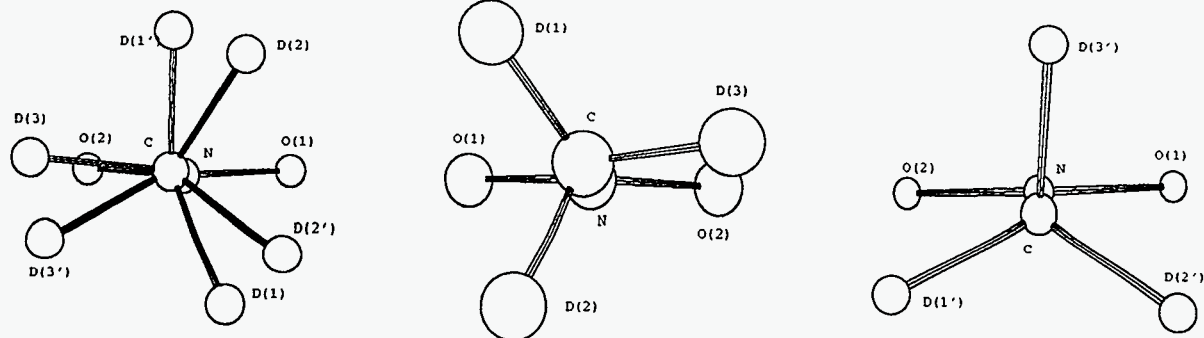
Experiment report:

The pressure dependence of the structure of nitromethane was investigated at pressures up to 55kbar on HIPD employing the "Paris-Edinburgh" pressure cell. The deuterated nitromethane was loaded into the cell made up into a paste with aerogel powder and salt (as pressure calibrant). Aerogel is a low density/high surface area amorphous material which promoted rapid crystallization of the nitromethane thus assuring that a fine grained powder was produced with no pressure induced preferred orientation. Earlier attempts using nitromethane liquid samples produced apparently coarse grained powders with very strong texture. The first figure illustrates this difference; the plot on the left is of pure nitromethane and the one on the right is from the nitromethane/aerogel paste at approximately the same pressure (ca. 50kbar).



Analysis of the texture free data taken at 15kbar and 40kbar gave essentially the same result as obtained earlier by single crystal x-ray work in a diamond anvil cell at similar pressures(1). The methyl group is disordered at 15 and 25kbar and at 40kbar it is "locked-in" rotated ~45° from its position at low temperatures and ambient pressure. At higher pressure (55kbar) a further rotation of the methyl group occurs so that it returns back to the orientation seen at ambient pressure although the molecule as a whole has been repositioned in the unit cell. The three figures below show how the methyl group reorients as a function of pressure for 15kbar, 40kbar and 55kbar.

Experiment report (continued):



The first view shows the methyl group disordered over two orientations, the second shows it rotated so that one of the C-D bonds is nearly in the same plane as the NO₂ group, and the third shows the methyl rotated back to its orientation in the ambient pressure structure with one C-D perpendicular to the NO₂ plane.

References:

- (1) D.T. Cromer, R.R. Ryan & D. Schiferl, *J. Phys. Chem.* 89, 2315-2318 (1985).

Instrument Used: <i>(please type)</i> HIPD	Local Contact R.B. Von Dreele	Proposal Number: <i>(for LANSCE Use Only)</i> 6055
Title: High Pressure Structure of Acetic Acid: Does it dimerize?		Report received: <i>(for LANSCE Use Only)</i> 5/6/94
Authors and affiliations: Robert B. Von Dreele, LANSCE, Los Alamos National Laboratory		
Experiment report: <p>The proposed experiment was to investigate the possible dimerization of acetic acid at high pressure. Although the ambient pressure/low temperature structure of acetic acid is known (1,2) nothing is known of a high pressure phase originally noted by Bridgeman(3). We have obtained powder diffraction patterns from d4-acetic acid at 3 pressures in the range 15-25kbar. The figure below shows that the pattern from acetic acid is quite weak apart from two peaks near 2.3Å. A trial model composed of acetic acid hydrogen bonded dimers proposed by Derissen & Smit (4) was used in an attempt to fit this data with no success. The figure shows a reasonable fit to the NaCl but completely misses the two strong features from the acetic acid. Evidently, the high pressure form is different from the proposed dimer structure.</p> <div style="text-align: center;"> <p>ACETIC ACID 20T Bank 3, 2-Theta 90.0, L-S cycle 6 Obsd. and Calc. Profiles</p> </div> <p style="text-align: right; font-size: small;">6-MAY-94 13 12 12</p>		

Experiment report (continued):

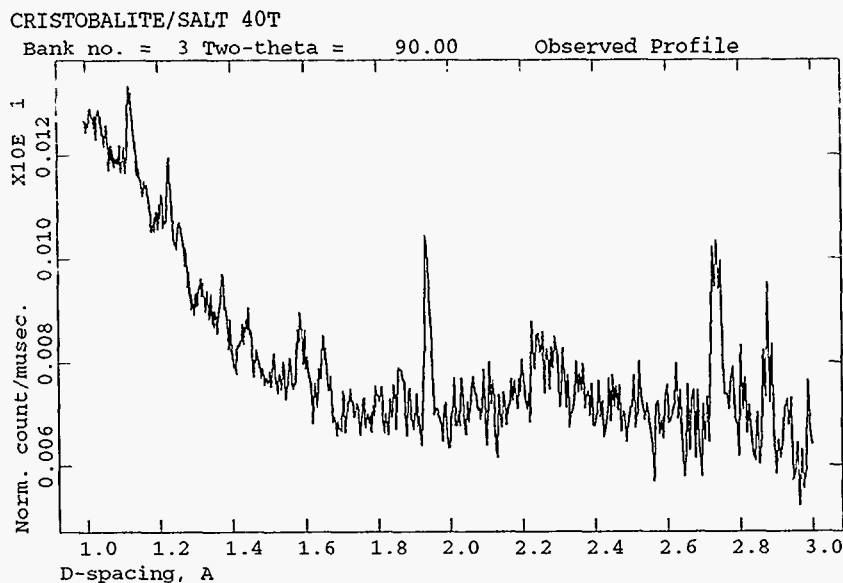
References:

- (1) R.E. Jones & D.H. Templeton (1958), *Acta Cryst.* 11, 484-487.
- (2) I. Nahringsbauer (1970), *Acta Chem Scand.* 24, 453-462.
- (3) P.W. Bridgeman (1916). *Proc. Amer. Acad. Arts. Sci.* 52, 92-187.
- (4) J.L. Derissen & P.H. Smit (1977), *Acta Cryst.* A33, 230-232.

Instrument Used: <i>(please type)</i> HIPD	Local Contact R.B. Von Dreele	Proposal Number: <i>(for LANSCE Use Only)</i> 6056
Title: Phase Transitions in Cristobalite at High Pressure		Report received: <i>(for LANSCE Use Only)</i> 5/6/94
Authors and affiliations: Robert B. Von Dreele, LANSCE, Los Alamos National Laboratory John Parise, Department of Earth and Space Science, SUNY, StonyBrook, NY		

Experiment report:

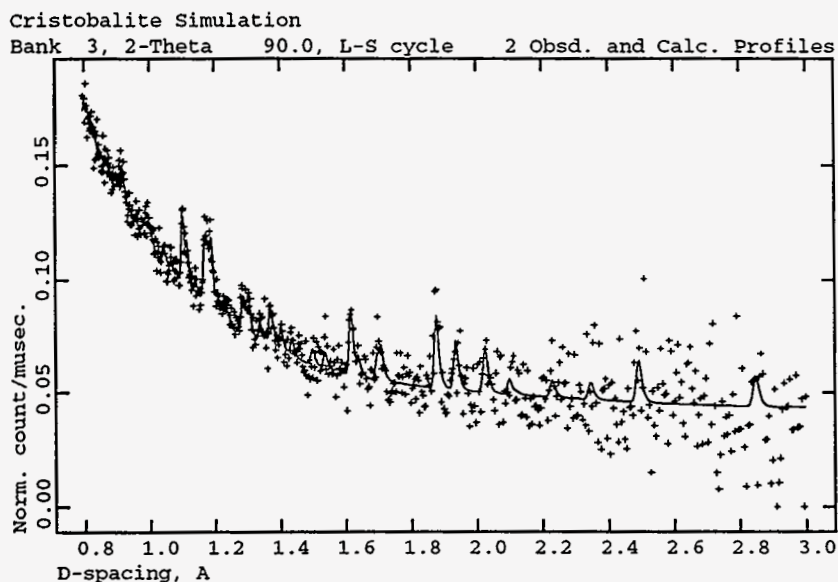
We proposed to examine the phase transitions in the cristobalite form of SiO₂ at high pressure in an attempt to understand the compression mechanism in this geologically important mineral. As can be seen from the first figure we did not succeed in obtaining diffraction data which were suitable for structure analysis.



6-MAY-94 10:56:22

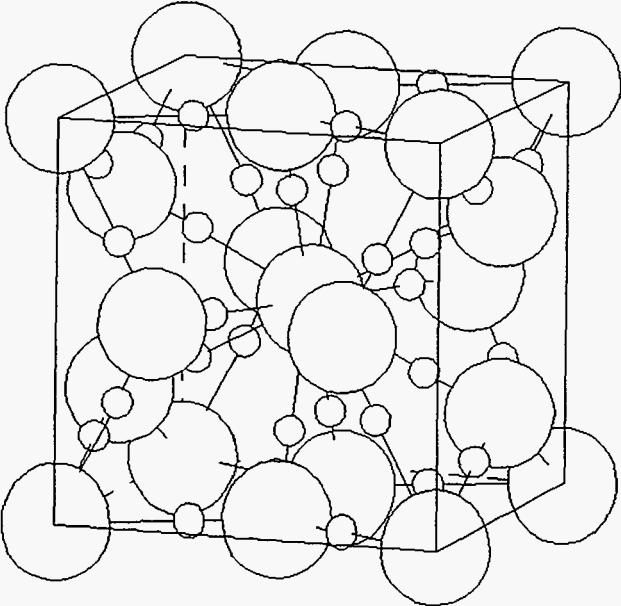
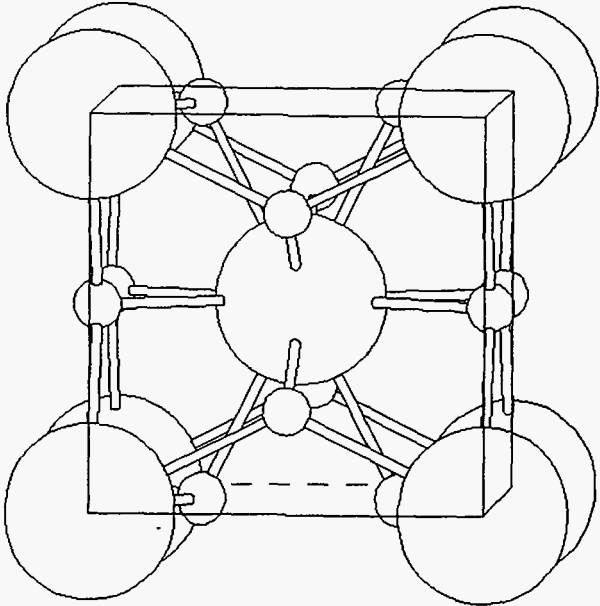
The only peaks visible in this pattern belong to the salt which was included as a pressure calibrant. In an attempt to understand the lack of diffraction peaks from the cristobalite we have calculated a simulated pattern using the known ambient pressure structure of cristobalite and the values of various other coefficients obtained (scale, background, etc.) from successful high pressure experiments. The resulting computed pattern is shown in the next figure.

Experiment report (continued):



It is evident that, apart from two peaks at 1.1 and 1.2Å, there is insufficient intensity in the diffraction pattern for this experiment to be successful. Although some diffraction peaks can be seen in the simulated pattern, there isn't enough of them to be usable in a Rietveld refinement. Moreover, we expected that there would have been a phase transition by this pressure (28kbar) and a pattern this weak precludes identifying the new phase.

References:

Instrument used: <i>(please type)</i> <p style="text-align: center;">HIPD</p>	Local contact: <p style="text-align: center;">R. B. Von Dreele</p>	Proposal number: <i>(for LANSCE use only)</i> <p style="text-align: center;">6072</p>
Title: <p style="text-align: center;">Structural Properties of α- and β-UD₃</p>		Report received: <i>(for LANSCE use only)</i> <p style="text-align: center;">2/24/94</p>
Authors and affiliations: <p style="text-align: center;">A. C. Lawson, MTL-5, and J. W. Conant NMT-5 Los Alamos National Laboratory</p> <p style="text-align: center;">G. L. Powell, Y-12 Oak Ridge National Laboratory Martin Marietta Corporation</p>		
Experiment report: <p>Uranium hydride crystallizes in two different crystal structures. They are both cubic, with space group Pm3n, and both structures are related to the β-W structure. The latter is more familiar as the structure of the superconductor Nb₃Sn. The β form, which is the one obtained by ordinary preparation techniques, has the structure shown in Fig. 1. There are two types of uranium atom, one of which is the Nb analog, the other the Sn analog. The hydrogen is interstitial. A revealing structural formula is U₃UD₁₂. The α-form, which can be obtained only by low-temperature preparation techniques, has the structure shown in Fig. 2. In this structure, U is analogous to Sn, and hydrogen to Nb. β-UD₃ is a ferromagnet, with a Curie temperature of 170 K. It has the curious property that the magnetic moments on the two uranium sites are identical within experimental error. As far as is known, α-UD₃ is non-magnetic.</p> <div style="display: flex; justify-content: space-around; align-items: flex-end;"> <div style="text-align: center;">  <p>Fig. 1. Structure of β-UD₃.</p> </div> <div style="text-align: center;">  <p>Fig. 2. Structure of α-UD₃.</p> </div> </div>		

Experiment report (continued):

We undertook the study of newly prepared material on HIPD with the hope that it would be single phase a material. Unfortunately, our diffraction patterns showed that the material was only 63% (by volume). Since the structures are so simple, we were able to refine the parameters for the α - and β -phases simultaneously. The lattice constants for the two phases are shown in Fig. 3. There is a pronounced minimum in the lattice constant curve for the α -phase. This does not correlate with any obvious structural or magnetic anomaly of this phase. There is also a shallow minimum in the β -phase, but it is very much less pronounced than that previously observed for pure β -phase. [1] These observations are consistent with an earlier measurement [2], but there is a consistent overall shift in the lattice constants. We do not know whether this is caused by a calibration error in the earlier measurements or by a difference in samples.

Debye-Waller factors [3] for the two phases are shown in Figs. 4 and 5. The Debye-Waller temperatures of the β -phase are roughly consistent with those reported for single phase material [1] The Debye-Waller temperatures for the α - phase are overall somewhat lower than for the β phase. As in the previous experiment [2,4], no sign of magnetism in the α -phase was found above 15 K. The magnetism of the β -phase was clearly observed at low temperatures.

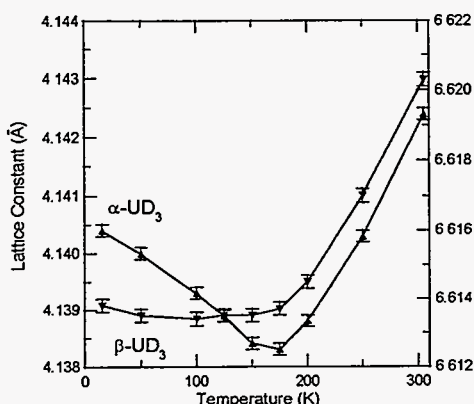


Fig. 3. Lattice constants of α - and β -UD₃ versus temperature.

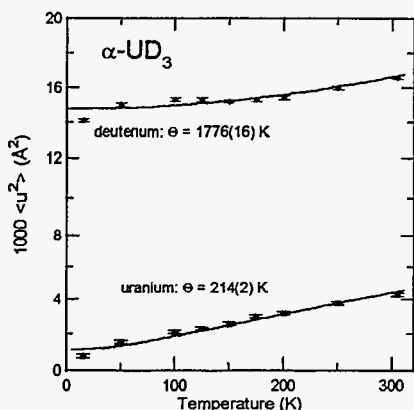


Fig. 4. Debye-Waller factors of α -UD₃ versus temperature

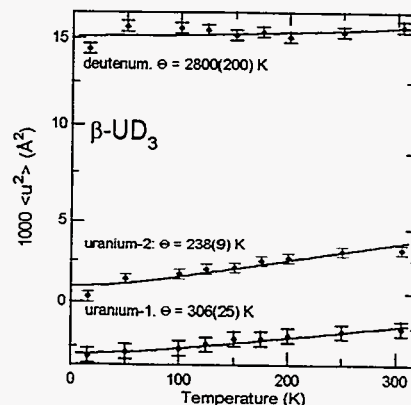


Fig. 5. Debye-Waller factors of β -UD₃ versus temperature.

References:

- [1] "Vibrational and Magnetic Properties of β -UD₃," A. C. Lawson, A. Severing, J. W. Ward, C. E. Olsen, J. A. Goldstone and A. Williams, *J. Less-Common Metals*, **158** 267-274 (1990).
- [2] "Neutron Powder Diffraction Study of α - and β -UD₃," A. C. Lawson, J. Conant, G. Burr, W. Tadloch and D. Kirk, LANSCE Experiment Reports, Los Alamos National Laboratory, LA-119338-PR (October 1990) p 56.
- [3] "Elastic Properties of Materials by Pulsed Neutron Diffraction," A. C. Lawson, A. Williams, J. A. Goldstone, D. T. Eash, R. J. Martinez, J. I. Archuleta, D. J. Martinez, B. Cort, and M. F. Stevens, *J. Less-Common Metals* **167** 353 (1991).
- [4] "Magnetic Structures of Actinide Materials by Pulsed Neutron Diffraction," A. C. Lawson, J. A. Goldstone, J. G. Huber, A. L. Giorgi, J. W. Conant, A. Severing, B. Cort and R. A. Robinson, *J. Appl. Physics*, **69** 5112-5117 (1991).

Instrument used: (please type) HIPD	Local contact: R. Von Dreele	Proposal number: <i>(for LANSCE use only)</i> 6073
Title: STRUCTURE OF MIXED ELECTRODES, $\text{Bi}_3 \text{M}_2 \text{SbO}_{11}$ M = Ir, Ru		Report received: <i>(for LANSCE use only)</i> 5/5/94
Authors and affiliations: B.J. Kennedy The School of Chemistry The University of Sydney Sydney, NSW 2006 Australia		
Experiment report: <p>Powder neutron diffraction patterns for 2 mixed metal oxides $\text{Bi}_3 \text{Ru}_2 \text{SbO}_{11}$ and $\text{Bi}_3 \text{Ir}_7 \text{SbO}_{11}$ have been collected on HIPD.</p> <p>Analysis of the data is in progress, the presence of small amounts of a monoclinic phase, SbBiO_4 is complicating the refinement, especially in attempting to detect any non-stoichiometry at the oxygen sites.</p>		

Instrument used: <i>(please type)</i> HIPD	Local contact: R. B. Von Dreele	Proposal number: <i>(for LANSCE use only)</i> 6083
Title Local Structure of $\text{La}_{1.875}\text{Sr}_{0.125}\text{CuO}_4$: Differential Pair Distribution Function Study		Report received: <i>(for LANSCE use only)</i> 5/9/94
Authors and affiliations: S.J.L. Billinge, MST-10 G. H. Kwei, MST-10 S. Ikeda, National Lab. for High Energy Physics (KEK), Japan		
Experiment report: <p>A growing number of experiments now indicate that the <i>local</i> atomic structures of the high-T_c materials are distorted away from the average crystal structure [1]. There is also evidence that these structural distortions couple to the carriers and therefore affect the properties of these important materials [1]. It is therefore very important to study the local structure of these materials in detail. We have used the pair distribution function (PDF) technique to study local structure in the 2:1:4 $[(\text{La}, \text{Sr}, \text{Ba})_2\text{CuO}_4]$ class of materials [2]. These systems are simple, single-plane, materials which, nonetheless, exhibit all of the canonical behavior of the cuprate superconductors.</p> <p>The superconductivity is associated with the CuO_2 planes. It is, thus, most important to consider structural distortions which involve primarily copper and oxygen atoms. It is possible to study only the atomic correlations in the material which involve copper by considering a differential-PDF (DPDF). In this function, which is experimentally accessible, all of the La-La, La-O and O-O correlations disappear, allowing us to concentrate on the important Cu-Cu, Cu-O and Cu-La correlations. We have obtained this function using powder diffraction data from HIPD.</p>		

Experiment report (continued):

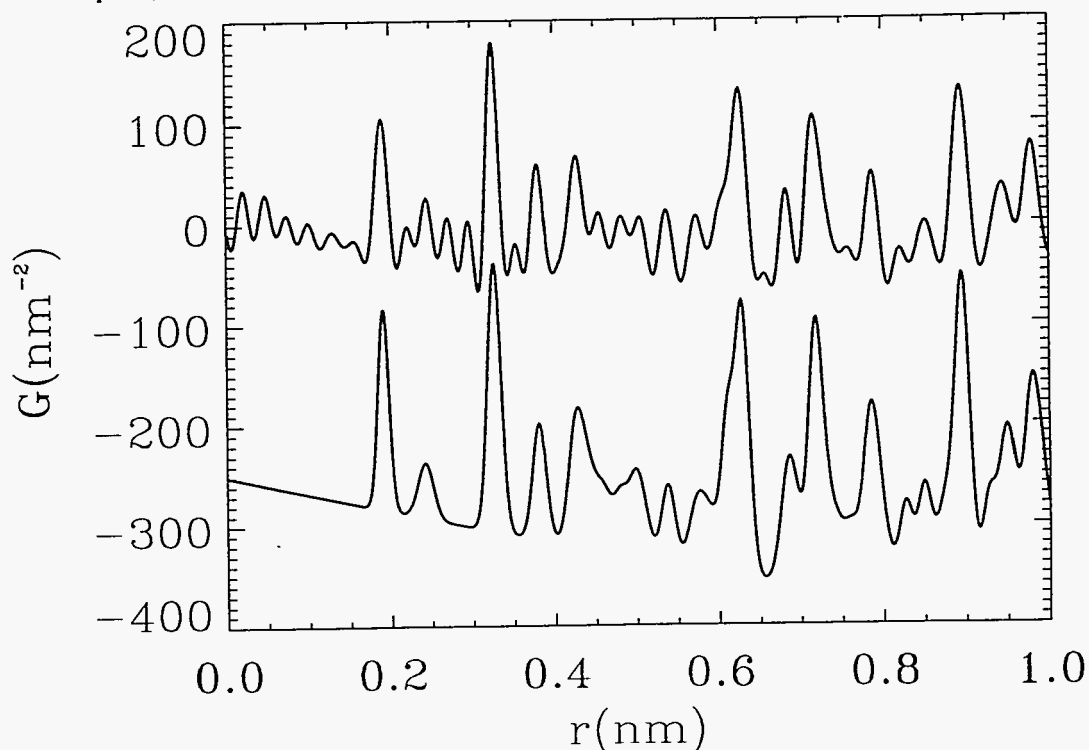


Figure 1. Copper differential PDF's from $\text{La}_{1.875}\text{Sr}_{0.125}\text{CuO}_4$. The upper curve is from powder diffraction data collected on HIPD, the lower curve is calculated from the crystallographic LTO structure.

Data were collected over a range of temperatures around T_c from two 10g samples of $\text{La}_{1.875}\text{Sr}_{0.125}\text{CuO}_4$: one sample was made with isotopically enriched ^{65}Cu and the other with isotopically enriched ^{63}Cu . After taking a difference the data were Fourier transformed yielding the copper DPDF. To our knowledge, this is the first differential PDF obtained from a crystalline material. The Cu-DPDF from the 10K data is shown in Fig. 1 as the upper curve. Below it is a model calculation for the Cu-DPDF assuming the crystallographic LTO model for the structure. The general features of the model are reproduced very nicely in the data; however, there are some discrepancies. The data are at an early stage in the analysis and it is difficult to draw definite conclusions at this point. We intend to analyse the temperature dependence of the Cu-DPDF and investigate in detail the origin of the discrepancies between the model and the data.

References:

- [1] for a review see S. J. L. Billinge, G. H. Kwei and J. D. Thompson, *Los Alamos Symposium 1993: Strongly Correlated Electronic Materials*, ed. K. Bedell (Addison-Wesley, 1994).
- [2] S. J. L. Billinge, G. H. Kwei and H. Takagi, *Phys. Rev. Lett.* **72**, 2282 (1994).

Instrument Used: (please type) HIPD	Local Contact: R. A. Robinson	Proposal Number: (for LANSCE Use Only) 6499																				
Title: Magnetic Ground State of UCoGa		Report received: (for LANSCE Use Only) 4/13/94																				
Authors and affiliations: L. Havela, V. Sechovský ; Charles University, Prague, Czech Republic H. Nakotte, F. R. de Boer ; Van der Waals-Zeeman Lab., The Netherlands A. Purwanto*, R. A. Robinson ; LANSCE, LANL *and NMSU																						
Experiment report: UCoGa belongs to the large group of UTX compounds (T =transition metal, X = p -electron metal) which has been studied extensively in order to understand the role of $5f-d$ hybridization in U-moment formation. Previous bulk magnetic investigations[1] revealed magnetic order at about 47 K, but the results were inconclusive regarding whether the ground state is ferromagnet, which exhibits domain effects, or antiferromagnet with a spin-flip transition in very low fields. That is, the coercivity of the hysteresis loop is too small to distinguish between the ferromagnet and antiferromagnet. UCoGa crystallizes in the hexagonal ZrNiAl structure (space group $P\bar{6}2m$). The structural parameters obtained from our data at 60 K (see Fig. 1) are : <table border="0" style="width: 100%;"> <tr> <td>U (3g)</td> <td>x</td> <td>0</td> <td>1/2</td> <td>$x = 0.580018 \pm 0.000026$</td> </tr> <tr> <td>Co (2c)</td> <td>1/3</td> <td>2/3</td> <td>0</td> <td></td> </tr> <tr> <td>Co (1b)</td> <td>0</td> <td>0</td> <td>1/2</td> <td></td> </tr> <tr> <td>Ga (3f)</td> <td>x</td> <td>0</td> <td>0</td> <td>$x = 0.239151 \pm 0.000034$</td> </tr> </table> $a(\text{\AA})=6.66456 \pm 0.00010$ $c(\text{\AA})=3.92653 \pm 0.00006$ Below the Néel temperature (47 K), although there are no purely magnetic peaks, magnetic contributions to nuclear peaks appear at 110, 200, 111, and 210. The possible magnetic structures were derived from the space group analysis (see Fig. 2). The fact that there are no 00 l magnetic contribution does not mean that the magnetic structure must be ferromagnetic (as in Fig. 2(c)) since two noncollinear models (Fig. 2(a) and (b)) also have no 00 l magnetic contribution. This is easily understood since the net moments in the 00 l basal plane are zero for both non-collinear models. Model 2(b) is excluded due to the absence of the calculated 110 magnetic contribution which we observe in the data. Model 2(c) gives a slightly better fit compared to model 2(a). The moment magnitude corresponding to model 2(c), which is ferromagnetic in c -direction, is $(0.74 \pm 0.03) \mu_B$ per U-atom. This result is in a good agreement with the value of $0.78 \mu_B$ per f.u obtained from the high-field magnetization [1]. Note that the Co moment is zero to within experimental error of $\pm 0.1 \mu_B$ per Co-atom. Also note that model 2(a) yields much larger U-moment of $(1.04 \pm 0.04) \mu_B$ per U-atom. This work has been submitted for publication[2].			U (3g)	x	0	1/2	$x = 0.580018 \pm 0.000026$	Co (2c)	1/3	2/3	0		Co (1b)	0	0	1/2		Ga (3f)	x	0	0	$x = 0.239151 \pm 0.000034$
U (3g)	x	0	1/2	$x = 0.580018 \pm 0.000026$																		
Co (2c)	1/3	2/3	0																			
Co (1b)	0	0	1/2																			
Ga (3f)	x	0	0	$x = 0.239151 \pm 0.000034$																		

Experiment report (continued):

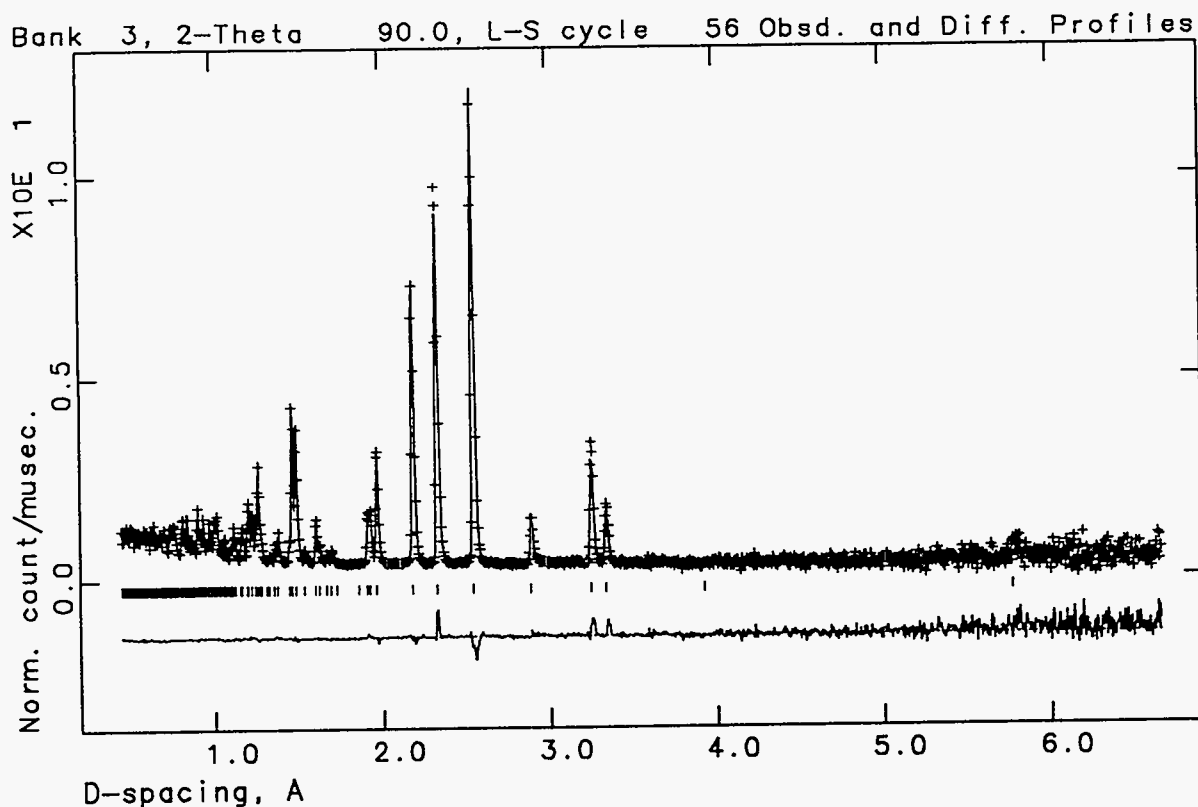


Fig. 1. Plot of the time-of-flight spectra, along with Rietveld fits, reflection markers and residual, from one 90° bank of HIPD at 60 K. The intensities have been divided by the incident spectrum.

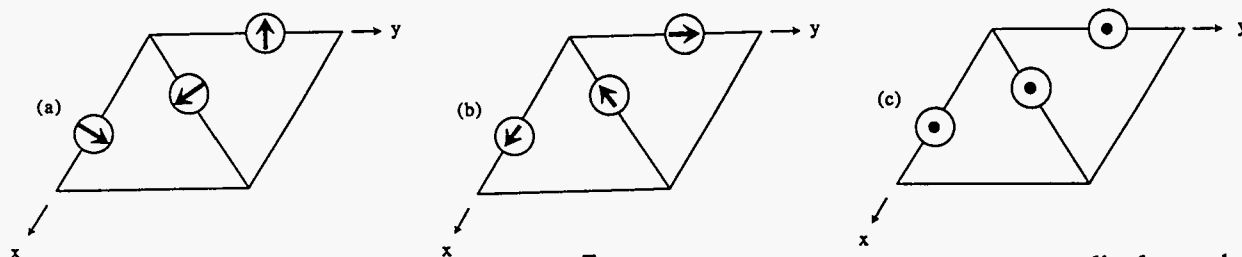


Fig. 2. The Shubnikov magnetic subgroups of $P\bar{6}2m$. In (a), the U-moments are perpendicular to the mirror planes. In (b) and (c), the U-moments are parallel to the mirror planes. The moments in (a) and (b) lie in the hexagonal basal plane, while in (c) are ferromagnetically coupled along the c -axis. Our data indicate that model 2(c) is the right one.

References:

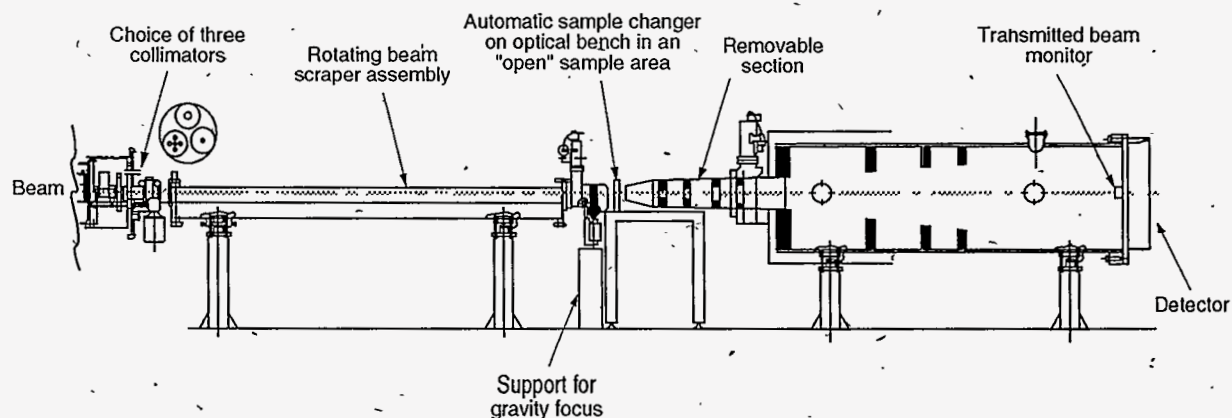
- [1]. H. Nakotte, F. R. de Boer, L. Havela, P. Svoboda, V. Sechovský, Y. Kergadallan, J. C. Spirlet, and J. Rebizant, *J. Appl. Phys.* 73, 6554 (1993)
- [2]. A. Purwanto, R. A. Robinson, K. Prokes, H. Nakotte, F. R. de Boer, L. Havela, V. Sechovský, N. C. Tuan, Y. Kergadallan, J. C. Spirlet and J. Rebizant, submitted for MMM/Intermag Conference - 1994, to be published in *J. Appl. Phys.*

*Low-Q Diffractometer
(LQD)*

Low-Q Diffractometer (LQD)

The Low-Q Diffractometer (LQD) is designed to study structures with dimensions in the range from 10 to 1000 Å. A significant feature of the LQD is that it measures a broad range of Q (0.003 to 0.5 \AA^{-1}) in a single experiment without any changes to the instrument's physical configuration. The LQD requires an intense source of long-wavelength ("cold") neutrons. Therefore, a liquid-hydrogen moderator is used, which produces a neutron spectrum that peaks at about 2.4 \AA and has usable flux from 0.3 to 20 \AA . A pair of single-aperture collimator plates yields an angular resolution of 0.09° and a penumbra diameter of 10 mm at the sample. An optional five-hole-

aperture converging collimator allows a four times increase in intensity without affecting the resolution. At 20 Hz, the slowest neutrons used on the LQD fall 12 mm under the influence of gravity. Rather than increasing the size of the beam-stop, neutrons whose parabolic trajectories strike the detector at its center are selected. The gravity-focusing device accomplishes this task by pushing the collimator exit plate upward at constant acceleration during each beam pulse. The LQD is useful in addressing problems of critical phenomena, colloid structure, biomolecular organization, phase separation, and phase morphology and molecular conformation in polymers.



Instrument Details

Wavelength range	0.2–15 Å at 20 Hz	
Scattering angle	6–60 mrad	
Q range	0.003–0.5 Å ⁻¹	
Sample size:		
Single-aperture collimator	10 mm x 13 mm	
Multiple-aperture collimator	24 mm x 27 mm	
Detected intensity (single aperture, 30 μA):	0.2 < λ < 1.6 Å	0.2 x 10 ⁴ n/s
	1.6 < λ < 5.0 Å	8.0 x 10 ⁴ n/s
	5.0 < λ < 15 Å	2.0 x 10 ⁴ n/s
Detector	1 multiwire, 59 cm in diameter	
Moderator	Liquid hydrogen at 20 K	
Sample environment	Air; vacuum; closed-cycle refrigerator; pressure cell (up to 3 kbar); shear cell; or user supplied	
Experiment duration	20 minutes to 12 hours	

Rex P. Hjelm, Jr., instrument scientist
Dennis Martinez, instrument technician

LQD Experiment Reports

5409	<i>Characterization of Void Arrays in Alumina Filaments</i>	71
6042	<i>Magnetic Correlation Length Determination in an Amorphous Magnetic Material</i>	73
6043	<i>Microstructure of Cationic Microemulsions Containing Metal Electrolytes</i>	75
6044	<i>Characterization of Polymer Molecules at Interfaces by Small- Angle Neutron Scattering</i>	80
6060	<i>Sans on Thin Homopolymer Films</i>	82
6061	<i>Lower Critical Ordering of Diblock Copolymers</i>	83
6071	<i>Neutron Scattering Studies of the Muscle Protein Complex Troponin C/Troponin I</i>	85
6074	<i>Structure of LCP-LCT Composites</i>	87
6075	<i>Study of Aqueous Biphasic Systems under Dynamic Conditions</i>	89
6097	<i>Trial Experiment for Time-of-Flight Protein Crystallography</i>	91
6099	<i>Alumina Gel Structures by SANS</i>	92
6103	<i>Neutron Scattering Studies on N-Terminal Trypsin Trimmed Nucleosome Core Particles</i>	94
6108	<i>Symmetric Isotopic Blends of PDMS</i>	96
6403	<i>Beta-Layering</i>	98
6405	<i>Small-Angle Neutron Scattering by Aged ²³⁹Pu δ-Phase Samples</i>	100

Instrument used: <i>(please type)</i> LQD	Local contact: Philip A. Seeger	Proposal number: <i>(for LANSCE use only)</i> 5409								
Title: Characterization of Void Arrays in Alumina Filaments		Report received: <i>(for LANSCE use only)</i> 9/21/93								
<p>Authors and affiliations:</p> <table border="0"> <tr> <td data-bbox="161 517 393 549">David S. Phillips</td> <td data-bbox="550 517 678 619">LANL MST-4 MS G771</td> <td data-bbox="1029 517 1095 549">USA</td> <td data-bbox="1224 517 1318 549">7-5128</td> </tr> <tr> <td data-bbox="161 666 384 697">Philip A. Seeger</td> <td data-bbox="550 666 678 768">LANL LANSCE MS D408</td> <td data-bbox="1029 666 1095 697">USA</td> <td data-bbox="1224 666 1318 697">7-8843</td> </tr> </table>			David S. Phillips	LANL MST-4 MS G771	USA	7-5128	Philip A. Seeger	LANL LANSCE MS D408	USA	7-8843
David S. Phillips	LANL MST-4 MS G771	USA	7-5128							
Philip A. Seeger	LANL LANSCE MS D408	USA	7-8843							
<p>Experiment report:</p> <p>The objective of this experiment was to measure the density and long-range order of the void array in a single crystal sapphire filament grown by the edge-defined film-fed growth process (EFG.) These voids were identified previously by transmitted light microscopy (with accompanying resolution limits). It was hypothesized that the voids order in an approximately helical arrangement, though it was difficult to quantify this impression in direct microscopy.</p> <p>We (actually Phil) ran this experiment for six of the eight hours of beam time allocated. At the end of this period, no measurable scattering attributable to the void array had been observed, so the experiment was terminated. This is probably a consequence of simply inadequate void fraction, at roughly 10^{-3} of the 50 micron diameter by ca 1 cm sample.</p> <p>For the last two hours of beam time allocated this project, Phil substituted a titanium-doped sapphire crystal previously designated as a backup experiment. Although the precipitates under study here are also dilute, 8×10^{-4}, this sample scattered very well and permitted a statistically significant measurement of the mean needle radius at an early stage of the precipitation reaction ultimately leading to star sapphire. This information is useful, since the major traditional tool for studying the precipitation (transmission electron microscopy) gives notoriously poor counting statistics. The measure obtained, $R_c = 235 \text{ \AA}$, is in qualitative agreement with microscopic images. The backup plan was as follows:</p> <p>The precipitation of rutile (TiO_2) needles in sapphire (Al_2O_3) single crystals is well known. These form twinned needles with the [011] direction in rutile parallel to the [1010] direction in sapphire; both are orientations of close oxygen packing. The needles grow to great length and coarsen rather slowly in width. The detailed structure of the needles has been thoroughly</p>										

Experiment report (continued):

studied by TEM. Rutile needles, though the most stable form of titanium dioxide, are still metastable in sapphire with respect to the pseudobrookite intermediate compound Al_2TiO_5 .

Two other precipitates in $\text{Ti}:\text{Al}_2\text{O}_3$ have more recently been discovered -- a TiO_2 analog to PbO_2 and a yet undetermined phase. Both form (qualitatively) at lower temperatures than rutile, though no decent measure of the precipitation kinetics of any of these at any temperature is yet available.

To measure the kinetics of any of these reactions, one would need a bulk technique capable of measuring particle volume fraction (and ideally, size as well) for samples quenched from various ageing times and temperatures. It is important for the measurements to be rapid and to interrogate substantial numbers of particles. If the scattering factors of rutile and sapphire are sufficiently distinct for neutrons, small angle neutron scattering would appear to be an ideal technique. Last summer's experiment confirms these assumptions and demonstrates the unique attractiveness of SANS to this problem -- it samples cubic millimeter sized volumes and returns useful dimensions and statistics in single experimental runs.

References:

Instrument used: <i>(please type)</i> LQD (Small angle scattering)	Local contact: Rob Robinson	Proposal number: <i>(for LANSCE use only)</i> 6042
--	------------------------------------	---

Title: Magnetic Correlation Length Determination in an Amorphous Magnetic Material	Report received: <i>(for LANSCE use only)</i> 4/25/94
--	--

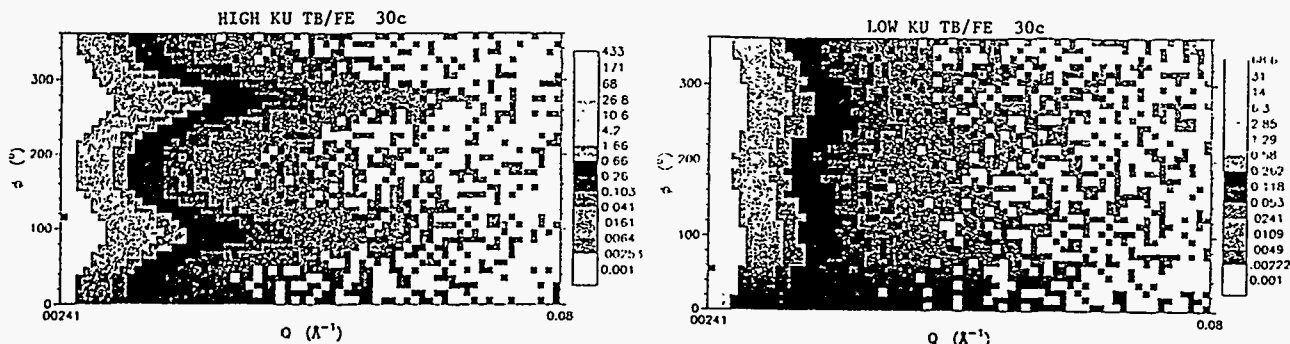
Authors and affiliations:

Frances Hellman, Department of Physics, University of California, San Diego
 Susan Watson, Department of Physics, University of California, San Diego
 Alex Shapiro, Department of Physics, University of California, San Diego
 Rob Robinson, LANSCE, Los Alamos National Laboratory, Los Alamos, NM
 Jim Rhyne, National Institute of Standards & Technology, Gaithersburg, MD

Experiment report:

A large number of magnetic materials exhibit "spin-glass-like" properties, meaning that although they possess strongly interacting local magnetic moments, the interactions are frustrated in such a way as to lead to a disordered magnetic state with no net moment. One group of "spin-glass-like" magnets are the amorphous rare earth-containing alloys in which the frustration arises from a competition between exchange and randomly-directed local magnetic anisotropy (due to local "crystal fields").^{1,2} These disordered magnets are characterized by a spin freezing temperature below which they possess only a finite magnetic correlation length ξ , defined as the length over which the directions of the local magnetic moments are correlated. The amorphous rare earth alloys possess an interesting and important additional attribute: the degree of randomness in the local axis directions can be precisely controlled and measured; in other words, we can introduce a coherence to the directions of these local axes.³ This coherence gives the materials a *macroscopic* magnetic anisotropy K_U which is easily measured. It has been theoretically predicted, but never experimentally confirmed, that even finite values of such a coherence will restore long range magnetic order and cause ξ to diverge above a critical value of K_U .^{4,5} Small angle neutron scattering (SANS) allows us to measure ξ in a material with controlled amounts of macroscopic anisotropy.

Amorphous Tb-Fe samples were prepared at UCSD in an ultra-high vacuum deposition system and protected from oxidation by Nb overlayers. To reach the necessary sample thickness (10 μm was desired), each sample consisted of a stack of 6-10 individual substrates, with a 1-1.5 μm thick α -Tb-Fe layer on each. Two sets



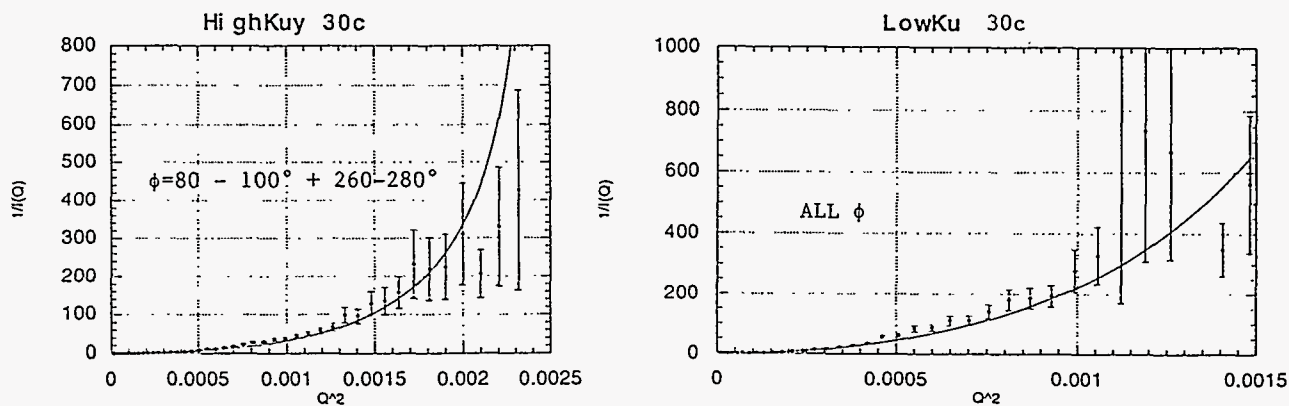
Experiment report (continued):

of sample were prepared; one with high values of K_U and one set with low K_U . These samples were characterized by magnetization measurements which gave the moment, magnetic ordering temperature and macroscopic anisotropy constant K_U . Structural and compositional characterization was made by Rutherford back-scattering and by x-ray diffraction including EXAFS analysis. SANS measurements were made in a vacuum furnace at LANSCE at a series of temperatures below the magnetic ordering temperature and then normalized by the non-magnetic background (nuclear) scattering above T_C . For a random anisotropy material, the scattering cross-section should be represented by the sum of a Lorentzian plus a Lorentzian-squared with the inverse correlation length, $\kappa = \xi^{-1}$, common to both terms^{6,7}:

$$\frac{d\sigma}{d\Omega} = \frac{A}{Q^2 + \kappa^2} + \frac{B}{(Q^2 + \kappa^2)^2} \quad (1)$$

Typical results are shown in figure 1 and 2 for data taken at room temperature. Figure 1 shows the normalized intensity of the scattering I from the high K_U and the low K_U sample in a grey scale $\phi(Q)$ plot. The most striking result, and a completely unexpected one, is the asymmetry in the plane of the sample of the high K_U material. This effect is presumably growth-induced, but there is no evidence (to quite high accuracy) for any in-plane asymmetry in any of the macroscopic magnetic properties. Since the low K_U samples do not show this effect, it is not a trivial consequence of the sample preparation technique. We are currently exploring models for the asymmetry. Future neutron scattering experiments on this problem would involve the effect of an applied magnetic field on the scattering, from which longitudinal and transverse spin fluctuation effects can be separated.

Figure 2 shows plots $1/I$ versus Q^2 with a polynomial fit to the data. The data shown is for relatively low values of Q , where the scattering in amorphous magnetic materials is not well understood and does not fit the form shown in Eqn. 1. At higher values of Q , the data is dominated by noise. As a result, no sensible values for ξ could be derived. In the future, we plan to count for longer at each temperature, taking data at fewer temperatures, and to work with different substrates which would allow more data at each Q to be included (the Si substrates used for this experiment gave large Bragg peaks due to multiple forward scattering-type events; only the longer wavelength events could therefore be analyzed).



References:

1. K. Moorjani and J. M. D. Coey, "Magnetic Glasses," Elsevier (1984).
2. R. Harris, M. Plischke, and M. J. Zuckermann, *Phys. Rev. Lett.* **31**, 160 (1973).
3. F. Hellman and E. M. Gyorgy, *Phys. Rev. Lett.* **68**, 1391 (1992).
4. Y. Goldschmidt and A. Aharony, *Phys. Rev. B* **32**, 264 (1985).
5. E. M. Chudnovsky and R. A. Serota, *IEEE Trans. Magn.* **20**, 1400 (1984) and *J. Phys. C* **16**, 4181 (1983).
6. J. J. Rhyne, *IEEE Trans. Magn.* **MAG-21**, 1990 (1985) and *Physica* **130B**, 253 (1985).
7. J. J. Rhyne, S. J. Pickart, and H. A. Alperin, *Phys. Rev. Lett.* **29**, 1562 (1972).

Instrument Used: (please type) LQD	Local Contact Phil Seeger	Proposal Number: <i>(for LANSCE Use Only)</i> 6043
Title: Microstructure of Cationic Microemulsions Containing Metal Electrolytes		Report received: <i>(for LANSCE Use Only)</i> 3/15/94
Authors and affiliations: Jess Wilcoxon, Sharon Craft, Organization 1153, Sandia National Labs, Albuquerque, NM		
Experiment Report Introduction <p>The purpose of this experiment was to learn more about the microstructure and interactions of inverse cationic microemulsion systems with added electrolyte. These systems consist of droplet-like structures with hydrophobic entities forming an interface with the majority oil phase, and an interior hydrophilic environment friendly to both water and electrolyte species (salts). We are particularly motivated to investigate these systems since they provide excellent environments to carry out simple chemical reactions such as reduction and coprecipitation.¹⁻³ Examples of reactions which we have successfully executed using inverse microemulsions include formation of a wide range of useful metal sulfides such as FeS₂ (cubic pyrite), MoS₂, CdS and metal oxides such as Fe₃O₄. Nanosize clusters of these materials formed in inverse microemulsions have enormous technological importance, particularly in the areas of catalysis and photocatalysis. By investigating the initial size and interactions in several of these systems we hope to gain insight into the relationship between micelle size, polydispersity, interactions and final metal oxide or sulfide cluster size, shape, and polydispersity. This is a very ambitious goal in view of the large complexity inherent to these multicomponent systems, and makes interpretation of scattering data difficult. Our approach is to use both SANS measurements and static and dynamic light scattering to investigate structure, dynamics, and interactions on length scales from ~500 nm to ~1 nm. The light scattering is typically done using normal hydrogenated alkanes, while SANS utilizes the more expensive deuterated alkanes, and this has important consequences on the microemulsion microstructure as we discovered.</p> Materials and Methods <p>The cationic surfactant, DTAC Dodecyltrimethylammonium, CH₃(CH₂)₁₁N(CH₃)₃Cl was investigated since it has an exceptionally large single phase microemulsion region when combined with an appropriate cosurfactant such as hexanol. In addition, unlike the surfactant CTAB, studied previously, no water is required to form a stable spherical droplet structure. This has major advantages from a synthetic standpoint since many strong reducing agents used to form metal clusters cannot abide the presence of water. The continuous phase aliphatic oils were all deuterated to improve both contrast and reduce the incoherent scattering contribution of hydrogen.</p>		

Experiment report (continued):

Results and Discussion

As mentioned above, we choose the DTAC system to take advantage of its extraordinarily large single phase microemulsion region for which light scattering investigations had suggested a droplet-like microstructure even very close to the phase separation boundary. Near this boundary at a water weight fraction $\sim w \sim .25$ the measured hydrodynamic radius was only ~ 18 nm, indicating a compact, non-interacting microstructure. In contrast, nonionic systems exhibit huge increases in scattering and apparent size near their phase boundaries, consistent with strong inter-micellar interactions. These interactions complicate the interpretation of SANS data, of course. Therefore, we anticipated this system would be ideal for SANS investigations.

Another remarkable feature of the DTAC system is that certain highly ionic electrolytes (e.g. Li_2S) can be added to the system in large amounts (up to nearly 0.5 M) and even facilitate expansion of the stable single phase region up to $\phi_w \sim .55$! This observation is quite different than any other system of which we are aware. In fact, in most cases addition of such highly ionic species tends to disperse the microemulsion stability. We wondered what type of microstructure existed near this phase boundary. It is difficult to imagine a droplet like structure with this little surfactant and containing this much water. But light scattering along with the low viscosity suggested this was precisely the case.

As so often happens in science, we made a serendipitous discovery in the process of preparing our deuterated SANS samples which gave us a significant and unconventional insight into one of the key factors responsible for inverse microemulsion stability. For example, we had previously mapped out the single phase region of the surfactant DTAC in octane and found stable microemulsions for water weight fractions $\sim w$, between 0 and 0.26. Thus, we were quite surprised that upon substituting deuterated octane this region decreased to only $0 < w < 0.08$. We noted similar dramatic changes with certain added electrolytes. These observations strongly implied that inverse microemulsion stability is determined primarily by interactions between the oil and the surfactant tails, not at the interior head group-water interface, as is commonly assumed. These observations also limited our ability to study the very interesting large single phase structures alluded to in the introduction.

In our first series of experiments we added water to an initially 8.5 wt% DTAC inverse micelle system containing 10% hexanol as a cosurfactant and examined changes in the scattering behavior. The changes we observed are shown for this system in figure 1. The limiting slope exhibits Porod law behavior as expected for a droplet-like micelle with a sharp interface between the surfactant and the oil. This limiting behavior does not change with addition of water, unlike some nonionic systems. Unfortunately it is not possible to make a direct comparison to light scattering data with respect to size changes because of the very different phase boundaries for the deuterated compared to the hydrogenated systems.

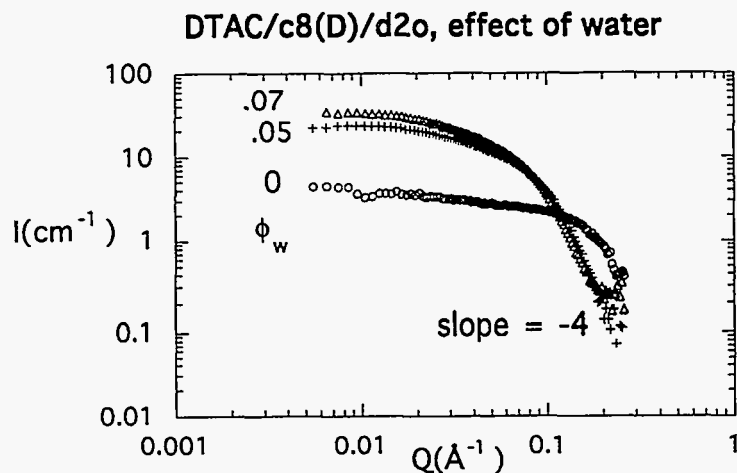


Figure 1. The effect of addition of water to the DTAC/hexanol/octane inverse micelle system is shown as a function of water weight fraction, ϕ_w .

Experiment Report (continued)

Due to the obvious importance of the oil interface interactions in determining phase stability, we decided to examine a longer chain hydrocarbon, hexadecane and also a cyclic hydrocarbon, cyclohexane in a water titration experiment. As the hydrocarbon number k increases, the amount of water that can be solubilized without phase separation decreases as shown in figure 2. No major changes in microstructure were observed however. In this regard this system is very similar to nonionic systems. No significant changes in scattering near the phase boundary at $\phi_w = 0.015$ were observed, indicating intermicellar interactions are quite weak in this system compared to nonionic micelles.

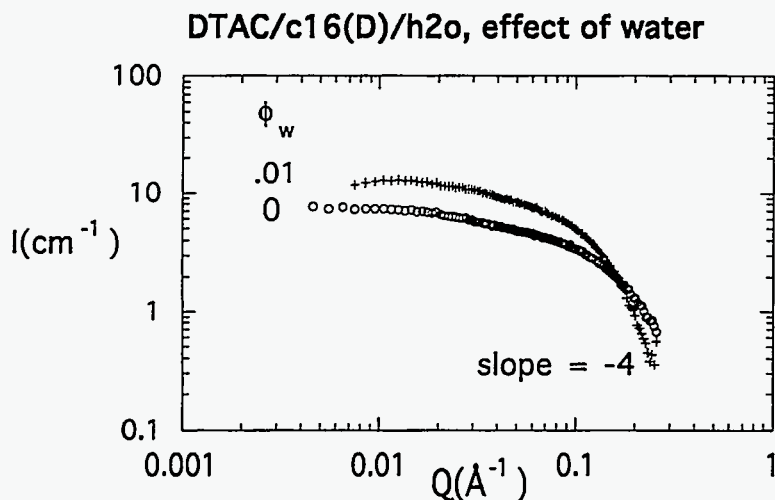


Figure 2. The effect of addition of water to the DTAC/hexanol/hexadecane inverse micelle system is shown as a function of water weight fraction, ϕ_w .

By contrast, use of a cyclic hydrocarbon affects the microstructure as shown in figure 3 where a slight minima develops. This change emphasizes the importance of packing (which determine interface curvature) and interactions at the oil interface. It is interesting to note that titration with either H₂O or D₂O did not affect the shape of the scattering curves shown in figure 1-3, instead simply altering the contrast factor. This implies that the inner interface of the micelle which is commonly thought to govern microemulsion stability and structure, has a much more limited role than expected.

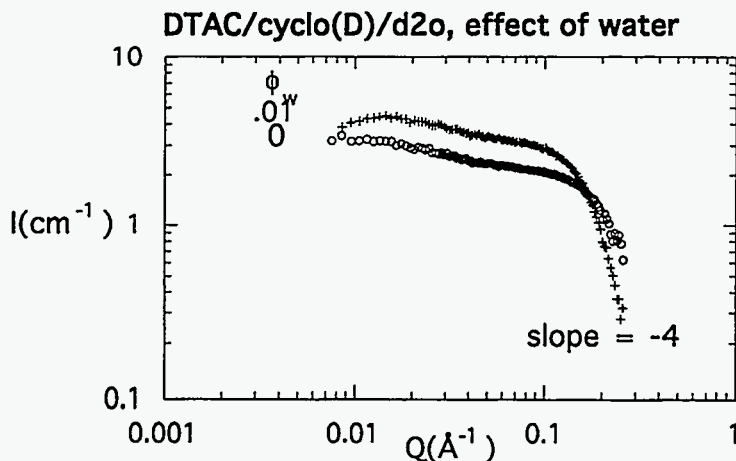


Figure 3. The effect of addition of water to the DTAC/hexanol/cyclohexane inverse micelle system is shown as a function of water weight fraction, ϕ_w .

We also investigated the effect of the presence of an electrolyte on the microstructure and stability of the DTAC/hexanol/octane system shown in figure 1. The single phase microemulsion decreased in size as shown in figure 4, but the structure remained droplet-like. The preservation of the microstructure in the presence of this salt explains the high quality of the spherical Sn clusters formed in the corresponding non-deuterated system by reduction of this metal salt.

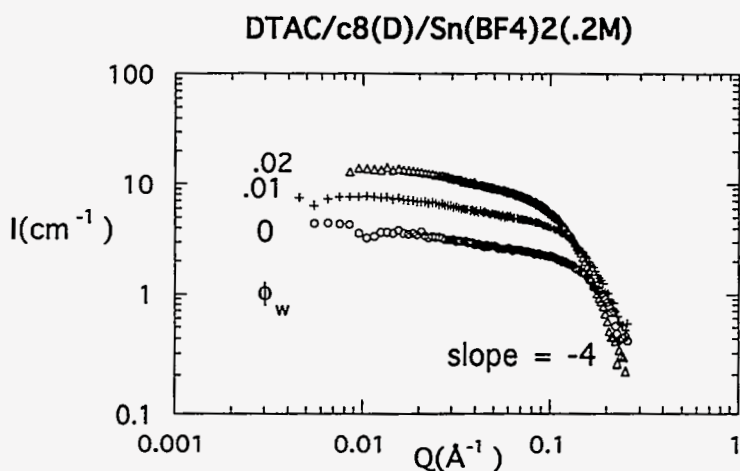


Figure 4. Effect of addition of a tin salt to the DTAC/hexanol/octane inverse micelle system as a function of water weight fraction, (ϕ_w).

However, not all salts had the same effect on the microstructure in this micelle system. For example, as shown in figure 5, addition of the corresponding iron salt at the same ionic strength did not decrease the size of the single phase region compared to the bare micelle, but the apparent mass reflected by the $I(0)$ value of nearly 1000 at (ϕ_w .07 is significantly larger than the value of ~20 seen near the phase boundary in both figures 1 and 4. This surprising result implies that a very strong increase in intermicellar attractive interactions due the presence of the salt may occur. These interactions cannot be simply explained by either the ionic strength nor the charge (oxidation state is two in both cases). They must be related to the ionic radius of Fe(II) compared to Sn(II) and geometric constraints at the inner interface of the micelle. However, the structure factor is still consistent with a spherical geometry.

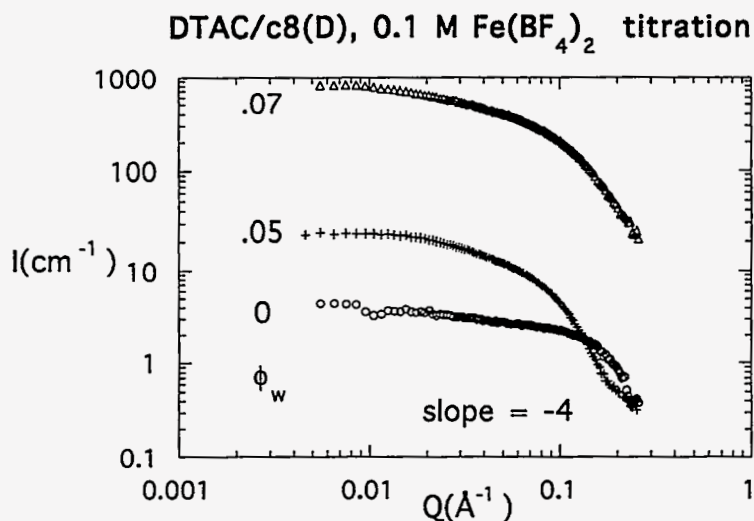


Figure 5. Effect of addition of a iron salt to the DTAC/hexanol/octane inverse micelle system as a function of water weight fraction, (ϕ_w).

Experiment Report (continued)

Finally, as mentioned in the introduction, we hoped to explore the unusual microstructure which we assumed must be present in the DTAC/hexanol/octane system when titrated with Li_2S . Unfortunately, in the case of the deuterated system investigated, the single phase microemulsion region actually decreased in size as shown in figure 6. No change in microstructure was observed and the single-phase region size remained roughly the same. Again, the well defined spherical cavities containing the salt can account for the monodisperse metal sulfide clusters formed using this system. For example, using the systems shown in figure 5 and 6 iron pyrite nanoclusters are easily formed.

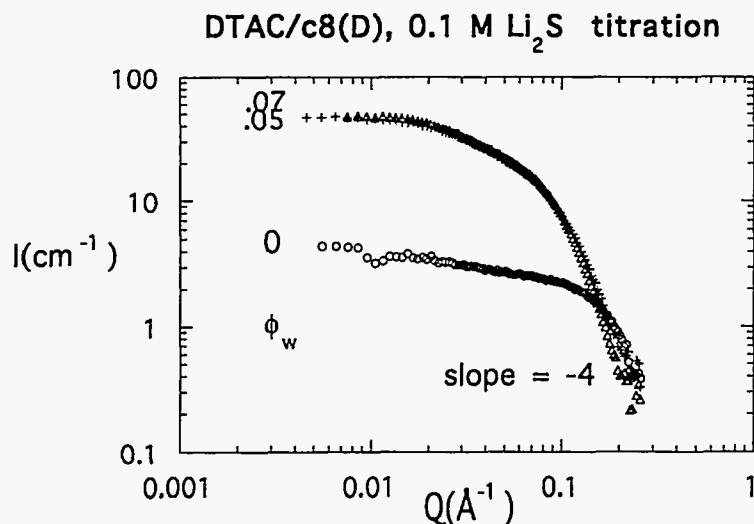


Figure 6. Effect of Li_2S titration on microstructure in the DTAC/hexanol/octane system.

References:

1. Wilcoxon J.P., Baughman R.J., and Williamson, R.L., *Formation of Catalysts in Inverse Micelles*, in Novel Methods for Catalyst Preparation, Symposium S, Proceedings of the Fall Meeting of the Materials Research Society, Boston, MA, Nov, (1990).
2. Wilcoxon, J.P., DOE patent #5,147,841, DOE control #S 70621, entitled "Method for the Preparation of Metal Colloids in Inverse Micelles and Product preferred by the method", issued Sep. 15, 1992.
3. DOE patent disclosure SD-5102 entitled, "Use of Highly Dispersed Materials as Coal Liquefaction Catalysts", submitted Feb 28, 1992, by Paul J. Nigrey, A.P. Sylwester, Jess P. Wilcoxon, Mark J. Hampden-Smith, and Zhibang Duan, assigned number SD-5102, S-75, 545.
4. Wilcoxon J.P., Critical Behavior of an Inverse Micelle System, Phys Rev A, 43, 1857, (1991).

Instrument used: <i>(please type)</i> LQD	Local contact: Dr. R.P. Hjelm, Jr.	Proposal number: <i>(for LANSCE use only)</i> 6044
Title: CHARACTERIZATION OF POLYMER MOLECULES AT INTERFACES BY SMALL-ANGLE NEUTRON SCATTERING		Report received: <i>(for LANSCE use only)</i> 6/20/94
<p>Authors and affiliations:</p> <p>W.C. Forsman and Peter Dreux Department of Chemical Engineering University of Pennsylvania Towne Building 220 S. 33rd Street Philadelphia, PA 19104-6393</p>		
<p>Experiment report:</p> <p>The goal of this experiment was to use small-angle neutron scattering (SANS) to examine the conformation of polymer molecules confined to solid-liquid interfaces in dispersions of finely divided particles. The polymer conformation is characterized by the <i>polymer density profile</i>, $\phi(Z)$, which is the volume fraction of polymer as a function of the distance Z from the surface of the particle.</p> <p>The work reported here is an extension of previous experiments on narrow molecular-weight-distribution poly(n-butyl methacrylate) chains chemically bonded (grafted) by one chain-end to nearly-monodisperse, 2300 Å SiO₂ spheres.</p> <p>In this work, bare SiO₂ spheres (850 Å in diameter) and identical spheres with physically adsorbed block copolymers were dispersed in isopropanol (IPA). The polymers used were di-block copolymers of non-adsorbing poly(n-butyl methacrylate) and adsorbing blocks of poly(dimethyl aminoethyl methacrylate). The adsorbing block might or might-not lie close to the adsorbing surface with the non-adsorbing block being more extended out into the continuum liquid.</p> <p>The polymers are designated [15,40], [10,492] and [200,500] where the first number in the square brackets is the degree of polymerization of the adsorbing block and the second number is the degree of polymerization of the non-adsorbing block. Total molecular weights were 8000, 71400 and 102400 g/mol. In all cases the data could only be successfully modeled by assuming that the polymer density profiles demonstrated a depletion layer. That is, there is very little polymer at the surface, $Z = 0$, and the density profile increases with increasing Z until it reaches a maximum. Indeed, satisfactory agreement between experimental results and model predictions could be obtained by assuming density profiles of the form:</p> $\phi(Z) = \left(\frac{\phi_M}{he^{-1}} \right) Z e^{(-Z/h)} \quad (1)$ <p>where ϕ_M is the maximum volume-fraction of the density profile and h is a measure of the extension of the profile out into the continuum liquid. Detailed results on sample [200,500] are shown graphically below. Comparing experimental results with model predictions is by examining difference scattering, <i>i.e.</i>, difference in scattering cross-section between spheres with adsorbed polymer and bare spheres (all values corrected for solvent scattering and background). Assuming $\phi_M = 0.2$ and $h = 120$ Å gives agreement between experimental difference scattering and model predictions shown in figures 1-3. The three figures give results over various ranges of Q. There is satisfactory agreement over 3 orders of magnitude in difference scattering. The model for the polymer density profile is shown in figure 4.</p>		

Experiment report (continued):

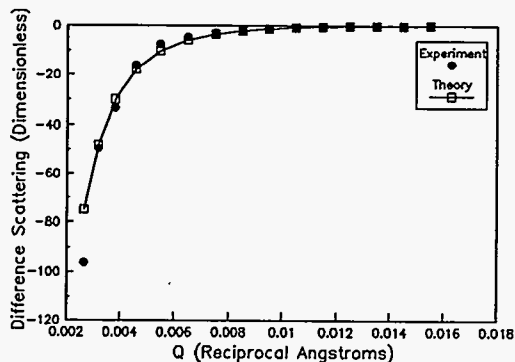


Figure 1. Agreement between theory and experiment for Polymer [200,500] over a low range of Q.

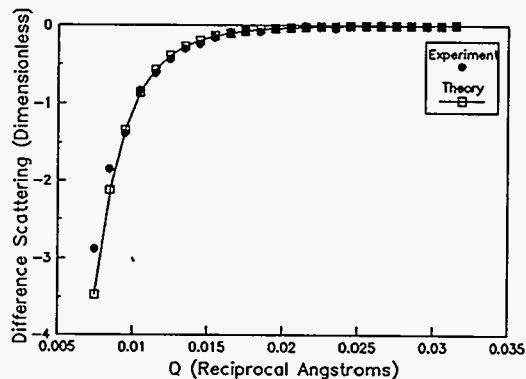


Figure 2. Agreement between theory and experiment for Polymer [200,500] over the mid-range of Q.

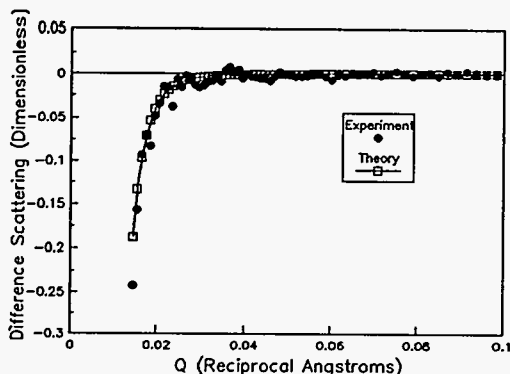


Figure 3. Agreement between theory and experiment for Polymer [200,500] over the high range of Q (tail of the difference scattering).

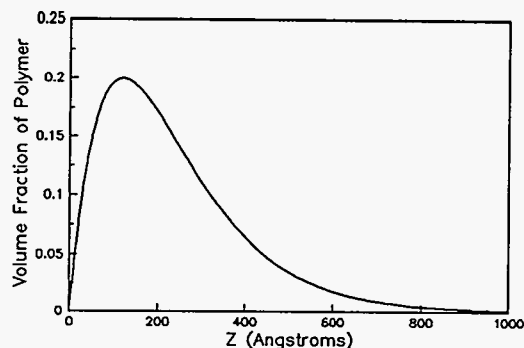


Figure 4. The polymer density profile for Polymer [200,500] according to equation (1) with $\phi_w = 0.2$ and $h = 120 \text{ \AA}$.

This profile gives a surface coverage of 5.5 mg/m^2 and a root-mean-square extension of polymer out into the continuum liquid of 290 \AA . This extension is approximately one-half of the root-mean-square radius of gyration for this polymer in IPA solution, 570 \AA , which was determined by SANS measurements from solution.

Similar results were obtained for the other polymer samples. With the limited number of samples studied, we observed that the amount of polymer adsorbed increases with the ratio of adsorbing to non-adsorbing repeat units, and with increasing overall molecular weight.

The number of cases reported here is limited. But for the examples studied, we conclude that none demonstrated the "parabolic" brush behavior described in the extensive review by Milner⁽¹⁾. Our experimental results were, however, qualitatively in agreement with predictions of Scheutjens and Fleer.⁽²⁾ Curiously, however, our results were also in qualitative agreement with a model for grafted polymer chains under theta conditions that was published 49 years ago.^{(3),(4)}

References:

1. S.T. Milner, *Science* 251, 905 (1991).
2. J.M.H.M. Scheutjens, personal communications.
3. S. Chandrasekhar, *Reviews of Modern Physics*, 15, 1 (1943).
4. A paper showing the relationship between Chandrasekhar's analysis and the polymer density profile of grafted chains has been submitted and is now being revised.

Instrument used: <i>(please type)</i> LQD	Local contact: REX HJELM	Proposal number: <i>(for LANSCE use only)</i> 6060
Title: SANS ON THIN HOMOPOLYMER FILMS		Report received: <i>(for LANSCE use only)</i> 11/7/94
Authors and affiliations: <p style="text-align: center;">T. P. Russell IBM Almaden Research Center, San Jose, California 95120</p>		
Experiment report: <p>Small angle neutron scattering experiments were performed on thin films of polystyrene, PS, to determine the configuration of the polymer molecules confined to a thin film geometry. Experiments were performed on 50/50 mixtures of PS and d-PS, each having a molecular weight of 5.0×10^5. In the bulk, PS molecules of this molecular weight will have a radius of gyration of $\sim 225 \text{ \AA}$. Individual film thickness of 200 \AA were used for this study.</p> <p>Samples were prepared by spin coating a 200 \AA thick film onto the surface of a thin, quartz coverslip. Forty layers of films, each having a thickness of 200 \AA were transferred onto the top of the quartz coated coverslip by floating the film on the surface of de-ionized water and retrieving the film with the coverslip. Four such samples were prepared on coverslips 7.5 cm in length. These were mounted on top of one another with the incident neutron beam impinging on the narrow side of the coverslips. In this geometry a total scattering volume of $3.0 \times 10^{-3} \text{ cm}^3$ was achieved. A typical polymer sample with a diameter of 1 cm and a thickness of 1 mm has a scattering volume of $7.9 \times 10^{-2} \text{ cm}^3$. Consequently, the scattering volume of the thin film samples was only a factor of 25 smaller than the usual specimen. However, the contrast and the concentration were maximized to optimize the possibility of seeing the scattering arising from the individual polymer chains.</p> <p>SANS experiments performed on LQD were ambiguous. While there was ample scattering arising from the polymer chains, there was an additional component to the scattering. This was manifest as a peak in the scattering profile occurring at a spacing of $\sim 200 \text{ \AA}$ which corresponded to the thickness of the individual layers. It is apparent that, during the sample preparation, impurities were entrapped between successive layers giving rise to a periodic variation in the scattering length density. It should be noted that entrapment of hydrogenous impurities would be sufficient to give rise to the observed scattering. Resolving the scattering parallel to the layers was difficult in that the dimensions of the polymer chain are large in that plane and, consequently, the scattering falls off quite rapidly. Therefore, while these particular experiments failed, an improved sample preparation should provide information on the configuration of the entrapped polymer chains. The flux and resolution capabilities of LQD were sufficient for the experiments and the scattering from the polymer chains was resolvable.</p>		

Instrument used: (please type) <p style="text-align: center;">LQD</p>	Local contact: <p style="text-align: center;">REX HJELM</p>	Proposal number: <i>(for LANSCE use only)</i> <p style="text-align: center;">6061</p>
Title: <p style="text-align: center;">LOWER CRITICAL ORDERING OF DIBLOCK COPOLYMERS</p>		Report received: <i>(for LANSCE use only)</i> <p style="text-align: center;">11/7/94</p>
Authors and affiliations: <p style="text-align: center;"> T. P. Russell IBM Almaden Research Center, San Jose, California 95120 A. M. Mayes MIT, Mat. Sci. & Eng., Cambridge, MA 02139 Y. Gallot Institut Charles Sadron, CRM, Strasbourg Cedex, France </p>		
Experiment report: <p>Small angle neutron scattering experiments were performed on symmetric diblock copolymers of perdeuterated polystyrene, d-PS, and poly(n-butylmethacrylate), P(n-BMA), denoted P(d-S-b-nBMA) as a function of temperature under an atmosphere to prevent oxidative degradation. Heating and cooling cycles were used to ensure reproducibility of the results. Copolymers having weight average molecular weights of 2.6×10^4, 6.8×10^4, 9.9×10^4 and 1.7×10^5 were investigated.</p> <p>SANS measurements on the 26K copolymer at 60°C showed a diffuse reflection centered at 0.04 \AA^{-1} corresponding to a spacing of 157 \AA and is characteristic of a diblock copolymer in the phase mixed state. With increasing temperature, the peak intensity in the maximum decreased slightly (up to 80°C) and then increased with increasing temperature up to $\sim 160^\circ\text{C}$.</p> <p>SANS measurements on the 68K copolymer, again showed a diffuse, but intense reflection occurring at 0.018 \AA^{-1} corresponding to a spacing of 347 \AA. As with the 26K copolymer, at 100°C, the 68K copolymer is in the phase mixed state. However, with increasing temperature the peak intensity increased markedly up to 200°C. Increasing temperature further resulted in a flow of the copolymer sample from the sample cell. The increase in the SANS intensity clearly indicates that this copolymer is approaching an ordering transition at elevated temperatures. This is the reverse, from what is ordinarily seen in diblock copolymers where a transition from the disordered state to the ordered state upon cooling occurs. By analogy to the lower critical solution temperature in polymer mixtures, this new transition in diblock copolymers has been called the lower critical ordering transition, LCOT.</p> <p>In an attempt to reduce the transition temperature into an observable range, SANS studies were performed on the 170K P(d-S-b-nBMA). Here an intense reflection was observed at 0.011 \AA^{-1} corresponding to a period of 580 \AA. Higher order reflections indicated that the copolymer was ordered over the entire temperature range studied.</p> <p>Consequently, SANS studies were performed on the 99K copolymer. The SANS results from this copolymer were most unusual. At low temperatures, $\sim 120^\circ\text{C}$, the SANS profile was isotropic and in keeping with the x-ray scattering results. With increasing temperature, the intensity of the scattering increased in keeping with the copolymer undergoing an ordering transition. However, a distinct asymmetry in the scattering pattern emerged which increased with increasing temperature. At</p>		

Experiment report (continued):

temperatures in excess of 130°C, according to the x-ray scattering measurements, the copolymer is ordered. The asymmetry of the scattering pattern suggests that a residual orientation of the copolymer chains remained from the initial film preparation process. The temperature range over which the copolymer is disordered and the time that the copolymer was in the disordered state must not have been sufficient to fully relax the chains. In the ordered state, increasing the temperature causes the copolymers to order more fully, enhancing the anisotropy.

Measurements were also performed on an asymmetric P(d-S-b-nBMA) having 26% d-PS and 74% PnBMA where the total molecular weight of the copolymer was 99K. Here, a distinct reflection was observed at a spacing of 314Å. With increasing temperature, the peak intensity increased and at 180°C a distinct second order reflection was evident. The appearance of the second order reflection clearly shows that the copolymer has undergone a transition from the disordered to ordered state upon heating.

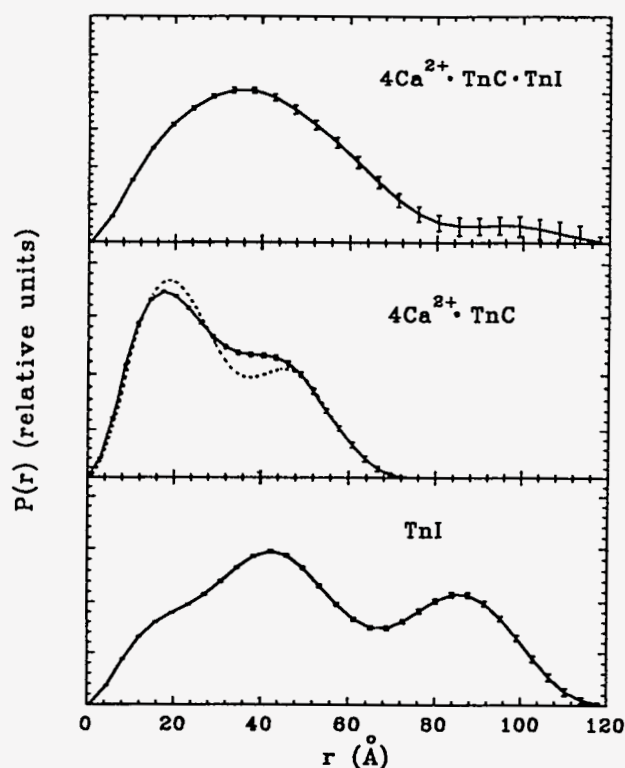
The major finding of the experiments is the confirmation of the LCOT in P(d-S-b-nBMA). However, more quantitative work is necessary to define clearly the transition temperature. This will require the design of a new temperature cell which allows a better control of the temperature and that prohibits the flow of the sample from the cell. Nonetheless, the findings of these experiments were critical in the definite establishment of the LCOT in diblock copolymers and opens another realm in the complex morphological behavior of block copolymers.

References:

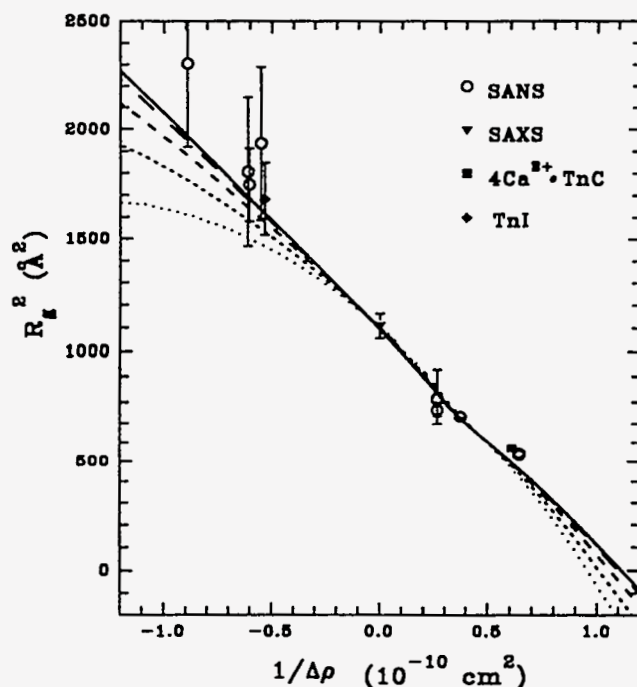
Instrument used: (please type) LQD	Local contact: Philip Seeger	Proposal number: <i>(for LANSCE use only)</i> 6071
Title: Neutron Scattering Studies of the Muscle Protein Complex Troponin C/Troponin I		Report received: <i>(for LANSCE use only)</i> 3/15/94
Authors and affiliations: Glenn A. Olah, Sue Rokop, and Jill Trehwella Chemical Science and Technology Division Spectroscopy and Biochemistry Group Los Alamos National Laboratory		
Experiment report: <p>Muscle contraction is one example of a multitude of diverse biochemical processes regulated by the divalent calcium ion. In the sliding-filament model of muscle action, thin and thick filaments move past each other causing contraction or relaxation. The filaments are composed of proteins. The thin filaments consist of a double stranded helical assembly of actin monomers. Tropomyosin is polymerized head-to-tail in the grooves of the actin helix (one tropomyosin to every 7 actin monomers), and each tropomyosin has one troponin complex bound to it. Troponin consists of three protein molecules: troponin I (TnI), troponin C (TnC), and troponin T (TnT), with molecular weights 24000, 18000, and 37000, respectively. The regulation of muscle contraction is associated with an increase in calcium concentration and is mediated through the TnC component of the troponin complex. When TnC binds calcium, a signal is transmitted via TnI and TnT to the tropomyosin and the interactions of the thick and thin filaments are modulated to give rise to the sliding mechanism. The experiments reported here were aimed at understanding the interactions between TnI and TnC and the nature of the conformational changes that are involved in the transmission of the calcium-induced signal that stimulates muscle contraction.</p> <p>With our beam time allocation in 1993, we completed a full contrast series on deuterated TnC complexed with TnI. Specifically we measured the very weakly scattering sample of this complex in 100% D₂O. By combining these data with data from previous measurements at LANSCE, and with data obtained using the small-angle neutron scattering station NG3 at NIST, we were able to derive the structural parameters for both the TnC and TnI components of the complex and their relative dispositions. The figure below (left) shows the P(r) functions for each component, along with the P(r) function derived from X-ray scattering data for the overall complex. The P(r) for the TnC component is consistent with the crystal structure of that component which shows an extended dumbbell shape with two globular domains connected by an extended helix. Below and to the right is a plot showing the Sturhmann analysis of the radius of gyration data as a function of contrast. This analysis indicates the centers-of-mass of the two</p>		

Experiment report (continued):

components are approximately coincident and the TnI is more toward the outside of the complex than the TnC. With the structural constraints placed on the complex and its components by the scattering data, plus known physical parameters such as the volume of the complex, we have derived a three dimensional model of the complex describing the molecular boundaries and relative dispositions of the two components. This model provides new insights into the molecular basis for the calcium-sensitive switch that regulates muscle contraction. We are currently refining this model for publication.



Solid lines indicate the vector distribution functions, $P(r)$, derived from the scattering data. The dotted line indicates the crystal structure $P(r)$ calculated for TnC



The solid line is the straight line fit of the data (i.e. 0 Å separation of the centers of mass for each component). The dashed lines are fits with increasing curvature expected for 5, 10, 15, 20 Å separations, respectively.

References:

- (1) Heidorn, D.B., & Trewhella, J. *Biochemistry* 27, 909 (1988).
- (2) Trewhella, J., Liddle, W. K., Heidorn, D. B., & Strynadka, N. *Biochemistry* 28, 1294 (1989)
- (3) Heidorn, D.B., Seeger, P.A., Rokop, S.E., Means, A.R., Crespi, H., & Trewhella, J. *Biochemistry* 28, 6757 (1989).
- (4) Trewhella, J., Blumenthal, D.K., Rokop, S.E., & Seeger, P.A. *Biochemistry* 29, 9316 (1990)
- (5) Blechner, S. L., Strynadka, N. C. J., Olah, G. A., and Trewhella, J. *Biochemistry* 31 11326, (1993).

Instrument used: <i>(please type)</i> LQD	Local contact: Rex Hjelm	Proposal number: <i>(for LANSCE use only)</i> 6074
Title: Structure of LCP-LCT Composites		Report received: <i>(for LANSCE use only)</i> 11/10/94
Authors and affiliations: Rex P. Hjelm, LANSCE Brian C. Benicewicz, MST-7 Elliot P. Douglas, MST-7		
Experiment report: <p>INTRODUCTION: Our understanding of the phase behavior and structure of solutions of long and short rigid rodlike molecules in a quasispherical solvent comes largely from the work of Abe and Flory [1] who described these systems in terms of interactions between rodlike molecules governed totally by excluded-volume effects. A complex phase behavior is predicted by this theory. According to this description (Fig. 1) at low solute concentrations an isotropic solution is formed. At sufficiently high volume fraction a biphasic results, consisting of an anisotropic (nematic) phase rich in long rods and an isotropic phase rich in short rods. This effect is driven by the entropy of packing the long rods.</p> <p>In real systems, however, the polymers are better described as semirigid rods [2] and there are often attractive interactions between the solute molecules and between the solvent and solute. Thus the question arises as to how the phase behavior and solution structure of real systems might correspond to the theoretical predictions.</p> <p>We have become interested in this problem as a result of our recent work on the realization of molecular composites [3]. These materials are predicted to have greatly enhanced mechanical properties [4], but there is presently little information to validate this notion. Approaches to produce stable molecular composites are limited by immiscibility between the reinforcement and matrix components [5]. To circumvent this problem, we proposed using liquid-crystal polymers (LCP) as the reinforcing component, with structurally similar liquid-crystal thermosets as the matrix. The two components should have better miscibility than systems used in earlier work [5] and therefore should approach the ideal molecularly-dispersed state more readily. Our initial studies on birefringent films [3] indicated by the open circle in the mixed nematic part of the phase map showed enhanced miscibility, as indicated by weak segregation of components into two randomly interpenetrating phases having a characteristic size of 8 nm [3]. These appeared to be equilibrium structure, as they did not change with extensive annealing of the films. A comparison of theoretical predictions with the experimental behavior of these systems as they are processed by drying from solution is important in developing concepts for the nanoscale engineering of these systems.</p> <p>In this work, we study the solution structure in N-methyl-2-pyrrolidinone (NMP) of the deuterated polyamide LCP, poly(p-phenylene-2-nitroterephthalamide) alone and in mixtures with any one of three liquid-crystal thermosets by small-angle neutron scattering (SANS). The use of SANS allows study of nanostructure over length scales from 1 to 50 nm. The solution compositions studied should form isotropic solutions according to the theories for rigid [1] and semiflexible [2] hard core-interacting rods.</p> <p>EXPERIMENTAL: The deuterated LCP and the three thermosets used in this study were prepared as previously described [3,6]. Solutions of LCP in NMP were prepared at different concentrations (expressed as (grams of LCP)/(100 ml NMP) = w/v %) of 3, 5 and 9 w/v%, and contained 100/0, 80/20, and 60/40 w/w% LCP/LCT. All measurements were done at room temperature (22° C). Scattering data were reduced to differential scattering crosssection per gram of LCP, $I(Q)$, ($m^2 g^{-1}$), as a function of momentum transfer, $Q = 4\pi/\lambda \sin \theta$, where 2θ is the scattering angle and λ is the neutron wavelength. The methods of data reduction for LQD are outlined elsewhere [8,9].</p> <p>RESULTS: The solutions of LCP in NMP and the ternary mixtures of LCP, LCT and NMP were yellow for the 3 w/v% LCP mixtures to light brown for the 5 w/v% LCP mixtures to dark brown for the 9 w/v% LCP mixtures. There was no sign of turbidity in the samples. All samples were observed to be isotropic by polarized optical microscopy. The 3 w/v% samples were viscous. Viscosity increased with increasing concentration. The 9 w/v% solutions were highly viscous and could not be poured.</p> <p>The 9 w/v% solution of LCP scattering intensity follows $I \propto Q^{-4}$. All mixtures containing 9 w/v% LCP with the different LCT's in 80/20 and 60/40 w/w% proportions show the same basic shape of the scattering curve with $I \propto Q^{-4}$ for $Q < 0.1 \text{ nm}^{-1}$ (Fig. 1). This Porod law scattering is indicative of domain-like structure. The main source of contrast in these solutions is from the deuterated LCP; thus the domains correspond to LCP-rich and -depleted microphases. The characteristic size of the domains is too large to be resolved with available SANS instrumentation ($> 50 \text{ nm}$), but too small to be observed in the polarized optical microscope.</p> <p>The 5 w/v% solution of LCP shows the same steep decline, $I \propto Q^{-4}$, for $Q < 0.15 \text{ nm}^{-1}$ (Fig. 2) as the 9 w/v% LCP solutions. The 5 w/v% LCP-LCT solutions on the other hand show very different behavior. In all but one of the measured ternary mixtures the scattering intensity goes as Q^{-1} for $Q < 0.4 \text{ nm}^{-1}$, as illustrated for two of these in Fig. 2,</p>		

Experiment report (continued):

suggesting a low-dimensional, filamentous structure. An exception is the 80/20 w/w% mixture with LCT II (Fig. 2). In this case the scattering for $Q < 0.2 \text{ nm}^{-1}$ goes approximately as Q^{-2} .

The 3 w/v% LCP solution shows significantly different scattering from the more concentrated solutions in that the low Q scattering shows Q^{-3} dependence (Fig. 3), which suggests some breakup of the domain-like organization into smaller, perhaps rougher-surfaced structures. The 3 w/v% LCP mixtures with LCT (Fig. 5) show scattering that is identical to that observed with the majority of the 5 w/v% LCP/LCT solutions for $Q > 0.05 \text{ nm}^{-1}$ (Fig. 2). However, there is a crossover to a Q^{-3} dependence at lower Q (Fig. 3) that could have been missed in the measurements of the 5 w/v% solutions, which accessed only for $Q > 0.05 \text{ nm}^{-1}$ (Fig. 2). The very low- Q scattering measured from the 3 w/v% LCP/LCT solutions suggests that the structure seen in the 3 w/v% LCP solutions (Fig. 5) is still present.

DISCUSSION: The presence of LCT in NMP solutions with LCP breaks up the domain-like structure inherent in the LCP solutions when the solute concentration is low. The region of the phase map explored by these measurements lies in the isotropic phase, according to the prediction of rigid rod [1] and semiflexible rod [2] theory. These theories, as well as the interpretation of the phase behavior of rigid-rod/flexible coil matrix blends [4], emphasizes the importance of entropic effects in the organization of the rods. Our results show [10,11] that the situation is more complex for systems involving a semiflexible, associating liquid-crystal polymer and rodlike short molecule than suggested by theories [1,2] that do not include the enthalpy of interaction between each of the components.

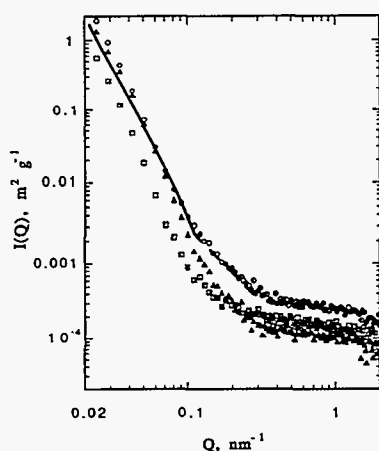


Fig. 1

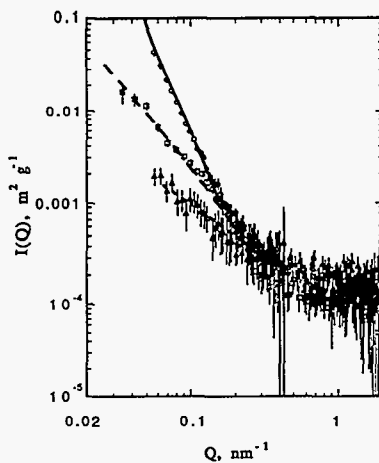


Fig. 2

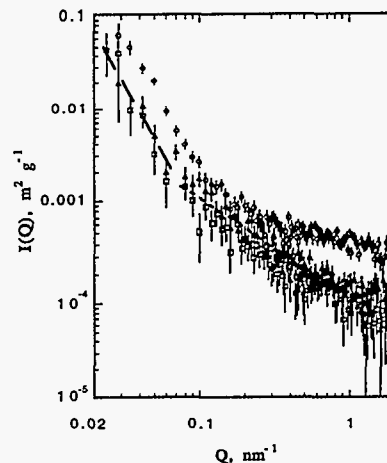


Fig. 3

Fig. 1. Small-angle neutron scattering from 9 w/v% LCP and LCP-LCT solutions in NMP. \circ , LCP only; \square , LCP with LCT, 80/20 w/w% LCP/LCT; Δ , LCP with LCT, 60/40 w/w% LCP/LCT. Lines indicate scattering law behavior: —, Q^{-4} ; - - -, Q^{-2} .

Fig. 2. Small-angle neutron scattering from 5 w/v% LCP and LCP-LCT solutions in NMP. Symbols are the same as for Fig. 1. Lines indicate scattering law behavior: —, Q^{-4} ; - - -, Q^{-2} ; ····, Q^{-1} .

Fig. 3. Small-angle neutron scattering from 3 w/v% LCP and LCP-LCT solutions in NMP. Symbols are the same as for Fig. 1. Lines indicate scattering law behavior: - - -, Q^{-3} ; ····, Q^{-1} .

References:

1. A. Abe and P.J. Flory, *Macromolecules* 11: 1122 (1978).
2. T. Sato, T. Shoda, and A. Teramoto, *Macromolecules* 27: 164 (1994).
3. B.C. Benicewicz, E.P. Douglas, and R.P. Hjelm, in *Liquid Crystalline Polymers*, C. Carfagna, ed., (Pergamon, New York, 1994), p. 87.
4. W.-F. Hwang, D.R. Wiff, C.L. Benner, and T.E. Helminiak, *J. Macromol. Sci. - Phys.* B22(2): 231 (1983).
5. G.T. Pawlikowski, D. Dutta, and R.A. Weiss, *Annu. Rev. Mater. Sci.* 21: 159 (1991).
6. A.E. Hoyt and B.C. Benicewicz, *J. Polymer Sci.* A28: 3403 (1990).
7. P.A. Seeger, R.P. Hjelm, and M. Nutter, *Mol. Cryst. Liq. Cryst.* 180A: 101 (1990).
8. R.P. Hjelm, *J. Appl. Cryst.* 21: 618 (1988).
9. P.A. Seeger, and R.P. Hjelm, *J. Appl. Cryst.* 24: 467 (1991).
10. R.P. Hjelm, E.P. Douglas, and B.C. Benicewicz, *Polym. Mat. Sci. Eng.*, 71, 287 (1994).
11. R.P. Hjelm, E.P. Douglas, and B.C. Benicewicz, *Inter. J. Thermophys.* (in press).

Instrument used: (please type) LQD	Local contact: Rex P. Hjelm	Proposal number: <i>(for LANSCE use only)</i> 6075
Title: Study of Aqueous Biphasic Systems under Dynamic Conditions		Report received: <i>(for LANSCE use only)</i> 6/20/94
Authors and affiliations: <p>P. Thiyagarajan¹, D. J. Chaiko² and R. P. Hjelm. Jr.³</p> <p>¹Intense Pulsed Neutron Source and ²Chemical Technology Divisions Argonne National Laboratory, Argonne, IL 60439. USA.</p> <p>³LANSCE, Physics Division, Los Alamos National Laboratory, Los Alamos, NM 87545, USA.</p>		
Experiment report: <p>Aqueous biphasic systems are heterogeneous liquid/liquid systems that result from appropriate combinations of inorganic salts and water-soluble polymers such as polyethylene glycol (PEG). These solvent extraction systems have received considerable attention for biotechnology related separations. We have been developing aqueous biphasic systems for use in separating dissolved metal ions and colloid sized particulates. Because aqueous biphasic systems are inexpensive, nontoxic, and are capable of highly selective separations, they are currently being examined for applications in waste treatment and environmental remediation (1-3)</p> <p>It is known that salts containing anions such as PO_4^{3-} are more effective at promoting biphasic formation than salts containing divalent anions like SO_4^{2-}, which in turn are more effective than monovalent anions like OH^-. However, multivalent cations tend to interact strongly with the ether oxygens of PEG and thus "salt in" rather than "salt out" the PEG. In general, ethoxylated polymers exhibit an inverse solubility relationship with temperature.</p> <p>During measurements of phase diagrams, we noticed that small shifts in the binodal curve occurred with time after vigorous mixing of the two phase system. We have also observed that partition equilibrium for low molecular weight solutes takes longer to attain as the biphasic system is mixed more vigorously. In addition, during the extraction of certain metal complexes from the salt phase into the PEG phase, we have found that the partition coefficient increases from zero at $t=0$ to well over 100 at $t=30-60$s. However, the partition coefficients then begin to decrease if the mixing time is extended beyond 60s. All of these observations suggest that shear forces can lead to changes in the PEG aggregate size/shape and that the return to thermodynamic equilibrium is slow.</p> <p>In order to understand the nature of the partition coefficient inequilibrium exhibited by PEG-3400 upon vigorous shaking we conducted SANS studies on PEG solutions under shear <i>in situ</i>. Three cases were studied, 10 PEG in the nonbiphasic forming NaCl solution, PEG in Na_2CO_3 solution under conditions in which they are in rod-like aggregate and the biphasic system. The first sample has formed large 3-dimensional aggregate upon shearing the PEG solution at 35 rps. The large aggregates might have formed through entanglements between the PEG molecules whose tertiary structure may be similar to that of the monomer as the high q</p>		

Experiment report (continued):

regions of SANS data for the monomeric PEG and the aggregate match reasonably well, but the low q region of the sheared sample shows a power law behavior with a slope of -3.0 (Fig. 1). The rod-like PEG aggregate in Na_2CO_3 aggregated further into much thicker and longer rods upon shearing the sample and they do not become smaller rods upon releasing of the shear forces (Fig. 2). Their lengths seem to be changing under different shearing conditions as seen from the variation in intensity of the low q regions signal under different shear rates (Fig. 3). The biphasic system got mixed upon shearing into a white dispersion and the scattering signal was an order of magnitude larger than those for the other two cases. These systems are very large colloids which become dispersed into the salt solution and thus we are seeing the scattering from their surfaces (log-log slope $= -3.83$). Comparison of the data in the whole q region suggests that the tertiary structure of PEG might be changing under these three conditions as evidenced by the completely different shapes of the SANS curves through out the q region (Fig.4).

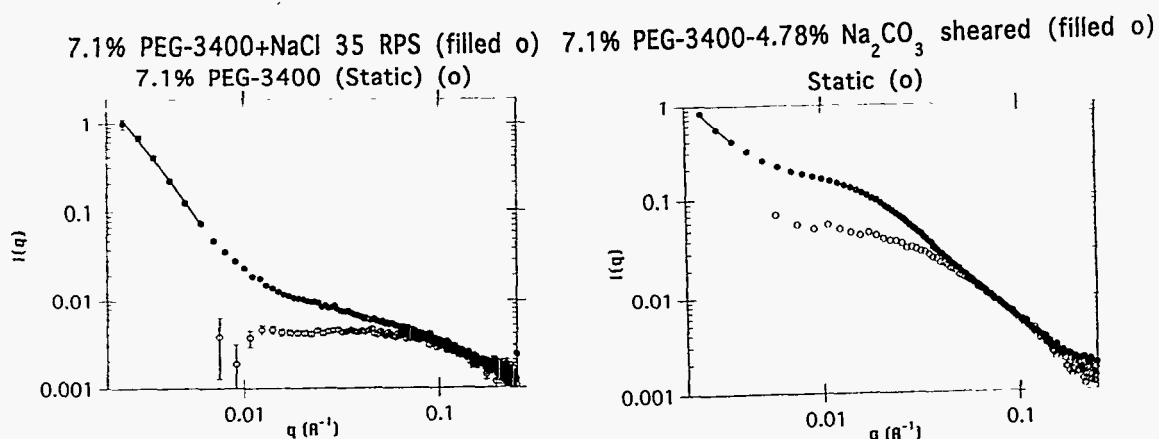
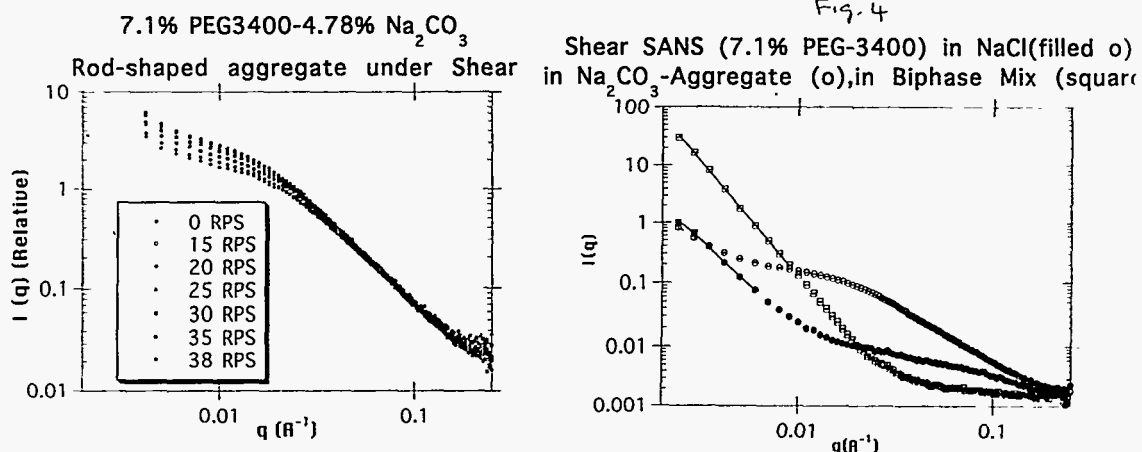


Fig. 3

Fig. 4



References:

- 1) D. J. Chaiko-1989 et al., Development of a Process for Treating Red Water by Organic/Inorganic Separation and Biodegradation," in Proceedings 14th Annual Army Environmental R&D Symposium, USATHAMA Report CETHA-TE-TR-90055, p. 303 (1989).
- 2) D. J. Chaiko, R. Mensah-Biney, C. J. Mertz, and A. N. Rollins, Actinide Recovery Using Aqueous Biphasic Extraction: Initial Developmental Studies, ANL-92/36 (1992).
- 3) D. J. Chaiko, R. Mensah-Biney, C. J. Mertz, and A. N. Rollins, Sep. Sci. Technol. **28**, 765 (1993).

Instrument used: <i>(please type)</i> LQD	Local contact: Rex P. Hjelm	Proposal number: <i>(for LANSCE use only)</i> 6097
Title: Trial Experiment for Time-of-Flight Protein Crystallography		Report received: <i>(for LANSCE use only)</i> 12/8/94
Authors and affiliations: Benno Schoenborn, LS-2		
Experiment report: <p>A trial experiment using the SANS spectrometer was carried out to test the feasibility of TOF measurements on proteins. It was planned to collect data for a very low resolution map contrasting an H₂O vs a D₂O myoglobin crystal.</p> <p>It was planned to use the difference between the H₂O and the D₂O reflections to phase a low resolution neutron map using a search function based on the known x-ray structure. Such an approach should provide improved phases for the low resolution data and will serve to initiate a solvent refinement to calculate the solvent density used in subsequent crystallographic refinements.</p> <p>The design parameters for the SANS station are far from ideal but trial calculations showed that it should be possible to collect the low order reflections needed for the solvent refinement.</p> <p>A large (27mm³) crystal was mounted and exposed for 15 minutes per position, with crystal rotations of 10°. Inspection of the data showed some large ill-defined peaks with a very nonlinear background. Subsequent tests showed a detector resolution larger than 5mm--with such a resolution single peaks cannot be resolved. The uneven detector response suggested degradation of the 2D counter by previous overexposure to gammas and neutrons. It is planned to repeat this experiment with longer beam time and a high resolution detector.</p>		

Instrument used: <i>(please type)</i> LQD	Local contact: Philip A. Seeger	Proposal number: <i>(for LANSCE use only)</i> 6099								
Title: Alumina Gel Structures by SANS		Report received: <i>(for LANSCE use only)</i>								
Authors and affiliations: <table border="0" style="width: 100%;"> <tr> <td style="width: 30%;">David S. Phillips</td> <td style="width: 30%;">LANL MST-4 MS G771</td> <td style="width: 15%;">USA</td> <td style="width: 25%;">7-5128</td> </tr> <tr> <td>Philip A. Seeger</td> <td>LANL LANSCE MS D408</td> <td>USA</td> <td>7-8843</td> </tr> </table>			David S. Phillips	LANL MST-4 MS G771	USA	7-5128	Philip A. Seeger	LANL LANSCE MS D408	USA	7-8843
David S. Phillips	LANL MST-4 MS G771	USA	7-5128							
Philip A. Seeger	LANL LANSCE MS D408	USA	7-8843							
Experiment report: <p>The objective of this experiment was to understand better the structural development during the peptization of alumina sols prepared by the Yoldas (1975) technique. It is part of a longer-term plan to understand the evolution of particle size and morphology through the individual stages of hydrolysis, peptization, and drying which are roughly separable in alumina-based sol/gel technology. The behavior of alumina gels is drastically different from the better-understood silicates particularly in this peptization step, which involves the acid digestion of the crystalline precipitate resulting from an initial rapid hydrolysis.</p> <p>Three groups of alumina sol samples were prepared using derivatives of the Yoldas (1975) technique designed to improve peptization kinetics. These included one sample aged in light water with the recommended 0.07 mole HNO₃ per mole AlOOH (AX23), one aged with 0.15 mole acid (AX22), and a sample both hydrolyzed and peptized with D₂O in order to reduce the background in its scattering profile. All samples were aged in sealed flasks in a 90 C convection oven for times between 0 and 328 hours. The deuterated sample yielded a coarse non-dispersible solid on initial hydration which did not digest perceptibly; it was not suitable for further study. Samples from both light-water peptizations were extracted at various ageing times, transferred to 1 mm suprasil cuvettes, and their SANS spectra measured in LQD.</p> <p>Scattering results show three features of interest (Figure 1). First, all show a "Porod" slope of roughly 2, indicating that the scatterers are fibrous and "infinitely" long. Second, the radii of the fibers decrease with increasing digestion time, confirming that the received treatment is effective. Third, the "expedited" high-acid samples seem coarser at 168 hours than the "by-the-book" low-acid ones, though this conclusion is compromised by an unusual "peak" (rather than shoulder) introduced into their low-Q profiles by long-range interfiber correlations.</p>										

Experiment report (continued):

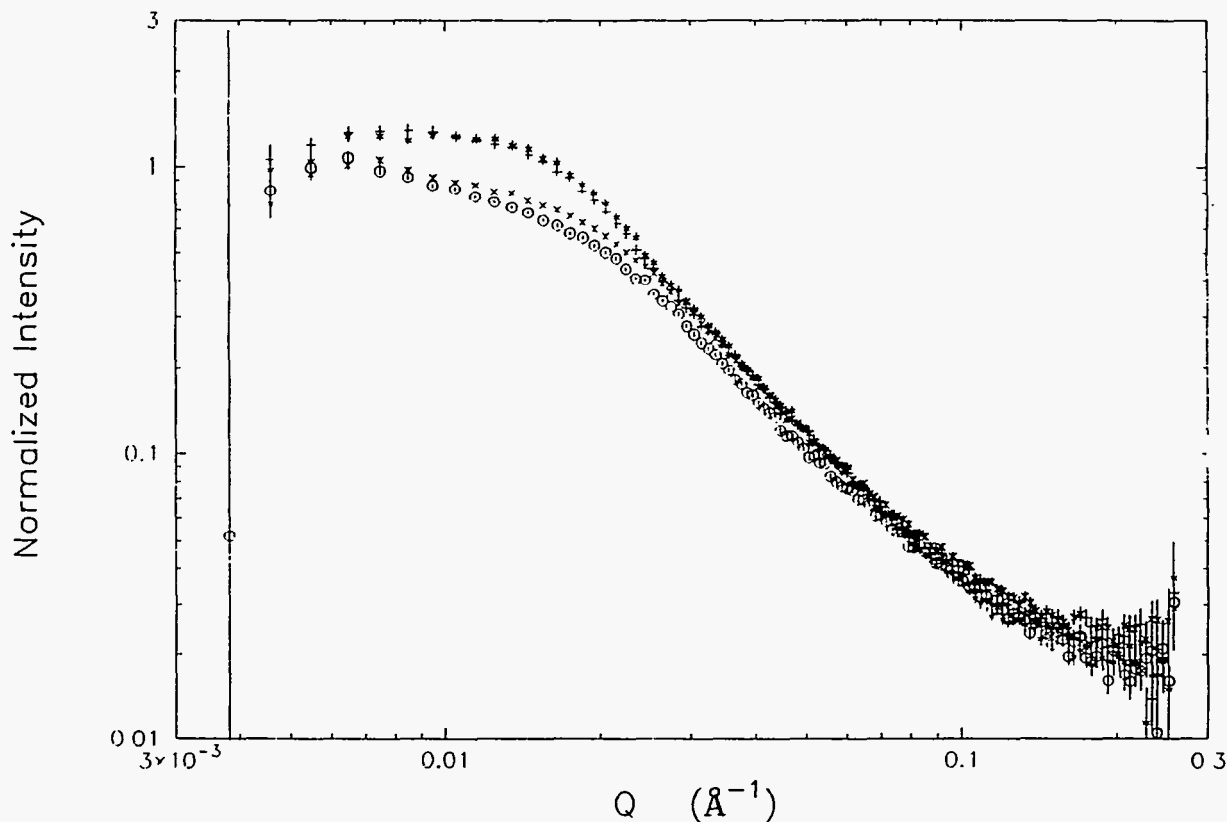
Alumina Gels — H₂O

+ AX22/168

* AX22/326

o AX23/28

x AX23/169



Moreover, this information is *pragmatically useful* in improving our processing of finer sols! Fibrous alumina gel structures were long ago reported for several other preparation routes (reviewed by Gitzen, 1970), but the Yoldas recipe has been believed to form platelets. The difference makes a difference, especially in understanding the low solid contents normally observed at the gel points of these systems. Furthermore, these results do not suggest that this feature can be readily changed by adjustment of peptization conditions. Second, the information that the mean fiber radius decreases with ageing time tells us that none of these samples is overaged, even at 328 hours, even with expediting additions of excess acid. Several previous efforts to refine these sols have ended too soon, not too late. We have characterized several of these samples in parallel by measuring capillary condensation in nitrogen adsorption isotherms and by direct observation in TEM, both of which confirm the results of this SANS study.

References:

Bulent E. Yoldas, *Bull. Am. Cer. Soc.* 54, 286 (1975).

Walter H. Gitzen, *Alumina as a Ceramic Material*, Columbus, Ohio: American Ceramic Society (1970).

Instrument used: <i>(please type)</i> <p style="text-align: center;">LQD</p>	Local contact: <p style="text-align: center;">Rex P. Hjelm</p>	Proposal number: <i>(for LANSCE use only)</i> <p style="text-align: center;">6103</p>										
Title: <p style="text-align: center;">Neutron scattering studies on N-terminal Trypsin Trimmed Nucleosome Core Particles.</p>		Report received: <i>(for LANSCE use only)</i> <p style="text-align: center;">4/13/94</p>										
Authors and affiliations: <p>Brian S. Imai. Life Sciences Division, LS-2 Mail Stop M880, Los Alamos National Laboratory, Los Alamos, NM 87545.</p> <p>Rex P. Hjelm. Manuel Lujan Neutron Scattering Center, Los Alamos National Laboratory, Los Alamos, NM 87545.</p> <p>E. Morton Bradbury. Life Sciences Division, LS-2 Mail Stop M880, Los Alamos National Laboratory, Los Alamos, NM 87545.</p> <p>Peter M. Yau. Department of Medical Biological Chemistry, MSI-A, University of California, Davis, CA 95616.</p> <p>John P. Baldwin. Physics Division, School of Information Science and Technology, Liverpool Polytechnic, Byrom Street, Liverpool L33AF, U.K.</p>												
Experiment report: <p>Background. The nucleosome core particle is the fundamental repeating unit of the eukaryotic chromosome, and is composed of 1.75 left-handed superhelical turns of DNA wrapped around a histone protein core (an octamer of two each of H2A, H2B, H3 and H4). The histones are subject to reversible N-acetylation of specific lysine residues in their N-terminal regions. This acetylation has long been associated with transcriptional activity and has been the subject of intense investigation from both a structural and functional perspective. The possible interactions of the positively charged histone N-termini with DNA both within and outside the core particle have also been the subject of a great deal of conjecture.</p> <p>In order to resolve some of these questions, many structural studies have been performed on isolated core particles. The dimensions of the disc shaped core particle have been determined to be roughly 110 Å in diameter by 55 Å in height by both solution scattering and crystallography. However, a significant discrepancy exists between the calculated R_G of 29.7 Å for the histone octamer in the crystal structure (1) and the measured R_G of 33-35 Å determined by neutron solution scattering (2). This discrepancy has been ascribed to the inability of crystallography to resolve the mobile, apparently randomly organized, N-terminal tails of the histones. Roughly 20% of the amino acid residues of the histones are found in the mobile tails and this additional mass was thought to account for the difference in the R_G values.</p> <p>The histone N-terminal tails can be selectively removed through limited trypsinization of intact core particles. This does not cause a significant change in the stability of the core particle or the incorporated histone octamer, but does cause a loss of protein mass corresponding to the missing mass in the core particle crystal structure. A neutron and x-ray solution scattering study done on isolated trypsinized histone octamers gave an R_G of 29.8 Å (3) which agreed well with the crystal structure calculated R_G of 29.7 Å. A neutron scattering contrast series experiment was undertaken at LQD on trypsinized nucleosome core particles in order to determine the effect of trypsinization on the intact core particle.</p> <table border="1" data-bbox="194 1640 789 1923"> <thead> <tr> <th>D₂O Concentration (% vol.)</th> <th>Radius of Gyration, R_G (Å)</th> </tr> </thead> <tbody> <tr> <td>0</td> <td>40.5</td> </tr> <tr> <td>25</td> <td>37.1</td> </tr> <tr> <td>63</td> <td>30.2</td> </tr> <tr> <td>100</td> <td>37.1</td> </tr> </tbody> </table> <p>Results. Scattering curves were obtained at 0, 25, 63 and 100% D₂O solvent compositions. R_G values were</p>			D ₂ O Concentration (% vol.)	Radius of Gyration, R_G (Å)	0	40.5	25	37.1	63	30.2	100	37.1
D ₂ O Concentration (% vol.)	Radius of Gyration, R_G (Å)											
0	40.5											
25	37.1											
63	30.2											
100	37.1											

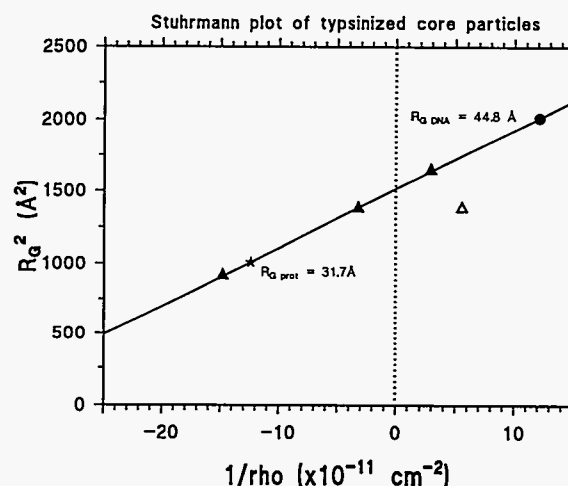
Experiment report (continued):

obtained by Guinier analysis of the resulting scattering curves. These values are summarized in the table.

The figure below shows these points plotted on a Stuhrmann plot. The 25% point (open triangle) did not appear to be in the linear portion of the plot and was not included in the regression analysis. The star and circle correspond to the theoretical DNA (65%) and protein (40%) match points and give R_G values for the protein and DNA components of 31.7 Å and 44.8 Å, respectively. The radius of gyration at infinite contrast is calculated to be 38.94 Å.

Conclusions. The R_G of 31.7 Å determined for the trypsinized histone octamer component of the core particle is significantly smaller than the R_G previously determined for intact core particle octamers of 33-35 Å. This is in accord with the idea that the loss of the tails leaves only the smaller, globular histone octamer core. Interestingly, this value is somewhat larger than the value of 29.8 Å previously obtained for the isolated trypsinized histone octamer and 29.7 Å obtained for the crystal structure. This may indicate that there may be some adjustment in the core particle structure which occurs upon the loss of the histone tails. This may also be reflected in the smaller value obtained for the R_G of the DNA component of 44.8 Å compared to 47-49 Å previously determined for intact core particles. The radius of gyration at infinite contrast is within the values previously determined of 39-41 Å.

Trypsinization of the N-terminal histone tails is often considered to mimic the effects of histone acetylation. Acetylation of the lysine *epsilon*-amino group results in a loss of a positive charge and this is presumed to reduce the interactions between the tails and the DNA, potentially affecting the structure of the nucleosome. While trypsinization also eliminates these interactions, all other potential interactions of the tails with DNA, including interactions of positively charged arginine residues are also eliminated. These results support the argument that trypsinization may have effects beyond simple positive charge elimination.



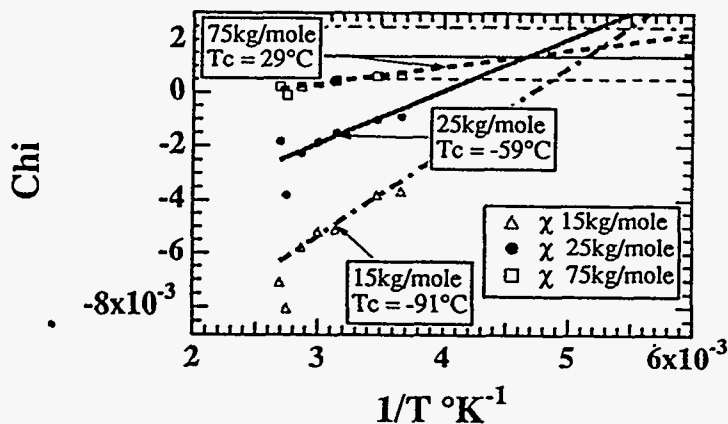
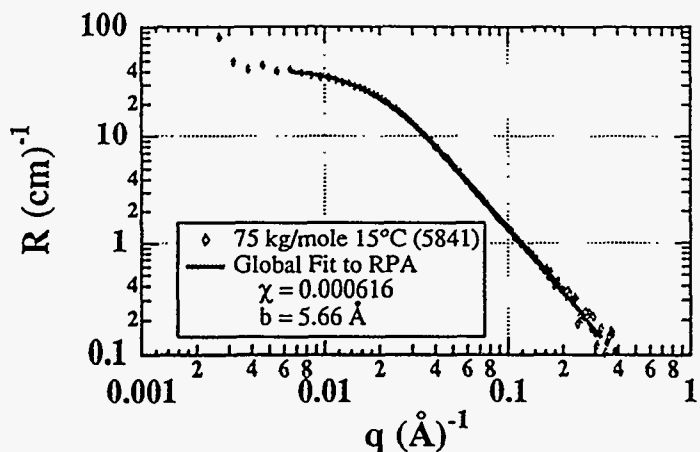
References:

1. Richmond, TJ, Finch, JT, Rushton, B, Rhodes, D and Klug, A (1984) *Nature* **311**, 532-537.
2. Imai, BS, Yau, P, Baldwin JP, Ibel, K, May RP and Bradbury, EM (1986) *J Biol Chem* **261**, 8784-8792.
3. Wood, MJ, Yau, P, Imai BS, Goldberg, MW, Lambert, SJ, Fowler, AG, Baldwin, JP, Godfrey, JE, Moudrianakis, EN, Koch, MHJ, Ibel, K, May, RP, and Bradbury, EM. (1991) *J Biol Chem* **266** 5696-5702.

Instrument used: <i>(please type)</i> LQD	Local contact: Rex Hjelm/Phil Seeger	Proposal number: <i>(for LANSCE use only)</i> 6108
Title: Symmetric Isotopic Blends of PDMS.		Report received: <i>(for LANSCE use only)</i> 11/9/94
<p>Authors and affiliations:</p> <p>G. Beaucage, Department of Materials Science and Engineering University of Cincinnati, Cincinnati, OH.</p> <p>M. Kent, Group 1815, Sandia National Laboratories, Albuquerque, NM.</p>		
<p>Experiment report: This experiment was aimed at determining thermodynamic parameters that describe the miscibility of symmetric, isotopic blends of PDMS, Poly(dimethylsiloxane). A comprehensive study of miscibility in these blends has not been reported. Lapp, Picot and Benoit¹ determined the interaction parameter for d-PDMS/PDMS (267/14.6kg/mole) at room temperature using a radius of gyration approach for the analysis of SANS data (extrapolation to zero concentration d-PDMS). The interaction parameter was calculated to be 1.7×10^{-3} at room temperature. Using $\chi_n = 2$ at the critical point Lapp predicts that phase separated blends will occur at room temperature for symmetric blends of about 100 kg/mole. This is very close to our experimental results discussed below. In this work the random phase approximation approach, RPA, was used to determine the interaction parameter directly from scattering data. All blends were composed of equal volumes of the two isotopic components. Molecular weights within a blend pair were closely matched. The nominal molecular weights were 15 kg/mole, 25 kg/mole, 75 kg/mole and 300 kg/mole. The 300 kg/mole blend appears to be phase separated at all accessible temperatures. This is deduced by the inability of the RPA equation to describe scattering data from this blend under the assumption of a single phase. We have obtained direct evidence of phase separation in the 15 and 25 kg/mole samples in measurements done at NIST using a cryostat to achieve very low temperatures.</p> <p>Generally, the RPA equation is used only at low-q since it is difficult to obtain good fits over a wide range of q and because the thermodynamic parameter of interest is a global parameter that can best be measured at the largest accessible sizes or the lowest-q. LANSCE data has the added advantage that a wide span of q is collected. Given that this is an extremely ideal blend system, it was hoped to fit the LANSCE data globally using the RPA equation to understand issues related to the limits of the applicability of the RPA approach. The RPA approach requires a knowledge of the scaling behavior that relates the radius of gyration of a polymer coil to the molecular weight. Using a Gaussian model for the chains R_g is related to the degree of polymerization, n by, $R_g^2 = n b^2/6$, where b is a scaling factor called the statistical segment length. This scaling factor can be obtained using rheology or light scattering. A value for b of 5.61 Å can be obtained from data presented in the Polymer Handbook, 3rd edition, VII/44 [2, 3]. We found that this value was appropriate in some cases for global fitting of the PDMS blends, particularly for the 75kg/mole blends close to room temperature. For the remaining blends there appear to be a shift in b with temperature and with molecular weight of the blends. We therefore used b as a fitting parameter to globally fit the entire data set. The</p>		

interaction parameter, χ was the second fitting parameter. Monotonic dependencies in temperature were observed for both parameters with b always showing a value larger than the expected value of 5.61. This dependency may be due to end-group effects in the blends at lower molecular weights or may account for expansion of the coils at high temperatures.

A typical global fit to the RPA equation over a wide range of q is shown below. "R" is the Rayleigh ratio or absolute intensity and "q" is the scattering vector. Values obtained in this way for χ and calculated for χ_{critical} are plotted against $1/T$ below. The horizontal lines are calculated values for the critical χ . Linear fits to the measured values are shown and the estimated critical temperature is shown. Negative values for χ may be due to end-group effects in the low molecular weight samples. The temperature dependence of χ indicates UCST behavior.



References:

1. A. Lapp, C. Picot and H. Benoit, *Macromolecules*, **18**, 2437 (1985).
2. G.V. Schultz, A. Haug, *Z. Phys. Chem. (Frankfurt)*, **34**, 328 (1962).
3. Also see A. Lapp, C. Strazielle, *Makromol. Chem., Rapid Commun.*, **6**, 591 (1985).

Instrument Used: LQD	Local Contact: Rex Hjelm	Proposal Number: <i>(for LANSCE Use Only)</i> 6403
Title: Beta-Layering		Report received: <i>(for LANSCE Use Only)</i> 3/15/94
Authors and affiliations: James K. Hoffer and Robert J. Candler, MTL-10		
Experiment report: <h3>Introduction</h3> <p>Beta-layering is an effect whereby solid tritium, or a solid deuterium-tritium (D-T) mixture, automatically redistributes itself into a uniform layer on the inside of the container walls¹. The driving force is the self-heating due to beta-decay of tritium into ³He . The redistribution occurs by sublimation/condensation at the solid-vapor interface, following an exponential rate constant $\tau \approx 30$ min. in 50-50 D-T. The effect is noticeably slowed down by the presence of non-condensable ³He in the vapor space. The National Inertial Confinement Fusion Program, funded by the DOE Defense Programs, is hoping to exploit the use of ICF target capsules containing uniform shells of solid D-T fusion fuel. The Omega Upgrade facility being built at the University of Rochester will incorporate a cryogenic target chamber for fielding both D₂ and D-T-filled targets. The next generation ICF driver, the so-called "National Ignition Facility (NIF), certainly will be built around a cryogenic target chamber. Although there are several issues about beta-layering which are not yet well understood, it remains the layering technique of choice for ICF target designers². The combination of high initial fuel density, increased implosion efficiency, and targeting stability afforded by a uniform <u>solid</u> D-T fuel layer gives beta-layered ICF targets considerable advantages over other known capsule designs.</p> <p>Although the basic equilibration rates for beta-layering can be predicted by simple theory, the degradation of the rate constants that occur with aging (an effect of ³He accumulation) are usually addressed by assuming that <u>all</u> of the ³He produced in the solid resides in the central, interior vapor region.³ However, it has been observed^{3,4,5} that shortly after solidifying, the normally transparent D-T solid layers develop optically dark defects which migrate only very slowly toward the interior. After several days, the solid layers become optically opaque. These defects, which appear to nucleate at or near the container wall and then grow as they sweep through the solid, are thought to be finite-sized ³He bubbles . In principle, the formation and morphology of these ³He bubbles can be studied by small-angle neutron scattering experiments. Likewise, the question of <u>where</u> the ³He really is; in the central vapor region, in the slowly moving defects, or both, is best answered by neutron radiography experiments.</p> <h3>Experiments</h3> <p>During the 1993 LANSCE run cycle, two different experiments were carried out on an aluminum cylindrical target with internal dimensions: 4.0 mm diameter x 4.0 mm length. The target was filled with 6000 psia of D-T (19.9 Ci) at EG&G Mound just two days prior to the first experiment and shipped to Los Alamos overnight. The amount of D-T is sufficient to yield a 200 μm-thick solid layer following beta-layering. The target was installed in the cryostat and cooled to 25 K (liquid state) prior to installation in the LQD cave on the first day of scheduled beam.</p>		

Experiment report (continued):

Initial SANS experiments revealed scattering from the surface of the liquid D-T, indicating that the target had been properly filled. Following background and alignment runs at 30 K (gaseous state), the cryostat was cooled to 17.0 K (the triple point of the DT molecule is 19.8 K) and several scans were recorded as beta-layering proceeded. To probe ^3He droplet evolution as a function of temperature, the measurements were repeated at 14 K and at 13 K. However, none of the data showed any significant departure from background scattering. It was later estimated that the average scattering length for D-T, as represented by the DT molecule, would be very close to that of ^3He . Thus any ^3He bubbles would be undetectable as long as there is no significant density difference between them and the D-T background.

Following the SANS experiments, the cryostat was relocated to the SPEAR cave and aligned in the positioning mount. Following beta-layering at 17.9 K on day 0, the first radiographic scan was not completed until late the following day. Subsequent scans were measured on day 10 and day 18, all while keeping the temperature in the cryostat constant to 17.90 ± 0.02 K.

Results

SANS - In spite of the 'nul' results, the following conclusions can be made:

- 1) The optical defects observed in solid D-T are probably not due to coalescence of voids or 'tracks' caused by beta-particles, because voids would scatter neutrons strongly owing to the density mismatch.
- 2) For the range of sizes observable by small angle neutron scattering experiments (10 to 1000 Å), ^3He bubbles produced during beta-decay of tritium in D-T solid have approximately the same density as the parent solid.

SPEAR - Although inconsistent beam intensity during each of the three day-long scans made it difficult to properly normalize the SPEAR data, the following conclusions can be drawn:

- 1) The formation of ^3He was easily detectable. The amount of neutron absorption observed matched that predicted from the known decay rate of tritium and the measured cross section for ^3He .
- 2) It was obvious that the ^3He produced from beta-decay of the tritium in the D-T solid was not held back in the solid layer.
- 3) Although the resolution of the measurements (~ 0.5 mm) do not permit us to distinguish the solid layer from the rest of the target interior, the data suggest that the density of ^3He in the solid layer is approximately the same as that observed in the central void space, i.e., there is no abrupt cut-off of ^3He intensity at the (calculated) interior edges of the D-T solid layers.

References:

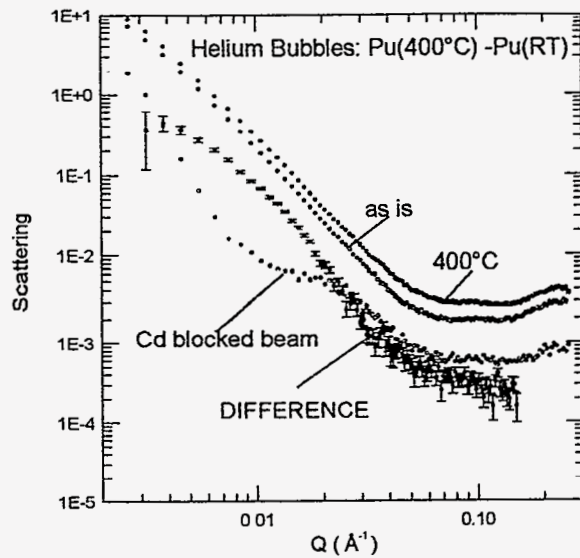
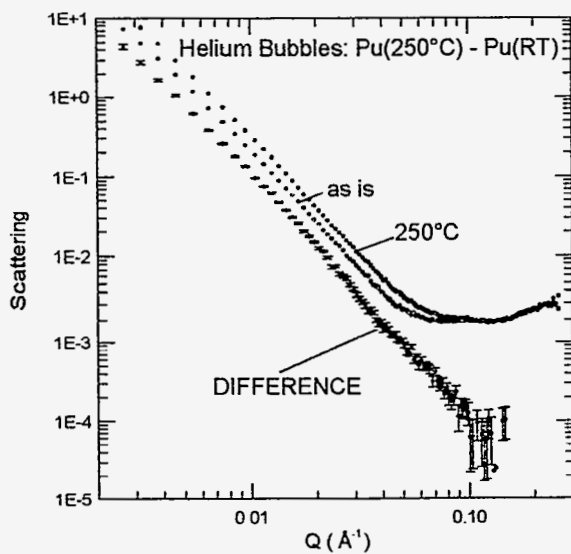
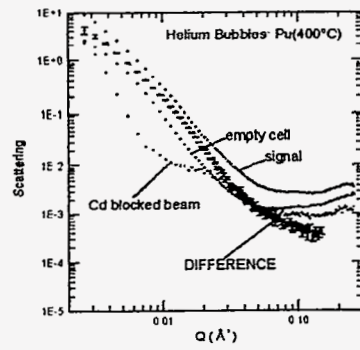
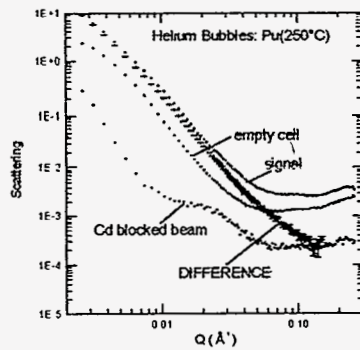
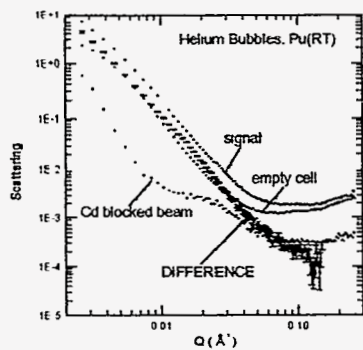
1. "Radioactively Induced Sublimation of Solid Tritium,"
J. K. Hoffer and L. R. Foreman, Phys. Rev. Lett. **60**, 1310 (1988).
2. "Solid Fuel Targets for the ICF Reactor,"
L. R. Foreman and J. K. Hoffer, Nuclear Fusion **28**, 1609 (1988).
3. "Temperature- and Age-Dependence of Redistribution Rates of Frozen Deuterium-Tritium"
T. P. Bernat, E. R. Mapoles, and J. J. Sanchez, Lawrence Livermore National Laboratory
Inertial Confinement Fusion Quarterly Report, **1**, 57 (1991).
4. "Uniform Solid Deuterium-Tritium Fuel Layers Resulting from Radioactively Induced Sublimation,"
J. K. Hoffer and L. R. Foreman, J. Vac. Sci. Technol. **A7**, 1161 (1989).
5. "Beta-Layering of Solid Deuterium-Tritium in a Spherical Polycarbonate Shell," John D. Simpson,
James K. Hoffer and Larry R. Foreman, Fusion Technology, **21**, 330, (1992).

Instrument used: <i>(please type)</i> LQD	Local contact: P. A. Seeger	Proposal number: <i>(for LANSCE use only)</i> 6405
Title: Small-Angle Neutron Scattering by Aged ²³⁹Pu δ-Phase Samples		Report received: <i>(for LANSCE use only)</i> 3/15/94

Authors and affiliations:

T. G. Zocco, J. I. Archuleta, A. C. Lawson and P. A. Seeger
 Los Alamos National Laboratory
 Los Alamos, NM 87545

Experiment report:



Experiment report (continued):

Self-irradiation damage of plutonium metal and its long term effects are of particular interest to plutonium metallurgists. With each radioactive decay event (α -decay), a helium nucleus and subsequent ^4He atom is formed, and over a long period of time these atoms can collectively add to a substantial amount of trapped helium in the lattice of the metal. It is important to know the distribution of trapped helium in order to predict its effects (e.g., swelling) on plutonium components.

It is not known *a priori* what happens to the helium. One possibility is that it will form small bubbles, or voids, and these are sometimes seen with electron microscopy. Bubble formation can be influenced by heat treatment.

In 1993 we continued our small-angle scattering experiments to look for helium bubbles in aged plutonium. We measured three samples of 22 year old ^{239}Pu . The samples are δ -phase, stabilized with 1.5 w/o gallium. The first was measured in an "as is" condition. A second sample was annealed at 250°C for two hours, and the third for 400°C for two hours. We measured the scattering and transmissions of all three samples on LQD, and we used a cadmium blank sample to determine the background.

The samples were doubly contained in aluminum sample holders with windows of very high purity aluminum. The signal from the sample holders must be precisely subtracted, so that good data are necessary. ^{239}Pu is highly absorbing, and this leads to two kinds of difficulties. First, very thin samples were required. We thinned our samples to about 0.003" before annealing. This gave satisfactory measurements, but very long counting times (20-30 hours) were required. The high absorption imposes a wavelength-dependent attenuation on the measured background, so that the measured background must be corrected. We solved this problem by developing a "pseudo-transmission" formalism for data reduction.

The accompanying figures show the results of the measurements; in each case, the curve marked "difference" is the final reduction. (In the case of "Pu(250C)-Pu(RT)", the pseudo-transmission corrections were negligible.) The data are much better than those obtained last year. There are two reasons for this: the samples were in much better condition than last year's samples, and the new "pseudo-transmission" gave a more reliable data reduction. The data from the sample annealed at 250°C data seem to be about the same as the unannealed (RT) sample, but the data for the sample annealed at 400°C are quite different. These data deserve a proper analysis by the maximum entropy method.

References:

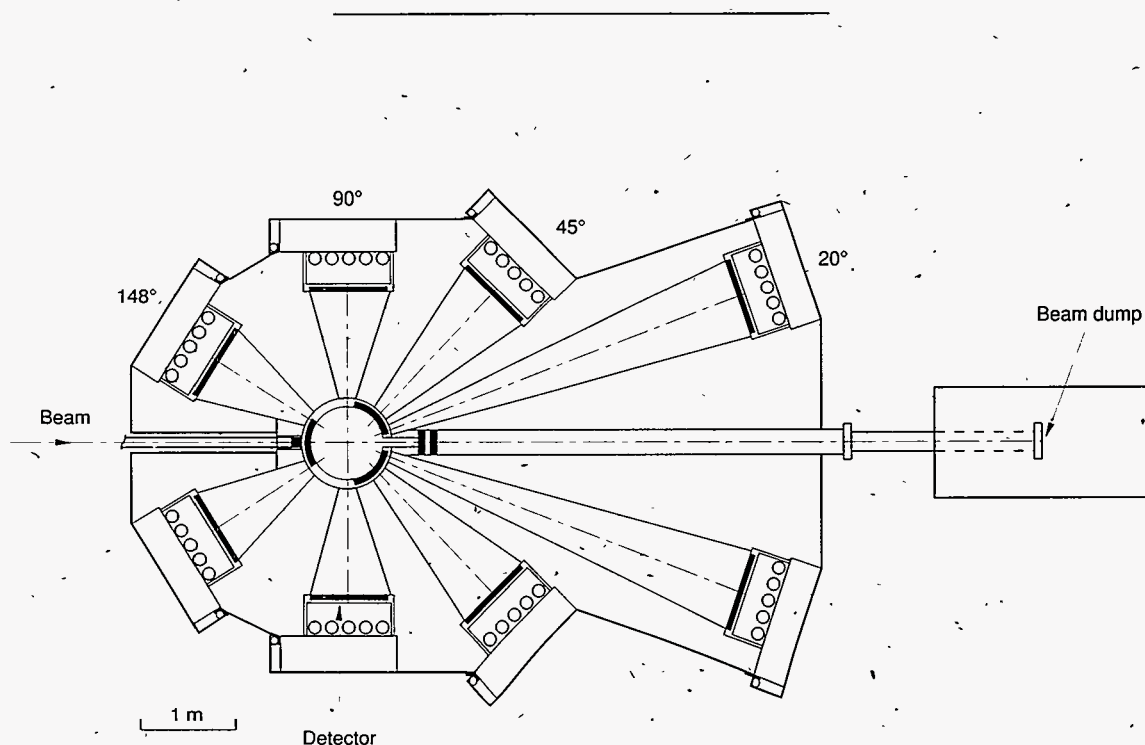
- D. L. Rohr, K. P. Staudhammer and K. A. Johnson, Los Alamos Report LA-9965-MS (1984).
- D. L. Rohr and K. P. Staudhammer, J. Nuclear Mat. 144 202 (1987).
- T. G. Zocco and D. L. Rohr, Mat. Res. Soc. Symp. Proc. 115 259 (1988).
- A. C. Lawson, T. G. Zocco, P. A. Seeger, R. Martinez, J. Cost and R. Hjelm, LANSCE Experiment Reports, 1992 Run Cycle, LA 12647-PR, p. 132.

*Neutron Powder
Diffractometer (NPD)*

Neutron Powder Diffractometer (NPD)

The Neutron Powder Diffractometer (NPD) design allows for studies of complex structures, internal strain measurements, and studies in which precise data are needed to extract electron distributions for x-ray and neutron comparisons. Standard collimation in the beam line produces a 5.0 x 1.0-cm beam at the sample position, which is 32 m from the source. Placed at five points along the beam, variable apertures permit adjustment of both the beam size on the sample and the viewed region of the moderator. The instrument has detectors placed symmetrically at several angles to cover short d-spacings (0.25 to 3.1 Å) at a

resolution ($\Delta d/d = 0.15\%$ to 2.5%). Both sides of the instrument have identical resolution because the incident beam is normal to the moderator. A large sample chamber (74 cm in diameter) accepts special environment devices such as a liquid helium cryostat, a vacuum furnace, and a closed-cycle helium refrigerator. The NPD accommodates a beam collimation and sample manipulation system mainly for residual stress measurements and a stress rig that provides uniaxial compression or tension up to ± 1000 MPa and at the same time is capable of heating components to approximately 1200 K in vacuum.



Instrument Details

Detector banks, d-spacing
range (approximate),
and resolution:

$\pm 20^\circ$ (future)	1.2–15.8 Å	0.91–1.5%
$\pm 45^\circ$ (future)	0.65–7.6 Å	0.37–0.62%
$\pm 90^\circ$	0.35–4.2 Å	0.25%
$\pm 148^\circ$	0.25–3.1 Å	0.15%

Moderator

Chilled water at 283 K

Sample environment

10–300 K; closed-cycle refrigerator;
room-temperature-access liquid-He dewar, 1.2–300 K;
compact stress rig with heating, limit 1200 K;
vacuum furnace, limit 1000 K;
manipulation and collimation system

Maximum beam size
at sample:

5.0 cm in height x 1 cm in diameter

Experiment duration

4 to 48 hours

Joyce Goldstone, instrument scientist

NPD Experiment Reports

6001	<i>UAuSn: Is There an Orthorhombic Distortion below the Néel Point?</i>	107
6004	<i>Phase Transition at 200K in Y_2In</i>	109
6016	<i>Neutron Diffraction Strain Measurements in a Near Titanium Alloy Subjected to Applied Loading</i>	111
6017	<i>Crystal Structure of Nacrite, $Al_2Si_2O_5(OH)_4$, at ~10K</i>	113
6019	<i>Residual Strains in Multilayer Ceramic/Metal/Ceramic Composites</i>	115
6053	<i>Pressure Induced Hydrogen Bonding: Neutron Diffraction Studies of Brucite, $Mg(OD)_2$, to 9 GPa</i>	117
6058	<i>Measurement of Residual Strains in Al-TiC Metal Matrix Composites Induced by Fabrication and Subsequent Thermo-mechanical Testing</i>	119
6059	<i>In Situ Measurement of Strain in CuNb & CuAg during Loading</i>	121
6067	<i>Test of a Boron-Phosphide Neutron Detector</i>	123
6076	<i>Implications of the Morphology of the Evolution of Elastic Macro-strain in a Metal Matrix Composite</i>	126
6077	<i>Internal Strain Measurements of Bulk and Reinforced NiTi Shape Memory Alloys</i>	128
6098	<i>Elastic Constant Determination in Zinc and NiAl by Neutron Diffraction</i>	130
6100	<i>Structure of the Super-Heavy-Fermion Compound YbBiPt</i>	132
6104	<i>Strains in Alumina/Silicon Carbide Composites and Nanocomposites</i>	134
6406	<i>In Situ Measurement of Elastic Strains at High Temperature and under Load in Polycrystalline Materials</i>	136

Experiment report (continued):

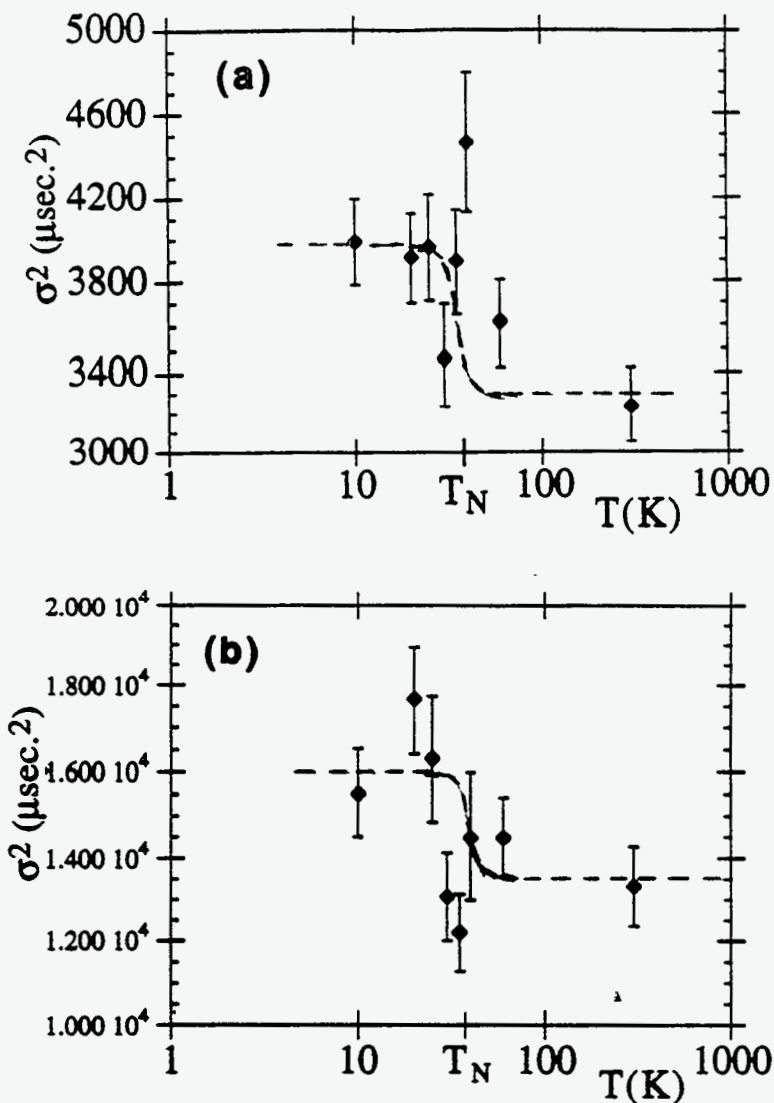
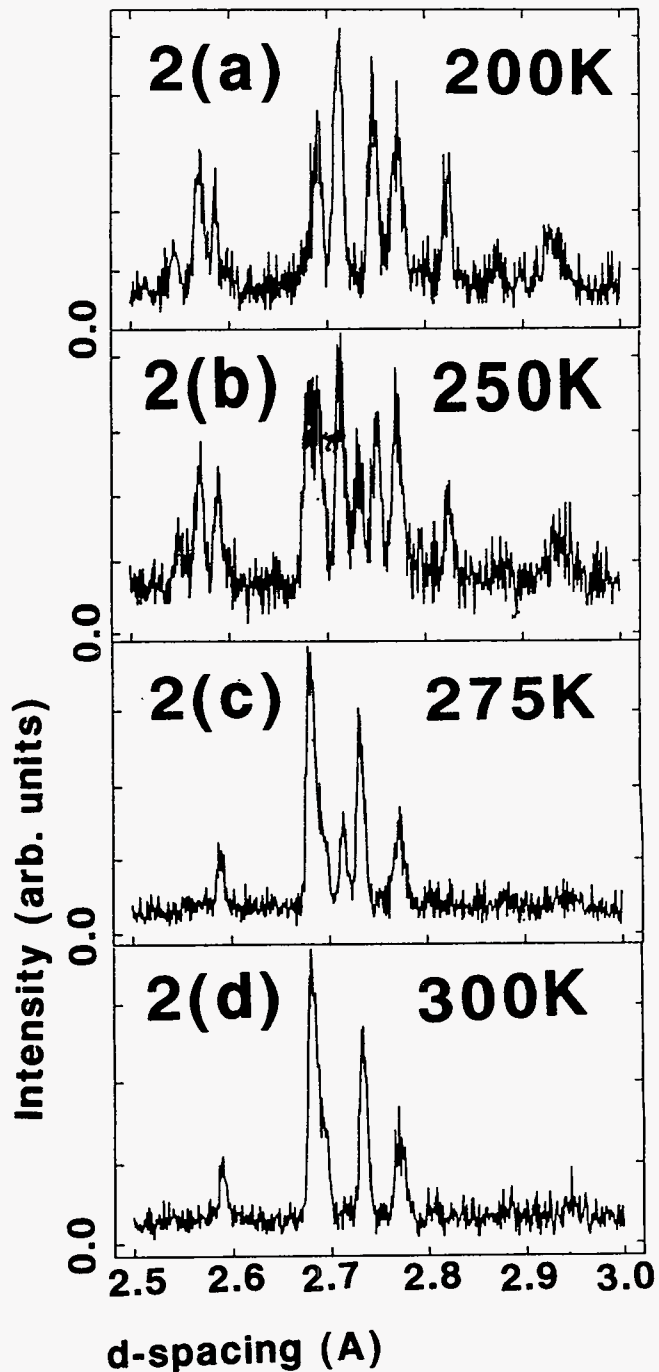
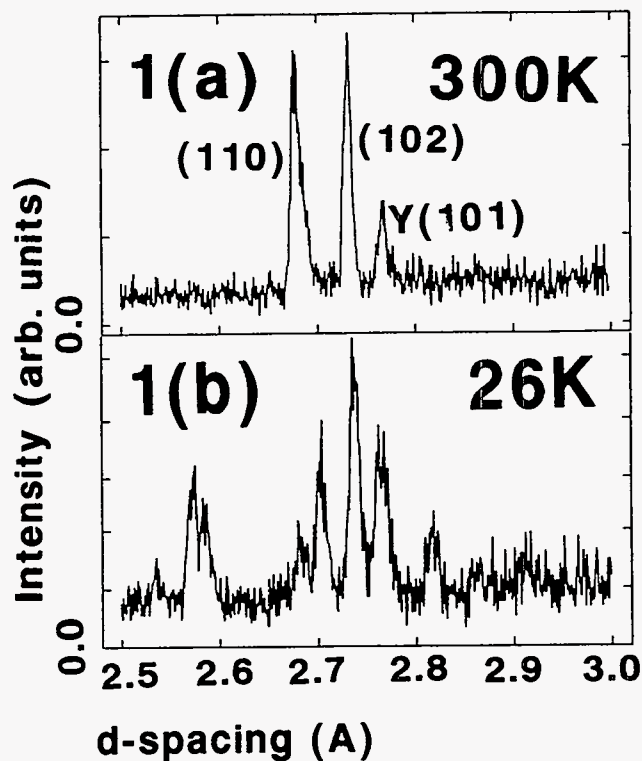


Fig. 1. Variation of σ^2 line-shape parameter with temperature for (a) 110_{hex} and (b) 102_{hex} reflection. T_N indicates the Néel temperature which is 37 K. The dashed-lines are guides to the eye and have no theoretical significance.

References:

- [1] R. A. Robinson, A. C. Lawson, J. A. Goldstone and K. H. J. Buschow, *J. Magn. Magn. Mater.* 128, 143 (1993)
- [2] R. A. Robinson et al., *Phys. Rev. B* 47, 9, 5090 (1993)
- [3] J. A. Goldstone, private communication.

Experiment report (continued) :



References:

- [1] E. Franceschi, J. Less-Common Metals 37, 157 (1974).
- [2] Z. Fisk, unpublished data

Instrument used: (please type) NPD	Local contact: Goldstone J, Bourke, M	Proposal number: <i>(for LANSCE use only)</i> 6016
Title: Neutron Diffraction Strain Measurements in a near Titanium Alloy subjected to Applied Loading		Report received: <i>(for LANSCE use only)</i> 12/13/93
Authors and affiliations: Ezeilo, A.N. Dept of Mechanical Engineering, Imperial College, London, SW7 2BX Webster, G.A. Dept of Mechanical Engineering, Imperial College, London, SW7 2BX Webster, P.J. Dept of Civil Engineering, University of Salford, Salford, M5 4WT		
Experiment report: <p>Introduction Residual stress measurements by neutron diffraction typically rely on the accurate measurement of the shift of a single Bragg peak to determine the residual lattice strains, which in turn are converted into residual stresses using elastic constants. Because the elastic constants of a particular reflection are unknown the bulk modulus is usually used or constants are calculated from the single crystal elastic constants found in the literature. It is known that use of these constants can give stresses which are in error by up to 33% in some materials [1]. By applying known loads to samples insitu, accurate values of the elastic constants can be obtained. Also, by loading a material into the plastic regime and then unloading, it is possible to obtain an indication of the residual microstresses introduced by plasticity. This is useful in selecting the most suitable reflection for performing engineering residual stress measurements. The aims of this experiment were to determine the (hkil) elastic constants, and also the most suitable reflection for performing engineering residual stress measurements in a near α titanium alloy, by loading samples in tension insitu while making neutron diffraction measurements.</p> <p>Samples The samples were titanium alloy IMI 834 with chemical composition as follows; Al 5.8%, C 0.06%, Sn 4.5%, Zr 4%, Nb 0.7%, Mo 0.5%, Si 0.4% and Ti the balance. IMI 834 has a bulk elastic modulus of 119 GPa, a Poissons ratio of 0.32 and a yield strength of 1030 MPa.</p> <p>Experiments Instrument NPD was used to perform the neutron diffraction measurements on the samples. Tensile tests were performed insitu on two identical tensile samples using the NPD stress rig. Each sample had two strain gauges attached to it to measure the engineering strain parallel to the direction of the applied load. The first sample was loaded to 600 MPa, within the elastic region, and the (hkil) elastic constants obtained both parallel and perpendicular to the applied load. The second sample was given 1 cycle of plastic loading to 1.5 % plastic strain and then 5 cycles of plastic loading to 2% plastic strain. The residual (hkil) lattice strains after cycling were then obtained.</p>		

Experiment report (continued):

Results

The modulus of elasticity as measured by the strain gauges was 126 GPa. The powder pattern revealed the hexagonal close packed crystal structure of titanium. The elastic constants obtained for each reflection are given in the table below. By using profile refinement techniques the elastic deformation of the entire lattice was calculated by obtaining refined values of the lattice parameters a and c for each load increment. The elastic constants as measured by profile refinement techniques were 119 GPa for a and 147 GPa for c and Poissons ratio ν , was 0.30 for a and 0.27 for c .

d (Å)	(hkil) reflection	E (hkil) (MPa)	ν	σ_{res} MPa (after 1 cycle)	σ_{res} MPa (after 5 cycles)
2.54	(10-10)	126	0.28	13	13
2.34	(0002)	154	0.28	38	19
2.23	(10-11)	126	0.33	-9	-12
1.72	(10-12)	128	0.32	-59	-124
1.46	(11-20)	123	0.27	-64	247
1.32	(10-13)	136	0.29	-82	40
1.24	(11-22)	127	0.31	40	39
1.22	(20-21)	126	0.35	-29	-22

Discussion

It is clear that most reflections give a value of the elastic constant E that is close to that measured using strain gauges. The (0002) reflection should be avoided for engineering applications because of its high stiffness. The (10-12) and the (11-20) reflections should also be avoided for engineering residual stress measurements as they both retain high residual microstresses when there is no engineering residual stress present. The (hkil) values of ν seem quite reasonable compared to the bulk value of 0.32 quoted in the literature. Profile refinement methods can be used to obtain residual stresses but the appropriate elastic constants must be used. In addition, for good neutron diffraction strain measurements the reflection chosen should have a high neutron count rate. From the complete diffraction profile (not shown) the (10-11) reflection gave the best neutron intensity. It is therefore suggested that for neutron diffraction engineering residual stress measurements the (10-11) reflection be used.

Acknowledgments

I would like to thank Mark Bourke, Joyce Goldstone and Armando for their help with the experiments.

References:

References

- [1] Ezeilo A.N. "Neutron Diffraction Calibration Measurements on Udimet 720 using Test Beam at ISIS" Internal report, dept of Mech Eng., Imperial College, London.

Instrument Used: <i>(please type)</i> NPD	Local Contact Joyce Goldstone	Proposal Number: <i>(for LANSCE Use Only)</i> 6017
Title: CRYSTAL STRUCTURE OF NACRITE, $\text{Al}_2\text{Si}_2\text{O}_5(\text{OH})_4$, AT ~10K		Report received: <i>(for LANSCE Use Only)</i> 3/15/94
Authors and affiliations: David L. Bish, EES-1, Mail Stop D469, Los Alamos National Laboratory (505-667-1165)		
Experiment report: <p>Nacrite is an uncommon polymorph of $\text{Al}_2\text{Si}_2\text{O}_5(\text{OH})_4$ and is one of the four kaolin minerals. The structures of two of the four polymorphs, kaolinite and dickite, are well known and have been studied using both X-ray and neutron diffraction methods (Bish and Von Dreele, 1989; Bish, 1993; Joswig and Drits, 1986; Bish and Johnston, 1993). Halloysite, the third polymorph, is not amenable to full three-dimensional study by diffraction methods because it exhibits extreme two-dimensional diffraction effects due to stacking disorder. Much effort has gone into determining the accurate structures of the kaolin minerals, particularly the details of the hydroxyl group orientations and the interlayer bonding. Currently, the presence of one hydroxyl group within the silicate layers for every three hydroxyl groups in the interlayer region is well accepted for the kaolin minerals. Nacrite, kaolinite, and dickite differ primarily in the manner in which their aluminosilicate layers are stacked, and it appears that partial explanation for the comparative rarity of nacrite lies in its interlayer bond energy.</p> <p>The structure of nacrite was first determined and refined in space group <i>Cc</i> using single-crystal X-ray methods (Blount et al., 1969). Unfortunately, the resultant structure model is incomplete and inaccurate, due in part to twinning of the analyzed crystal. The positions of the hydrogen atoms that are so important in determining and understanding the interlayer bonding were not determined. In addition, a number of interatomic distances are obviously in error. Blount et al. (1969) proposed that angular strain in the directed interlayer hydrogen bonds was a partial explanation for the lesser abundance of nacrite. In addition, they suggested that the nacrite layer (7.186Å) is slightly thicker than the dickite (7.162Å) and kaolinite (7.124Å) layers. This difference appears to be due to a slightly greater interlayer separation in nacrite than in dickite and kaolinite. Blount et al. suggested that this difference is due to a less favorable packing of layers.</p> <p>High-quality X-ray powder diffraction data were obtained at room temperature from the sample to be used for neutron data collection. Rietveld refinement of the structure was performed and I obtained a structure model that appears to be superior to that published by Blount et al. (1969). The room temperature unit-cell parameters are $a = 8.9168(4)\text{Å}$, $b = 5.1553(2)\text{Å}$, $c = 15.6766(9)\text{Å}$, and $\beta = 113.606(2)^\circ$. Neutron diffraction data were collected at 10K using NPD and the X-ray sample of well-crystallized nacrite. Although incoherent scattering from the hydrogen in the mineral apparently</p>		

Experiment report (continued):

degraded the diffraction information somewhat, the data were sufficient to allow location of at least two of the four hydrogen atoms. In addition to the incoherent scattering, the diffraction information for nacrite was somewhat degraded by the presence of approximately 38% dickite in the sample, estimated from the refined scale factors. The room temperature structure of nacrite (Blount et al., 1969) was used as the starting model for nacrite, and the dickite in the sample was represented by the refined low-temperature dickite structure, including H atoms, of Bish and Johnston (1993). Atomic positions for dickite were fixed, and profile, preferred orientation, and thermal parameters for nacrite and dickite were constrained to be equal. To locate hydrogen atoms, difference-Fourier techniques were used after performing a Rietveld refinement using only the aluminosilicate framework of nacrite (without the hydrogen atoms) and the low-temperature structure of dickite. During this process, only profile, scale, and lattice parameters were refined, keeping the positions of the aluminosilicate framework fixed. After refinement of these parameters, a difference-Fourier map was calculated to search for the hydrogen atoms. Probable positions of the interlayer H2 and H3 atoms were obtained from the difference-Fourier map; however, consistent positions for the interlayer H3 atom and the inner H1 atom were not located. Instead, positions for these two H atoms were taken from the results of electrostatic energy modeling. To-date, the positions of the H atoms have been refined, along with unit-cell and profile parameters. The profile parameters show that the observed peak broadening is due primarily to strain rather than finite crystallite size. Refined low-temperature unit-cell parameters for nacrite are $a = 8.893(2)\text{\AA}$, $b = 5.147(1)\text{\AA}$, $c = 15.690(4)\text{\AA}$, and $\beta = 113.944(3)^\circ$ (including refinement of the instrument parameters). The a and b parameters are significantly smaller at low temperature, but the c parameter is significantly larger. By analogy with the behavior of dickite, it was expected that the greatest thermal *contraction* would be along the c axis. The unusual behavior in unit-cell parameters with temperature may have resulted from an apparent sample displacement due to the highly absorbing nature of the hydrogenous sample. The refined preferred orientation correction, 1.017(3), is consistent with the platy nature of the sample and the sample holder geometry.

One of the the refined H positions is significantly different from those proposed by Blount et al. (1969). The inner H atom and the interlayer H(3) and H(4) atoms give OH orientations similar to those previously proposed, but the interlayer H(2) atom gives an OH orientation that is much closer to being in the plane of the silicate layers. Full three-dimensional refinement of the structure, including the H atoms located here, should clarify the details of the interlayer H bonding and provide an explanation for the relative rarity and instability of the mineral. Ultimately, the best structural results will probably be obtained when a purer sample of nacrite is discovered.

References:

- Bish, D. L. (1993) Rietveld refinement of the kaolinite structure at 1.5K. Clays and Clay Minerals, in press.
- Bish, D. L. and Johnston, C. T. (1993) Rietveld refinement and Fourier-transform infrared spectroscopic study of the dickite structure at low temperature. Clays & Clay Minerals, **41**, 297-304.
- Bish, D. L. and Von Dreele, R. B. (1989) Rietveld refinement of non-hydrogen atomic positions in kaolinite. Clays and Clay Minerals, **37**, 289-296.
- Blount, A. M., Threadgold, I. M., and Bailey, S. W. (1969) Clays & Clay Minerals, **17**, 185-194.
- Joswig, W. and Drits, V. A. (1986) The orientation of the hydroxyl groups in dickite by X-ray diffraction. N. Jb. Mineral. Mh., 19-22.

Instrument used: <i>(please type)</i> NPD	Local contact: Mark Bourke	Proposal number: <i>(for LANSCE use only)</i> 6019
---	--------------------------------------	---

Title: Residual Strains in Multilayer Ceramic/Metal/Ceramic Composites	Report received: <i>(for LANSCE use only)</i> 2/24/94
--	--

Authors and affiliations:

Michael R. James
Rockwell Science Center
Thousand Oaks, CA 91360

Multilayer Composites consisting of bonded alternating ceramic and metal layers offer attractive structural properties. Thermal residual stresses are usually present which affect both the integrity of the bond and crack propagation across the interface. Complementary studies were made with neutron and x-ray diffraction to provide an understanding for the development of the residual thermal stresses.

Neutron Diffraction Measurements - Experimental Procedure

Measurements were made on three multilayer samples of Al₂O₃ with either Cusil or Al metallic layers and on equivalent monolithic reference samples of Al₂O₃, Cusil and Al which were used to provide unstrained references. Specimens were placed in the Neutron Powder Diffractometer (NPD) at 45° to the neutron beam. Time-of-flight diffraction patterns were recorded in each of the four detector banks. The 90° detectors recorded the strain parallel and normal to the multilayer lay-up.

The diffraction pattern for the Cusil braze (nominal composition 63wt%Ag, 1.75%Ti, balance Cu) gave definitive Cu and Ag peaks indicating they are separate and immiscible phases. There was no indication of a ternary phase of Cu, Ag and Ti. Well separated Bragg reflections were fitted individually and strains were calculated by comparing equivalent reflections between the multilayer samples and the monolithic reference standards. For example, for Al₂O₃, eight diffraction peaks were used. The values reported are the average strain over all the peaks and the corresponding standard deviation.

The diffraction data was also analyzed using Rietveld refinement to calculate the lattice parameters for the multilayer and monolithic standard states. Because of inconsistent peak shifts of the Cu and Ag phases, the accuracy of the lattice parameters for the multilayer samples was too low to be worthwhile. However, Rietveld refinement lattice

Experiment report (continued):

parameters calculated for the standard Al_2O_3 were used for estimating the thermal expansion coefficient.

Room Temperature Neutron Diffraction Compared to X-ray Diffraction Results

The in-plane strain (ϵ_1) values in the Al_2O_3 phase of the multilayer samples were very reasonable for all three samples with a magnitude close to that predicted by an elastic-perfectly plastic analysis. Neutron and x-ray (surface measurement) measured values are compared in Table 1. However, the in-plane strain in the metal layers are very different from that predicted for a homogeneous layer and further though must be given to the behavior of the metal layers.

Table 1 In-Plane Residual Strain ($\times 10^{-6}$)

		Predicted	Neutron	Neutron Scatter	X-ray
1 layer Cusil/ Al_2O_3	Al_2O_3	-820	-763	± 82	-790
3 layer Cusil/ Al_2O_3	Al_2O_3	-560	-500	± 109	-540
Al/ Al_2O_3	Al_2O_3	-170	-66	± 72	-90

Significant strains were measured by neutron diffraction in the ϵ_3 direction (i.e., through the thickness) in the metal layers although interpretation of this remains as perplexing as that for the in-plane strains in the braze alloy. Both the Cu and Ag phases exhibited significant variation among different lattice planes making the determination of an average strain unwarranted. For the Al_2O_3 phase, measurable but statistically zero strains were found.

Elevated Temperature Results

Elevated temperature data were analyzed the same way, i.e., individual diffraction peaks were fit and compared. The furnace data was plotted as lattice strain vs. temperature for the Al_2O_3 phase as calculated from the difference between the averaged room temperature and elevated temperature interplanar spacings. Extrapolation of the elevated temperature slope gave a stress free temperature of about 700 °C. The composite was consolidated at 825°C. Further details on these results can be found in Ref. 1.

References:

1) M.A.M. Bourke, J.A. Goldstone, N. Shi, G.T. Gray III, M. R. James and R. Todd, *The Use of Pulsed Neutron Diffraction to Measure Strain in Composite Materials*, Forth Int. Conf. on Residual Stress, June 8-10 1994, Baltimore MD.

Instrument used: <i>(please type)</i> NPD	Local contact: Robert Von Dreele	Proposal number: <i>(for LANSCE use only)</i> 6053
Title: PRESSURE INDUCED HYDROGEN BONDING: NEUTRON DIFFRACTION STUDIES OF BRUCITE, Mg(OD)₂, TO 9 GPa .		Report received: <i>(for LANSCE use only)</i> 12/8/93
<p>Authors and affiliations:</p> <p>J. B. Parise, K. Leinenweber, D. J. Weidner, ESS, SUNY, Stony Brook and R. B. Von Dreele, LANSCE.</p>		
<p>Experiment report:</p> <p>Knowledge of the pressure dependence of hydrogen bonding in O-H bearing minerals and other solids is of importance in understanding their stability and crystal chemistry. In the earth context, pressure induced H-bonding could increase the stability of OH-bearing phases under conditions of the earth's interior^{1,2}; the limit to the stability of hydrous materials at high temperature is the entropy gain associated with dehydration. Stronger H-bonding might inhibit this dehydration. Indeed our recent results^{3,4} suggest this mechanism operates to stabilize brucite at high pressure to its melting point; this contrasts to its behavior under ambient conditions⁵. The geophysical implications for the dehydration behavior is adequately reviewed in several publications^{6,7}. A further interest in weakly H-bonded systems which may strengthen with pressure pertains to recent efforts to model these materials theoretically^{8,9}. Structures derived from data at high pressures place powerful constraints on these theoretical models. The studies of prototypical hydrous phases and comparisons with theoretical calculation are useful for evaluating the theoretical stability of the more complex phases proposed to exist in the earth's mantle².</p> <p>Powder neutron diffraction is THE technique for structure determination of hydrogenous materials at high pressure. Since the introduction of the Paris-Edinburgh cell¹⁰ at HIPD the prospect for gaining new insights into changes in H-bonding with pressure has greatly improved. This cell provides pressures in excess of 10 GPa - a usable range at least 4 times greater than previously attainable - with large sample volume and no interference from the sample holder. Its installation at a spallation source provides for superior data of the type required for Rietveld refinement. This apparatus has enabled us to recently complete a study of deuterated brucite, Mg(OD)₂, the results of which are summarized in the figure below.</p> <p>Rietveld analysis of the data collected at four pressures (Table 1) suggests the deuterium moves from the 2<i>d</i> site in P3m1 to 6<i>i</i>. Strengthening of the H-bonding is indicated by increase in the O-D...O angle and decrease in the D...O distance (Figure). The splitting of 1/3-occupied D-sites increases with pressure. This feature of the structure can also be modeled with an anisotropic thermal parameter which flattens considerably at high pressures. Interestingly the low pressure data, obtained here and reported by others in the literature, also show a flattening perpendicular to <i>c</i>, suggesting there may be some weak H-bonding in this solid under ambient conditions.</p>		

Experiment report (continued):

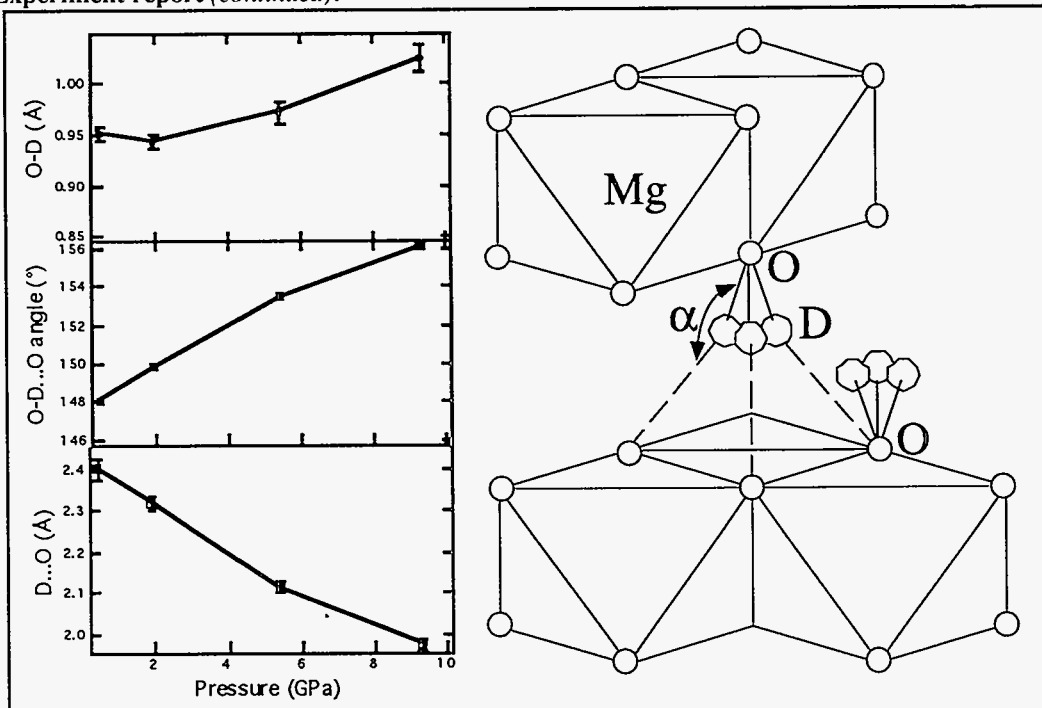


Figure 1. Variation in structural parameters O-D (top), O-D..O angle (middle) and D...O (bottom) for brucite up to 9 GPa.

Table 1. Refined atomic parameters* for the "split atom model" of deuterated brucite

pressure (GPa)	0.4	1.9	5.4	9.3
<i>a</i>	3.1382(2)	3.1167(3)	3.0728(4)	3.0365(6)
<i>c</i>	4.713(1)	4.630(1)	4.496(1)	4.403(2)
<i>z</i> O	0.214(3)	0.219(2)	0.229(2)	0.232(2)
Uiso (O)**	0.5(1)	0.7(1)	1.0(1)	1.0(1)
<i>x</i> D	0.367(4)	0.373(3)	0.389(2)	0.402(2)
<i>z</i> D	0.412(2)	0.417(2)	0.435(2)	0.449(2)
Uiso (D)**	1.7(4)	1.3(3)	1.2(3)	1.0(4)
Rwp	4.28	3.77	3.98	3.90
Rp	3.01	2.70	2.68	2.83
χ^2	1.56	1.87	1.79	1.93

* Space group P3m1, Mg at site 1*a*, (0,0,0); oxygen at (1/3,2/3,*z*);

D moved from site 2*d* at (1/3,2/3,*z*) to 6*i* at (*x*,*-x*,*z*).

** ($\times 10^2$); thermal parameters for Mg constrained to equal those for oxygen.

References:

- (1) L.-g. Liu *Phys. Earth. Planet. Inter.* , 1987, **49**, 142.
- (2) R. E. Pacalo and J. B. Parise *Am. Mineral.* , 1992, **77**, 681.
- (3) K. Leinenweber et al, 1993, *in preparation*
- (4) J. B. Parise, K. Leinenweber, D. J. Weidner, K. Tan and R. B. Von Dreele *in preparation* , 1993,
- (5) S. A. T. Redfern and B. J. Wood *American Mineralogist* , 1992, **77**, 1129.
- (6) J. A. Tyburczy, T. S. Duffy, T. A. Ahrens and M. A. Lange *J.of Geophysical Research* , 1991, **96**, 18.
- (7) A. B. Thompson *Nature* , 1992, **358**, 295.
- (8) D. M. Sherman *Amer. Mineral.* , 1991, **76**, 1769.
- (9) P. D'Arco, M. Causa, C. Roetti and B. Silvi *Phys. Rev. B* , 1993, **47**, 3522.
- (10) R. J. Nelmes, et al. *Physical Review Letters* , 1993, **71**, 1192.

Instrument Used: (please type) <p style="text-align: center;">NPD</p>	Local Contact <p style="text-align: center;">Mark Bourke</p>	Proposal Number: <i>(for LANSCE Use Only)</i> <p style="text-align: center;">6058</p>
Title: Measurement of residual strains in Al - TiC metal matrix composites induced by fabrication and subsequent thermomechanical testing.		Report received: <i>(for LANSCE Use Only)</i> <p style="text-align: center;">12/6/94</p>
Authors and affiliations: <p style="text-align: center;">J.E. Allison, Ford Mo Co., Dearborn Mi. M.A.M. Bourke, MST5 / LANSCE, MS H805 (665 1386) J.A. Goldstone, LANSCE, MS H805 (667 3629)</p>		
Experiment report: <p>Metal matrix composites (MMC) are an important new material for the automotive industry. Ford Motor Company has been investigating the mechanical behavior (1,2) and applications of this class of materials for over 8 years. Interest has focussed on particle reinforced aluminum MMCs because of their superior cost-performance ratio compared to whiskers or continuous fiber reinforced material. In general the differences that exist between the thermal expansion coefficients (CTE) of the reinforcing particles and the matrix induce residual stresses, which have a significant effect on mechanical propoerties of the bulk material.</p> <p>The measurements we performed in this experiment addressed the evolution of residual stresses following differing thermal treatments. A high strength aluminum alloy containing varying volume fractions of SiC (see figure 1) was subjected to 1)a solution treatment (500°C), followed by rapid quenching to room temperature and 2) an aging treatment (150-200°C) followed by moderate cooling to room temperature. Stresses were determined after both treatments as well as in several identically treated specimens to assess the degree of variation.</p> <p>In a second study measurements were performed to assess the influence of small plastic strains of less than .001 since this is an important strain regime for many automotive components. Because of the directionality of these strained specimens measurements along the straining axis of a cylindrical specimen required that the cylindrical specimens were placed horizontally in the neutron beam.</p>		

Experiment report (continued):

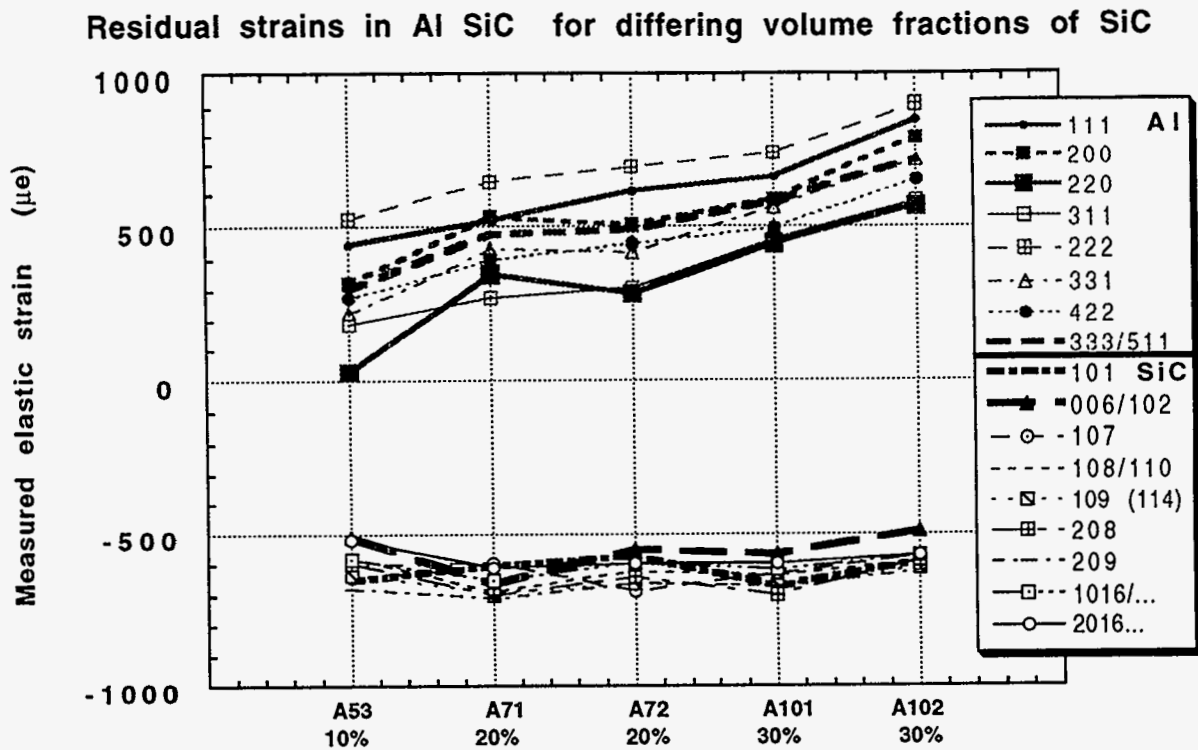


Figure 1 Residual strains measured in 5 samples containing, 10,20,20,30, and 30vol% SiC

References:

1. Bonnen, Allison and Jones, Metal. Trans. A, Vol 22A, p 1007 (1991).
2. Vyletel, VanAken and Allison, Scripta Met., Vol 25, p 2405 (1991).

Instrument Used: <i>(please type)</i> <p style="text-align: center;">NPD</p>	Local Contact <p style="text-align: center;">Mark Bourke</p>	Proposal Number: <i>(for LANSCE Use Only)</i> <p style="text-align: center;">6059</p>
Title: <i>In situ</i> measurement of strain in CuNb & CuAg during loading		Report received: <i>(for LANSCE Use Only)</i> <p style="text-align: center;">11/10/94</p>
Authors and affiliations: <p style="text-align: center;">M.A.M. Bourke, MST5 / LANSCE, MS H805 (665 1386) J.A. Goldstone, LANSCE, MS H805 (667 3629) G.T. Gray III, MST5, MS G755 (667 5452) M.A. Hill, MST6, MS G770 (667 3629)</p>		
Experiment report: Using the NPD, we measured strains in both copper-niobium and copper-silver alloys during applied loading to help understand the development of residual strains in codeforming composite systems being considered as possible winding materials for high field pulsed magnets Alloys containing two insoluble ductile phases can be heavily cold worked by rolling or swaging to produce <i>in-situ</i> composites, termed HDISC (heavily deformed <i>in-situ</i> composites). Studies of their mechanical properties reveal that their strengths often exceed predictions based on the simple "rule-of-mixtures". This strengthening is presumed to result from cold working of the individual phases. Understanding their strength and hardening behavior requires a knowledge of the residual strains produced within each phase by plastic deformation. Previously, we measured residual strains in each phase of a copper-niobium alloy resulting from deformation at different temperatures and strain rates (1). In this experiment, we complement that work by exploring the respective phase behavior of Cu 15%vol Nb and Cu-16%vol Ag composites, during slow strain rate, room temperature, uniaxial loading. The microstructure of the two systems were very different; the niobium reinforcement was essentially spherical and quite soft (following annealing) while the Ag was filamentary and much harder (following extensive cold drawing). Figure 1 shows the elastic strains (parallel to the load axis at a series of static load levels) of 4 Cu reflections and 2 Ag reflections from the CuAg sample during uniaxial tensile loading. The small initial strains were produced by a preload to 500MPa and do not include any contribution from the initial thermal residual stresses. The sample had a rectangular cross section of 4x6 mm and a volume of $\approx 140\text{mm}^3$ was irradiated by the neutron beam. At the maximum load of 775 MPa, which is just larger than the nominal yield stress (763MPa), there was evidence of load transfer from the Ag to the Cu as indicated by the Cu 200 and the Ag 111 reflections. The assumption that this was due to yielding of the Ag filaments is supported by the residual strains measured on unload (not shown). Figure 2 shows measured elastic strains of Cu and Nb reflections from a 10mm diameter cylindrical specimen of CuNb during a uniaxial compression test. Following anneal the niobium is spherical and relatively soft. Cu Nb in this state would not be used in any practical mechanical applications but was selected for ease of comparison with FE models. Clearly the moduli of the Cu and the Nb are substantially different. On loading to -280MPa, load transfer is evident from changes in slope of the stress-strain data. Upon unload a range of residual strains were noted for the different Nb reflections.		

Experiment report (continued):

Unlike the Cu Ag, in the CuNb the residual strains on unload indicate that the copper yielded first transferring load to the Nb. Finite element calculations are currently being performed to see if quantitative predictions of these results are possible.

Applied tensile stress vs Measured elastic strain (parallel to the loading direction) Cu Ag

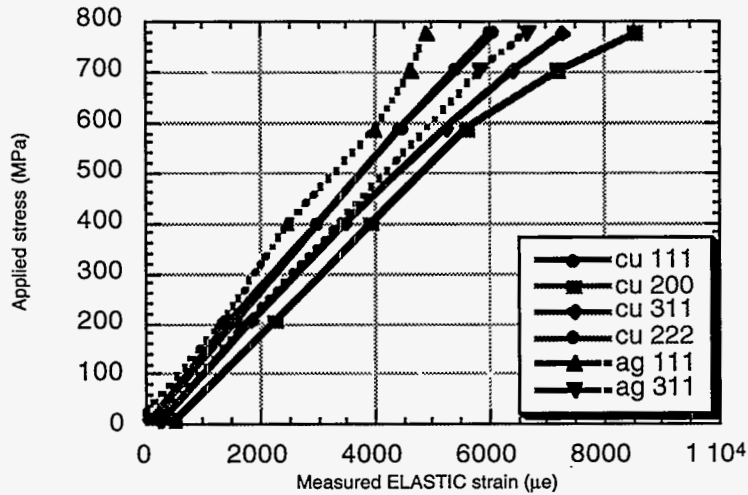


Figure 1: (0 to 775MPa unload not shown)

Compressive stress vs Measured elastic strain (parallel to the loading direction) Cu Nb

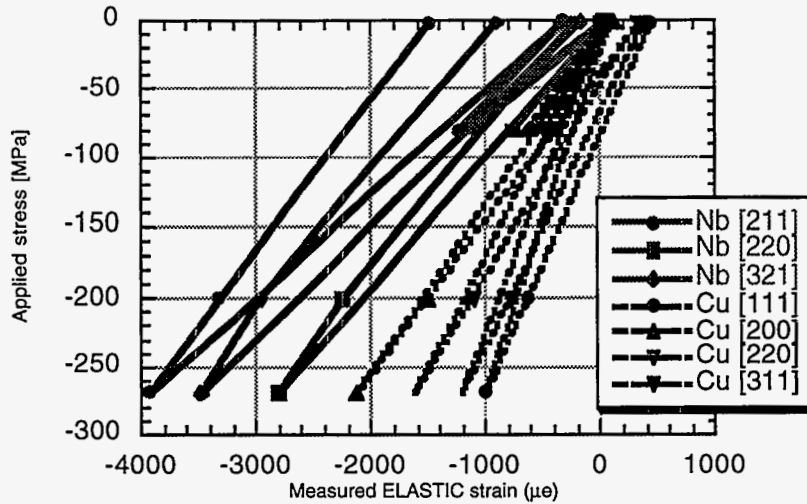


Figure 2: (0 -80, 0 , -270,-200,0)

References:

The use of pulsed neutron diffraction to measure strain in composites; M.A.M. Bourke, J.A. Goldstone et al, pp. 539-548, Proceedings of fourth international conference on residual stress, Published by S.E.M. (1994).

Instrument Used: (please type) NPD	Local Contact M.R. Fitzsimmons	Proposal Number: <i>(for LANSCE Use Only)</i> 6067
Title: Test of a Boron-Phosphide Neutron Detector		Report received: <i>(for LANSCE Use Only)</i> 3/8/94
Authors and affiliations: M.R. Fitzsimmons, LANSCE, LANL J. Lund, Radiation Monitoring Devices, Inc, MA		
Experiment report: <p>We tested a boron-phosphide (BP) solid state neutron detector. The detector consisted of a 12mm thick single crystal film of BP grown on silicon. The BP-silicon interface formed an ohmic contact as did the aluminum contact to the silicon substrate. A Schottky barrier at the interface between the surface of the BP film and a gold contact provided the rectifying barrier used to measure charges produced during the conversion of boron to lithium and α-particles. Curve (a) in Fig. 1 shows the intensity measured by the BP detector as a function of time-of-flight. Curve (b) is the intensity measured by the detector after the neutrons are absorbed by a one centimeter thick piece of boron-nitride. The oscillation in curves (a) and (b) are believed to be the result of grounding loops at the instrument. The difference between these curves is shown as curve (c) and represents the neutron spectrum measured by the BP detector. The similarity of curve (c) in Fig. 1 to the spectrum measured by a conventional BF₃ gas detector (Fig. 2) suggests that semiconducting BP can be used to detect neutrons.</p>		

Experiment report (continued):

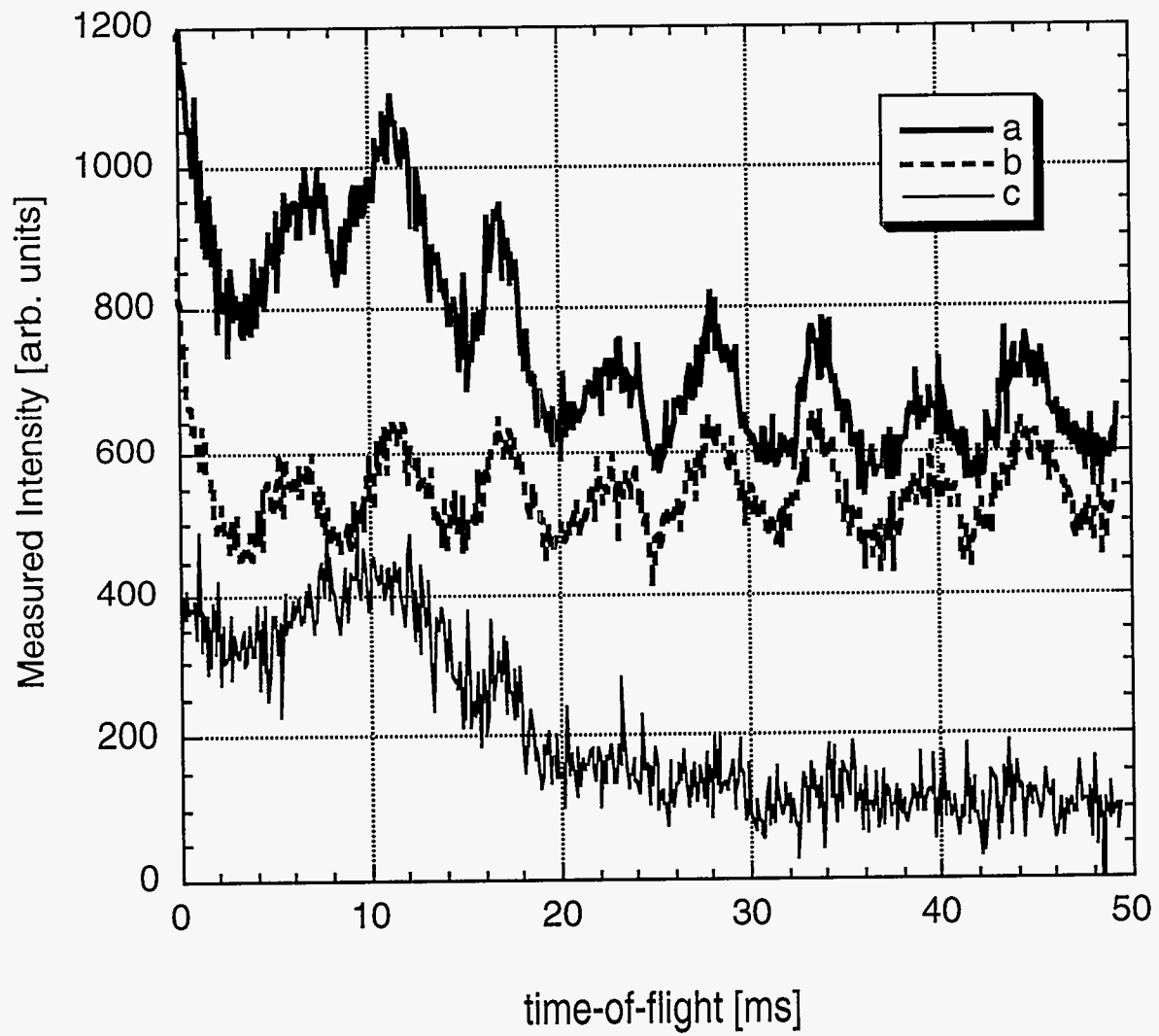


Fig. 1

References:

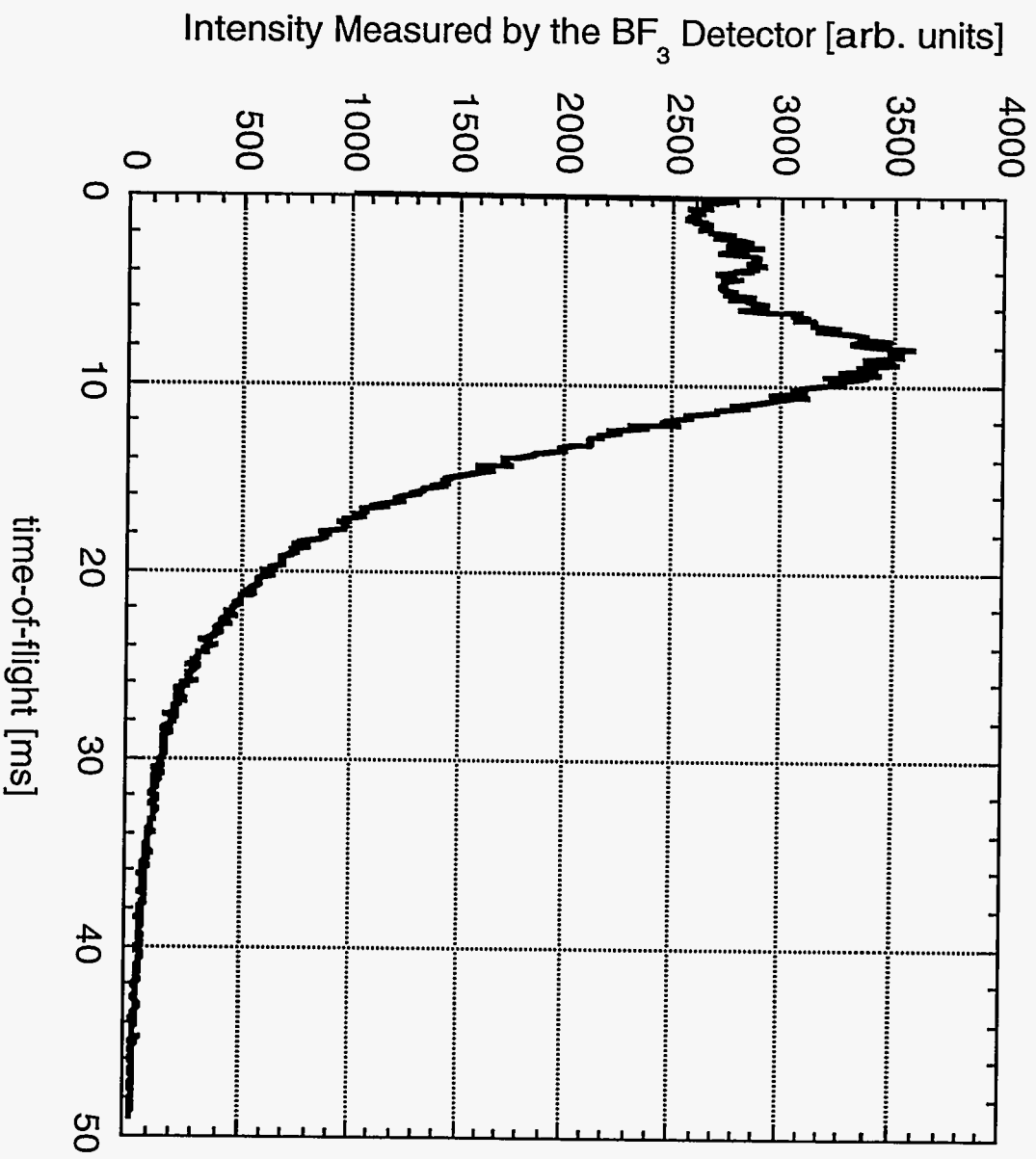


Fig. 2

Instrument used: <i>(please type)</i> NPD	Local contact: N. Shi	Propos al number: <i>(for LANSCE use only)</i> 6076
Title: Implications of the Morphology of the Evolution of Elastic Macro-Strain in a Metal Matrix Composite		Report received: <i>(for LANSCE use only)</i> 4/12/94
Authors and affiliations: N. Shi, CMS/LANSCE, MS H805, 7-2944; M.A.M. Bourke, MTL-5/LANSCE, MS H805, 5-1386; J.A. Goldstone, LANSCE, MS H805, 7-3629; J.E. Allison, Ford Motor Co., (313)845-7224.		
<p>Experiment report:</p> <p>Unlike a single-phase material, the load-induced average elastic strain (elastic macro-strain) in a two-phase material may be nonlinear with the applied load [1]. It was found that the tangent of the curve of elastic macro-strain vs. applied stress in a multiphase composite is a function of not only the elastic properties of each phase, but also load sharing between phases, i.e. the ratio of stresses between the reinforcement and the matrix. Recent analytical and numerical analyses suggest that [1] the slope of the curve of a uniaxial stress vs. elastic macro-strain can be rigorously expressed as the following:</p> $\text{slope} = \frac{(\lambda_{matrix} + 2G_{matrix})[1 + f(R-1)]}{1 + f\left[\frac{R}{E_{particle}}(\lambda_{matrix} + 2G_{matrix}) - 1\right]} \quad (1)$ <p>where f is the reinforcement volume fraction, G, E and λ are the elastic constants of the individual phases, R is the load sharing ratio, i.e. the ratio between the change of stresses in the reinforcement and the matrix ($\Delta\sigma_{zz}^r/\Delta\sigma_{zz}^m$) as induced by an increment of applied stress. In a composite, the individual phases elastic properties are independent of the applied load. Therefore, the slope changes only with the load sharing ratio "R." It can be further shown that the slope increase with the load sharing ratio, R, when the ratio of Young's modulus between the reinforcement and the matrix is approximately greater than 0.5. A significant implication of this finding is that the onset of reinforcement fracture may be identified during loading since fracture of reinforcement will relief load from the reinforcement, whereas matrix plastic flow will induce transfer of load to the reinforcement.</p> <p>In 1993, we have measured the evolution of elastic macro-strain of a 2080 Al reinforced by 15 vol. pct SiC particulates. Figure 1 displays the evolution of the elastic macro-strain from averaging of the lattice phase-strain obtained from Rietveld refinement. The sample was loaded in steps of 50 MPa (10 MPa intervals when the applied stress is greater than 450 MPa). At the end of each steps, neutron diffraction data was taken, and the sample was put into a constant-stress control mode (rather than a constant cross-head displacement control) to minimize creep-induced relaxation of applied stress. Each data acquisition step took about four hours. From Figure 1, the following is observed during loading:</p>		

Experiment report (continued):

When the applied load is lower than about 350 MPa, the elastic macro-strain remains approximately linear to the applied load; At about 350 MPa, the slope increases; At about 440 MPa, the slope decreases again.

Based on the prediction by Eq. (1), we propose that the following physical process takes place during loading. When the applied load is small, the matrix remain largely elastic and no significant internal stress redistribution takes place during this period, this warrants a linear relationship between the applied load and the elastic macro-strain. As a significant part of the matrix in the composite starts to plastically yield (350 MPa), the matrix becomes more compliant and load is transferred to the reinforcement. From Eq. (1), this is accompanied by an increase of slope.

Figure 1 displays this increase of slope as marked by "Plastic Flow." As the applied load further increases (440 MPa), fracture of brittle SiC reinforcement is inevitable [2]. These fractured particles, then, are released from load-carrying process, and, in contrast to matrix plastic flow, load is transferred back to the matrix. As predicted by Eq. (1), such a process is accompanied by a decrease of slope. This decrease of slope is marked by "Particle Fracture" in Fig. 1.

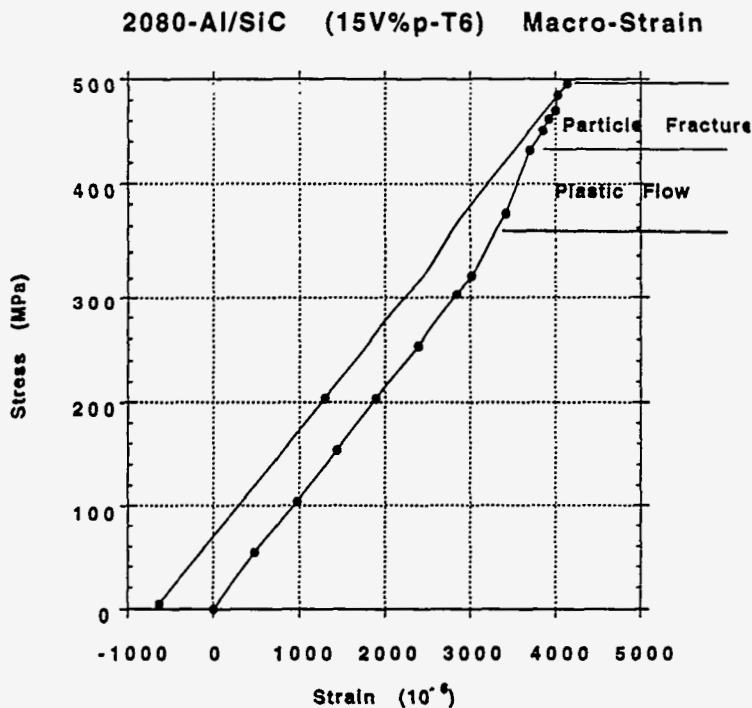


Figure 1: Evolution of the elastic macro-strain with the applied load. The elastic macro-strain is derived from averaging of lattice phase-strain obtained from Rietveld refinement.

One other aspect that is important in understanding the changes of slope is the role of anelastic relaxation during neutron data acquisition. First, the 2080 Al/SiC composite did not experience

significant anelastic relaxation as evidenced by the fact that no significant time-dependent deformation was observed during the iso-stress holding for neutron diffraction measurement. Second, a separate measurement of the 6091 Al matrix composite on the anelastic relaxation shows that a progressive anelastic relaxation will induce further increase of slope. Therefore, the decrease of slope at applied stress greater than 440 MPa may best be described by reinforcement fracture.

References:

1. N. Shi, M.A.M. Bourke, J.A. Goldstone, to be submitted.
2. P.M. Mummery, B. Derby, C.B. Scruby, *Acta metall. mater.* **41**, 1431 (1993).

Instrument used: <i>(please type)</i> NPD	Local contact: M.A.M. Bourke J.A. Goldstone	Proposal number: <i>(for LANSCE use only)</i> 6077
Title: Internal Strain Measurements of Bulk and Reinforced NiTi Shape Memory Alloys		Report received: <i>(for LANSCE use only)</i> 12/8/93
Authors and affiliations: D.C. Dunand and D. Mari* Department of Materials Science and Engineering, Massachusetts Institute of Technology, Cambridge, MA 02139 * currently at Amysa, 10 route de Lausanne, 1400 Yverdon, Switzerland M.A.M. Bourke and J.A. Goldstone LANSCE, Los Alamos National Laboratory, Los Alamos, NM 87545		
Experiment report: <u>Introduction</u> - The shape-memory intermetallic alloy NiTi exhibits a thermoelastic phase transformation near room-temperature. When deformed in the low-temperature martensitic phase, NiTi exhibits large strains as the result of twinning and reorientation of martensite variants. These strains can be fully recovered by heating above the transformation temperature and cooling the resulting austenite back to the martensitic structure, a phenomenon called "shape memory effect". The introduction of an elastic, non-transforming phase such as TiC in a NiTi matrix is expected to induce large internal stresses as a result of the strain incompatibility between the two phases during deformation and transformation. Since both twinning and shape memory are sensitive to stresses, the purpose of the experiment is to investigate the effect of internal stresses on these properties in deformed NiTi-TiC composites, by measuring elastic internal strains by neutron diffraction. <u>Experimental Procedures</u> - Bulk martensitic NiTi samples (containing 0 and 20 vol% TiC particles), as well as control powder samples of NiTi, TiC and NiTi-20vol%TiC contained in vanadium cans were investigated by neutron diffraction in the Neutron Powder Diffractometer (NPD). The two annealed bulk samples were outfitted with strain-gauges and subjected to a complete compressive loading-unloading cycle in the NPD mechanical rig. Neutron diffraction measurements were made to measure the lattice strains parallel and perpendicular to the following applied compressive stresses: -3 MPa, -100 MPa, -210 MPa, -280 MPa, -100 MPa and -3 MPa. Furthermore, the unloaded samples were examined after shape-memory recovery of the macroscopic anelastic compressive strains by applying a 5 minute anneal at 150 °C. <u>Results and Discussion</u> - Two phenomena take place upon mechanical loading of martensitic NiTi: (i) elastic deformation and (ii) twinning and reorientation of martensite, resulting in a "pseudo-plastic" deformation that can be recovered upon cycling above the phase transformation temperature. Figures 1a and b show the material behavior during loading. Below 100 MPa, both NiTi and NiTi-TiC exhibit elastic behavior, as measured from strain gauges. However, comparison with lattice strains in the loading direction measured by neutron diffraction shows that the strain gauge strains are much larger, resulting in a low apparent modulus of 60 to 66 GPa for NiTi-TiC and NiTi, as compared to neutron moduli of between 100 and 150 GPa. It is concluded that twinning deformation takes place at very low stresses. Above 100 MPa, where twinning plasticity is observed macroscopically, load is transferred in NiTi to certain plane families as variant reorientation occurs: diffraction peak intensities (Fig. 2a)		

show that the fraction of variants with (100) and (011) planes perpendicular to load decreases and increases, respectively. The opposite phenomenon is observed for these same planes oriented parallel to load. Comparing NiTi to NiTi-TiC, variant reorientation is enhanced in the composite (Fig. 2b), while the lattice strains at the maximum loading are decreased (Fig. 1b), indicative that the reinforcement is carrying some of the load. As seen from the curvature of stress vs strain data in Fig. 1b, most planes transfer load to the reinforcement with increasing load, and, at the highest load, planes (-121) and (021) actually shed load upon stressing of the composite.

Unloading curves show purely linear behavior, resulting in residual strains after unloading that are, relative to the starting state of the material, both positive and negative depending on the crystallographic planes. The planes also tend to revert towards their annealed intensity (Figs. 2), indicating that moderate reverse twinning is taking place, as also observed in the macroscopic strain measured by the strain gauge. This phenomenon is more marked in the unreinforced samples showing that the TiC reinforcement prevents recovery upon mechanical unloading.

After shape-memory recovery, the sample recovers macroscopically most of its deformation, while the stresses on different crystallographic planes are on average reduced, and near zero. Also, both samples exhibit peak intensities for all planes near or below their initial anneal value, the largest difference being the reorientation of plane (100).

In summary, the strains in different planes of martensitic NiTi and NiTi-TiC have been measured by neutron diffraction as a function of external loading. Load transfer in the composite is observed; furthermore, in both samples, twinning is recorded, resulting in preferential orientation of some of the planes perpendicular or parallel to the macroscopic stress. Upon shape-memory recovery of both samples, stresses and plane orientations are recovered at the microscopic level.

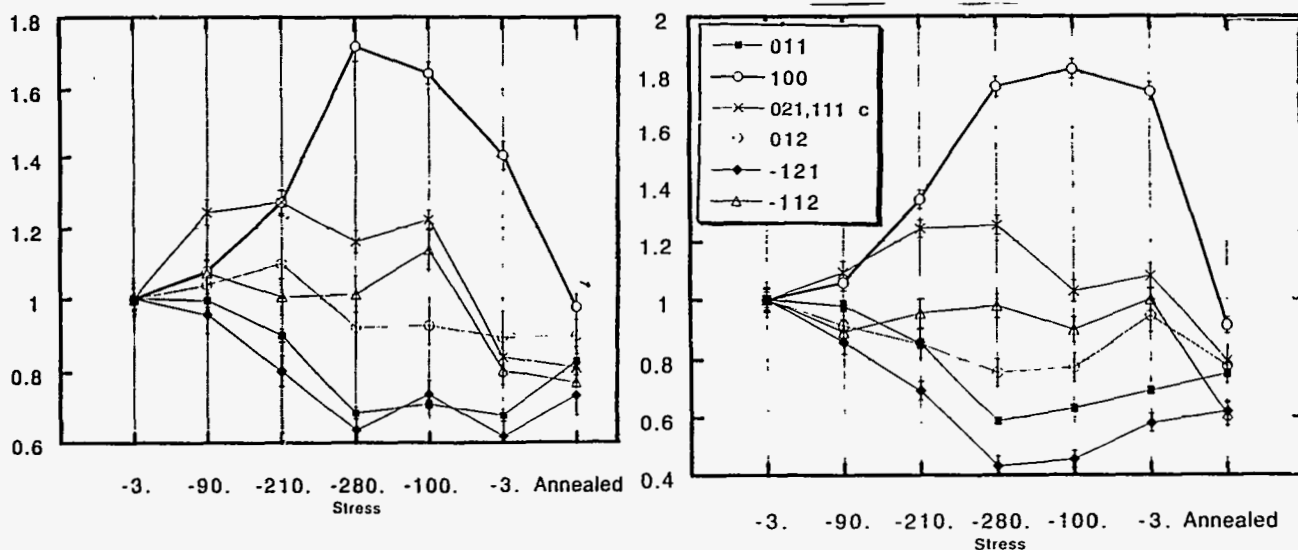


Fig. 2a and b - Normalized peak intensity as a function of applied stress for NiTi and NiTi-TiC

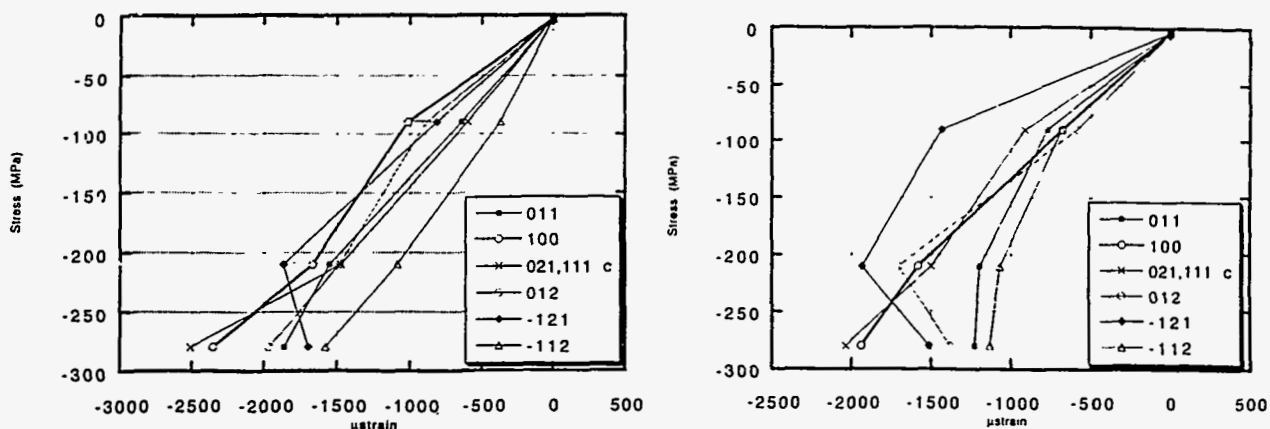
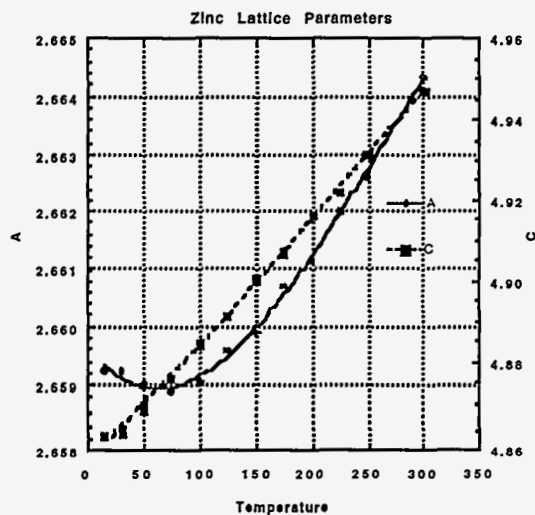


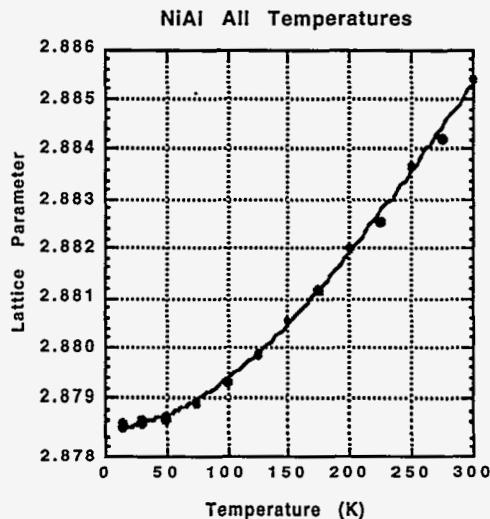
Fig. 1a and b - Applied Stress as a function of lattice strains for NiTi and NiTi-TiC

Instrument Used: <i>(please type)</i> <p style="text-align: center;">NPD</p>	Local Contact <p style="text-align: center;">Joyce A. Goldstone</p>	Proposal Number: <i>(for LANSCE Use Only)</i> <p style="text-align: center;">6098</p>
Title: <p>Elastic Constant Determination in Zinc and NiAl by Neutron Diffraction</p>		Report received: <i>(for LANSCE Use Only)</i> <p style="text-align: center;">3/15/94</p>
Authors and affiliations: <p>Joyce A. Goldstone, LANSCE, H805, Los Alamos Natl. Lab, Los Alamos, NM 87545</p> <p>Andrew C. Lawson, MTL-5, H805, Los Alamos Natl. Lab, Los Alamos, NM 87545</p> <p>James D. Cotton, MTL-6, G770, Los Alamos Natl. Lab, Los Alamos, NM 87545</p>		
Experiment report: <p>We have had success using neutron diffraction for the measurement of isotropic Debye-Waller factors. [1] Proving the validity of this technique for anisotropic materials is important. In many materials, the atomic sites do not have cubic symmetry, even in cubic materials. In particular, we have in the past assumed isotropic values for hydrogen atoms sitting in tetrahedral or octahedral sites in the cubic hydrides. Most actinide materials crystallize in anisotropic structures and undergo multiple phase changes to other anisotropic structures. Examining the variations in anisotropic Debye-Waller factors through these phase transitions can give important clues about the driving forces for these structural changes. To validate the anisotropic approach, this year we conducted careful Debye-Waller measurements on an anisotropic material for which the elastic constants are well known and highly anisotropic, namely zinc. In addition we looked at a simple cubic binary alloy, NiAl.</p> <p>Data were collected on the NPD at several temperatures, 10K to 300K, using a closed cycle helium refrigerator and automatic temperature control to ± 1K. All data were analyzed using Rietveld refinement of the Generalized Structure Analysis System (GSAS) developed at LANSCE. Care was taken to use the correct background function -- one that correctly models the physics of the background scattering and thus is temperature independent. [2]. The figures below show the lattice parameters and thermal parameters for zinc and NiAl as a function of temperature. The thermal parameter data are fit to a model [1], which requires fitting a Debye-Waller temperature and offset for atom to a single Debye formula. Thus in the case of zinc, the anisotropic Debye temperatures are obtained for the two crystallographic directions, while for NiAl, the Debye temperatures for Ni and Al are obtained. For zinc the values are 260(1)K for the a-axis and 163.4(3)K for the c-axis. For NiAl, the values obtained are 335(1)K for Ni and 596(5)K for Al.</p> <p>One important reason for studying zinc is that anisotropy is large. The c_{11} constant is 165 GPa and the c_{33} constant is 61.8 GPa. [3] According to the model presented in reference [1], the Debye-Waller temperature is proportional to the square root of the elastic constant. For the case of zinc, $c_{11}/c_{33} = 2.67$ and $(\langle E^a_{DW} \rangle / \langle E^c_{DW} \rangle)^2 = 2.54$, which is good agreement. Thus measurement of the temperature dependence of thermal parameters offer a good alternate for obtaining the anisotropy of elastic constants in polycrystalline materials. In particular for radioactive materials that require containment this technique is possibly the easiest method for gaining this information.</p> <p>For the NiAl, the Debye temperatures reported here are significantly different from the elemental Debye temperatures. For nickel, the reported Debye temperature is 450K and for aluminum it is 428K. The bulk modulus for NiAl is 193 GPa. [4] This value gives an average Debye temperature of 590K.</p>		

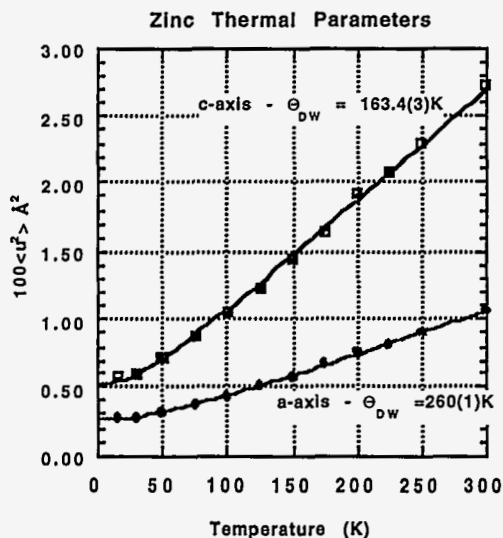
Experiment report (continued):



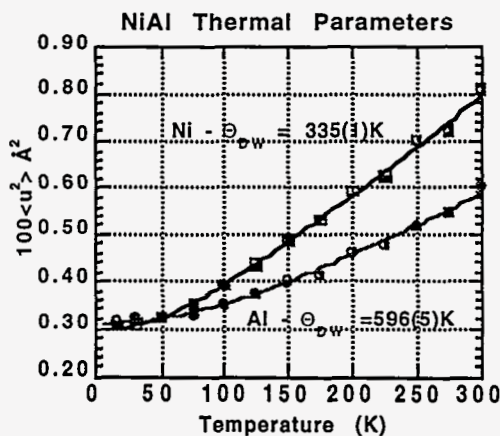
Variation of the lattice parameters of zinc as a function of temperature. The lines through the data are cubic polynomial fit



Variation of the lattice parameter of NiAl as a function of temperature. The line through the data is cubic polynomial fit.



Thermal parameters of zinc in the a and c lattice directions. Data have been fit to the equation in ref [1] to obtain the Debye temperature for each lattice direction.



Thermal parameters of NiAl for both Ni and Al. Data have been fit to the equation in ref [1] to obtain the Debye temperature for each element.

References:

- [1] "Elastic Properties of Materials by Pulsed Neutron Diffraction" A. C. Lawson, A. Williams, J. A. Goldstone, D. T. Eash, R. J. Martinez, J. I. Archuleta, D. J. Martinez, B. Cort, and M. F. Stevens, *J. Less-Common Metals* 167 (1991) 353-363.
- [2] A. C. Lawson, J.A. Goldstone, B. Cort, and R. B. Von Dreele, "Debye-Waller Factors of α -Plutonium", LANSCE Experiment Reports, 1992 Run Cycle, LA-12647-PR, p.46.
- [3] G. Grimvall, *Thermophysical Properties of Matter*, (North-Holland, Amsterdam, 1986).
- [4] R. D. Noebe, R. R. Bowman, and M. V. Nathal, "Physical and Mechanical Properties of the B2 compound, NiAl", *International Materials Reviews*, 38 (1993) 193.

Instrument used: <i>(please type)</i> NPD	Local contact: R.A. Robinson	Proposal number: <i>(for LANSCE use only)</i> 6100
Title: Structure of the Super-Heavy-Fermion Compound YbBiPt		Report received: <i>(for LANSCE use only)</i> 3/30/94
Authors and affiliations: R. A. Robinson, LANSCE, LANL A. Purwanto, LANSCE, LANL & NMSU P. C. Canfield, Ames Laboratory		
Experiment report: The cubic intermetallic compound YbBiPt[1,2] has the largest electronic specific heat of any heavy fermion compound: $\gamma = 8 \text{ Jmol}^{-1}\text{K}^{-2}$, and order of magnitude more than that of typical heavy fermion compounds like UPt_3 . It crystallises in the Cl_b or MgAgAs structure type (with space group F43m), which is a common Heusler-alloy structure. There is one formula unit per unit cell and the atoms are distributed on 3 of the 4 sites along the [111] body diagonal. The sequence is not arbitrary in that one site is vacant, two have vacancies as nearest neighbours and the final site is <i>special</i> in that it has no vacant nearest-neighbour sites. The previous x-ray study[2] reported that Bi was on the special site, and to date, two band-structure calculations have assumed this sequence. However, refinement of room temperature data taken on NPD (see Fig. 1) indicates that Pt is on the special site: With Pt special we get reduced $\chi^2 = 1.554$, while with Bi special $\chi^2 = 1.751$. This makes more sense from a chemical and atomic size point of view, as the Pt ion is smaller than Bi. We also find approximately 8% elemental Bi in the sample, and this not altogether surprising as the sample was grown from a bismuth flux. However, this is more important than one might think at first. A long-standing puzzle has been the fact that the high-temperature magnetic susceptibility is significantly lower than that one could obtain from the full Hund's rule moment for Yb^{3+} . Our data indicate that this discrepancy is partly due to miscalculation of molarities, as a consequence of the Bi impurity. In fact, the structure on YbBiPt turns out to be closely related to that of Bi, which is rhombohedral, as shown in Fig. 2. If the x parameter were 0.25 rather than 0.23, and the rhombohedral c/a ratio was $\sqrt{6} = 2.449$ rather than 2.608, then Bi would be cubic. Then, if half the Bi atoms were systematically replaced with Yb, one would have the fictitious rock-salt structure compound YbBi. Finally, the smaller Pt atom can be inserted into half of the "vacant" sites as an interstitial to give the true MgAgAs structure for YbBiPt.		

Experiment report (continued):

Finally, there is evidence from inelastic neutron scattering experiments on the crystal-field levels of Yb^{3+} that the symmetry is lower than cubic. We searched very carefully for both rhombohedral and tetragonal distortions, and also intra-cell rhombohedral displacements, but have no evidence for any such symmetry breaking.

This work has been submitted for publication in Phys. Rev. B. [3]

Figure 1

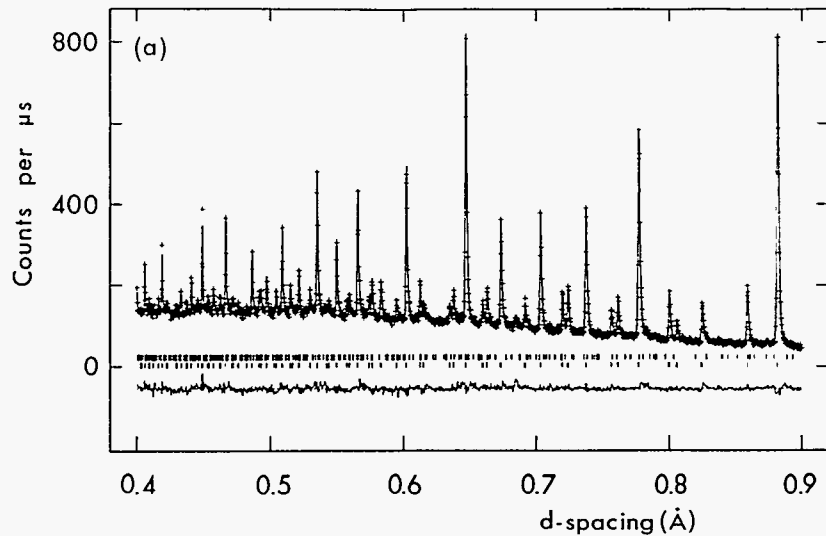
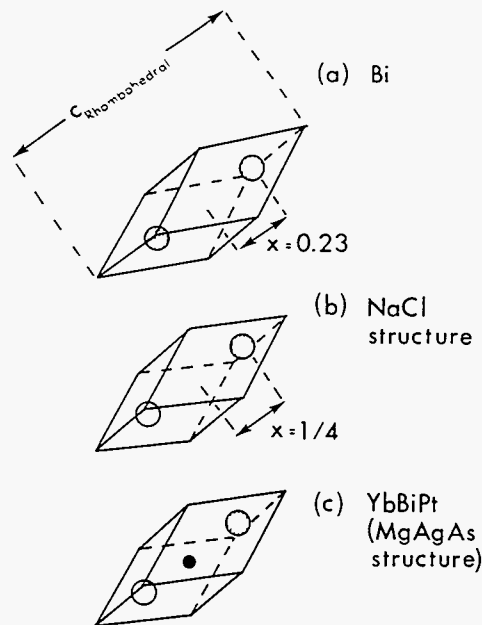


Figure 2



References:

- [1] P. C. Canfield, J. D. Thompson, W. P. Beyermann, A. Lacerda, M. F. Hundley, E. Peterson, Z. Fisk and H. R. Ott, J. Appl. Phys. 70, 5800 (1991).
- [2] Z. Fisk, P. C. Canfield, W. P. Beyermann, J. D. Thompson, M. F. Hundley, H. R. Ott, E. Felder, M. B. Maple, M. A. Lopez de la Torre, P. Visani and C. Seaman, Phys. Rev. Lett. 67, 3310 (1991).
- [3] R. A. Robinson, A. Purwanto, M. Kohgi, P. C. Canfield, T. Kamiyama, T. Ishigaki, J. W. Lynn, R. Erwin and E. Peterson, submitted to Phys. Rev. B, Los Alamos preprint LA-UR-94-727.

Instrument used: <i>(please type)</i> NPD	Local contact: Dr. M. A. M. Bourke	Proposal number: <i>(for LANSCE use only)</i> 6104
Title: Strains in Alumina/Silicon Carbide Composites and Nanocomposites		Report received: <i>(for LANSCE use only)</i> 4/12/94
<p>Authors and affiliations:</p> <p style="text-align: center;">R. I. Todd</p> <p style="text-align: center;">University of Oxford, Department of Materials, Parks Rd., Oxford, OX1 3PH, UK</p> <p style="text-align: center;">From 13/6/94: The Manchester Materials Science Centre, Grosvenor St., Manchester, M1 7HS, UK</p>		
<p>Experiment report:</p> <p>A number of subjects were investigated within the unifying theme of discontinuously reinforced ceramic-ceramic composites. A summary of the main conclusions follows.</p> <p><u>1. Derivation of Measured Strain Distributions from Peak Shape Changes.</u> There are two aspects to this technique: (i) deconvolution of 'pure' diffraction peaks for the composite using peaks from a strain free reference specimen, and (ii) interpretation of the results in terms of the measured strain distribution function (MSD). Both were investigated. Pure diffraction peaks were successfully deconvolved for the matrices of Al₂O₃/30vol% SiC_p (3µm) microcomposite, Al₂O₃/30vol% SiC_p (200nm) nanocomposite and Al₂O₃/20vol% SiC_p (200nm) nanocomposite specimens. The success of the deconvolution method used [1] depends critically on the broadening of the composite peak relative to the corresponding peak from the unstrained reference specimen, and as a result it was not possible to obtain similar results for lower volume fractions of SiC, or for the SiC phase.</p> <p>The strains in the microcomposite specimen have previously been examined using the HRPD on the ISIS spallation source (UK), and although the quality of the pure diffraction peaks deconvolved using the NPD was lower owing to its lower resolution, there was a high degree of agreement between the peaks obtained from the two instruments.</p> <p>For the pure diffraction peak to be interpreted directly in terms of the MSD, the MSD derived from different orders of the same reflection, or simply from different peaks for isotropic cases, must be the same, which is equivalent to there being no difference in particle size broadening between the reference specimen and the composite specimen [2]. In addition, the MSDs from microcomposites, in which the spacing of the reinforcement is about the same as the diffracting domain size, and from nanocomposites with the same composition, in which the reinforcement spacing is less than the domain size, should have the same shape. Both of these requirements were borne out in all cases by the results.</p> <p>It is of great interest that there is no extra particle size broadening in the composite matrix compared to the reference specimen. Methods which attempt to analyse diffraction peak broadening in composites by assuming the measured strain distribution to be Gaussian invariably conclude that a significant proportion of the broadening is caused by the particle size effect, and deduce suspiciously small domain sizes. The present results show that such methods are invalid, and make clear the reason for their failure, viz. the MSDs were found to be markedly non-Gaussian. This is not surprising, since elastic models for the matrix strains predict non-Gaussian MSDs[1].</p>		

Experiment report (continued):

2. Internal Stresses in Al_2O_3/SiC_p Nanocomposites Significant mechanical property improvements over monolithic alumina have been reported for these materials, and many of the suggested mechanisms to explain these depend on thermal mismatch internal stresses. The average strains in uniaxially hot pressed (25MPa, 1700°C) nanocomposites containing 4, 12, 24 and 35 vol% 200nm SiC were measured. The variation of the strain in both phases had the variation with volume fraction predicted by elastic models, and corresponded to a relaxation free temperature drop of 1650°C. The strains in the SiC corresponded to hydrostatic stresses of ~1.5GPa.

The strains were 25% higher than those found in similar microcomposites (3 μ m SiC). This may be because most of the SiC in the nanocomposites resides within the alumina grains, and therefore requires volume diffusion rather than grain boundary diffusion to relax the stresses by diffusion, and because the nucleation of prismatic dislocation loops around the particles should be inhibited by their small size.

The average strains in both phases were ~15% greater in the plane of the hot pressed discs used, presumably because of alignment of slightly elongated particles in this direction. The strains from individual reflections in the alumina matrix ranked in the order expected from the anisotropy in Young's modulus.

3. Internal Stresses in $Al_2O_3/20\%TiN_p$ Nanocomposites The strains measured in both phases were large (~1000 μ s) and positive. This is clearly a spurious result since the force balance between the two phases is not satisfied. In addition, the peak shapes from the alumina reference specimen and the corresponding peaks in the composite were almost identical, showing none of the characteristic strain broadening of other systems. The most likely explanation for these effects is a reaction between the two phases, and the investigation is continuing using TEM in Oxford.

4. Influence of Heat Treatment on Internal Stresses in Al_2O_3/SiC Whisker Composites The stress levels in specimens air quenched from 1600°C were 16% higher than in furnace cooled specimens. It is hoped to compare the toughness of the two materials to determine the effect of the residual stress level on the mechanical properties directly. The average strains were greater in the plane of the hot pressed plates, presumably because of the alignment of the SiC whiskers in that direction.

5. Internal Stresses in Al_2O_3/SiC Platelet Composite The stress levels measured were about half as big as in the corresponding SiC particle and whisker reinforced composites. This may be the result of microcracking caused by the large diameter (70 μ m) of the platelets. Ceramographic and mechanical studies of the material are being carried out.

6. Internal Stresses in Monolithic Alumina The strains normal to the {006} and {300} planes have been measured in a hot pressed alumina disc. It is hoped to relate these to an elastic model for the strains caused by the thermal expansion anisotropy for alumina, and to assess the extent of any texture caused by hot pressing.

References:

1. R. I. Todd & B. Derby, in "Residual Stresses in Composites", E. V. Barrera and I. Dutta (eds.), p.147, TMS-AIME, Warrendale, PA, 1993
2. R. I. Todd and B. Derby, accepted for publication in proc. ICRS-4, June 1994, Baltimore, MD

Instrument Used: <i>(please type)</i> <p style="text-align: center;">NPD</p>	Local Contact <p style="text-align: center;">Joyce A. Goldstone</p>	Proposal Number: <i>(for LANSCE Use Only)</i> <p style="text-align: center;">6406</p>															
Title: In-Situ Measurement of Elastic Strains at High Temperature and under Load in Polycrystalline Materials		Report received: <i>(for LANSCE Use Only)</i> <p style="text-align: center;">11/14/94</p>															
Authors and affiliations: <table border="0" style="width: 100%;"> <tr> <td style="width: 25%;">Mark Bourke,</td> <td style="width: 25%;">MST-5/LANSCE</td> <td style="width: 50%;">MS H805, LANL, Los Alamos, NM 87545</td> </tr> <tr> <td>Joyce Goldstone</td> <td>LANSCE</td> <td>MS H805, LANL, Los Alamos, NM 87545</td> </tr> <tr> <td>Ning Shi</td> <td>CMS/LANSCE</td> <td>MS H805, LANL, Los Alamos, NM 87545</td> </tr> <tr> <td>Andrew Lawson</td> <td>MST-5,</td> <td>MS H805, LANL, Los Alamos, NM 87545</td> </tr> <tr> <td>John Allison,</td> <td>Ford Motor Co.</td> <td>MD 3182, Research Laboratory , 20000 Rotunda Drive Dearborn, MI 48121-2053</td> </tr> </table>			Mark Bourke,	MST-5/LANSCE	MS H805, LANL, Los Alamos, NM 87545	Joyce Goldstone	LANSCE	MS H805, LANL, Los Alamos, NM 87545	Ning Shi	CMS/LANSCE	MS H805, LANL, Los Alamos, NM 87545	Andrew Lawson	MST-5,	MS H805, LANL, Los Alamos, NM 87545	John Allison,	Ford Motor Co.	MD 3182, Research Laboratory , 20000 Rotunda Drive Dearborn, MI 48121-2053
Mark Bourke,	MST-5/LANSCE	MS H805, LANL, Los Alamos, NM 87545															
Joyce Goldstone	LANSCE	MS H805, LANL, Los Alamos, NM 87545															
Ning Shi	CMS/LANSCE	MS H805, LANL, Los Alamos, NM 87545															
Andrew Lawson	MST-5,	MS H805, LANL, Los Alamos, NM 87545															
John Allison,	Ford Motor Co.	MD 3182, Research Laboratory , 20000 Rotunda Drive Dearborn, MI 48121-2053															
Experiment report: <p>Measuring phase strains during the static load tests has provided insight into the mechanisms and onset of load transfer in metal matrix composite materials. Since diffraction measure <i>elastic</i> strains nonlinearity in plots of applied loading vs. elastic strain for individual phases in composite materials indicates load transfer. Although observed nonlinearities do not unambiguously distinguish between possible deformation mechanisms, it does provide a test for material models¹. Using a stress rig on the NPD all lattice reflections in a specimen are recorded simultaneously, corresponding to strain directions parallel and perpendicular to an applied load. In this experiment we demonstrated simultaneous high temperature and applied load measurements are possible and that in at least one situation creep relaxation measurements are possible.</p> <p>The perennial metal matrix material AlSiC has many potential applications in the automobile industry, including connecting rods, brake rotors or drive shafts all of which may see sustained or periodic temperature fluctuations. To examine its high temperature behavior, a uniaxial tension specimen of a 15 vol% SiC Al material (DWA) was heated using 1" long (125W) cartridge heaters. The sample was 160 mm long with a circular cross section and a diameter at the gauge section of 10 mm. Only a 14 mm length was irradiated by the neutron beam which was controlled at 110°C (although the ends were hotter). The specimen was surrounded by a vanadium heat shield.</p> <p>Figure 1 shows the data during both load and unload; for clarity only a few reflections are given. The inset shows the macroscopic strain recorded using a strain gauge. Measurements were made at static loads and took approximately 4 hours. Above 200 MPa the sample was creeping over the duration of each stress level. On unload the aluminum reflections were left slightly in tension ($\approx 100\mu\epsilon$) relative to the starting state of the material and the silicon carbide in compression ($< -100\mu\epsilon$). Apart from the Al 200, not surprisingly the unloaded residual strains were small compared to equivalent tests performed at room temperature to the same final plastic strain. Although small the sign of the residual strains suggests that diffusional rather than plastic relaxation of the aluminum occurred. Further analysis of the morphology of the loading curves may allow inferences about the material deformation².</p> <p>In figure 1 the strains reported correspond to one measurement at each stress level, however in reality the elastic strains may evolve over the duration of a measurement at each load. This evolution at temperature at a given load has been recorded in an aluminum Al2219 alloy (T6 condition) reinforced with 15 % vol. TiC particles. This material has no immediate applications but is an excellent system</p>																	

Experiment report (continued):

for comparison with numerical modeling by virtue of its microstructure with approximately spherical TiC particles (formed in-situ using the XD™ process) that possess clean interfaces and do not appear to fracture under either monotonic or cyclic loading. Previous room temperature measurements on this material have been compared to finite element (FE) modeling³. On examination of the strain contours in the model it was shown that the presence of thermal residual stress alters the strain field so that the site of matrix initial yielding changes which in turn alters the morphology of the loading curve.

To examine its creep behavior, a uniaxial tension specimen was used as described above. As in the previous example, the specimen was aligned so that strains parallel and perpendicular to the applied load were measured simultaneously. The sample was heated to 150°C then measured unloaded and at initial loads of 150 MPa, 200 MPa, and 225 MPa. At each load level data were collected at 40 minute intervals for approximately 4 hours. Although 40 minutes is not a long enough count to allow individual reflections to be fitted Rietveld refinement (using GSAS) of the overall patterns is more than adequate to allow the bulk phase behavior to be measured. Figure 2 shows the data for the lattice parameter of Al and TiC parallel to the loading direction. The test was performed under stroke control so that the stress decreases over the duration of a hold level resulting in a decrease in the elastic strains. Analysis of these data is not complete.

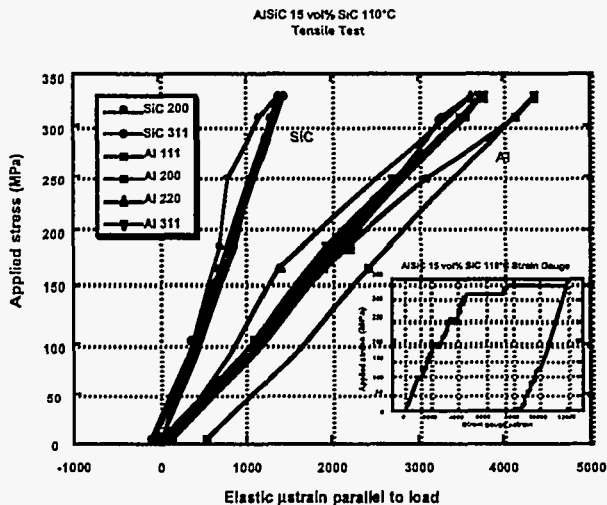


Figure 1: Strain relative to initial material state in a uniaxial tension test of a 15 vol% SiC Al 6091 (T6) particulate MMC

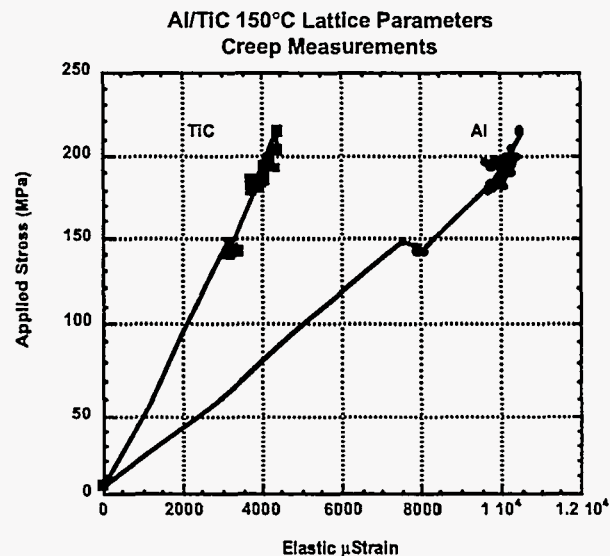


Figure 2: Parallel strain relative to initial material state in a uniaxial tension creep test of a 15 vol% TiC Al particulate MMC. Data were taken in 40 minute intervals at a given load.

References:

1. A. Allen, M. Bourke, S. Dawes, M. Hutchings, and P. Withers, *Acta Metall Mater.* **40**, 2361 (1992).
2. N. Shi, M. A. M. Bourke, and J. A. Goldstone, *Neutron Scattering in Materials Science, Symposium*, Boston Ma. Nov. 1994.
3. M. A. M Bourke, J.E. Allison, J. A. Goldstone, N. Shi, M. G. Stout, A. C. Lawson, *Scripta Met. Metall.* **29**, 771 (1993)

*Neutron Transmission
Flight Path (NTFP)*

Neutron Transmission Flight Path (NTFP)

The Neutron Transmission Flight Path (NTFP) is designed for transmission experiments in which a downstream detector measures the neutron intensity passing through a sample in the neutron beam. The flight path consists of a shielded cave that is approximately 2.5 m wide and 4.5 m deep along the beam path, the center of which is located about 7.75 m from the target moderator. Various experiment apparatus can be placed in this cave to accommodate samples and special sample environment equipment. Detectors can also be mounted in the cave. At the downstream end of the cave, a 0.75-m diameter, 45-m-long pipe extends along the beam path. This pipe can be evacuated and leads to a room in which detectors can be placed. With detectors approximately 59 m from the neutron moderator, a resolution of about 5×10^{-4} can be achieved in time-of-flight experiments.

NTFP Experiment Reports

6400	<i>Phonon Spectrum Information from Neutron Resonance Broadening</i>	142
6402	<i>Investigation of the Austenite-Bainite Transformation in Gray Iron Using Real-Time Neutron Transmission</i>	144

Instrument used: <i>(please type)</i> 56m Neutron Transmission Flight-Path	Local contact: Walter Trela	Proposal number: <i>(for LANSCE use only)</i> 6400
Title: Phonon Spectrum information from Neutron Resonance Broadening		Report received: <i>(for LANSCE use only)</i> 3/15/94
Authors and affiliations: Walter J Trela, P-17, MS H803 J Eric Lynn, P-17, MS H803 Kay Meggers, Kiel University, Germany Andrew C Lawson, MST-5, MS H805 Barbara Cort, NMT-5		
Experiment report: <p>Basic statistical information on the phonon frequency spectrum $g(\nu)$ of a material can be obtained from the study of narrow low energy neutron resonances of its atomic nuclei. Plutonium, for which single crystals suitable for neutron inelastic scattering measurements on a triple-axis spectrometer, is a prime candidate for Doppler broadening experiments. In the experiment undertaken here the aim was to measure the effective cross sections of a few of the resonances of plutonium isotopes over a range of temperatures and in sufficient detail to extract some of the low-order moments and "quasi-moments" of the phonon spectrum. ("Quasi-moments" are weighted by temperature dependent functions of the frequency). In these experiments the samples can be metallic foils or cylinders in normal micro-crystalline form, or even powders. It should be noted that Doppler broadening gives phonon information specific to the frequencies residing on the atom with the resonance cross section. Thus the method, if successful, could be applied to a range of alloys and other materials with suitable elemental constituents containing narrow neutron resonances.</p> <p>In the crudest approximation Doppler broadening is treated in a classical gas model. This gives rise to an effective cross-section in which the true nuclear cross section in the centre-of-mass frame is convoluted with a Gaussian function (of the energy transferred to or from the surrounding medium) with dispersion parameter related to the average recoil energy R given to the compound nucleus from the momentum of the bombarding neutron and the ambient temperature of the target material. In the next approximation, for a crystalline target, the temperature in the dispersion parameter is replaced by the mean energy of occupied oscillator states; this is the "quasi-moment" (of order 1)</p> $\langle h\nu \rangle_T = \int d\nu h\nu g(\nu) \coth(h\nu/2kT) \quad (1)$ <p>In practice, this approximation works quite well for neutron resonances measured at normal room temperatures and above, the difference between $\langle h\nu \rangle_T$ and kT being a few percent or less. Higher order approximations can be achieved by adding to</p>		

Experiment report (continued):

the Gaussian convolution function extra terms that are the products of Hermite polynomials (in the energy transfer to the crystal lattice) with the Gaussian. The coefficients of these can be expressed in terms of the moments and "quasi-moments" of the phonon frequency spectrum. Beyond the unadorned Gaussian, one may expect the "skew" and "kurtosis" terms (involving third and fourth order polynomials, respectively) to be significant. The coefficients of these terms can be expressed using the second phonon moment $\langle (h\nu)^2 \rangle$ and the quasi-moment of order 3.

Such expansions of the convolution function can be very accurate with a reasonably small number of terms (fewer than ten) except for resonances below a few eV. At these low energies a substantial fraction of the resonance cross section resides in a recoilless "line", the neutron analogue of gamma-ray Mossbauer spectra. The fraction of the resonance cross section in this recoilless profile is given by the Debye-Waller factor. The recoilless line arises from a delta function in the Doppler-broadening convolution function. The delta function is not amenable to a treatment based on moments. Hence such cases are best treated by first separating out the recoilless line and then treating the remainder of the convolution function by the moments method. It should be noted, however, that the Debye-Waller factor contains the quasi-moment of order -1, and hence also gives important information on the phonon spectrum. Indeed, this quantity has been extracted for this purpose from powder diffraction measurements in thermal neutron scattering.

It is the objective of this experiment to determine the first 3 or 4 moments (or quasi-moments) of the phonon spectrum of plutonium metal, stabilised in its delta phase by alloying with a few percent of lighter elements, from accurate measurements of the low energy neutron resonance total cross sections of the plutonium isotopes at different temperatures. The cross sections are measured by the transmission method. To make accurate measurements over resonance peaks and well down on to their wings, and to cover resonances of widely different peak cross-section, a broad range of sample thicknesses has to be used.

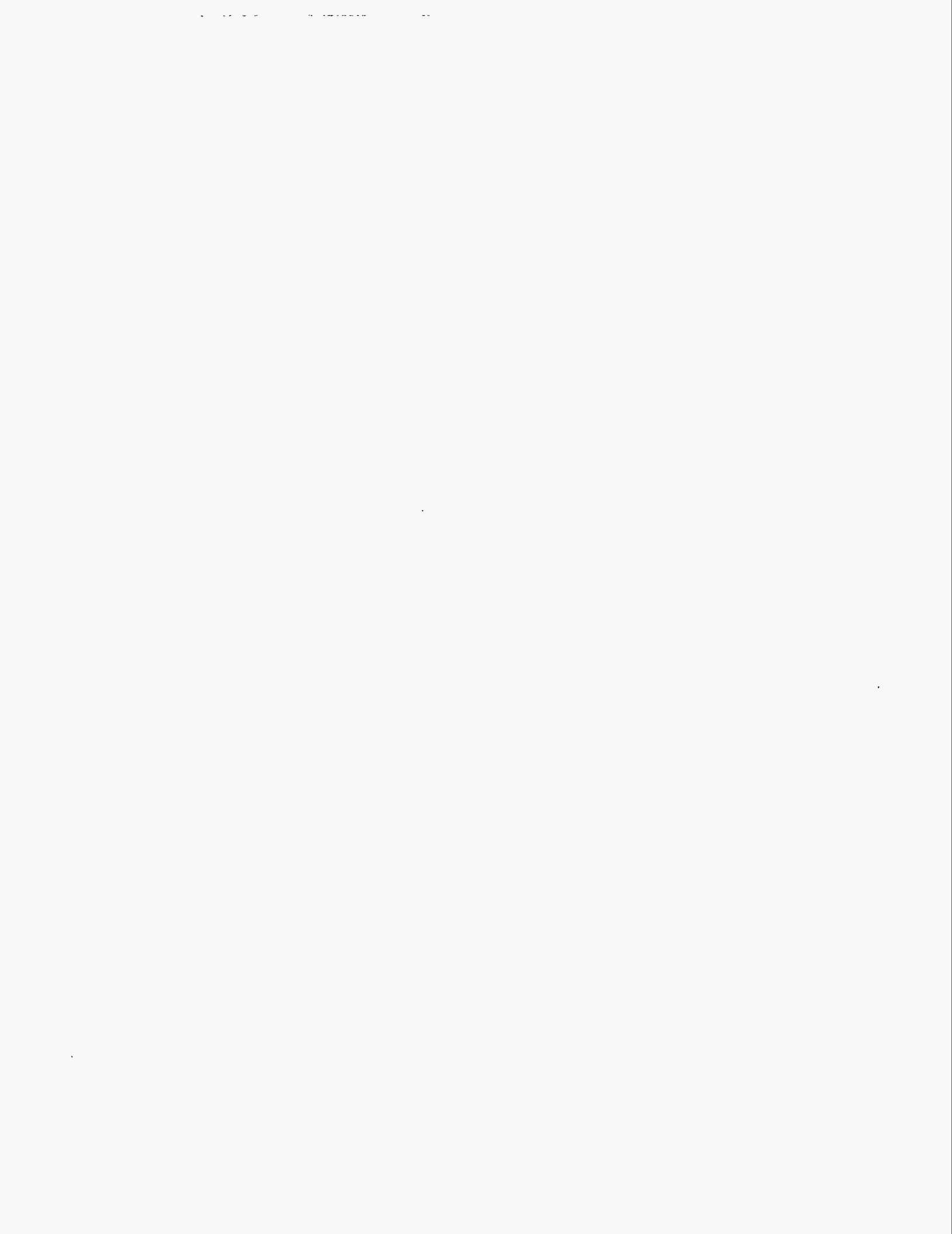
Owing to difficulties last year in obtaining and fabricating the plutonium samples required for these experiments, many fewer measurements than envisaged were completed in 1993. In fact data were obtained on only one sample giving information on the cross section over the centre of the 2.67 eV resonance of ^{242}Pu at several temperatures from 15 K upwards, but with inadequate data on the resonance wings. No data were acquired on other suitable resonances, such as the 1.04 eV resonance of ^{240}Pu . Background runs, open beam runs and runs suitable for calibration were completed. Also valuable data were acquired on a series of tantalum and tungsten metal samples; these will be used for "proof of principle" of the method. The large amount of data is taking considerable time to process. So far they have been tested for temperature equilibration over time, and consistent temperature-stable data sets have been obtained for each sample-temperature combination. Work on detailed fitting of the resonances, with careful treatment of background and resolution effects has now started.

Instrument used. <i>(please type)</i> Flight Path 5	Local contact: Walter Trela	Proposal number: <i>(for LANSCE use only)</i> 6402
Title: Investigation of the Austenite - Bainite Transformation in Gray Iron Using Real Time Neutron Transmission.		Report received: <i>(for LANSCE use only)</i> 3/30/94
<p>Authors and affiliations:</p> <p>Walter J. Trela/ Los Alamos National Laboratory Kay Meggers/ Kiel University, Kiel Germany Hans G. Priesmeyer/ Kiel University, Kiel Germany</p>		
<p>Experiment report:</p> <p>Nucleation and growth problems, so called TTT (time - temperature - transformation) processes, pervade much of materials research. However, the measurement of such processes remains largely unexplored. The determination of structure and the measurement of (e.g. study of quenched specimens or use of ambient structural data to interpret properties under extreme conditions), and usually with different specimens. We have developed a short burst neutron transmission technique that now allows investigation at many points of time during a phase transformation. Spectra are recorded continuously in-situ from a single sample.</p> <p>We have measured in-situ the decomposition of austenite (fcc structure) into bainite (bcc structure) within globulitic gray iron (3.6 wt.% C, 2.4 wt.% Si, and 0.45 wt.% Mn) in real time. This is a diffusion controlled, eutectoid solid state phase transformation. The measurement was accomplished by recording continuously 30 sec. transmission spectra of thermal neutrons from the sample. Our results show that the transformation follows the Avrami law (see figure 1.) during its intermediate stages (between 250 sec. and 500 sec.). However, for the Avrami law the transformation quickly reaches its completion, whereas we see the progression of the transformation break off after approximately 500 sec. Thereafter, the transformation proceeds slowly for the next 2500 sec. to about 80% completion and then stops.</p>		

Experiment report (*continued*):

The reason for this behavior is that the driving force for the transformation is not constant. At first the energy balance is dominated by the increase of free energy of the single atoms. During the initial growth of the new phase, the bainite grains grow very quickly and relatively undisturbed for the first 500 sec. But, after that the bainite grains start to impinge against each other and the gain in free energy is more and more compensated by an increasing energy of distortion. The latter occurs because the specific volume of the austenite is very much smaller than that of the bainite. Further, the transformation is retarded because it proceeds through a martensite-like intermediate stage and the specific volume of martensite is even larger. This causes residual stresses of the 2nd kind and reduces the driving force of the transformation. Thus, the decomposition of the austenite becomes more and more retarded until it finally almost completely stops. In summary, we have shown that through this neutron transmission technique it is possible to follow a structural phase transformation in-situ in real time and to produce a complete TTT diagram.

References:

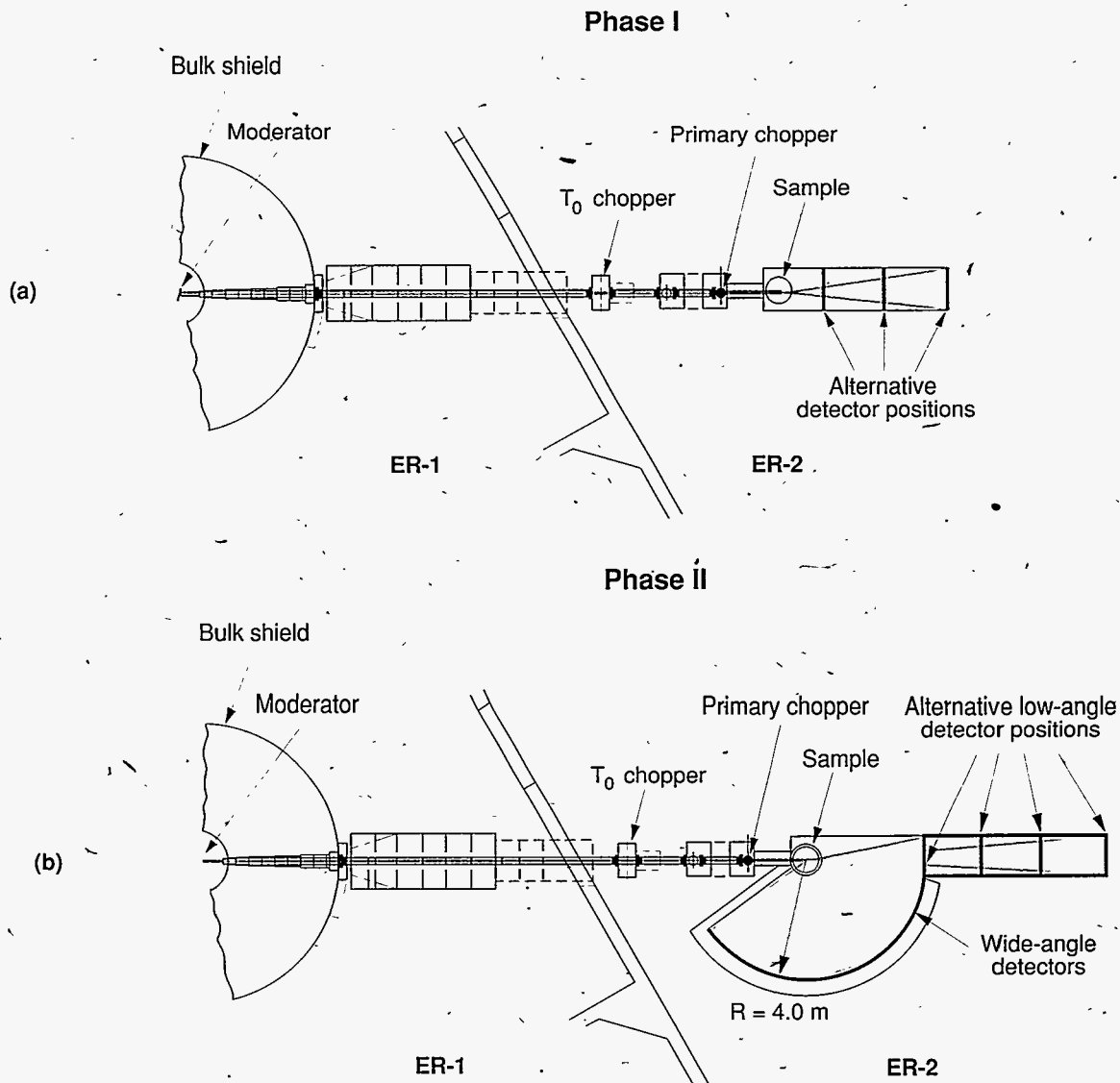


PHAROS

Chopper Spectrometer (PHAROS)

The chopper spectrometer, PHAROS, is designed for low-angle studies such as neutron Brillouin scattering and magnetic excitations. The instrument provides 0.5% incident energy resolution for incident energies between 50 meV and 2 eV. The sample is positioned 20 m from the moderator, which is currently water at room temperature. Phase I is complete (Fig. a), and the spectrometer consists of an evacuated, shielded flight path for low-angle scattering ($1^\circ < \phi < 10^\circ$). When Phase II is completed (Fig. b), the spectrometer will be a high-resolution, general-purpose chopper spectrometer with 10 m² of detectors covering scattering angles between -10° and 140° . PHAROS will then be able to accommodate the full range of inelastic scattering experiments, including phonon densities of states, magnetic excitations, momentum distributions, crystal-field levels, chemical spectroscopy, and measurements of $S(Q, \omega)$ in disordered systems. In addition, the low-angle detectors will be available for use at distances between 4 and 10 m, with scattering angles down to 0.65° , thus making it suitable for high-resolution inelastic studies at low Q :

spectrometer with 10 m² of detectors covering scattering angles between -10° and 140° . PHAROS will then be able to accommodate the full range of inelastic scattering experiments, including phonon densities of states, magnetic excitations, momentum distributions, crystal-field levels, chemical spectroscopy, and measurements of $S(Q, \omega)$ in disordered systems. In addition, the low-angle detectors will be available for use at distances between 4 and 10 m, with scattering angles down to 0.65° , thus making it suitable for high-resolution inelastic studies at low Q :



Instrument Details

Moderator-chopper distance	18 m
Chopper-sample distance	2 m
Moderator	Chilled water at 283 K
Chopper frequency	600 Hz
Chopper diameter	10 cm
Chopper slit spacing	1 mm or more
Sample size	up to 5 cm x 7.5 cm
Incident energy resolution	$\Delta E_i/E_i = 0.5\%$

Phase I

1 m² of detectors at 3.5 m from the sample; scattering angle between 1° and 10°.

Phase II

9 m² of detectors at 4 m from the sample; scattering angle between -10° and 140°;

1 m² of detectors in forward scattering position at 4 to 10 m from the sample.

Robert Robinson, instrument scientist

Eric Larson, instrument technician

PHAROS Experiment Reports

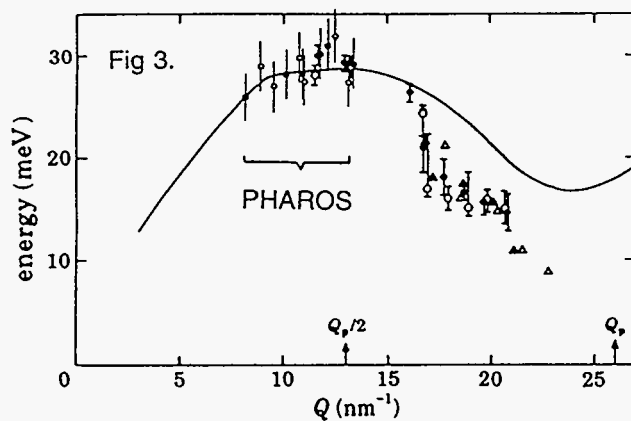
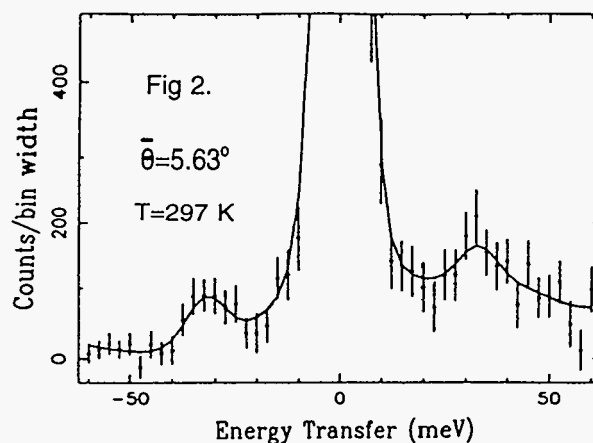
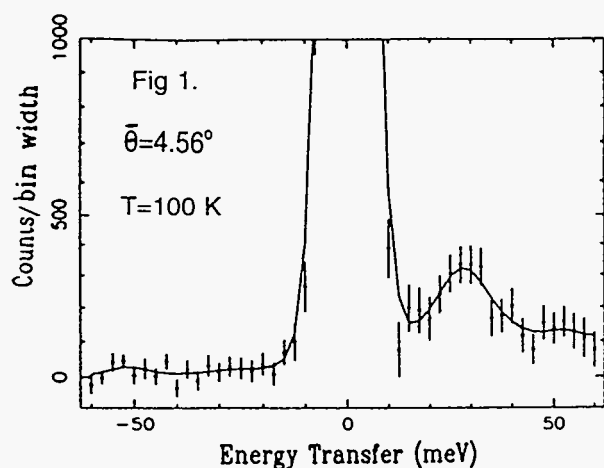
6082	<i>Neutron Brillouin Scattering</i>	151
6409	<i>Vibrational Spectra of TiH₂ and KHF₂</i>	153

Instrument used: <i>(please type)</i> PHAROS	Local contact: Dr. R. Robinson	Proposal number: <i>(for LANSCE use only)</i> 6082
Title: Neutron Brillouin Scattering		Report received: <i>(for LANSCE use only)</i> 2/23/94
<p>Authors and affiliations:</p> <p>P.A. Egelstaff[*], J-B. Suck^{**}, R.A. Robinson[#], B.J. Olivier[#] and C.J. Benmore[*].</p> <p>[*] Dept. of Physics, University of Guelph, Guelph, Ontario N1G 2W1 Canada. ^{**} Institut Laue-Langevin, BP156 F-38042, Grenoble, Cedex 9, France. [#] Los Alamos National Laboratory, LANSCE, Los Alamos, New Mexico, 87545, USA.</p>		
<p>Experiment report:</p> <p>This report describes the results from the neutron Brillouin scattering (NBS) study of the amorphous metal $Mg_{70}Zn_{30}$ performed on the high resolution chopper spectrometer PHAROS. NBS experiments refer to inelastic neutron scattering measurements made at momentum transfers $\hbar Q$ within the first pseudo-Brillouin zone ($Q < 13.0 \text{ nm}^{-1}$ for $Mg_{70}Zn_{30}$). As an experimental tool NBS plays an important role in the investigation of the collective dynamics in liquids and amorphous materials [1], [2]. This type of experiment is possible using the PHAROS instrument, as a sufficiently large ω-range is covered at momentum transfers within the zone [3].</p> <p>Strips of the $Mg_{70}Zn_{30}$ melt-spun glass (of mean density 1.72 g cm^{-3}) were pressed into a flat container of sample volume $8.0(\text{height}) \times 5.5(\text{width}) \times 2.0(\text{thickness}) \text{ cm}^3$ intersected by a $6 \text{ mm} \times 6 \text{ mm}$ square grid of 0.5 mm thick cadmium blades. An incident energy of 187 meV (close to the absorption maximum for neutrons in Cd) was chosen to maximize the effect of the grid and thereby reduce the large multiply scattered neutron background. An identical grid was also used for the empty sample container and placed either side of a 3 mm Vanadium plate for the calibration run. Forty, 10 atm, linear position sensitive ^3He detectors, arranged in vertical rows and placed in the forward scattering direction, gave a low-angle scattering range of 1.3° to 8.8°. At the time of the experiment the instrument resolution was measured to be constant at 4.8% ($\text{FWHM} = 9.0 \text{ meV}$ at $\hbar\omega = 0$) over the entire angular range.</p> <p>Two experiments were performed on the metallic glass at temperatures of 100 K and 297 K using epithermal neutrons. However due to the relatively low count rate at high incident energies and attenuation of the scattered beam by the Cd grid, sample run times of 9 days at 100 K and 4.5 days at 297 K were required for acceptable statistics on the sample alone. In addition long empty container and Vanadium runs were required so that a total of 22 days good running took place. Detector calibration measurements were also performed before and after the experiment and showed a high degree of detector stability.</p> <p>The raw x-y detector data were corrected to form Debye-Sherrer rings. In this analysis the data were grouped into 5 concentric rings, at fixed θ. Other detector groupings are also possible, for example at constant Q increments, and will be examined at a later stage in the analysis. The final ringed data were rebinned from time-of-flight onto a constant energy scale using 2.5 meV bins, corrected for detector efficiency and normalised to the lowest angular ring using the number of counts under the elastic peak in the Vanadium spectrum. The empty container scattering was then removed and an absorption correction made. A two-channel maximum entropy method [4] was used to separate out the sharp, one-phonon scattering events from the large, broad background comprising multiphonon and multiple scattering events.</p>		

Experiment report (continued):

In figures 1 and 2 the error bars denote the data and the solid line is the maximum entropy fit to the data. The dotted line shows the background term.

The dispersion relation, determined by plotting the maxima of the measured excitation peaks as a function of momentum transfer (shown by the squares and diamonds in figure 3) is in good agreement with the theoretical predictions of Hafner [5] (solid line). A comparison between the overlapping results obtained on the HET time-of-flight spectrometer at ISIS ([1], circles fig. 3) and this study for the range $11.5 < Q \text{ (nm}^{-1}\text{)} < 13.3$ also show good agreement within experimental error. A unique advantage of NBS experiments is the ability to distinguish between longitudinal and transverse excitations, as whilst neutrons couple directly to longitudinal vibrations they only couple to transverse vibrations via Umklapp processes outside the first Brillouin zone. The collective excitations observed in this study can therefore unambiguously be identified as longitudinal vibrations since the dispersion relation extends far inside the first Brillouin zone. Further analysis of the data is in hand, which may extend the measured data to lower Q values. The present results clearly demonstrate the viability of performing successful NBS experiments on the PHAROS spectrometer, and at the same time, a need for long run times and improved resolution.



Figs. 1 & 2 show examples of the data at 100K and 297K, and their interpretation using Maximum Entropy methods.

Fig. 3 Dispersion curve for glassy $\text{Mg}_{70}\text{Zn}_{30}$.

References:

- [1] Suck J-B, Egelstaff P, Robinson R, Sivia D, Taylor A (1992) *Europhys. Lett.*, **19**(3) 207.
- [2] Suck J-B, Egelstaff P, Robinson R, Sivia D, Taylor A (1992) *J. Non-Cryst. Solids* **150** 245.
- [3] R Robinson (1989) in 'Advanced Neutron Sources 1988' IOP conf. series, *Topics in Applied Physics* **97** 311.
- [4] D Sivia (1990) in 'Maximum Entropy and Bayesian Methods' edited by Fougere P (Kluwer Academic, the Netherlands) p195.
- [5] Hafner J (1983) *J. Phys. C* **16** 5773.

Instrument used: <i>(please type)</i> PHAROS	Local contact: R.A. Robinson	Proposal number: <i>(for LANSCE use only)</i> 6409
Title: Vibrational Spectra of TiH₂ and KHF₂		Report received: <i>(for LANSCE use only)</i> 4/8/94
<p>Authors and affiliations:</p> <p>B. J. Olivier, LANSCE, LANL R. A. Robinson, LANSCE, LANL</p>		
<p>Experiment report:</p> <p>As test experiments, we took data at various temperatures and incident energies on TiH₂ and KHF₂. A sample of the results are shown in Figures 1-3.</p> <p>TiH₂ is a classic metal-hydride system and it has often been used as a test sample for new inelastic scattering spectrometers, by virtue of its large scattering cross-section and simple vibrational dynamics. Essentially it is a classical Einstein oscillator (with characteristic frequency given by $\hbar\omega \sim 150$ meV), but with slight dispersion. This results in the splitting shown in Figure 1. The only unusual thing about this spectrum is that the lower energy peak (at 140 meV) is weaker in intensity than the high energy peak (at 155 meV). This is the reverse of what is normally seen in spectra from TiH₂[1]. We believe this is due to our measurement being made at much smaller Q than is customary: PHAROS currently records data at scattering angles less than 10°. Much the same has been seen in low-Q measurements on a similar metal hydride ZrH₂[2]. In this experiment 24.4g of sample was used and the total counting time was 23 hours.</p> <p>KHF₂ is a classic hydrogen-bonded system, which exhibits internal HF₂⁻ molecular modes between 140 and 200 meV, as shown in Figure 2. The broad peak centred at 180 meV is a "phonon wing"[3]. The peak at 155 meV is in fact split into an asymmetric stretch mode and a doubly degenerate bending mode. This can be seen more clearly in the higher resolution data shown in Figure 3. In this experiment 100g of sample was used. The counting time was 17 hours for the data in Figure 2, and 3 hours for the data in Figure 3.</p>		

Experiment report (continued):

Figure 1. Excitation spectrum from 24.4g of TiH_2 at 40K. $E_I = 300\text{meV}$, Chopper frequency = 600 Hz

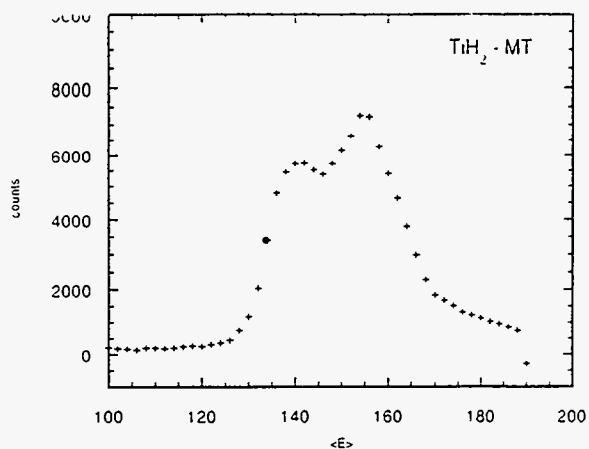


Figure 2. Excitation spectrum from 100g of KHF_2 at 50K. $E_I = 300\text{ meV}$, Chopper frequency = 600 Hz

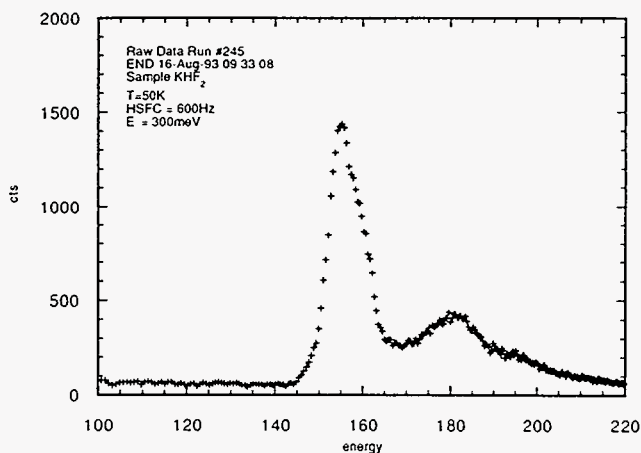
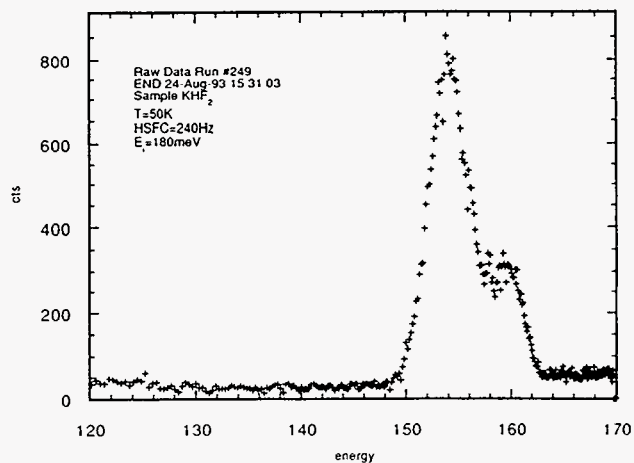


Figure 3. Excitation spectrum from 100g of KHF_2 at 50K. $E_I = 180\text{meV}$, Chopper frequency = 240 Hz



References:

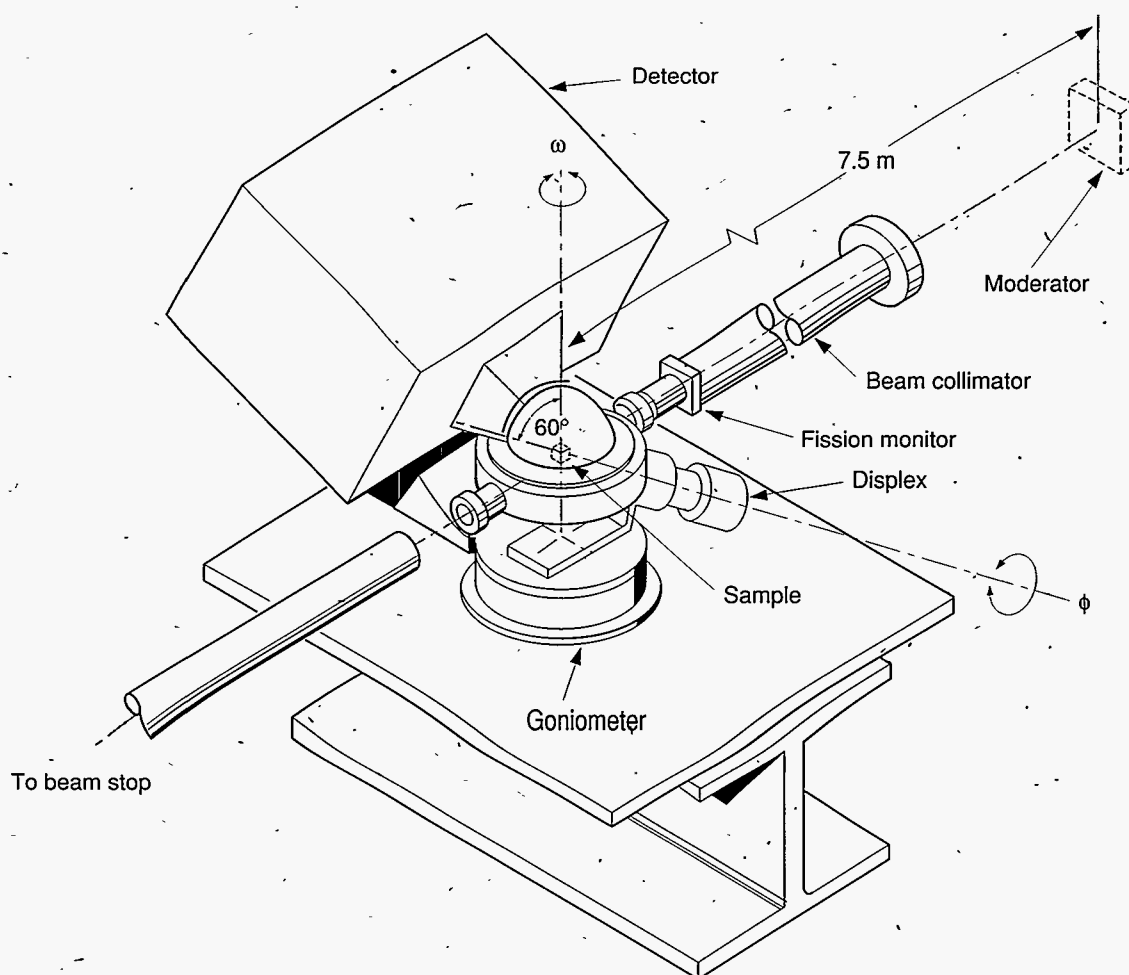
- [1] J. Eckert (private communication).
- [2] J. G. Couch, O. K. Harling and L. C. Clune, Phys. Rev. B4, 2675 (1971), Fig. 4.
- [3] J. Tomkinson, Spectrochimica Acta 48A, 329 (1992), Fig. 4.

*Single Crystal
Diffractometer (SCD)*

Single Crystal Diffractometer (SCD)

The Single Crystal Diffractometer (SCD) is used to determine the crystal structures of a wide variety of materials. Neutrons are scattered from the crystalline sample into an area detector ($25 \times 25 \text{ cm}^2$; position-sensitive; ^3He gas-filled proportional counter), and the wavelength of the neutrons is determined by their time of flight from the source to the detector. To collect all the required data for a particular crystal, the orientation of the sample can be changed by rotating the goniometer about ϕ and ω . The SCD has been used to study the structure of organometallic molecules that show a

unique binding of H_2 ; crystal-structure changes at solid-solid phase transitions; magnetic spin structure; twinned or multiple crystals; the texture analysis of polycrystalline materials that have been subjected to extreme geological environments; and crystal structures of materials under pressures of 10 to 20 thousand atmospheres. The instrument measures a large volume of reciprocal space at one time and, therefore, can be used for studies of unknown incommensurate structures, diffuse scattering, and so forth. The SCD also accommodates nonambient sample environments.



Instrument Details

Wavelength range	0.5–10 Å
Beam diameter at sample	1–5 mm
Time resolution	~1%
Maximum lattice constant	~20 Å
Detector	1 multiwire proportional counter (25 cm x 25 cm) at 90°
Detector resolution	2.5 mm
Moderator	Chilled water at 283 K
Sample environment	10–300 K
Sample size	0.5–10 mm ³
Experiment duration	2 to 4 days per octant of reciprocal space

Allen C. Larson, instrument scientist
Dennis Martinez, Instrument technician

SCD Experiment Reports

6013	<i>Magnetic Phases in UNiGe</i>	159
6034	<i>Study of Alignment in Ag-Sheathed $\text{Bi}_2\text{Sr}_2\text{CaCu}_2\text{O}_{8\pm\delta}$ Round Wires</i>	161
6039	<i>Neutron Diffraction Study of H in Clinohumite</i>	163
6049	<i>Single Crystal Neutron Diffraction Study of Apatite Exhibiting Growth Related Sectoral and Intrasectoral Dissymmetrization</i>	165
6063	<i>Velocity of Sound Measurements in the Linear Chain Antiferromagnet CsFeBr_3 by Means of the Diffraction Method</i>	167
6096	<i>Single Crystal Neutron Diffraction Study of the Structure of $\text{Ce}_{2-x}\text{Pt}_4\text{Ga}_{8+y}$</i>	169
6101	<i>Velocity of Sound Measurements in the Linear Chain Antiferromagnet CsFeBr_3 by Means of the Diffraction Method, Part II</i>	171
6109	<i>Neutron Diffraction Analysis of Neutron-Induced Damage in Spinel (MgAl_2O_4) Single Crystals</i>	173

Instrument Used: (please type) SCD	Local Contact: R. A. Robinson	Proposed Number: (for LANSCE Use Only) 6013
Title: Magnetic Phases in UNiGe		Revised Number: (for LANSCE Use Only) 4/12/94
Authors and affiliations: V. Sechovský, L. Havela ; Charles University, Prague, Czech Republic A. Purwanto*, A. C. Larson, R. A. Robinson ; LANSCE, LANL H. Nakotte, F. R. de Boer ; Van der Waals-Zeeman Lab., The Netherlands *and NMSU		
Experiment report: <p>Based on powder neutron-diffraction results, Murasik et al. [1] claimed that UNiGe crystallizes in the CeCu₂ structure type with Ni and Ge atoms being randomly distributed on copper sites. An antiferromagnetic structure with a propagation vector $\mathbf{q} = (1/2, 0, 1/2)$ and U-moments oriented along the <i>a</i>-axis was proposed below 43.3 K. At 13 K, the U-moment magnitude is $(1.37 \pm 0.07) \mu_B$. In contradiction, Kawamata et al. [2] claimed that they observed magnetic reflections coinciding with the nuclear ones on a UNiGe single crystal at 10 K. This suggests an identical size of the magnetic and nuclear unit cell. These inconsistent results have motivated our study on single crystalline UNiGe.</p> <p>The SCD experiment on UNiGe single crystal was done at LANSCE at zero external magnetic field for six different temperatures, i.e; 20 K, 44 K, 46 K, 48 K, 52 K and 60 K.</p> <p>To answer the question whether UNiGe crystallizes in the structure type of CeCu₂ (Imma space group) or TiNiSi (Pnma space group), we indexed the 60 K single crystal data using GSAS. We observe reflections both with $h+k+l=2n$ and $h+k+l=2n+1$. The latter are forbidden in Imma, but not in Pnma. Therefore, the space group of UNiGe is Pnma (TiNiSi structure type). The intensities fit well to this structure.</p> <p>Fig. 1 shows some qualitative observations obtained by SCD of LANSCE on the single crystalline UNiGe in zero external magnetic field. At 20 K, a magnetic Bragg peak appears at $0, 3/2, -1/2$ indicating a commensurate antiferromagnetic ordering with propagation vector $\mathbf{q} = (0, 1/2, 1/2)$. This commensurate phase is preserved up to around 41.5 K [3]. At 46 K, the Bragg peak is flanked by a pair of magnetic satellites at $\delta = \pm (0, .141, .141)$ suggesting an incommensurate antiferromagnetic phase. In fact, this incommensurate phase emerges just above 41.5 K and disappear around 50.5 K [4].</p> <p>More quantitative analysis of the magnetic neutron data is in progress.</p>		

Experiment report (continued):

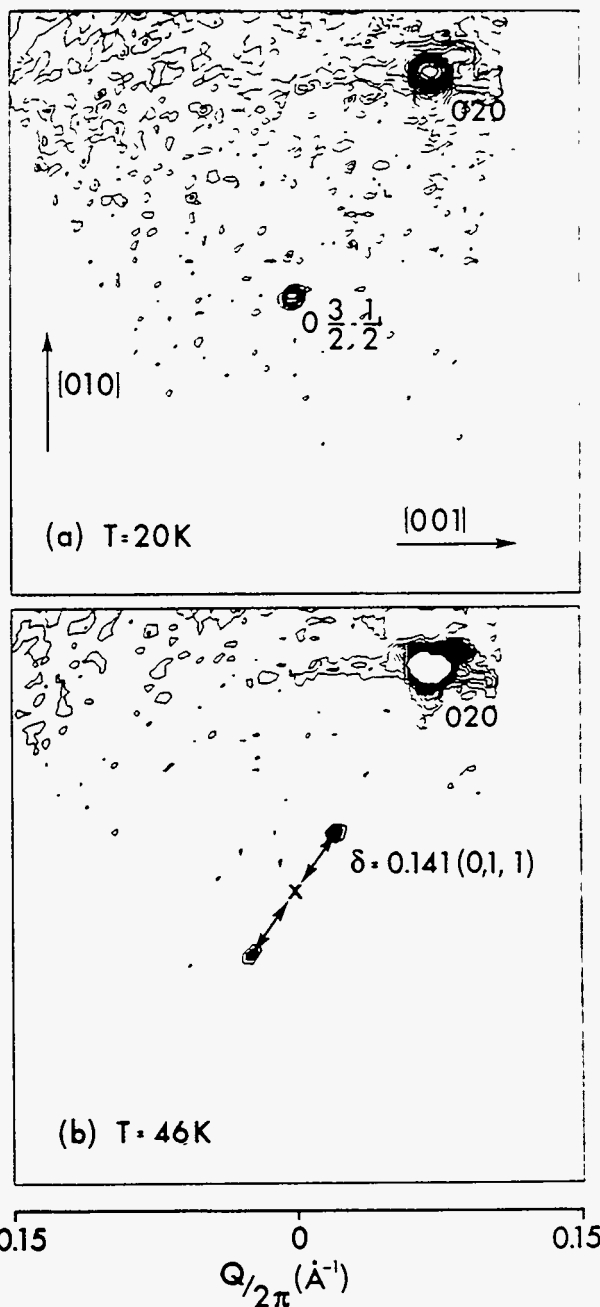


Fig. 1. Contour plots of the SCD raw data showing the magnetic reflection in the vicinity of $0, 3/2, -1/2$ at (a) 20 K and (b) 46 K.

References:

- [1] A Murasik, P. Fischer, R. Troc and V. H. Tran, *J. Phys. C: Condens. Matter.*, 3 (1991)1841
- [2] S. Kawamata, H. Iwasaki, N. Kobayashi, *J. Magn. Magn. Matter.*, 104-107 (1992)55
- [3] V. Sechovský, L. Havela, A. Purwanto, A. C. Larson, R. A. Robinson, K. Prokeš, E. Brück, F. R. de Boer, P. Svoboda, H. Maletta and M. Winkelmann, *J. Alloy & Comp.* (in press).
- [4] V. Sechovský, L. Havela, P. Svoboda, A. Purwanto, R. A. Robinson, H. Maletta, K. Prokeš, H. Nakotte and F. R. de Boer, submitted to MMM '94 Conference, Albuquerque, to appear in *J. Appl. Phys.*, LA-UR-94-1172.

Instrument used: <i>(please type)</i> SCD	Local contact: Allen C. Larson	Proposal number: <i>(for LANSCE use only)</i> 6034
Title: Study of Alignment in Ag-Sheathed $\text{Bi}_2\text{Sr}_2\text{CaCu}_2\text{O}_{8\pm\delta}$ Round Wires		Report received: <i>(for LANSCE use only)</i> 3/15/94
<p>Authors and affiliations:</p> <p>Eric E. Hellstrom Department of Materials Science and Engineering University of Wisconsin-Madison 1509 University Ave. Madison, Wisconsin 53706</p> <p>Allen C. Larson LANSCE Los Alamos National Laboratory Los Alamos, NM 87545</p>		
<p>Experiment report:</p> <p>Alignment is thought to be needed to attain high critical current density in the high temperature superconductors. Neutron diffraction pole figures studies were carried out to quantify the degree of alignment that developed in Ag-sheathed $\text{Bi}_2\text{Sr}_2\text{CaCu}_2\text{O}_8$ (2212) tapes and wires. These studies showed higher c-axis alignment in flat tapes that had been melt processed using step solidification compared to tapes melt processed using continuous cooling. In addition, they confirmed that there was no detectable alignment in large diameter (0.7mm) round wires made by Vacuumschmelze, but showed that radial alignment can be attained in small diameter (60μm) round wire that had been processed using step solidification melt processing.</p> <p>Ray¹ proposed a mechanism that explains the 2212 alignment that occurs during melt processing. (This is a process in which 2212 forms from a melt during cooling.) A key feature of this mechanism is that the chemical nature of the substrate material is not critical for alignment (so long as there is no chemical reaction), but the geometry of the substrate and superconductor region is critical. Specifically, the model predicts that in a two dimensional planar geometry, the grains will grow parallel to the plane with the c-axis aligned perpendicular to the plane. Extending the analysis to one dimension, it predicts that in a rod geometry, the grains will grow parallel to the long axis of the rod with the c-axes of the grains radially aligned around the long axis of the rod. The degree of alignment is expected to increase with decreasing oxide thickness in two dimensional geometries, and to increase with decreasing diameter of the oxide in the one dimensional rod geometry.</p> <p>A second point that was investigated was the effect of cooling conditions during melt processing on the alignment. Again, Ray developed a technique called step solidification melt processing that increases the degree of alignment in 2212 conductors.</p> <p>The table lists the samples that were investigated, their geometries, and the type of melt processing used to make the samples. Figure 1 shows the (0012) pole figures for the samples listed in the table. The table lists the maximum multiples of random distribution (mrd) for each sample.</p> <p>The flat 2212 tape that was slow cooled (Fig. 1a) had less alignment than the flat tape that was processed using the step-solidification method (Fig. 1b) described in the table. The continuous cooling at 10°C/hr yielded less alignment and more second phases in the fully-processed tape than did the step-solidified sample. These results show quantitatively that step-solidification processing is very conducive to forming well-aligned 2212.</p> <p>The neutron diffraction data showed that the round 2212 wire (0.7 mm diam.) that Vacuumschmelze makes is not aligned (Fig. 1c). This confirms their claim of not alignment,² and is particularly significant since the majority of work on 2212 is based on the premise that high alignment is needed to attain high J_c. These neutron diffraction results confirm that their reasonable J_c values can be achieved in unaligned samples.</p> <p>The 61-filament round wire that was step solidified showed radial c-axis alignment (Fig. 1d). These results show that it is indeed possible to generate radial c-axis alignment in small diameter wires when processing using step solidification melt processing. In the next cycle we plan to run the control experiments on small diameter (60μm) round wires using a heat treatment that is less conducive to attaining high alignment.</p>		

Conductor geometry	Superconductor dimensions	Heat treatment	MRD for (0012) pole	Conductor source	Comments
Flat tape (slow cool 10°C/hr) - 2d planar	2mmx40μm	Continuous Cooling 890°C, cool to 840°C @ 10°C/hr, hold 100hr	10.6 mrd - c-axis alignment perpendicular to plane of tape	Powder and tape made and heat treated at UW- Madison	Low C content in powder
Flat tape (step solidified) - 2d planar	2mmx40μm	Step Solidification 890°C, cool to 870°C @ 10°C/hr, hold 24hr, drop to 865°C, hold 24hr...through 840°C	17.3 mrd - c-axis alignment perpendicular to plane of tape	Powder and tape made and heat treated at UW- Madison	
Round wire - (monocore) - 1d rod	0.7mm diam.	890°C, fast cool to 840°C, hold 100hr	No alignment	Wire made and heat treated by Vacuumschmelze	Confirms Vac.'s claim of no alignment
61 fil. round wire (step solidif'd) 1d rod	60μm diam. (each filament)	See schedule for step solidified flat tape	1.8 mrd - radial c-axis alignment	Wire from Intermagnetics General Corp., heat treated at Wisconsin	Commercial powder - it contained C

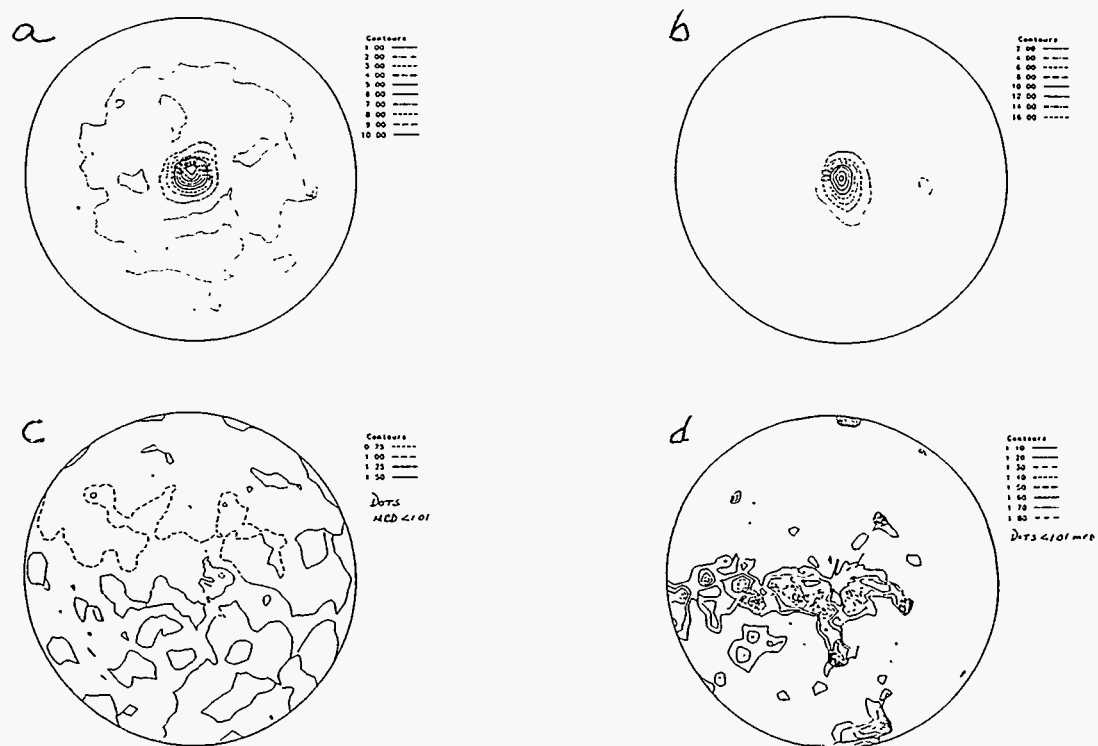


Fig 1. (0012) pole for (a) flat tape slow cooled at 10°C/hr (data from '92 run cycle), (b) flat tape (step solidified), (c) monocore round wire (0.7mm diam) (Vacuumschmelze), and (d) 61-filament round wire (step solidified) (60μm filaments) (Intermagnetics General Corp.).

References:

1. R.D. Ray II, Ph.D. Thesis, University of Wisconsin-Madison (1993)
2. K. Heine, J. Tenbrink, and H. Krauth, Appl. Phys. Lett. 55 (1989) 2441.

Instrument Used: <i>(please type)</i> <p style="text-align: center;">SCD</p>	Local Contact <p style="text-align: center;">Allen C. Larson</p>	Proposal Number: <i>(for LANSCE Use Only)</i> <p style="text-align: center;">6039</p>
Title: <p style="text-align: center;">Neutron Diffraction Study of H in Clinohumite</p>		Report received: <i>(for LANSCE Use Only)</i> <p style="text-align: center;">10/26/94</p>
Authors and affiliations: <p>JOSEPH R. SMYTH and R. JEFFREY SWOPE</p> <p>Department of Geological Sciences, University of Colorado Boulder, Colorado 80309-0250</p> <p>ALLEN C. LARSON</p> <p>Los Alamos Neutron Scattering Center, MS H805, Los Alamos National Laboratory, Los Alamos, NM 87545</p>		
Experiment report: <p>Clinohumite occurs as a vein and accessory phase in metamorphosed ultramafic rocks, and as a major phase in metamorphosed limestones and dolomites and carbonatites. Clinohumite has been reported in mantle-derived rocks from several localities including Moses Rock, Utah and Buell Park, Arizona. Clinohumite has been proposed as a possible host for H in rocks of the upper mantle. Trace amounts of H occur in mantle-derived olivines which show IR spectra similar to that of clinohumite, and it has been suggested that this H may occur in humite-like defects in the host olivine. H positions in the humite minerals have not been determined, so the objective of this experiment is to locate the H position in order to clarify the role of H in the clinohumite and possibly in the related olivine structure. Olivine is the dominant phase in the upper 400 km of the Earth and trace substitution of H in olivine may control the early de-volatilization of the planet.</p> <p>The structure of a natural, F-free titano-clinohumite $[(Mg_{7.33}Fe_{1.00}Ti_{0.47})(SiO_4)_4OOH]$ from Val Malenco, Italy had been previously refined from X-ray data collected at room temperature and the cell parameters determined by X-ray methods at several temperatures down to 100K. A relatively large, equant crystal of the hydroxyl titano-clinohumite measuring approximately 3 mm in diameter was selected for study and mounted on an Al pin in the vacuum shroud of an Air Products Co. Displex model 201 refrigerator. The crystal was cooled to approximately 30K and a short-duration histogram of data collected to determine the orientation matrix. A preliminary unit cell and angle coordinates for the twenty histograms of data required to cover a unique quadrant of reciprocal space were determined from these data. Twenty histograms of data, each approximately 4 hours duration, were recorded. The Bragg peaks were indexed and intensity data for 3108 reflections extracted from the histograms. Of these, 2454 were greater than zero, and 1832 were greater than $3\sigma(F^2)$ which includes all unique intensities with $\sin \theta / \lambda$ less than 1.00.</p>		

Experiment report (continued):

The lattice constants for the *a*-axis unique monoclinic unit-cell are $a = 4.7403(8)$, $b = 10.2607(18)$, $c = 13.6943(22)$, $\alpha = 101.119(12)^\circ$. The structure was refined to a final R value of 0.08 in space group $P2_1/b$. A hydrogen position with 50.0% occupancy was located at fractional coordinates $x = 0.083(7)$, $y = 0.013(1)$, $z = 0.0103(7)$; the titanium is fully ordered, occupying approximately 25% of the M3 site at a position displaced $\sim 0.25 \text{ \AA}$ from that of the Mg in M3. However, numerous reflections in violation of the *b*-glide in $P2_1/b$ were observed, as were several in violation of the 2_1 . It appears that the true space group is either $P1$, or possibly, made up of domains of $P2_1$ and Pb so that violations of the *b*-glide are due to ordering of both H and Ti. Refinement of the structure in the lower symmetry space groups, however, did not converge.

References:

Instrument used: <i>(please type)</i> SCD	Local contact: Allen Larson	Proposal number: <i>(for LANSCE use only)</i> 6049
Title: Single Crystal Neutron Diffraction Study of Apatite Exhibiting Growth Related Sectoral and Intrasectoral Dissymmetrization.		Report received: <i>(for LANSCE use only)</i> 1/19/94
Authors and affiliations: <p> John Rakovan and Richard J. Reeder. Department of Earth and Space Sciences, State University of New York at Stony Brook, Stony Brook, New York. Allen Larson. Manuel Lujan, Jr. Neutron Scattering Center, Los Alamos National Laboratory, Los Alamos, New Mexico. </p>		
Experiment report: <p> Surfaces play an important role in the partitioning of trace elements into crystals as well as in the ordering of trace and major elements during growth. Samples of natural hydroxy-fluorapatite have been found that show regions of dissymmetrization, from hexagonal to monoclinic or triclinic symmetry, that correlate directly to different growth sectors and subsectors within single crystals (see figure). Sectors formed under the {00.1} faces are uniaxial negative and exhibit a continuous extinction when viewed in optic axis sections under crossed polars. Sectors that have grown under the {10.1}, {11.1} and {10.0} faces, however, are not uniaxial. These regions are biaxial and show differential extinction orientation, in sections cut perpendicular to the c axial direction, between and within different sectors. Within time equivalent portions of a given sector, subsectors of different extinction orientation are polygonized and may show differences in optic angle (2V) as large as 13 degrees. </p> <p> Rakovan and Reeder (1994) studied a number of apatites from different locations, including those in this study, that display sectoral and intrasectoral zoning of a large number of trace elements. In all of these samples, compositional heterogeneities correspond directly to different faces and symmetrically nonequivalent growth steps on a given face. Hence, it is postulated that this differential distribution of trace elements occurred during growth and was controlled by the structure of the crystal surface. The optical observations suggest that differences in surface structure are also affecting the ordering of atoms as they are incorporated into the crystals. Thus far, sectoral and intrasectoral dissymmetrization are only seen in the hydroxy-fluorapatites investigated here. These samples are the only ones from Rakovan and reeder (1994) with a </p>		

Experiment report (continued):

detectable OH component. The lack of anomalous optical behavior in the OH-free apatites suggests that the most probable cause of the reduction of symmetry in the biaxial sectors is positional ordering of OH and or OH/F ordering.

Quantitative characterization of the differential ordering is essential for the interpretation of possible surface structural influences. Single, optically homogeneous, subsectors were cut for neutron diffraction. Intensity data from one full and one partial octant of reciprocal space were obtained. Structural refinement is not yet complete, however, the data collected are not consistent with $P2_1/b$ symmetry, which is the symmetry of almost all other non- $P6_3/m$ hexagonal apatites. Rather, the optical data combined with such observed reflections as $00l$, $l=3n$, indicate a nonhexagonal space group not yet observed in apatite.

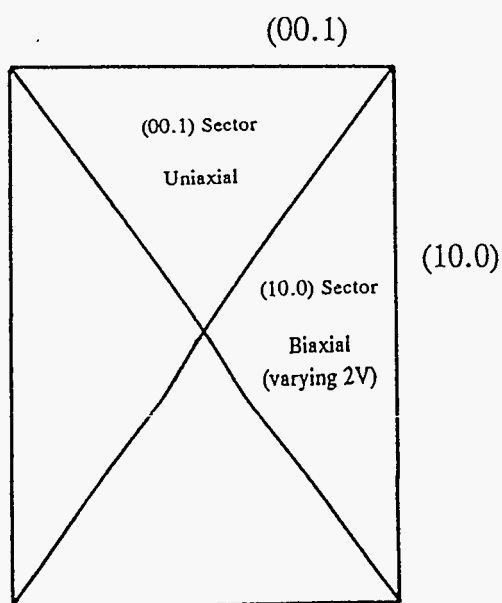


Fig. 1 Idealized crosssection of an apatite single crystal showing optical variation between $\{00.1\}$ and $\{10.0\}$ sectors.

References:

Rakovan and Reeder (1994) Dissymmetrization and differential incorporation of trace elements in apatite: The role of surface structure during growth. Submitted, American Mineralogist.

Instrument used: <i>(please type)</i> <p style="text-align: center;">SCD</p>	Local contact: <p style="text-align: center;">A.C. Larson</p>	Proposal number: <i>(for LANSCE use only)</i> <p style="text-align: center;">6063/SCD</p>
Title: <p style="text-align: center;">Velocity of sound measurements in the linear chain antiferromagnet CsFeBr₃ by means of the diffraction method.</p>		Report received: <i>(for LANSCE use only)</i> <p style="text-align: center;">6/17/94</p>
Authors and affiliations: <p style="text-align: center;">D. Visser. Department of Physics, Loughborough University of Technology, Loughborough LE11 3TU, UK A.C. Larson. LANSCE, Los Alamos National Laboratory, Los Alamos, New Mexico 87545, USA.</p>		
Experiment report: <p>CsFeBr₃ crystallizes with the hexagonal perovskite structure. At low temperatures the magnetic properties of this compound are governed by a singlet ground state and a low lying doublet state (1).</p> <p>Inelastic neutron scattering experiments showed that CsFeBr₃ is a pure singlet ground state system. Consequently no magnetic ordering has been observed and the gap between the singlet and doublet transition has a finite energy. The dispersion surface has a minimum energy (0.11 THz) at the soft mode point Q(1/3 1/3 1). The magnetic features of this system are well described by RPA theory.</p> <p>In one of the early experiments on CsFeBr₃ we observed extra scattering along the (111) direction which may be due to an unexpected second magnetic mode. A polarized neutron scattering study of these modes in CsFeBr₃ showed clearly that this second scattering process has a non magnetic origin (2). A possible explanation for this scattering process may arise from a multiscattering process where the neutron is first inelastically scattered by a low energy phonon followed by Bragg scattering (3).</p> <p>It is known for several hexagonal ABX₃ halides that low-lying phonons are present (4). In order to verify the predictions made it was necessary to measure the velocity of sound of the acoustic phonons in CsFeBr₃ as well as the texture of the crystals used in the inelastic neutron scattering experiments.</p> <p>It has recently been demonstrated on Graphite, BaF₂ and CaF₂ that one can get accurate information on the acoustic phonons and sound velocities using the 'diffraction' method on a pulsed neutron source (5).</p> <p>This approach has been followed in our case. A single crystal of CsFeBr₃ was mounted on the TOF single crystal diffractometer SCD at LANSCE with the [100] direction in backscattering position. The detector is placed under 90° to the incident flight path. We studied the three major symmetry directions: [100], [110] and [0 0 1] at room temperature.</p> <p>We were able to obtain information on the major directions of around 6 - 10 harmonics of the principal reflections, fig.1. In the case of the [100] direction we studied the dependence of the shape of the diffuse scattering in two different settings.</p> <p>It is clear from the obtained data that we observe a large amount of diffuse scattering and that the difference in shape of the diffuse scattering is directly related to the different regions of the neutron velocity.</p>		

Experiment report (continued):

For a crystal which shows an isotropic propagation of sound one will observe either one TDS (thermal diffuse scattering) peak when the one phonon scattering surface has the form of two ellipsoids or two when the scattering surface is a hyperbolic one.

Our data falls into the region of these two types of scattering processes. At present the data is being analyzed. The data will provide information on the velocity of sound in the different principle directions as well as parts of the phonon dispersion curves (surface).

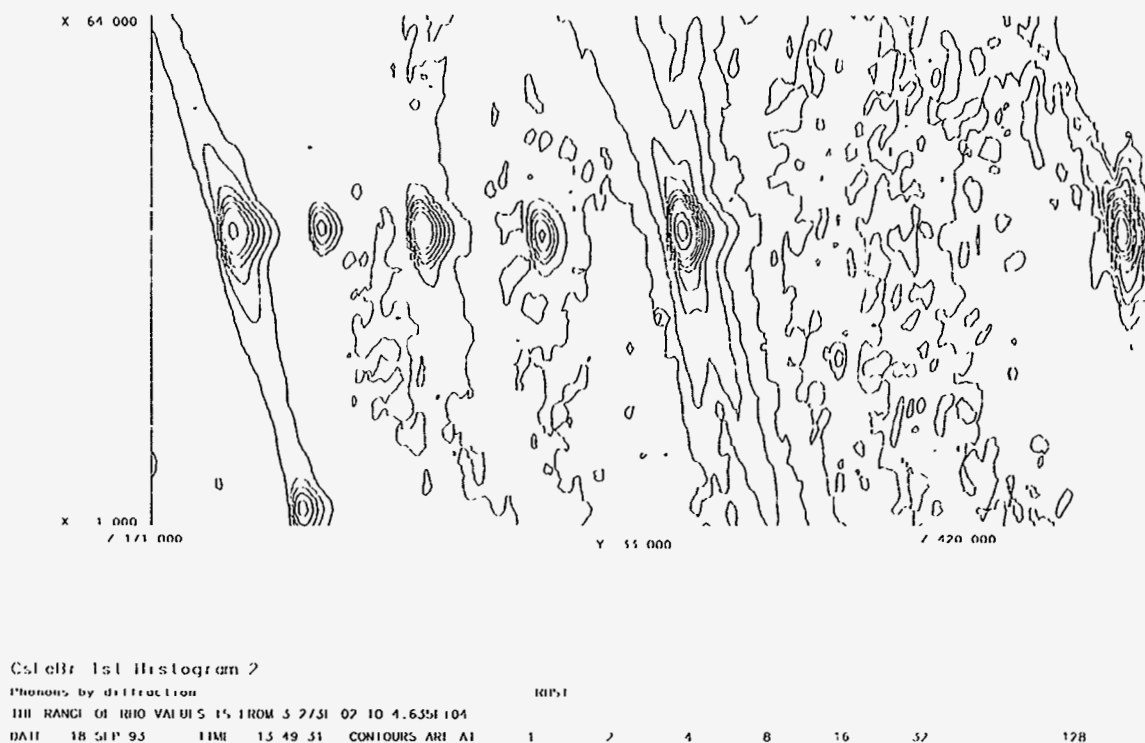
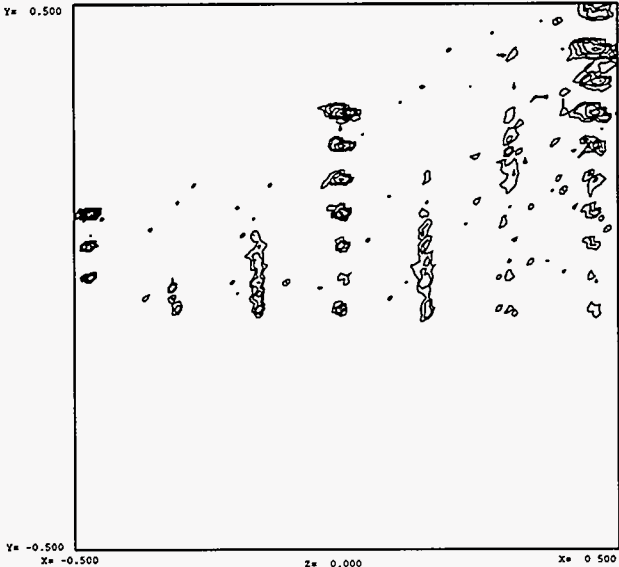


Fig.1 Elastic Bragg scattering and TDS in CsFeBr₃ along the [001] direction at room temperature.

References:

- (1) B.Dorner, D.Visser, U.Steigenberger, K.Kakurai & M.Steiner. Z. Phys. B 72; 487 (1988).
- (2) D.Visser, B.Dorner and M.Steiner. (submitted).
- (3) B.Schmid, B.Dorner, D.Visser and M.Steiner. Z. Phys. B86; 257 (1992).
- (4) D. Petitgrand, B.Hennion, C. escribe-Filippini and S.Legrand. J. de Phys. T42, C6 supp 12, 782 (1981).
- (5) C.J.Carlile, D.A.Keen and C.C.Wilson & B.T.M.Willis. Acta Cryst. A48; 826 (1992), and reference there in.

Instrument Used: <i>(please type)</i> SCD	Local Contact Allen Larson	Proposal Number: <i>(for LANSCE Use Only)</i> 6096
Title: Single Crystal Neutron Diffraction Study of the Structure of $Ce_{2-x}Pt_4Ga_{8+y}$		Report received: <i>(for LANSCE Use Only)</i> 6/2/94
Authors and affiliations: Allen C. Larson LANSCE George Kwei P-10 A. C. Lawson MST-5 Paul C. Canfield Iowa State University and Ames Laboratory		
Experiment report: <p>The newly discovered family of compounds $RE_{2-x}Pt_4Ga_{8+y}$ (where RE is rare earth) has been found to have many interesting transport properties. The material readily crystallizes into large hexagonal prismatic crystals, but the structures have been difficult to solve. Both neutron powder diffraction data and single crystal x-ray data had been collected, but refinements of coherent structural models against these data produced inconclusive results. The introduction of static disorder (vacancies and/or substitutional disorder) did not help the understanding of the structure although reasonably good refinement results were obtained. There was some indication that the unit cell found might be a sub-cell of the true cell. So a single crystal was examined on SCD which would produce conclusive data concerning the unit cell size and perhaps give an indication of the problem.</p> <div style="text-align: center;">  </div>		

Experiment report (*continued*):

A data set for a trigonal unit cell was collected on SCD. Examination of this data did not show the presence of any super lattice reflections, ruling out that as the cause of the problem. However, plots of the intensity data in various hkl nets showed the presence of diffuse scattering along the reciprocal lattice vectors $n/3, m/3, l$. A typical plot is shown above. This plot shows the $h, 2-h, l$ lattice net centered on the 310 reflection. The $h, 2-h, 0$ vector is horizontal increasing to the right and $00l$ points upward in the plot. The columns of discrete peaks are the $20l, 31l$ and $42l$ lattice rows. There are prominent streaks from diffuse scattering along the $8/3, 2/3, l$ and $10/3, 4/3, l$ lattice rows and the $7/3, 1/3, l$ and $11/3, 5/3, l$ lattice rows show somewhat weaker diffuse streaks.

These data can be interpreted in terms of a disordered structural model. These results are supported by data obtained from EXAFS data.

Further analysis of these data has not yet been carried out.

References:

Instrument used: <i>(please type)</i> SCD	Local contact: A.C. Larson	Proposal number: <i>(for LANSCE use only)</i> 6101/SCD
Title: Velocity of sound measurements in the linear chain antiferromagnet CsFeBr ₃ by means of the diffraction method. Part II.		Report received: <i>(for LANSCE use only)</i> 6/17/94
Authors and affiliations: D. Visser. Department of Physics, Loughborough University of Technology, Loughborough LE11 3TU, UK A.C. Larson. LANSCE, Los Alamos National Laboratory, Los Alamos, New Mexico 87545, USA.		
Experiment report: In the previous experiment we showed that for different values of Q different types of diffuse intensity distributions due to phonon scattering (thermal diffuse scattering) are observed in the diffraction data of CsFeBr ₃ . So far we have investigated the [001], [110] and [100] directions. We observe in all directions the predicted (3) different scattering regimes which are due to the change of the neutron velocity in respect to the velocity of sound (direction dependent) of the crystal. We also obtained information from the [001] direction that the space group of CsFeBr ₃ may have a lower symmetry than P6 ₃ /mmc. We observed reflections of the type 00 <i>l</i> ; <i>l</i> = odd. These reflections are forbidden in space group P6 ₃ /mmc. A similar observation has been made for CsMnBr ₃ . For this material it has been found that the (001) and (003) reflections are present in large crystals (D10 - ILL) at low temperatures and disappear at T = 70 K (1). In order to understand the diffuse scattering profiles in CsFeBr ₃ , it was necessary to redetermine the crystal structure of CsFeBr ₃ . We collected two sets of diffraction data on a small crystal at room temperature as well as at 20 K. This data is presently analysed. It became clear that these data sets do not show the forbidden reflections. Therefore we reexamined the big crystal in different settings (different scattering conditions). We found that the forbidden reflections disappear when changing the scattering conditions. This might indicate that a double diffraction process takes place (2).		

Experiment report (*continued*):

Further experiments were carried out on the big crystal of CsFeBr₃ at 20 K in order to determine the TDS scattering.

CsFeBr₃ contracts anisotropically, therefore one expects the phonon spectrum to change too. Such behaviour would be directly reflected in the diffuse scattering profile. One expects further that the profile of the diffuse scattering due to the energy gain process will not be present. Such indication have been observed.

References:

- (1) D.Visser & G.J. McIntyre. unpublished results.
- (2) J.C. Speakman. Acta Cryst. 18, 570 (1965).

Instrument used: <i>(please type)</i> Single Crystal Diffractometer	Local contact: Allen Larson	Proposal number: <i>(for LANSCE use only)</i> 6109
Title: Neutron Diffraction Analysis of Neutron-Induced Damage in Spinel (MgAl ₂ O ₄) Single Crystals		Report received: <i>(for LANSCE use only)</i> 5/6/94
Authors and affiliations: K.E. Sickafus, Los Alamos National Laboratory, Los Alamos, NM; A.C. Larson, Los Alamos National Laboratory, Los Alamos, NM; G.W. Hollenberg, Pacific Northwest Laboratory, Richland, WA; F.A. Garner, Pacific Northwest Laboratory, Richland, WA; R.C. Bradt, Univ. of Nevada-Reno, Reno, NV.		
Experiment report: The goal of the experiments described here is to use neutron diffraction to determine the extent of neutron-induced cation disorder in spinel (MgAl ₂ O ₄) single crystals, via measurement of the cation inversion parameter before and after irradiation. The general formula for spinel is given by: $(Mg_{g_{1-i}}^{2+} Al_i^{3+})^{A_{IV}} [Mg_{g_i}^{2+} Al_{2-i}^{3+}]_2^{B_{VI}} O_4 \quad \left\{ \begin{array}{l} i = 0 \quad \Rightarrow \quad normal \text{ spinel} \\ i = 2/3 \quad \Rightarrow \quad random \text{ cation arrangement.} \\ i = 1 \quad \Rightarrow \quad inverse \text{ spinel} \end{array} \right.$ The quantity in parentheses represents the average occupancy of A-sites (coordination IV), while the quantity in brackets represents the average occupancy of B-sites (coordination VI). The variable <i>i</i> is the so-called <i>inversion parameter</i> , which specifies the fraction of trivalent aluminum ions that occupy A-sites. Spinel single crystals were irradiated in the Materials Open Test Facility (MOTA) of the Fast Flux Test Facility (FFTF). The nominal irradiation conditions experienced by the crystals in the FFTF reactor were 24.9•10 ²⁶ n/m ² (<i>E_n</i> > 0.1 MeV) at 658K (249 dpa); 5.3•10 ²⁶ n/m ² at 678K (53 dpa); and 5.6•10 ²⁶ n/m ² at 1023K (56 dpa). One crystal was not irradiated, but stored under ambient conditions as a control sample (dpa represents displacements per atom). Irradiated crystals were analyzed using the single-crystal diffractometer (SCD) at the Manuel Lujan, Jr. Neutron Scattering Center (LANSCE), Los Alamos National Laboratory. The data reduction and structure refinement were carried out using the diffraction code GSAS (General Structure Analysis System [1]).		

Experiment report (*continued*):

Table 1 shows the results of the crystal structure refinements, based on the neutron diffraction data obtained from unirradiated and irradiated spinel samples. The only constraint in these refinements is that oxygen sites are fully-occupied by oxygen anions. Normalized, average scattering powers are shown for A- and B-site cations and for oxygen anion sites. Also indicated in Table 1 are the residual indices from the crystal structure refinement for each sample. The A-site (8(a)) scattering power, \hat{f}_A , is normalized by the coherent neutron scattering length for magnesium, $b_{Mg} = 5.375$ fm. Similarly, the scattering power \hat{f}_B for the B-site (16(b)) is normalized by $b_{Al} = 3.449$ fm, while \hat{f}_O for the oxygen-site (32(e)) is normalized by $b_O = 5.805$ fm. Coherent neutron scattering lengths were obtained from Koester *et al.* [2].

It is readily apparent in Table 1 that the scattering powers of both A- and B- cation sites in spinel are changed following neutron irradiation. It is observed that the average scattering power of an A-site diminishes following irradiation, while the scattering power of a B-site increases. Since the scattering length for Mg is much larger than for Al, these results suggest that the higher scattering power Mg atoms are replaced by Al atoms on A-sites and vice versa on B-sites, during neutron irradiation.

To determine the extent of inversion in each crystal, an additional *constrained* least-squares' refinement procedure was performed. The initial condition for this refinement procedure was a normal spinel lattice. The refinement required that (i) all A and B sites be occupied by a Mg or Al atom; (ii) occupancy of an A-site by an Al atom required simultaneous occupancy of a B-site by a Mg ion; (iii) the Al:Mg atom ratio in the crystal was fixed at 2:1. A summary of the results is presented in Table 2. Here, i is seen to increase from $i \sim 0.24$ in the unirradiated sample to inversion values ranging from 0.59 to 0.69 in the neutron irradiated samples. In fact $i \sim 0.69$ for the highest fluence sample (249 dpa) exceeds the value of i pertaining to randomized cation sublattices ($i = 0.67$).

These results suggest that in all neutron irradiated spinel samples, at least 35% of the A-sites (or equivalently, $\sim 17\%$ of the B-sites) in the irradiated spinel crystals have experienced Al^{3+} for Mg^{2+} disordering replacements. This retained dpa on the cation sublattices is the largest retained dpa ever measured in an irradiated spinel material (only 0.002 - 0.09% of the instantaneous dpa has ever been observed in the microstructure of irradiated spinel).

References:

- [1] A. C. Larson and R. B. VonDreele, "General Structure Analysis System (GSAS)," LA-UR 86-748, Los Alamos National Laboratory, Los Alamos, NM 87545, 1990.
- [2] L. Koester, H. Rauch, and E. Seymann, Atomic Data and Nuclear Data Tables **49** (1991) 66.

Table 1. Scattering power of tetrahedral and octahedral cation sites, and oxygen anion lattice sites, in unirradiated and neutron irradiated spinel crystals. Also tabulated are the residual indices from the crystal structure refinement for each crystal.

Sample	Scattering Power (normalized)			Residual Index	
	\hat{f}_A A-Site 8(a)	\hat{f}_B B-Site 16(d)	\hat{f}_O O-Site 32(e)	R	R_w
Unirradiated	0.862	1.001	1.000	0.076	0.065
56 dpa / 1023 K	.765	1.167	1.000	0.095	0.099
53 dpa / 678 K	.756	1.123	1.000	0.112	0.103
249 dpa / 658 K	.687	1.086	1.000	0.107	0.096

Table 2. Least-squares refinement results for inversion parameter, oxygen parameter, and residual indices for unirradiated and neutron irradiated spinel single crystals.

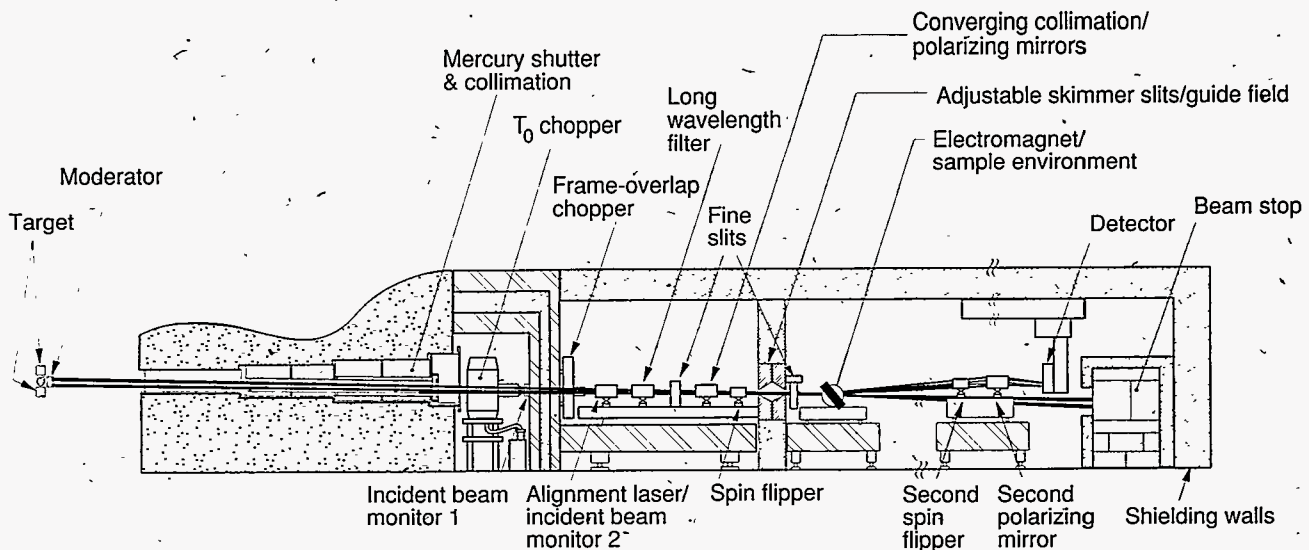
Sample	Inversion Parameter (i)	Residual Index	
		R	R_w
Unirradiated	.237 ± .020	0.074	0.066
56 dpa / 1023 K	.644 ± .016	0.093	0.072
53 dpa / 678 K	.592 ± .026	0.115	0.092
249 dpa / 658 K	.692 ± .026	0.109	0.099

*Surface Profile Analysis
Reflectometer (SPEAR)*

Surface Profile Analysis Reflectometer (SPEAR)

The Surface Profile Analysis Reflectometer (SPEAR) is designed to study solid/solid, solid/liquid, solid/gas, and liquid/gas interfaces. SPEAR's moderated neutrons are collimated into two beams inclined downwards at angles of 1.5° and 1.0° to the horizontal that converge at a common sample position, which is 8.73 m from the moderator. A specially designed shutter allows the beams to be operated either independently or simultaneously. The vertical resolution of each beam ($\Delta\theta/\theta$) is $\pm 5\%$ for horizontal surfaces and the horizontal resolution ($\Delta\theta$) is $+0.25^\circ$. A t-zero chopper, which interrupts the beam during the initial flash of high-energy neutrons and gamma rays, significantly reduces the background that may limit reflectivity measurements. A frame-overlap chopper, which defines the wavelength

band (1 to 16 Å or 16 to 32 Å) to be used, suppresses frame-overlap background problems. Polarizing supermirrors and spin-flippers can be inserted into the beam line before and after the sample position when polarized neutrons and analysis of the polarization state of the beam scattered by a sample are required. A goniometer at the sample position allows solid samples to be accurately tilted in order to change the angle of incidence of the beam relative to the reflecting surface. A vibration isolation system (Newport Corporation) supports the sample and actively dampens vibrations transmitted through the floor or air. SPEAR uses a single ^3He detector for low-reflectivity studies or a single linear position-sensitive detector with 2-mm resolution for studies of off-specular scattering.



Instrument Details

Moderator-to-detector distance	12.38 m
Wavelength frames at 20 Hz	$1 < \lambda < 16 \text{ \AA}$ $2 < \lambda < 7 \text{ \AA}$ (polarized beam) $16 < \lambda < 32 \text{ \AA}$
Q range (horizontal sample)	$0.007 < Q < 0.3 \text{ \AA}^{-1}$
Beam cross section at sample position (maximum sample <u>acceptance</u>)	5 mm high x 25 mm wide (1° beam) 7.5 mm high x 25 mm wide (1.5° beam) 1 mm high x 25 mm wide (polarized 1.5° beam)
Moderator	Liquid hydrogen at 20 K
Neutron flux at sample position for 1.5° beam at 60 μA :	$1 < \lambda < 6 \text{ \AA}$ $3.4 \times 10^5 \text{ n/cm}^2/\text{s}$ $6 < \lambda < 16 \text{ \AA}$ $3.3 \times 10^5 \text{ n/cm}^2/\text{s}$ $16 < \lambda < 32 \text{ \AA}$ $2 \times 10^5 \text{ n/cm}^2/\text{s}$
Detectors	Single ^3He tube 2-mm resolution linear ^3He position-sensitive detector
Sample environment	Solid/liquid interface cells; UHV evaporator; UHV oven; Langmuir trough; electromagnet (< 1 Tesla); controllable humidity oven; solid/liquid interface Poiseuille cell
Minimum reflectivity	$< 10^{-6}$
Experiment duration	30 minutes to 6 hours

Greg Smith, instrument scientist
Mike Fitzsimmons, instrument scientist
Ross Sanchez, instrument technician

SPEAR Experiment Reports

6009	<i>Characterization of the Surface Depletion Layer for a Tethered Chain (PDMS-PS Diblock Copolymer Monolayers at the Air Surface of Ethyl Benzoate)</i>	181
6021	<i>Studies of the Magnetic Structures and Properties of Thin Films Grown In Situ</i>	183
6028	<i>Analysis of the Structure and Orientation of Adsorbed Polymers in Solution Subject to Dynamic Shear Stress</i>	184
6033	<i>Effect of Rough Surfaces and Thin Films on the Diffuse Scattering Observed by Neutron Reflectometry</i>	186
6040	<i>Investigation of the Surface Structure and Molecular Orientation of Non-Newtonian Fluids under Shear Stress by Neutron Reflectometry</i>	189
6057	<i>Evolution of Order in Thin Block Copolymer Films</i>	191
6068	<i>Test of a Boron-Phosphide Neutron Detector</i>	193
6095	<i>A Study of Moisture Adsorption at the Molybdenum/Polyurethane Interface</i>	196
6102	<i>Neutron Reflectivity of Conducting Polymers</i>	198

Instrument used: (please type) SPEAR	Local contact: Greg Smith	Proposal number: <i>(for LANSCE use only)</i> 6009				
Title: Characterization of the Surface Depletion Layer For a Tethered Chain (PDMS-PS Diblock Copolymer Monolayers at the Air Surface of Ethyl Benzoate)		Report received: <i>(for LANSCE use only)</i> 3/15/94				
Authors and affiliations: <table style="width: 100%; border: none;"> <tr> <td style="width: 30%;">Michael S. Kent</td> <td>Sandia National Laboratories</td> </tr> <tr> <td>Greg S. Smith</td> <td>Los Alamos National Laboratories</td> </tr> </table>			Michael S. Kent	Sandia National Laboratories	Greg S. Smith	Los Alamos National Laboratories
Michael S. Kent	Sandia National Laboratories					
Greg S. Smith	Los Alamos National Laboratories					
Experiment report: <p>We have used neutron reflectivity to study the conformation of PDMS-PS diblock copolymers spread as monolayers on the surface of ethyl benzoate (EB). EB is a good solvent for PS and a nonsolvent for PDMS. PDMS homopolymer spreads to form an insoluble monolayer on the surface of EB. Since the copolymer also spreads on EB, the PDMS block is believed to lie flat on the surface while the PDMS block is submerged. The copolymer monolayer is spread by simply placing a dry grain on the EB surface. The PS block was fully deuterated while the PDMS block and EB were hydrogenated. Since the scattering length density of PDMS is nearly matched with air, only the PS block in EB was observed.</p> <p>In previous work¹ regarding a 4.5k-60k copolymer, we observed that the best fit profile required a maximum in PS segmental concentration away from the surface, or in other words, a depletion layer right at the surface. The goal of the present work was to characterize the variation of the form of the profile, and specifically the depletion layer, as a function of the PS molecular weight and the surface density. We therefore examined a new copolymer (21k-169k) at three surface concentrations covering nearly the entire range of surface density which is accessible in this experiment. In addition, we examined another copolymer (28k-330k), which, along with the 4.5-60 copolymer examined previously, should allow the characterization of the molecular weight dependence of the depletion layer.</p> <p>Representative curves for the 21-169 copolymer and the pure solvent are shown in Figure 1. The inset shows the low q region. Figure 2 shows the best fit profile using a parabolic function with a depletion layer and an exponential tail. In every case, the addition of a depletion layer in the profile significantly improved the quality of the fit. Our preliminary analysis indicates that the magnitude of the depletion layer is relatively insensitive to the surface density and the molecular weight of the PS block.</p>						

Experiment report (continued):

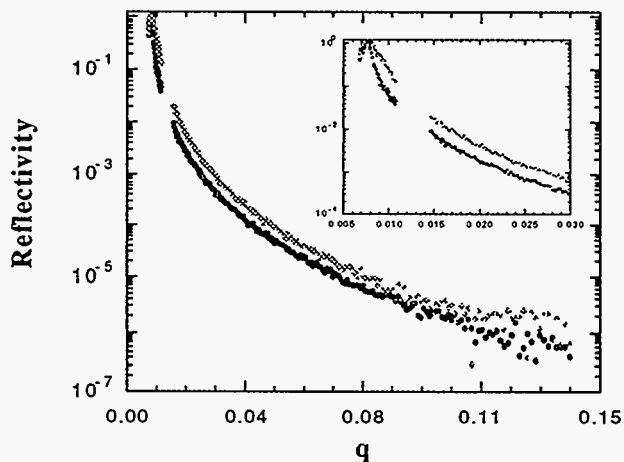


Figure 1. Reflectivity data for the pure solvent surface (lower) and with a monolayer of the 21-169 sample at high surface density (upper curve). The inset shows the low q region.

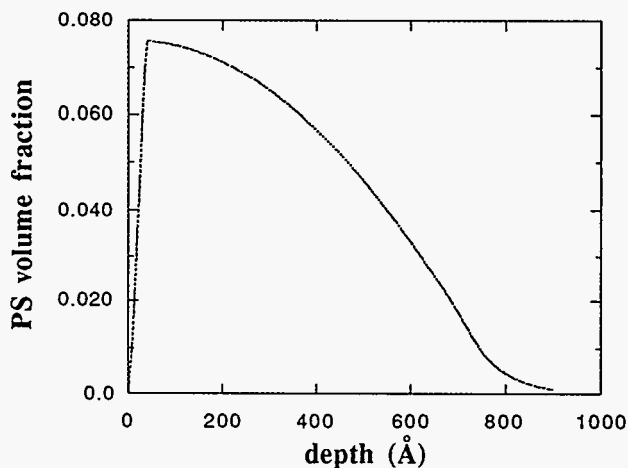


Figure 2. Best fit profile for the data in Figure 1 using a parabolic type profile with a depletion layer and an exponential tail.

References:

1. M. S. Kent, L. T. Lee, B. J. Factor, F. Rondelez, and G. S. Smith *Journal de Physique IV*, 3(8), (1993), 49.
2. M. S. Kent, L. T. Lee, B. J. Factor, F. Rondelez, and G. S. Smith submitted to *Macromolecules*

Instrument Used: <i>(please type)</i> SPEAR	Local Contact M.R. Fitzsimmons	Proposal Number: <i>(for LANSCE Use Only)</i> 6021
Title: Studies of the Magnetic Structures and Properties of Thin Films Grown In Situ		Report received: <i>(for LANSCE Use Only)</i> 3/7/94
Authors and affiliations: M.R. Fitzsimmons, LANSCE, LANL A. Röhl, Uni München, Germany E. Burkel, Friedrich-Alexander-Uni, Germany K.E. Sickafus, LANL G.S. Smith, LANSCE, LANL R. Pynn, LANSCE, LANL		
Experiment report: <p style="text-align: center;">Measured Enhancement of the Magnetic Moment of Nickel at a Large-Angle [001] Twist Grain Boundary</p> <p style="text-align: center;">M.R. Fitzsimmons[*], A. Röhl[†], E. Burkel[‡], K.E. Sickafus[§], G.S. Smith[*] and R. Pynn[*]</p> <p style="text-align: center;">[*]Manuel Lujan Jr., Neutron Scattering Center, Los Alamos National Laboratory, Los Alamos, New Mexico, USA [†]Sektion Physik der Universität München, München, Germany [‡]Friedrich-Alexander Universität, Erlangen-Nürnberg, Germany [§]Los Alamos National Laboratory, Los Alamos, New Mexico, USA</p> <p>Abstract— The atomic density and magnetization of a nickel twist grain boundary averaged over its lateral dimensions have been measured as a function of distance from the grain boundary plane. The magnetic moment of a nickel atom is found to be about 52% larger in a twist grain boundary than in the bulk. This enhancement is attributed to the reduced density of the grain boundary.</p> <p>PACS numbers: 61.72.Mm, 75.50.Rr, 75.70.Cn</p> <p>submitted to Phys. Rev. Lett., 1994.</p>		

Instrument Used: <i>(please type)</i> SPEAR	Local Contact Greg Smith	Proposal Number: <i>(for LANSCE Use Only)</i> 6028
Title: Analysis of the Structure and Orientation of Adsorbed Polymers in Solution Subject to Dynamic Shear Stress		Report received: <i>(for LANSCE Use Only)</i> 4/22/94
<p>Authors and affiliations:</p> <p>Shenda Baker Harvey Mudd College, Claremont, CA</p> <p>Greg Smith LANSCE</p> <p>Chris Toprakcioglu University of Patris, Greece</p>		
<p>Experiment report:</p> <p>Understanding the details of flow induced deformation of adsorbed and grafted polymer layers is especially important in applications such as size exclusion chromatography, adsorption and separation processes, waste water treatment, ultra filtration, enhanced oil recovery and microbial adhesion. Typically, the polymers are adsorbed to spherical colloidal particles in a column to maximize exposed surface area. By flowing a solution through the column past the polymer with an active binding ligand attached (occasionally, the polymer itself has binding capabilities), a specific component in the fluid can bound to the polymer and separation can be achieved. Depending on the interactions between the polymers, surface and solvent, the polymer geometry will be closely packed to the surface, tightly intermingled among themselves or extending out into the solution. Thus, the binding site may be exposed to the solvent or hidden in the entangled polymer chains.</p> <p>The effectiveness of these polymer based separation techniques depends on the interaction of molecules in the fluid flow with these adsorbed polymers of a certain geometry. Polymer detachment is also a concern when using high shear rates to increase throughput and is difficult to measure directly. Furthermore, the effect of shear and extent of solvent interactions on the polymer geometry may be drastically different after the selected macromolecule has adsorbed to the polymer support¹. As such, knowledge of the thickness, orientation, solvent and effect of shear rate on these polymer properties is imperative in the design of effective systems.</p> <p>A number of techniques have been used to measure, in static equilibrium, the average adsorbed layer thickness, called the effective hydrodynamic thickness (EHT). However, only the hydrodynamic flow method² and the ellipsometric technique³ have been used to examine the dynamic flow-induced deformation of adsorbed polymers. These techniques, though useful in obtaining an average polymer thickness, are unable to give information regarding the packing of the polymer, solvent interactions, or the location of the interactive end groups of the polymer in or out of the polymer "brush". Clearly, if the molecular portion of the polymer responsible for binding does not extend into the solution, any separation process will be thwarted.</p>		

Experiment report (continued):

To study these shear effects, we have began a series of neutron reflection experiments to measure the density profile of an adsorbed diblock copolymer in solution. The diblock chosen was the same as in previous studies, namely (poly)styrene-(poly)ethylene oxide. The solvent chosen was deuterated cyclohexane which is a poor solvent for both blocks at room temperature. The reflection measurements were made in a quartz cell as previously described⁴. Figure 1 shows our preliminary results where the reflectivity $X Q^4$ is plotted versus Q . The solid curve is for the case of zero shear. When the shear flow was established, the reflectivity curve changes dramatically as shown by the data represented by the triangles in the figure. We are currently in the process of analyzing this data in terms of models used previously for good solvents⁵.

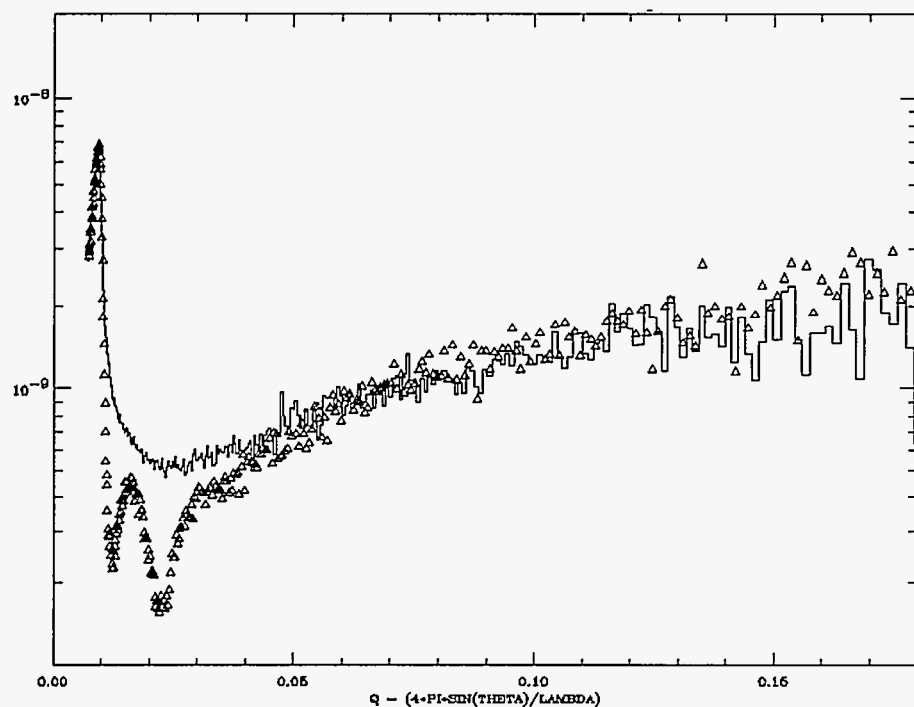


Figure 1. The measured reflectivity for a PS-PEO diblock copolymer in cyclohexane. The solid curve is for zero shear and the curve represented by triangles is for shear on.

References:

1. See Y. Cohen, *Macromolecules*, **21**, 494 (1988) and ref. therein.
2. Y. Cohen and F.R. Christ, *SPE Reservoir Eng.*, 113 (1986).
3. J.J. Lee and G.G. Fuller, *Macromolecules*, **17**, 375(1984).
4. S.M. Baker, S.S. Smith, R. Pynn, P. Butler, J Hayter, W. Hamilton, and L. Magid, *Rev. Sci. Instrum.*, **65**(2), 412 (1994).
5. J.B. Field, C. Toprakcioglu, L. Dai, G. Hadziioannou, G. S. Smith and W.A. Hamilton, *Journal de Physique II*, **2**, 2221,(1992).

Instrument Used: <i>(please type)</i> SPEAR	Local Contact Roger Pynn	Proposal Number: <i>(for LANSCE Use Only)</i> 6033
Title: Effect of Rough Surfaces and Thin Films on the Diffuse Scattering Observed by Neutron Reflectometry		Report received: <i>(for LANSCE Use Only)</i> 4/22/94
Authors and affiliations: Shenda Baker, Harvey Mudd College, Claremont, CA Roger Pynn, LANSCE Greg Smith, LANSCE Tom Russell, IBM, Almaden		
Experiment report: <p>Quantitative analysis of reflectivity data has traditionally been limited to the specular part of the scattering with a simple assumption of Gaussian roughness to explain the reduction in specular intensity due to diffuse scattering. While this approach may provide a satisfactory interpretation of the specular data (although we are beginning to see deviations from this assumption for very rough surfaces) little is learned about the nature of the rough surface itself. The diffuse scattering, which is easily measured using the PSD on SPEAR, contains information about the height-height correlations of the interfaces within a reflecting sample. In the simplest case of a bare substrate, the diffuse scattering is simply related to the Fourier transform of the height-height correlation function of the air/substrate interface. More complex situations arise for layered samples which display fringes of diffuse scattering either at constant k_{1z}, constant k_{2z}, or constant q_z. Here k_{1z} and k_{2z} are respectively the components of the incident and scattered neutron wavevectors perpendicular to the sample and $q_z = k_{1z} + k_{2z}$.</p> <p>Fringes at constant q_z are indicative of correlations between the roughness of parallel interfaces, while those at constant k_{1z} or constant k_{2z} result from interference between diffuse scattering from one interface and specular reflection from a nearby interface. [2] The profile of the fringes (ie the manner in which intensity dies off along the fringe) provides information about the degree of roughness of an interface and the healing length for roughness correlations between interfaces. The overall fringe intensity is related to the number of correlated rough interfaces. Intensities of the fringes can be calculated quantitatively within the distorted-wave Born approximation (DBWA).</p> <p>Last year we started experiments on several rough systems. [1] First, we wanted to examine the effect of a rough surface on the roughness of the air/liquid interface of a thin wetting film of polymeric material. A theoretical treatment of this case has already been provided by Robbins [3] who analyzed the way in which thin liquid films wet rough solid surfaces. The authors derive a general equation for the equilibrium shape of the surface, which depends strongly on wavevector. Surface height fluctuations on</p>		

Experiment report (*continued*):

length scales smaller than the film thickness or a "healing length", ξ , are strongly damped and produce little roughness of the film surface. At larger wavelengths, the films conform to the local fluctuations of substrate height. Second, we examined a multilayer of 30 bilayers of vanadium and carbon that was provided by Ovonic Corp. In fact, the design specifications called for this multilayer to be as perfect as possible with very smooth interfaces. Nevertheless, we observed significant diffuse scattering in a very distinctive pattern which we have been able to explain qualitatively by a DWBA calculation. Furthermore, we are presently performing calculations on polymer systems which form catenoids [4] having intense diffuse scattering.

Experiment

In order to complete the above studies, these experiments were done in 1993:

1--A detailed examination of "island" structures [5] prepared by T. Russell of IBM, Almaden was performed. Both "thick" and "thin" islands (200-500Å) were examined for both specular and diffuse scattering. To determine wetting effects of different layers, both carbon and gold were subsequently deposited on the rough surfaces.

2--Holographic and blazed gratings provide fairly uniform "rough" samples with which diffuse scattering of a known surface can be examined. Furthermore, nearly complete wetting on these surfaces can be done with Fomblin, provided that the grating of glass or silicon.

Analysis of these experiments is time consuming and computer intensive and are thus still in progress. However, we can see certain results already:

1--In both the thick and thin bare island samples, the diffuse scattering is spectacular. **Figure 1** shows a λ vs θ plot showing lines at constant k_z in addition to a line from the critical edge at constant q_z . We have shown this to be expected for the type of islands with facets that are present on this surface. Two-dimensional fitting routines are being developed as well as adequate theory to describe the bare surface.

When a film of carbon or gold is deposited on the surface, clear diffuse scattering is still observed, however the detailed nature of the scattering is difficult to discern by eye. When the 2-D fitting is operational, these distinctions will be accounted for.

2--Diffuse scattering from the gratings (bare) proved to be quite remarkable. By rotating the sample axis with respect to the incident neutron beam, we could effectively change the observed spacing of the grating and thus bring the diffuse scattering in and out of the range of our detector reproducibly. **Figure 2** shows a 3600grove/mm holographic grating rotated at 4° from perpendicular to the incident beam. We are still interpreting the details of the scattering, but can clearly state that we are observing overall roughness correlated in the x-direction (or y, depending on how you look at it) on the surface. We hope to incorporate the shape of the grating lines in our code since we have looked at both holographic (sinusoidal) and blazed (sharp known angle cuts). We also have wetted these surfaces with Fomblin, but have not begun analysis on those yet.

Figure 1 Specular and diffuse scattering from a thin island sample plotted as lambda as a function of theta.

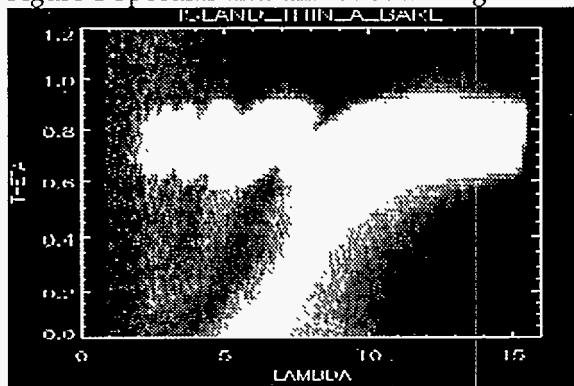
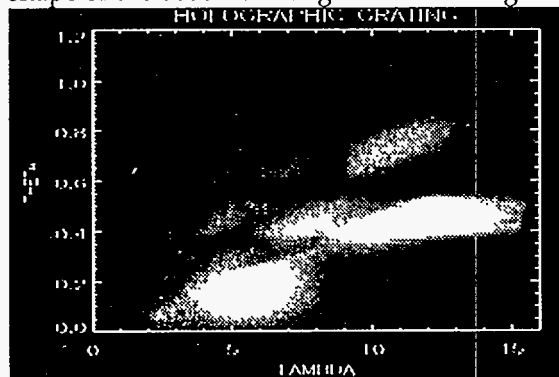


Figure 2 Specular and diffuse scattering from a holographic grating with 3600 grooves/mm. The diffuse peaks shown can be made to shift by varying the observed spacing of the grating with rotation relative to the incident beam. The shapes and intensities of the peaks also changes as would be expected since the shape of the observed rough surface changes.



References:

- [1] S. M. Baker *et al.* LANSCE Experiment Reports, 1992
- [2] R. Pynn *Phys. Rev. B* 45, 602 (1992)
- [3] M. O. Robbins, D. Andelman and J-F. Joanny *Phys. Rev. A* 43 (8), 4344 (1991)
- [4] Unpublished SPEAR results 1992 and M. O Delacruz, A. M. Mayes and B. W. Swift *Macromolecules* 20 (25), 944 (1992)
- [5] A.M. Mayes, T.P. Russell, P. Bassereau, S.M. Baker and G.S. Smith, *Macromolecules*, 27, 749(1994).

Instrument Used: <i>(please type)</i> SPEAR	Local Contact Greg Smith	Proposal Number: <i>(for LANSCE Use Only)</i> 6040
Title: Investigation of the Surface Structure and Molecular Orientation of Non-Newtonian Fluids Under Shear Stress By Neutron Reflectometry		Report received: <i>(for LANSCE Use Only)</i> 4/22/94
Authors and affiliations: Shenda M. Baker, Harvey Mudd College, Claremont, CA Greg Smith, LANSCE Roger Pynn, LANSCE John Hayter, ORNL Bill Hamilton, ORNL Lee Magid, University of Tennessee, Knoxville Paul Butler, University of Tennessee, Knoxville		
Experiment report: <p>A number of complex fluids exhibit viscoelastic properties which are widely exploited in industrial processes. There is however, little fundamental understanding of such systems at the molecular level. Our research has focused on this question, using the aqueous cetyltrimethylammonium dichlorobenzoate surfactants (denoted as i,j - indicating the position of the chlorine substituents on the benzene ring) as model systems. Indeed, 3,5 solutions, for example, are already viscoelastic at concentrations below 1%, while 2,6 solutions never show any elastic properties [1]. Adjusting the position and number of the chlorine substituents on the counterion provides a means of tuning the solutions through a range of behavior from Newtonian to highly viscoelastic. While the bulk properties of these systems are clearly important, and experiments in that area are ongoing, knowledge of the surface properties is critical to an understanding of some of the most important aspects of viscoelastic fluids, such as lubrication.</p> <p>Using a new shear cell for reflection measurements[2], results of our 1993 quartz shear cell reflection measurements on 3,5/D₂O solutions revealed two very interesting features. When the 3,5 solution is sheared a small peak appears at $Q=0.018 \text{ \AA}^{-1}$ (figure 1). This is probably due to the formation of a shear induced ordered state of characteristic length $\sim 400 \text{ \AA}$ in the near surface region. To our knowledge this is the first observation of such an effect, which saturated at surprisingly low flow rates and had a short relaxation time ($<15 \text{ min}$). Data from SANS [3], TEM [4], and light scattering [5] all indicate that the bulk 3,5 solution contains a mesh of very long rod-like micelles. Also, recent SANS measurements performed in the same quartz cell reveal that the rod-like micelles form an hexagonal lattice of rods when shear is applied[6]. Preliminary analysis of this data suggests that there is a monolayer of surfactant adsorbed to the quartz interface and that there is an oscillating density profile near the surface which decays within the first 2000 \AA from the surface.</p> <p>The second feature that we have seen in the data is the appearance of diffuse scattering when the shear flow is established (figure 2). This same diffuse scattering is absent when the shear flow is removed. This type of scattering is consistent with a roughened interface at the surface. This may be due to the local wiggles performed by the ordered rod-like micelles as they flow through the cell.</p>		

Experiment report (continued):

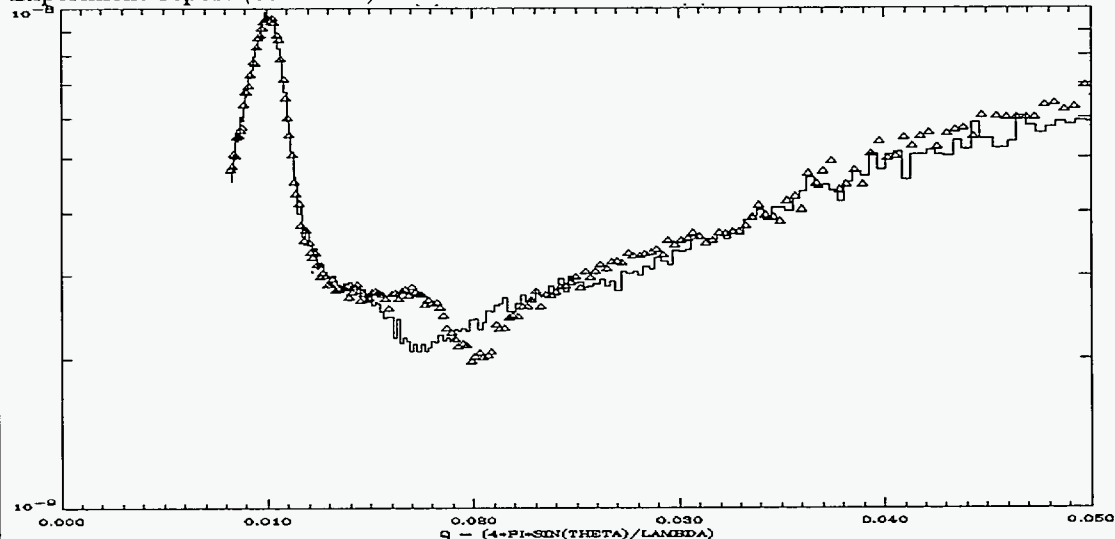


FIGURE 1. The measured reflectivity curve plotted as Reflectivity $\times Q^4$ versus Q . The solid line is the 0 shear data while the triangles are the data for the case of shear flow. We observe a peak in the shear data near $Q=0.017\text{\AA}^{-1}$.

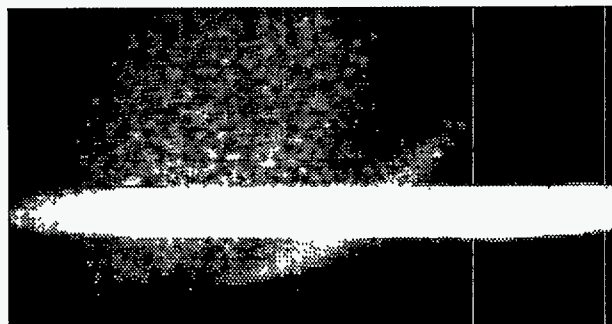


FIGURE 2. An intensity plot of the raw data. The x axis is the neutron wavelength going from 1.6 to 16 \AA while the y axis represents an angle of reflection from 0 to 1.2 degrees. the bright line across the data is the specular scattering. In addition, we see an arced curve of diffuse scattering which appears only in the sheared sample.

References:

- [1] M.T. Carver, PhD Dissertation, The University of Tennessee - Knoxville (1986).
- [2] S.M. Baker, G.S. Smith, R. Pynn, P. Butler, J. Hayter, W.H. Hamilton, and L. Magid, *Rev. Sci. Instrum.*, **65** (2), 412(1994).
- [3] J.C. Gee, PhD Dissertation, The University of Tennessee - Knoxville (1981).
- [4] L.J. Magid, J.C. Gee, and Y. Talmon, *Langmuir* **6**, 1609 (1990).
- [5] P.D. Butler, PhD Dissertation, The University of Tennessee - Knoxville (1991).
- [6] W.A. Hamilton, P.D. Butler, S.M. Baker, G.S. Smith, J.B. Hayter, L.J. Magid, and R. Pynn, "Shear Induced Hexagonal Ordering of a Dilute Solution of Threadlike Micelles," *Phys. Rev. Lett.*, April, (1994).

Instrument used: (please type) SPEAR	Local contact: GREG SMITH	Proposal number: <i>(for LANSCE use only)</i> 6057
Title: EVOLUTION OF ORDER IN THIN BLOCK COPOLYMER FILMS		Report received: <i>(for LANSCE use only)</i> 11/7/94
Authors and affiliations: <p style="text-align: center;"> T. P. Russell IBM Almaden Research Center, San Jose, California 95120 A. M. Mayes MIT, Cambridge, MA 02139 </p>		
Experiment report: <p>Neutron reflectivity measurements, in conjunction with x-ray reflectivity, was used to investigate the ordering of thin films of diblock copolymers¹. Symmetric diblock copolymers of perdeuterated polystyrene, d-PS, and poly(methyl methacrylate), PMMA, denoted, P(d-S-b-MMA), having $M_w = 8 \times 10^4$ with $M_w/M_n = 1.05$ were investigated in this study. Films of the copolymer with thicknesses of 680 and 800Å, corresponding to 2.1L and 2.5L, respectively, where L is the bulk period, were prepared on polished 5 cm diameter Si substrates by spin coating toluene solutions. For each thickness a matched sets samples were prepared and annealed 170°C for different periods of time to examine the evolution of the ordering of the copolymers. The identical samples investigated by neutron reflectivity were, also, studied by x-ray reflectivity. Neutron reflectivity is sensitive to the development of the internal structure of the copolymer, whereas x-ray reflectivity measurements are sensitive to the surface roughness.</p> <p>Shown in Figures 1-4 are a series of neutron reflectivity measurements on the 800Å film initially after spin coating (Fig.1) and after annealing at 170°C for 0.1 hr (Fig.2), 0.25 hr (Fig.3) and 4 hr (Fig.4). The development of the interferences arising from the multilayering of the diblock copolymer structure is clearly evident without a detailed analysis of the data. Shown along with each of the reflectivity profiles are the scattering length density profiles that yielded the best fit to the reflectivity data. In the as cast film, one clearly sees that the preferential interaction of the PMMA block with the substrate and the lower surface energy of the d-PS block, cause the development of oscillations in the concentration of the components from both the substrate and air interfaces. As a reference, the reflectivity profile shown as the dashed line in Figure 1 corresponds to that calculated from a homogenous film. Within a short period of annealing, the period of the oscillation has increased rapidly and has achieved basically the bulk period. This rapid change in the period corresponds to a rapid, local relaxation of the copolymer. As the annealing time increases, the period of the copolymer remains fixed, however, the ordering of the copolymer with respect to the improves markedly and, after four hours of annealing, the reflectivity profile shown in Figure 4 is obtained which is typical for a well order multilayered structure.</p> <p>Over this same time period, x-ray reflectivity results show that the surface roughness undergoes a dramatic increase initially. This corresponds to the time during which the copolymer is undergoing a rapid local relaxation. However, after the period</p>		

has been established and the periodic structure extends through the entire film, the surface roughness begins to diminish, becoming comparable to the roughness of the initial, as cast film. This behavior was observed for both the 2.1L and 2.5L thick samples suggesting a diffusive motion of copolymer chains over the surface of the film.

The results from these studies, coupled with corresponding electron microscopy studies², indicate that there are several different relaxation times associated with the ordering of the diblock copolymer. First, there is a rapid local relaxation of the chains to achieve their bulk equilibrium period. This results in the formation of a network type of structure within the film. This three-dimensional microphase separated network structure provides pathways of low resistance diffusion of the copolymer chains along the interface to produce the resultant multilayered structure. This, however, occurs over a much longer time scale.

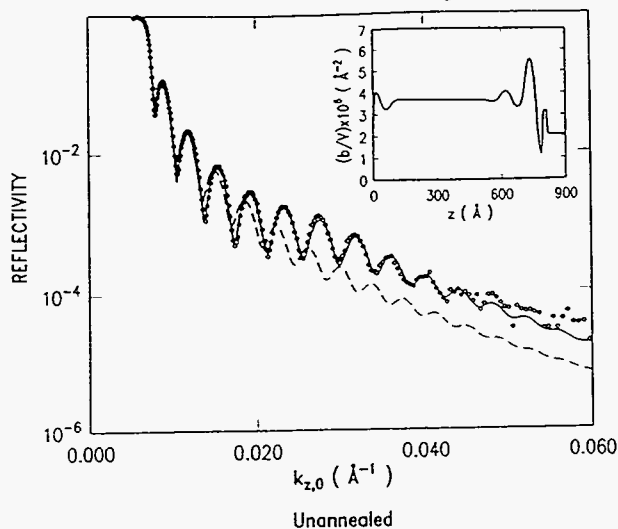


Figure 1. Neutron reflectivity profile for 800-Å film in the as-cast state. Dashed line through the data indicates best fit for a uniform film. Solid line corresponds to inset b/V profile. The air/polymer interface corresponds to 0 in the scattering length density profile.

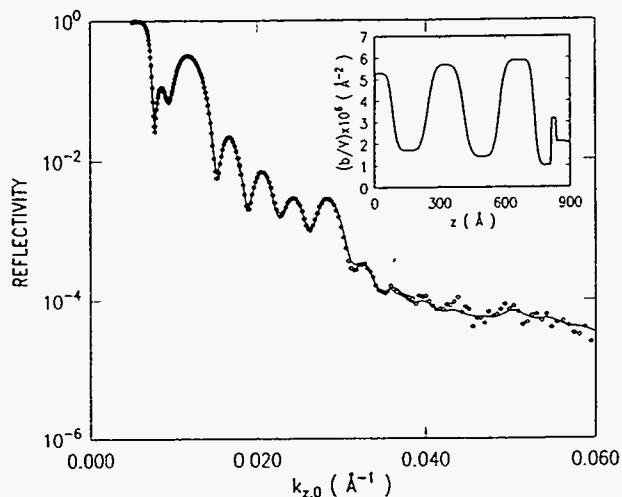


Figure 3. Neutron reflectivity profile and best-fit for 800-Å film annealed 0.25 h.

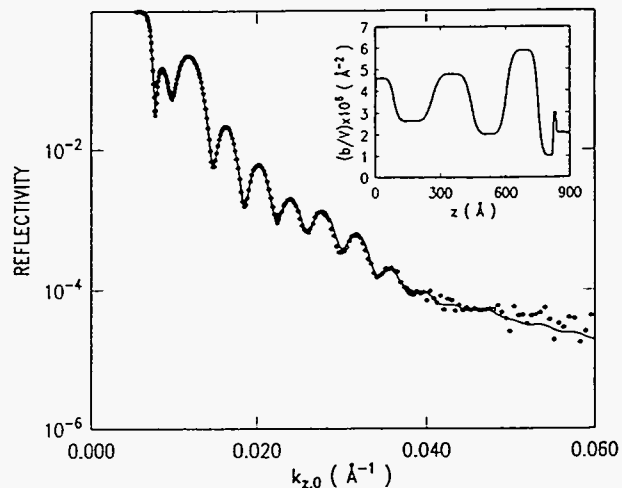


Figure 2. Neutron reflectivity profile for 800-Å film annealed 0.1 h. Solid line through data corresponds to inset b/V profile.

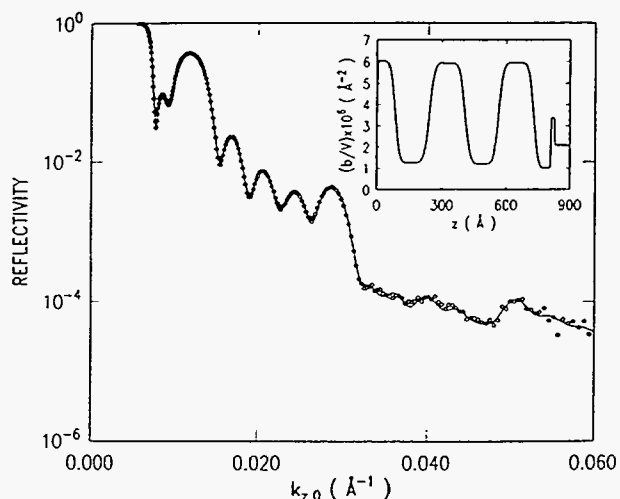


Figure 4. Neutron reflectivity profile and best-fit for 800-Å film annealed 4 h.

References

1. A. M. Mayes, T. P. Russell, P. Bassereau, S. M. Baker and G. S. Smith, *Macromolecules*, 27, 749 (1994).
2. T. P. Russell, A. M. Mayes and M. Kunz, in *Ordering in Macromolecular Systems*, A. Teramoto, M. Kobayashi and T. Norisuyi (Springer Verlag, Berlin), 1994.

Instrument Used: <i>(please type)</i> SPEAR	Local Contact M.R. Fitzsimmons	Proposal Number: <i>(for LANSCE Use Only)</i> 6068
Title: Test of a Boron-Phosphide Neutron Detector		Report received: <i>(for LANSCE Use Only)</i> 3/7/94
Authors and affiliations: M.R. Fitzsimmons, LANSCE, LANL J. Lund, Radiation Monitoring Devices, Inc, MA		
Experiment report: We tested a boron-phosphide (BP) solid state neutron detector. The detector consisted of a 12mm thick single crystal film of BP grown on silicon. The BP-silicon interface formed an ohmic contact as did the aluminum contact to the silicon substrate. A Schottky barrier at the interface between the surface of the BP film and a gold contact provided the rectifying barrier used to measure charges produced during the conversion of boron to lithium and α -particles. Curve (a) in Fig. 1 shows the intensity measured by the BP detector as a function of time-of-flight. Curve (b) is the intensity measured by the detector after the neutrons are absorbed by a one centimeter thick piece of boron-nitride. The oscillation in curves (a) and (b) are believed to be the result of grounding loops at the instrument. The difference between these curves is shown as curve (c) and represents the neutron spectrum measured by the BP detector. The similarity of curve (c) in Fig. 1 to the spectrum measured by a conventional BF ₃ gas detector (Fig. 2) suggests that semiconducting BP can be used to detect neutrons.		

Experiment report (continued):

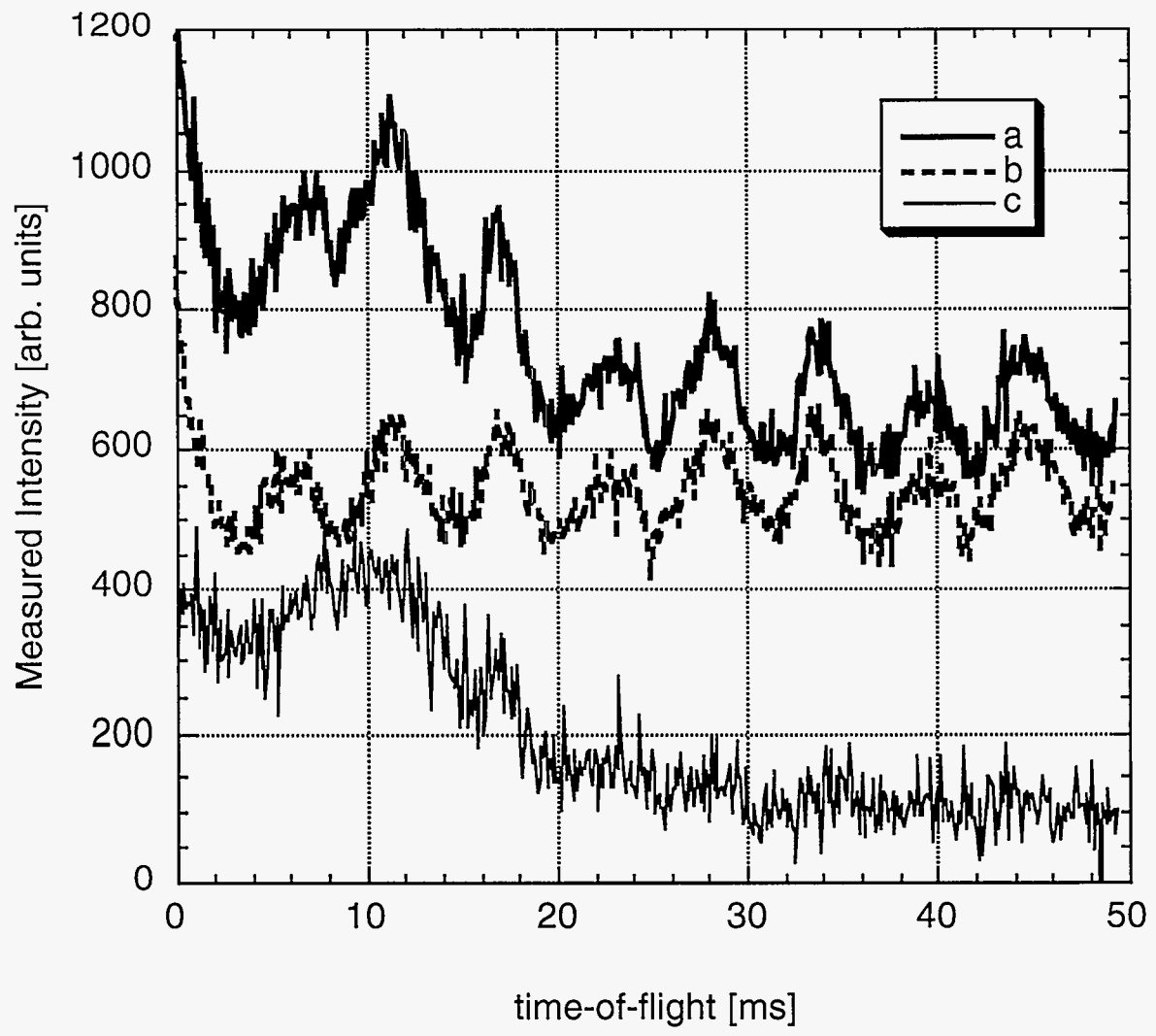


Fig. 1

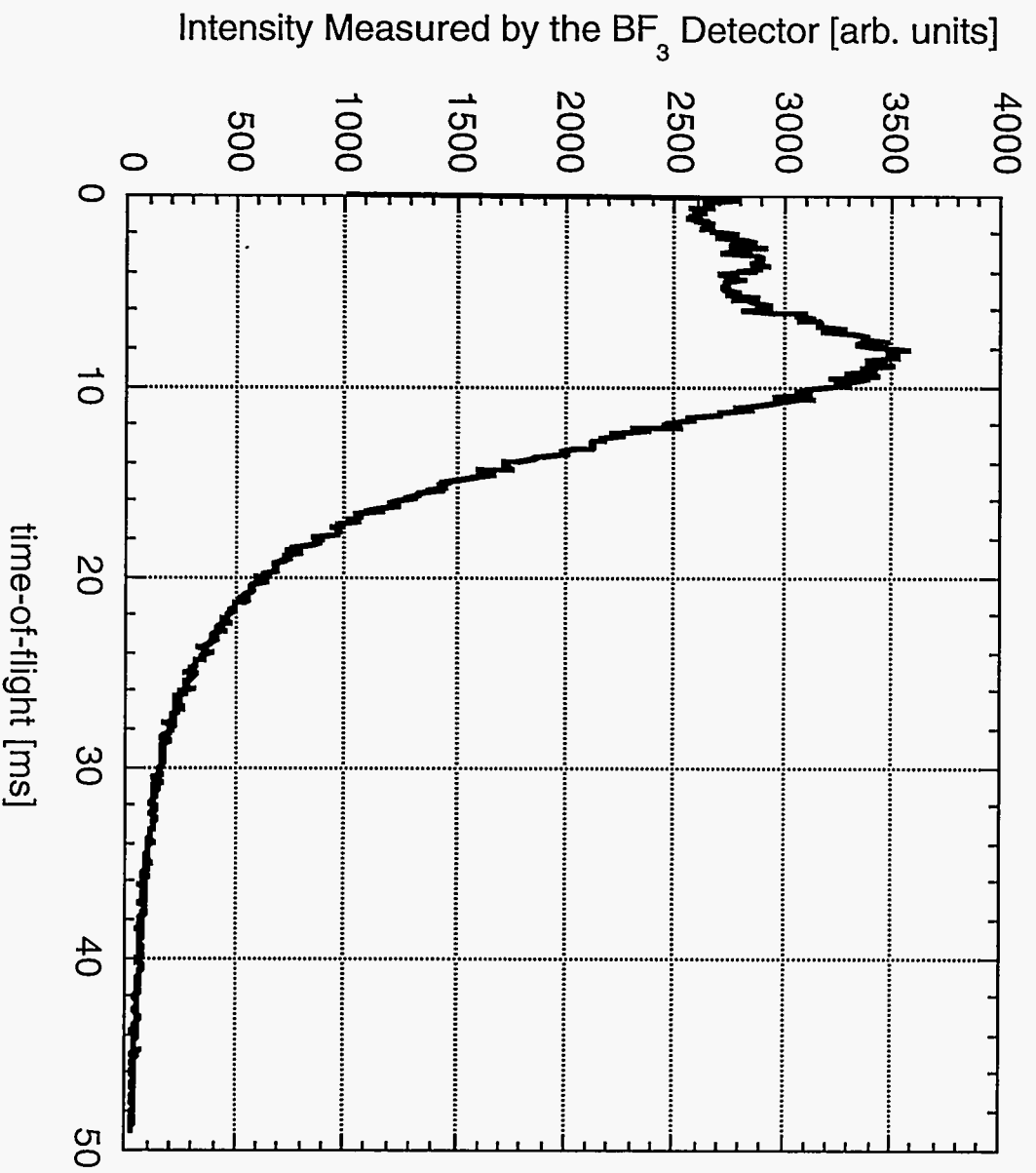


Fig. 2

References:

Instrument used: <i>(please type)</i> <p style="text-align: center;">SPEAR</p>	Local contact: <p style="text-align: center;">Greg Smith</p>	Proposal number: <i>(for LANSCE use only)</i> <p style="text-align: center;">6095</p>			
Title: <p style="text-align: center;">A Study of Moisture Adsorption at the Molybdenum/Polyurethane Interface</p>		Report received: <i>(for LANSCE use only)</i> <p style="text-align: center;">3/15/94</p>			
Authors and affiliations: <table style="width: 100%; border: none;"> <tr> <td style="width: 33%; vertical-align: top;"> Michael S. Kent Greg S. Smith Shenda Baker Steven Wages James Browning </td> <td style="width: 33%; vertical-align: top;"> Sandia National Laboratories Los Alamos National Laboratories Los Alamos National Laboratories Los Alamos National Laboratories Matrin Marietta Corp. </td> <td style="width: 33%;"></td> </tr> </table>			Michael S. Kent Greg S. Smith Shenda Baker Steven Wages James Browning	Sandia National Laboratories Los Alamos National Laboratories Los Alamos National Laboratories Los Alamos National Laboratories Matrin Marietta Corp.	
Michael S. Kent Greg S. Smith Shenda Baker Steven Wages James Browning	Sandia National Laboratories Los Alamos National Laboratories Los Alamos National Laboratories Los Alamos National Laboratories Matrin Marietta Corp.				
Experiment report: <p>We have used neutron reflectivity to study the profile of adsorbed moisture at the molybdenum/polyurethane (Mo/PU) interface as a function of the presence of a silane coupling agent. This work is part of a larger study of adhesion failure mechanisms at this interface.¹ To our knowledge, this is the first use of neutron reflectivity to study moisture adsorption at a metal/polymer interface. A recent report by Wu, et al. described the use of neutron reflectivity to study the adsorption of moisture to the interface between a polyimide and the native oxide surface of a silicon wafer.²</p> <p>The samples were prepared by first evaporating a thin (~ 1000 Å) layer of molybdenum onto the surface of a polished silicon single crystal. A 1000 Å PU film was then spin-coated onto the surface of the Mo from a toluene solution. Three samples were prepared containing 0.0, 0.63 and 1.93 wt. % 3-glycidoxypropyltrimethoxysilane in the PU. The neutron reflectivity for each sample was measured both in the dry state and upon exposure to a saturated D₂O atmosphere. Immediately upon exposure to D₂O, the reflectivity was measured as a function of time to determine the rate of diffusion of D₂O through the ~1000 Å PU film. The reflectivity curves for the three samples varied with time for the first ~ 30 minutes. The final time-independent curves for the 0.0 and 1.9 wt % silane samples, along with the curves for the dry state, are shown in Figures 1 and 2.</p> <p>For each sample, we observe an increase in the reflectivity of the wet samples relative to the dry state. With decreasing concentration of silane, the increase in reflectivity for the wet samples is greater and, in addition, there is a shift in the maxima toward lower q which increases in magnitude. This shift indicates the presence of a moisture rich layer at the interface. The data indicate a moisture content greater than 80% in this adsorbed layer (~ 15 Å) with no silane and roughly 50% for the 0.6 % silane sample. The 1.9 wt % silane sample shows no shift in the maxima, which indicates that the region adjacent to the Mo contains little or no excess moisture. In addition, the samples with no silane and 0.6 wt % silane indicate that moisture has penetrated into the oxide layer of the Mo. It is uncertain whether moisture penetration into the oxide occurs with the 1.9 % silane sample.</p> <p>In conclusion, we have demonstrated that the amount of moisture adsorbed to the Mo/Pu interface decreases with the amount of silane originally mixed into the bulk of the PU. The amount of silane needed to achieve a very low level of adsorbed moisture is</p>					

Experiment report (continued):

between 0.6 and 1.9 wt %. Further work relating this characterization information to mechanisms of adhesive failure for this and other systems is planned.

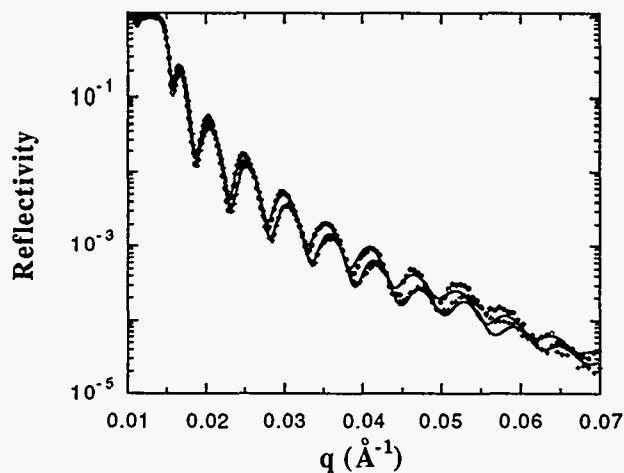


Figure 1. Reflectivity data along with best fit curves for the sample with 0.0 wt % silane. The upper and lower curves are for the wet and dry samples, respectively.

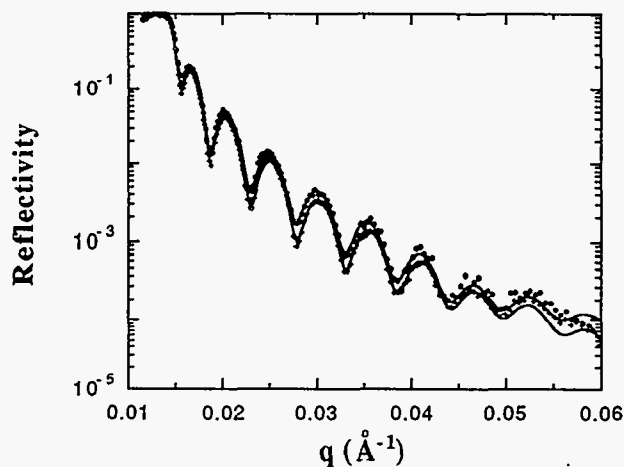


Figure 2. Reflectivity data along with best fit curves for the sample with 1.9 wt % silane. The upper and lower curves are for the wet and dry samples, respectively.

References:

1. M. S. Kent, D. MacIntyre, G. S. Smith, S. Baker, S. Wages, A. Nyitray, and J. Browning *Proceedings of the 17th Annual Meeting of the Adhesion Society*, 1994, pg 102.
2. W. L. Wu, W. J. Orts, C. J. Majkrzak, D. L. Hunston, Submitted to *Polym. Eng. and Sci.*

Instrument Used: <i>(please type)</i> SPEAR	Local Contact Greg Smith	Proposal Number: <i>(for LANSCE Use Only)</i> 6102															
Title: Neutron Reflectivity of Conducting Polymers		Report received: <i>(for LANSCE Use Only)</i> 4/8/94															
Authors and affiliations: <table border="0" style="width: 100%;"> <tr> <td style="width: 35%;">Greg Smith</td> <td style="width: 35%;">LANSCE</td> <td style="width: 30%;"></td> </tr> <tr> <td>Francisco Uribe</td> <td>MEE-11</td> <td></td> </tr> <tr> <td>Shimshon Gottesfeld</td> <td>MEE-11</td> <td></td> </tr> <tr> <td>Tom Zawodzinski</td> <td>MEE-11</td> <td></td> </tr> <tr> <td>Mike Fitzsimmons</td> <td>LANSCE</td> <td></td> </tr> </table>			Greg Smith	LANSCE		Francisco Uribe	MEE-11		Shimshon Gottesfeld	MEE-11		Tom Zawodzinski	MEE-11		Mike Fitzsimmons	LANSCE	
Greg Smith	LANSCE																
Francisco Uribe	MEE-11																
Shimshon Gottesfeld	MEE-11																
Tom Zawodzinski	MEE-11																
Mike Fitzsimmons	LANSCE																
Experiment report: <p>Conducting polymers have received significant attention in recent years as new materials with unique combinations of good electrical conductivity, mechanical flexibility, and ease of formation on surfaces. Furthermore, some conducting polymers have the additional qualities of high charge capacity and good charge cyclibility. For this reason, some of these materials emerge as candidates for use in electrochemical capacitors for use as car batteries etc.</p> <p>It has been shown using optical ellipsometry and quartz-crystal micro balance techniques that the overall morphology and density of conducting polymer films depend on the growth conditions of the film as well as the voltage cycling history of the films. Specifically, in polyaniline films, potential multicycling was shown to bring about an annealing effect in films using ellipsometry. Although much information has been inferred from these experiments, no direct measurements of the detailed structure of the films as a function of the various treatments have been undertaken.</p> <p>To perform these studies, we have designed an electrochemical cell for reflectivity studies. This cell is small and portable and may be transported to any neutron facility. The cell is made such that a polymer film is deposited onto a quartz crystal and the crystal is placed into an electrolyte solution. A platinum gauze is submerged in the same electrolyte to be the other plate of the capacitor. Then the density profile may be studied as a function of the cycling history of the potential. Also, the I/V curve may be measured as the cycling continues to match the behavior of the capacitor with the film's density profile.</p>																	

Experiment report (continued):

This will provide valuable information on the detailed morphological changes in the film as the capacitor is charged and discharged. This information will in turn help to modify film preparations so that the capacitors will be more robust. These studies will begin using polyaniline films, and will be expanded as new promising polymer materials are developed.

The first data taken in the cell is shown below. As can be seen, as a function of cycling history, the conducting polymer layer evolves with cycling. A cursory glance at the data suggests that the solvent-polymer interface is becoming more diffuse as a function of cycling. The data is presently being analyzed to obtain the detailed density profile.

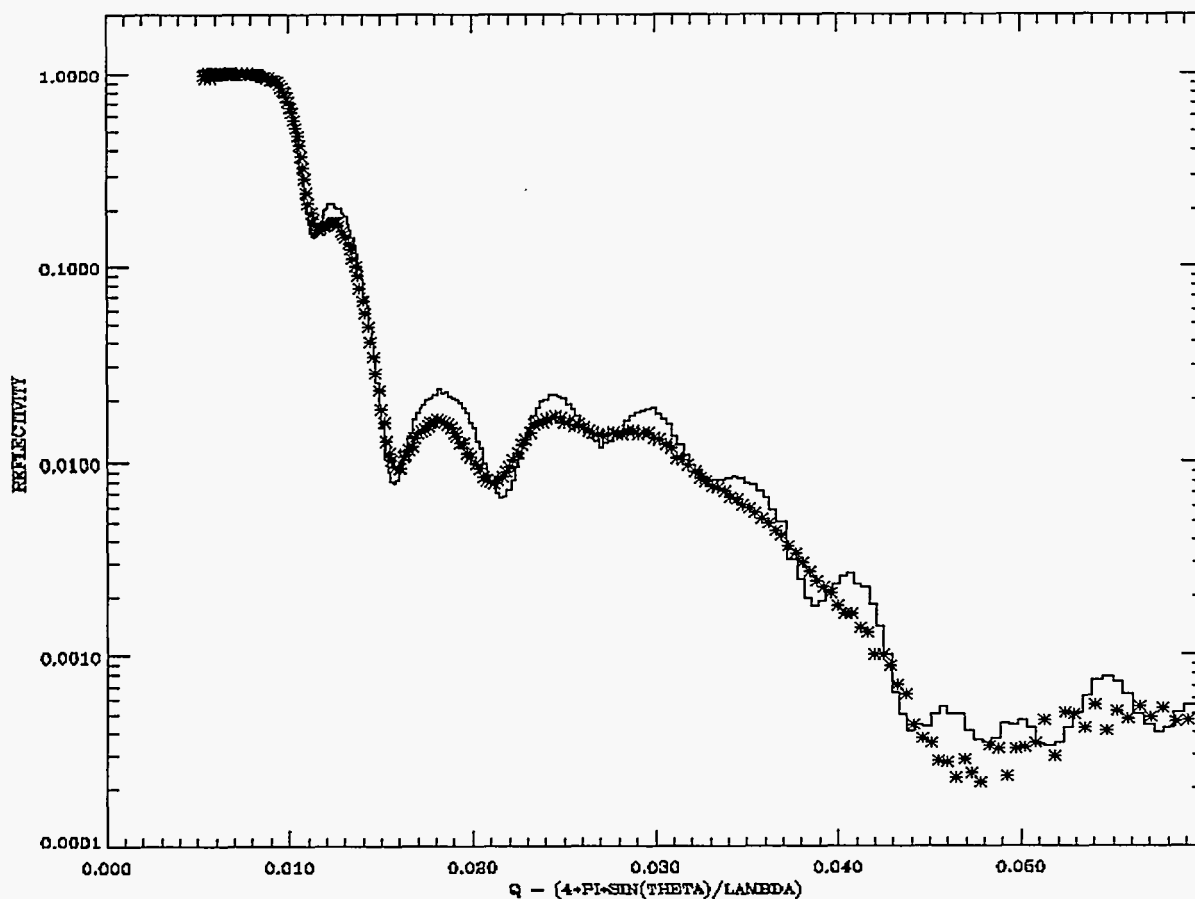


Fig1. The measured reflectivity for a conducting polymer. A quartz block was first prepared by depositing a film of titanium and then a film of platinum. The polymer was then deposited. The solid curve shows the reflectivity before any voltage cycling when the applied voltage was 0.6volts. The dashed curve is after cycling between 0.6v and -0.1v for ~1000 cycles.

Appendices

Condensed Matter Research.

Book Chapters

M. A. Bourke, J. A. Goldstone, M. G. Stout, and A. Needleman, "Characterization of Residual Stresses in Composites," *Fundamentals of Metal-Matrix Composites*, S. Suresh, A. Mortenson, and A. Needleman, Eds. (Butterworth-Heinemann, Boston, 1993), pp. 61-80.

R. B. Von Dreele, "Neutron Diffraction," *Materials Science and Technology, Vol 2B*, R.W. Cahn, P. Haasen, E.K. Kramer, Eds. (VCH Publishers, Inc., New York, 1994), chapter 19.

Published Articles

V. V. Grushin, B. E. Hauger, W. Klooster, T. F. Koetzle, R. K. McMullan, T. J. O'Loughlin, M. Pelissier, J. S. Ricci, M. P. Sigalas, and A. B. Vymenits, "Reaction of H₂ with IrHCl₂P₂ P = PiPr₃ or PtBu₂Ph): Stereoelectronic Control of the Stability of Molecular H₂ Transition Metal Complexes," *Journal of the American Chemical Society* **115**, 7300 (1993).

M. A. G. Aranda, J. P. Attfield, S. Bruque, and R. B. Von Dreele, "Chemical Switching of Magnetic Properties through Topotactic Lithium Exchange in Manganese(III) Arsenate Hydrate," *Chemical Communications* p. 155 (1994).

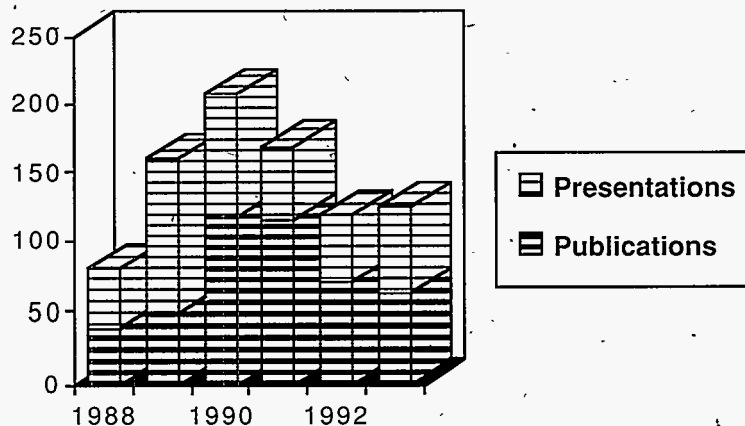
S. M. Baker, G. S. Smith, R. Pynn, P. Butler, J. B. Hayter, W. Hamilton, and L. Magid, "Shear Cell for the Study of Liquid-Solid Interfaces by Neutron Scattering," *Review of Scientific Instruments* **65**, 412-416 (1994).

M. Barthes, H. Kellouai, G. Page, J. Moret, S.W. Johnson, and J. Eckert, "H-Localized Mode in Chains of Hydrogen-Bonded Amide Groups," *Physica D*, **68**, 45-50 (1993).

G. Beaucage and R. S. Stein, "Tacticity Effects on Polymer Blend Miscibility," *Macromolecules* **26**, 1617-1626 (1993).

S. L. Billinge, G. H. Kwei, A. C. Lawson, J. D. Thompson, and H. Takagi, "Superconductivity and the Low Temperature Orthorhombic to Tetragonal Phase Transition in La_{2-x}Ba_xCuO₄," *Physical Review Letters* **71**, 1903-1906 (1993).

Presentations & Publications



- S. J. Billinge, G. H. Kwei, and H. Takagi, "Local Octahedral Tilts in $\text{La}_{2x}\text{Ba}_x\text{CuO}_4$: Evidence for a New Structural Length Scale," *Physical Review Letters* **72**, 2282-2285 (1994).
- S. J. Billinge, G. H. Kwei, and H. Takagi, "Local Structure and Superconductivity in $\text{La}_{2x}\text{Ba}_x\text{CuO}_4$ for $x = 0.125$ and 0.15 ," *Physica B* **199-200**, 244 (1994).
- M.A. Bourke, J. A. Goldstone, N. Shi, J. E. Allison, M. G. Stout, and A. C. Lawson, "Measurement and Prediction of Strain in Individual Phases of A 2219Al/TiC/15p-T6 Composite During Loading," *Scripta Metallurgica et Materialia* **29**, 771-776 (1993).
- P. C. Canfield, R. Movshovich, R. A. Robinson, J. D. Thompson, Z. Fisk, W. P. Beyermann, A. Lacerda, M. F. Hundley, R. H. Heffner, D. E. MacLaughlin, F. Trouw, and H. R. Ott, "Ground State Properties of YbBiPt ," *Physica B* **197**, 101-108 (1994).
- J. D. Corbett, J. Eckert, U. A. Jayasooriya, G. J. Kearley, and R. P. White, "Inelastic Neutron Scattering Study of the Metal Cluster Compound $\text{Li}_6[\text{Zr}_6\text{Cl}_{18}\text{H}]$," *Journal of Physical Chemistry* **97**, 8384 (1993).
- S. B. Dierker and P. Wiltzius, "Statics and Dynamics of a Critical Binary Fluid in a Porous Medium," *Physical Review Letters* **66**, 1185-1188 (1991).
- J. A. Eastman, M. R. Fitzsimmons, and L. J. Thompson, "Anomalous Defect Behavior Resulting from the Hydriding of Nanocrystalline Pd," *Philosophical Magazine Letters* **68**, 335-343, (1993).
- J. A. Eastman, M. R. Fitzsimmons, L. J. Thompson, A. C. Lawson, and R. A. Robinson, "Diffraction Studies of the Thermal Properties of Nanocrystalline Pd and Cr," *Nanostructured Materials* **1**, 465-470 (1993).
- J. Eckert and G. J. Kubas, "On the Barrier to Rotation of the Dihydrogen Ligand in Metal Complexes," *Journal of Physical Chemistry* **97**, 2378 (1993).
- J. Eckert, C.M. Jensen, G. Jones, E. Clot, and O. Eisenstein, "An Extremely Low Barrier to Rotation of Dihydrogen in the Complex $\text{IrClH}_2(\text{ETA}_2\text{-H}_2)(\text{PiPr}_3)_2$," *Journal of the American Chemical Society* **115**, 11056 (1993).
- M. R. Fitzsimmons, J. A. Eastman, R. A. Robinson, A. C. Lawson, J. D. Thompson, R. Movshovich, and J. Satti, "Unusual Magnetic Ordering in Nanocrystalline Cr," *Physical Review B: Condensed Matter* **48**, 8245 (1993).
- M. J. Geselbracht, A. M. Stacy, A. R. Garcia, B. G. Silbernagel, and G. H. Kwei, "Local Environment and Lithium Ion Mobility in LiNbO_2 : Inferences from Structure, Physical Properties, and NMR," *Journal of Physical Chemistry* **97**, 7102 (1993).
- R. Hjelm, P. Thiyagarajan, and H. Alkan-Onyuksel, "Organization of Phosphatidylcholine and Bile Salt in Rodlike Mixed Micelles," *Journal of Physical Chemistry* **96**, 8653-8661 (1992).
- L. John, E. M. Pearce, T. K. Kwei, W. A. Hamilton, G. S. Smith, and G. H. Kwei, "Hydrogen-Bonded Polymer Blends: The Influence of Annealing on the Interface Composition of Thin Films," *Macromolecules* **25**, 6770-6774 (1992).
- G. H. Kwei, J. M. Lawrence, W. P. Beyerman, P. C. Canfield, J. D. Thompson, Z. Fisk, A. C. Lawson, and J. A. Goldstone, "Thermal Expansion of $\text{Ce}_3\text{Bi}_4\text{Pt}_3$ at Ambient and High Pressure," *Physical Review B: Condensed Matter* **46**, 8067-8072 (1992).
- G. H. Kwei, A. C. Lawson, S. J. Billinge, and S.-W. Cheong, "Structures of the Ferroelectric Phases of Barium Titanate," *Journal of Physical Chemistry* **97**, 2368 (1993).
- G. H. Kwei, Y. T. Lee, M. F. Nicol, S. M. Sung, and R. N. Zare, "Preface - Dudley Herschbach 60th Birthday Festschrift," *Journal of Physical Chemistry* **97**, 2038 (1993).

- G. H. Kwei, J. E. Schirber, B. Morosin, E. L. Venturini, J. A. Voigt, J. A. Goldstone, and A. C. Lawson, "Phase Separation and Superconductivity in Superoxygenated $\text{La}_{2-x}\text{Sr}_x\text{CuO}_{4+\delta}$," *Physics and Chemistry of Solids* **54**, 1403 (1993).
- G. H. Kwei, J. O. Willis, T. Sakurai, J. A. Goldstone, A. C. Lawson, H. Yamauchi, and S. Tanaka, "Dopant Solubility, Phase Stability, and Superconductivity in Sr-doped $\text{La}_{2-x}\text{Sr}_x\text{CaCu}_2\text{O}_6$," *Physica C* **213**, 455 (1993).
- A. Lacerda, P. C. Canfield, W. P. Beyermann, M. F. Hundley, J. D. Thompson, G. Sparn, Z. Fisk, C. Burns, D. Barnhart, A. C. Lawson, G. H. Kwei, and J. A. Goldstone, "Possible Heavy-Fermion Behavior and Field-Induced Transitions in New R-Pt-Ga Compounds," *Journal of Alloys and Compounds* **181**, 191 (1992).
- A. C. Lawson, J. W. Conant, R. Robertson, R. K. Rohwer, V. G. Yound, and C. L. Talcott, "Debye-Waller Factors of PdD_x Materials by Neutron Powder Diffraction," *Journal of Alloys and Compounds* **183**, 174-180 (1992).
- A. C. Lawson, J. A. Goldstone, B. Cort, R. I. Sheldon, and E. M. Foltyn, "Atomic Thermal Vibrations of the Light Actinide Elements," *Journal of Alloys and Compounds* **213/214**, 426-428 (1994).
- A. C. Lawson, G. H. Kwei, J. A. Goldstone, B. Cort, R. I. Sheldon, E. Foltyn, J. Vaninetti, D. T. Eash, R. J. Martinez, and J. I. Archuleta, "Measurement of Atomic Elastic Constants by Pulsed Neutron Powder Diffraction," *Advances in X-Ray Analysis*, J. V. Gilfrich, et al., Eds. (Plenum Press, New York, 1993), Vol. 36, pp. 577-583.
- H. Nakotte, E. Bruck, J. H. Brabers, K. Prokes, F. R. de Boer, V. Sechovsky, K. H. Buschow, A. V. Andreev, R. A. Robinson, A. Purwanto, and J. W. Lynn, "Magnetic Properties of Single-Crystalline UCu_3Al_2 ," *IEEE Transactions Magnetics* **30**, 1217-1219 (1994).
- R. A. Robinson, P. C. Canfield, M. Kohgi, and T. Osakabe, "On the Low-Energy Excitations in YbBiPt ," *Bulletin of The American Physical Society* **38**, 79 (1993).
- R. A. Robinson, A. C. Lawson, J. A. Goldstone, and K. H. J. Buschow, "Magnetostuctural Distortions in the Noncollinear Hexagonal Antiferromagnet UPdSn ," *Journal of Magnetism and Magnetic Materials* **128**, 143-150 (1993).
- R. A. Robinson, A. C. Lawson, V. Sechovsky, L. Havela, Y. Kergadallan, H. Nakotte, and F. R. de Boer, "Magnetic and Crystallographic Structures in UTX Intermetallic Compounds," *Journal of Applied Physics* **213/214**, 528-532 (1994).
- R. A. Robinson, J. W. Lynn, A. C. Lawson, and H. Nakotte, "Temperature Dependence of Magnetic Order in Single-Crystalline UPdSn ," in *Proceedings of the 38th Annual MMM Conference*, Minneapolis, Minnesota, November 15-18, 1993, *Journal of Applied Physics* **75**, 6589-6591 (1994).
- R. A. Robinson, J. W. Lynn, A. C. Lawson, and H. Nakotte, "Temperature Dependence of Magnetic Order in Single-Crystalline UPdSn ," *Journal of Applied Physics* **75**, 6589-6591 (1994).
- V. Sechovsky, L. Havela, A. Purwanto, A. C. Larson, R. A. Robinson, K. Prokes, H. Nakotte, E. Brück, F. R. De Boer, P. Svoboda, H. Maletta, and M. Winkelmann, "Magnetic Phases in UNiGe ," *Journal of Alloys and Compounds* **293/294**, 536-539 (1994).
- N. Shi and R. J. Arsenault, "Influence of Thermally Induced Plasticity on the Bauschinger Effect of SiC/Al Composites," *Metallurgical Transactions A* **24**, 1879-1882 (1993).

Publications in Press or Submitted

M. Barthes, K. Kellouai, G. Page, J. L. Sauvajo, J. Eckert, S. Johnson, and J. Dianous, "Self-Trapping of Vibrational Energy in Chains of Hydrogen-Bonded Molecules," Los Alamos National Laboratory document LA-UR-93-1654 (submitted to *L'Actualite Chimique*).

J. Eckert, "Quasi-solutions or Conformation Substrates? Neutron Diffraction Study of Acetanilide," Los Alamos National Laboratory document LA-UR-93-3351 (submitted to *Physical Review Letters*).

G. H. Kwei and S. J. Billinge, "Pair Distribution Functions of Ferroelectric Perovskites: Direct Observation of Structural Ground States," Los Alamos National Laboratory document LA-UR-93-255 (submitted to *Ferroelectrics*).

E. W. Ong, J. Eckert, L. A. Dotson, and W. S. Glausinger, "Nature of Guest Species within Alkaline Earth-Ammonia Intercalates of Titanium DiSulfide," Los Alamos National Laboratory document LA-UR-93-3965 (submitted to *Chemical Materials*).

N. Shi, M. A. Bourke, J. A. Goldstone, M. G. Stout, A. C. Lawson, L. C. Davis, and J. E. Allison, "Influence of Thermal Residual Stresses on the Development of the Average Lattice Elastic Strain During External Loading in the Al/TiC Composite," Los Alamos National Laboratory document LA-UR-93-2106, (submitted to *Metallurgical Transactions A*).

Contributed Conference Presentations/Publications

B. Benicewicz, E. P. Douglas, and R.P. Hjelm, "Molecular Composites from Liquid Crystalline Polymers and Liquid Crystalline Thermosets," Los Alamos National Laboratory document LA-UR-93-2169, in *Proceedings of the International Workshop on Liquid Crystalline Polymers*, Capri, Italy, June 1-4, 1993.

M. A. Bourke, "Stress Measurement in Engineering Materials Using Pulsed Neutrons," Los Alamos National Laboratory document LA-UR-93-220, in *Proceedings of 1993 Meeting of American Crystallographic Association*, Albuquerque, New Mexico, May 23-28, 1993.

M. A. Bourke, J. A. Goldstone, and A. C. Lawson, "Pulsed Neutron Diffraction Measurement of Strain in Individual Phases of Metal Matrix Composites Before, During, and After Loading at Different Temperatures," Los Alamos National Laboratory document LA-UR-93-357, in *Proceedings of Fourth International Conference on Residual Stresses*, Baltimore, Maryland, June 8-10, 1994.

M. A. Bourke, J. A. Goldstone, A. C. Lawson, N. Shi, and J. E. Allison, "Measurement of Strain in Individual Phases of Composites Before, During, and After Mechanical Loading," Los Alamos National Laboratory document LA-UR-93-538, in *Proceedings of ICANS XII*, Abingdon, United Kingdom, May 24-28, 1993.

J. Eckert and S. Johnson, "Self-Trapped States in Chains of Hydrogen Bonded Molecules," Los Alamos National Laboratory document LA-UR-93-4125, in *Proceedings of Workshop on The Extension of the Concept of Localized States*, Universite Montpellier II, Montpellier, France, October 29-30, 1992.

M. R. Fitzsimmons, E. Burkel, and G. S. Smith, "The Magnetic Structures of Planar Interfaces," Los Alamos National Laboratory document LA-UR-93-894, in *Proceedings of Surface X-Ray and Neutron Scattering Conference*, Dubna, Russia, June 24-29, 1993.

M. R. Fitzsimmons, E. Burkel, G. S. Smith, and M. A. Natasi, "The Magnetizations of Phase and Grain Boundary Interfaces," Los Alamos National Laboratory document LA-UR-93-1750, in *Proceedings of the American Vacuum Society's 40th Symposium*, Orlando, Florida, November 16-18, 1993.

R. Hjelm, E. Douglas, and B. Benicewicz, "Towards the Realization of Molecular Composites from Liquid Crystalline Polymers and Liquid Crystalline Thermosets," Los Alamos National Laboratory document LA-UR-93-3430, *Materials Research Society Meeting*, Boston, Massachusetts, November 29-December 3, 1993.

R.P. Hjelm, W. A. Wampler, and P. A. Seeger, "Small Angle Scattering, Contrast Variation and the Study of Complex Composite Materials: A Study of the Structure of Carbon Black," Los Alamos National Laboratory document LA-UR-93-1657, in *Proceedings of the Annual Meeting of The Rubber Division of the American Chemical Society*, Denver, Colorado, May 18-22, 1993, (submitted to *Rubber Chemistry and Technology Journal*, 1993).

H. Küppers and J. Eckert, "Inelastic Neutron Scattering Study of the Extremely Short Intramolecular Hydrogen Bond in Quinolinic Acid," Los Alamos National Laboratory document LA-UR-93-539, in *Proceedings of International Union of Crystallography Congress XVI*, Beijing China, August 23-27, 1993.

A. C. Lawson, J. A. Goldstone, B. Cort, R. I. Sheldon, and E. Foltyn, "Debye-Waller Factors of the Light Actinide Elements," Los Alamos National Laboratory documents LA-UR-93-1802 & 3463, in *Proceedings of Actinides 93*, TMS Annual Meeting, San Francisco, California, February 1994.

H. Nakotte, E. Bruck, F. R. de Boer, K. H. Buschow, A. V. Adreev, R. A. Robinson, A. Purwanto, and J. W. Lynn, "Electronic Properties of UCu_xAl_{5-x} ," Los Alamos National Laboratory document LA-UR-93-1066, in *Proceedings of 23rd Journées des Actinides*, Schwarzwald, Germany, April 20-23, 1993.

H. Nakotte, E. Bruck, F. R. de Boer, V. Sechovsky, L. Havela, R. A. Robinson, A. C. Lawson, V. Nunez, J. W. Lynn, and K. H. Buschow, "Crystallographic and Magnetic Structures of $UPdSn$ and $UAuSn$," Los Alamos National Laboratory document LA-UR-93-1105, in *Proceedings of 23rd Journées des Actinides*, Schwarzwald, Germany, April 20-23, 1993.

E. W. Ong and J. Eckert, "Distinguishable Ammonia Species in Alkaline Earth-Ammonia Intercalated Titanium Disulfide," Los Alamos National Laboratory document LA-UR-93-1751, in *Proceedings for the American Chemical Society's National Meeting*, Chicago, Illinois, August 22-27, 1993.

R. Pynn, "Diffuse Neutron Scattering Signatures of Rough Films and Multilayers," Los Alamos National Laboratory document LA-UR-93-779, in *Proceedings of Surface X-Ray and Neutron Scattering* Dubna, Russia, June 24-29, 1993.

R. Pynn, "Plans for a New Pulsed Spallation Source at Los Alamos," Los Alamos National Laboratory document LA-UR-93-1972, in *Proceedings of ICANS XII*, Abingdon, United Kingdom, May 24-28, 1993.

R. Pynn, "Studying Surface Roughness with Neutrons," Los Alamos National Laboratory document LA-UR-93-1263, *Neutron Scattering Satellite Meeting*, Beidaihe, China, August 17-19, 1993.

R. A. Robinson, A. C. Lawson, A. C. Larson, R. B. Von Dreele, and J. A. Goldstone, "Rietveld Refinement of Magnetic Structures from Pulsed-Neutron-Source Powder-Diffraction Data," Los Alamos National Laboratory document LA-UR-93-0347, in *Proceedings of ICANS XII*, Abingdon, Oxford, May 24-28, 1993.

R. A. Robinson, A. C. Lawson, A. C. Larson, R. B. Von Dreele, and J. A. Goldstone, "Rietveld Refinement of the Crystal and Magnetic Structure of UPdSn from Spallation Neutron Source Powder Diffraction Data," Los Alamos National Laboratory document LA-UR-93-220, in *Proceedings of 1993 Meeting of American Crystallographic Association*, Albuquerque, New Mexico, May 23-28, 1993.

R. A. Robinson, A. C. Lawson, V. Sechovsky, L. Havela, Y. Kergadallan, H. Nakotte, and F. R. de Boer, "Magnetic and Crystallographic Structures in UTX Intermetallic Compounds," Los Alamos National Laboratory document LA-UR-93-2739, *International Conference on Actinides*, Santa Fe, NM, September 19-24, 1993.

T. P. Russell, A. M. Mayes, Y. Gallot, R. P. Hjelm, and P. A. Seeger, "The Lower Disorder to Order Transition in Diblock Copolymers," Los Alamos National Laboratory document LA-UR-93-3884, in *Proceedings of American Physical Society Meeting*, Seattle, Washington, March 22-26, 1993.

N. Shi, M. A. M. Bourke, J. A. Goldstone, and J. E. Allison, "Development of the Average Lattice Phase-Strain and Global Elastic Macro-Strain in Al/TiC Composites," Los Alamos National Laboratory document LA-UR-93-1107, in *Proceedings of the Fourth International Conference on Residual Stresses*, Baltimore, Maryland, June 8-10, 1994.

V. Sechovsky, L. Havela, A. Purwanto, A. C. Larson, R. A. Robinson, K. Prokes, H. Nakotte, E. Brück, F. R. De Boer, P. Svoboda, H. Maletta, and M. Winkelmann, "Magnetic Phases in UNiGe," Los Alamos National Laboratory document LA-UR-93-3350, *International Conference on Actinides*, Santa Fe, New Mexico, September 19-24, 1993.

G. Smith, A. M. Mayes, P. Bassereau, and T. P. Russell, "Time Evolution of the Ordering Process in Thin Copolymer Films," Los Alamos National Laboratory document LA-UR-93-425, in *Proceedings of American Physical Society*, Seattle, Washington, March 22-26, 1993.

Invited Talks

M. Barthes, H. Kellouai, G. Page, J. Eckert, S. Johnson, and R.K. McMullan, "Chains of Hydrogen-Bonded Molecules: Structural Data and Localized Modes," Los Alamos National Laboratory document LA-UR-93-1655, in *Proceedings of 8th International Workshop on Nonlinear Coherent Structures in Physics*, Bayreuth, Germany, June 1-4, 1993.

S. J. Billinge, J. D. Thompson, and G. H. Kwei, "Experimental Evidence for Lattice Effects in High Temperature Superconductors," Los Alamos National Laboratory document LA-UR-93-4363, in *High Temperature Superconductivity - Proceedings (The Los Alamos Symposium - 1993)*, K. Bedell, et al., Eds. (Addison Wesley, Redwood City, 1994).

M. A. Bourke, J. A. Goldstone, M. G. Stout, A. C. Lawson, and J. E. Allison, "Strain Measurement in Individual Phases of an Al/TiC Composite During Mechanical Loading," Los Alamos National Laboratory document LA-UR-93-3596, in *Proceedings of Annual TMS Meeting*, Denver, Colorado, February 21-25, 1993.

J. Eckert, "Origin of the Barrier to Rotation of the Dihydrogen Ligand in Metal Complexes," Los Alamos National Laboratory document LA-UR-93-1656, in *Proceedings of the American Chemical Society National Meeting*, Chicago, Illinois, August 22-27, 1993.

J. Eckert, "The Barrier to Rotation and Bonding Interactions of the Dihydrogen Ligand in Metal Complexes," Los Alamos National Laboratory document LA-UR-93-3860, in *Proceedings of American Chemical Society National Meeting*, Denver, Colorado, March 27, 1993.

J. Eckert, R. Varma, L. Diebolt, and M. Reid, "Inelastic Neutron Scattering Studies of Active Material From Discharged Ni Positive Plates," Los Alamos National Laboratory document LA-UR-93-1796, in *Proceedings of the Electrochemical Society Meeting*, New Orleans, Louisiana, October 10-15, 1993.

R.P. Hjelm, "Spontaneous Liposome Formation in Bile Salt-Phosphatidylcholine Mixed Aqueous Colloids," Los Alamos National Laboratory document LA-UR-93-2658, in *Proceedings of the 1st International Conference on Pharmaceutical Sciences and Technology*, Chicago, Illinois, August 24-38, 1993.

R. P. Hjelm, W. A. Wampler, and P. A. Seeger, "Microstructure of Composite Materials using Small-Angle Neutron Scattering of Contrast Variation," *Polymers and Polymer Composites* 1, 53A-70A (1993), Los Alamos National Laboratory document LA-UR-93-4371.

M. R. James, M. A. Bourke, J. A. Goldstone, and A. C. Lawson, "Diffraction Measurements of Residual Stress in Titanium Matrix Composites," in *Proceedings of TSM Spring Meeting*, Denver, Colorado, February 21-25, 1993, Los Alamos National Laboratory document LA-UR-93-3831.

A. C. Lawson, "Magnetic Structures by Neutron Powder Diffraction," Los Alamos National Laboratory document LA-UR-93-711, GSAS User's Workshop, Los Alamos, New Mexico, February 24-26, 1993.

R. Pynn, "Can Neutron Scattering Solve 'Real' Problems?," Los Alamos National Laboratory document LA-UR-93-1436, in *Proceedings of Neutron Scattering Satellite Meeting*, Beidaihe, China, August 17-19, 1993.

J. D. Thompson, W. P. Beyermann, P. C. Canfield, M. F. Hundley, G. H. Kwei, A. Lacerda, Z. Fisk, R. S. Kwok, J. M. Lawrence, and A. Severing, "Thermodynamics and Transport in $Ce_3Bi_4Pt_3$ and Related Materials," Los Alamos National Laboratory document LA-UR-92-2800, in *Transport and Thermal Properties of Electron Systems*, H. Fujii, T. Fujita, and G. Oomi, Eds. (Plenum Press, New York, 1993), p. 35.

Operations—Computers, Targets, Moderators

Contributed Conference Presentations

C. A. Beard, P. W. Lisowski, G. J. Russell, and L. S. Waters, "Comparison of Energy Deposition Calculations by the LAHET Code System with Experimental Results," Los Alamos National Laboratory document LA-UR-93-2582, in *Proceedings of the International Conference on Future Nuclear Systems: Emerging Fuel Cycles and Waste Disposal Options (Global '93)*, (American Nuclear Society, La Grange Park, 1993), p. 403.

T. O. Brun, C. A. Beard, L. L. Daemen, E. J. Pitcher, G. J. Russell, and W. B. Wilson, "LAHET Code System/CINDER'90 Validation Calculations and Comparison with Experimental Data," Los Alamos National Laboratory document LA-UR-94-269, in *Proceedings of the Twelfth Meeting of the International Collaboration on Advanced Neutron Sources (ICANS XII)*, Abingdon, United Kingdom, May 24-28, 1993.

L. L. Daemen, "A Tc-99 Burner for the Hanford Waste," Los Alamos National Laboratory document LA-UR-93-2974, abstract in *Transactions of the American Nuclear Society* 69, 440 (1993).

L. L. Daemen, E. J. Pitcher, and G. J. Russell, "A Hybrid Beryllium/Heavy Water Reflector for ISIS," Los Alamos National Laboratory document LA-UR-93-4259, in *Proceedings of the Twelfth Meeting of the International Collaboration on Advanced Neutron Sources (ICANS XII)*, Abingdon, United Kingdom, May 24-28, 1993.

L. L. Daemen, G. J. Russell, and E. J. Pitcher, "Moderator Materials and Neutronic Performance," Los Alamos National Laboratory document LA-UR-93-4257, in *Proceedings of the Twelfth Meeting of the International Collaboration on Advanced Neutron Sources (ICANS XII)*, Abingdon, United Kingdom, May 24-28, 1993.

G. J. Russell, "Los Alamos Pulsed Spallation Neutron Source Target Systems—Present and Future," Los Alamos National Laboratory document LA-UR-93-2976, abstract in *Transactions of the American Nuclear Society* 69, 431 (1993).

G. J. Russell, G. D. Baker, R. J. Brewton, A. Bridge, T. O. Brun, M. Cappiello, C. E. Cummings, L. L. Daemen, D. Davis, D. Grisham, R. P. Hjelm, J. S. Elson, A. Kernodle, M. A. Merrigan, E. J. Pitcher, H. Robinson, L. Walker, and R. Woods, "Target Station Design for a 1 MW Pulsed Spallation Neutron Source," Los Alamos National Laboratory document LA-UR-94-404, in *Proceedings of the Twelfth Meeting of the International Collaboration on Advanced Neutron Sources (ICANS XII)*, Abingdon, United Kingdom, May 24-28, 1993.

W. B. Wilson, T. R. England, E. D. Arthur, C. A. Beard, C. D. Bowman, L. L. Daemen, L. N. Engel, V. Gavron, D. C. George, H. G. Hughes, W. W. Kinnison, R. J. LaBauve, D. M. Lee, H. Lichtenstein, P. W. Lisowski, D. W. Muir, A. P. Palounek, R. T. Perry, E. J. Pitcher, R. E. Prael, G. J. Russell, G. H. Sanders, L. S. Waters, and P. G. Young, "Accelerator Transmutation Studies at Los Alamos with LAHET, MCNP, and CINDER'90," Los Alamos National Laboratory document LA-UR-93-3080, in *Proceedings of the Workshop on Simulating Accelerator Radiation Environments*, Santa Fe, New Mexico, January 15-19, 1993.

Invited Talks

G. J. Russell, E. J. Pitcher, and L. L. Daemen, "Split-Composite Spallation Neutron Source Targets and Accelerator Production of Tritium," Los Alamos National Laboratory document LA-UR-93-2975, abstract in *Transactions of the American Nuclear Society* 69, 429 (1993).

Spectrometer Development and User Interaction

Contributed Conference Presentations

M. R. Fitzsimmons, G. S. Smith, R. Pynn, and M. A. Nastasi, "Polarized Neutron Reflection at LANSCE," Los Alamos National Laboratory document LA-UR-93-0607, in *Proceedings of ICANS XII*, Abingdon, United Kingdom, May 24-28, 1993.

B. J. Olivier, J. P. Sandoval, P. Lysaght, M. Nutter, and R. A. Robinson, "First Results from Pharos, the New Chopper Spectrometer at LANSCE," Los Alamos National Laboratory document LA-UR-93-1752, in *Proceedings of ICANS XII*, Abingdon, United Kingdom, May 24-48, 1993.

R. A. Robinson, M. Nutter, R. L. Ricketts, E. Larson, J. P. Sandoval, P. Lysaght, and B. J. Olivier, "A New Chopper Spectrometer for Neutron Brillouin Scattering and Low-Angle Neutron Inelastic Scattering: PHAROS (Phase I)," Los Alamos National Laboratory documents LA-UR-93-396 & 1389, in *Proceedings of ICANS XII*, Abingdon, United Kingdom, May 25-28, 1993.

P. A. Seeger and R. P. Hjelm, "A Very-Low Q Diffractometer for an Advanced Spallation Source," Los Alamos National Laboratory document LA-UR-93-780, in *Proceedings of ICANS XII*, Abingdon, United Kingdom, May 24-28, 1993.

Invited Talks

P. A. Seeger and R. P. Hjelm, "Design and Implementation of Low-Q Diffractometers at Spallation Sources," Los Alamos National Laboratory document LA-UR-93-2213, in *Proceedings of American Crystallographic Association*, Albuquerque, New Mexico, May 23-28, 1993.

Beam Delivery

Contributed Conference Presentations

J. Donahue, D. Clark, S. Cohen, D. Fitzgerald, S. Frankle, R. Hutson, R. Macek, E. MacKerrow, O. van Dyck, C. Wilkinson, H. Bryant, M. Gulley, M. Halka, P. Keating, and W. Miller, "Measurement of HO Excited States Produced by Foil Stripping of 800-Mev H- Ions," Los Alamos National Laboratory document LA-UR-93-2038, *The 1993 Particle Accelerator Conference*, Washington, D. C., May 17-20, 1993.

S. Frankle, D. Fitzgerald, R. Hutson, R. Macek, and C. Wilkinson, "Application of a Simple Analytical Model to Estimate Effectiveness of Radiation Shielding for Neutrons," Los Alamos National Laboratory document LA-UR-93-1923, *The 1993 Particle Accelerator Conference*, Washington, D. C., May 17-20, 1993.

T. Hardek and A. Band, "Integrating Log-Ratio Position Processing for the Los Alamos Proton Storage Ring Extraction Line," Los Alamos National Laboratory document LA-UR-93-1955, *The 1993 Particle Accelerator Conference*, Washington D. C., May 17-20, 1993.

T. Hardek, R. Macek, M. Plum, and T. S. Wang, "Beam Pinging, Sweeping, Shaking, and Electron/Ion Collecting at the Proton Storage Ring," Los Alamos National Laboratory document LA-UR-93-1921, *The 1993 Particle Accelerator Conference*, Washington, D. C., May 17-20, 1993.

R. Hutson, D. Fitzgerald, S. Frankle, R. Macek, M. Plum, and C. Wilkinson, "Stripper-Foil Scan Studies of the First-Turn Beam Loss Mechanism in the LAMPF Proton Storage Ring (PSR)," Los Alamos National Laboratory document LA-UR-93-1867, *The 1993 Particle Accelerator Conference*, Washington, D. C., May 17-20, 1993.

A. J. Jason, R. A. Hardekopf, R. J. Macek, H. A. Thiessen, R. Woods, and S. O. Schriber, "A Los Alamos Design Study for a High-Power Spallation-Neutron-Source Driver," Los Alamos National Laboratory document LA-UR-93-1878, *The 1993 Particle Accelerator Conference*, Washington, D. C., May 17-20, 1993.

R. J. Macek, "Machine Studies at the Los Alamos Proton Storage Ring," Los Alamos National Laboratory document LA-UR-93-2941, in *Proceedings of the ICANS XII Meeting*, Abingdon, United Kingdom, May 24-28, 1993.

M. Sharirli, J. M. Butner, J. L. Rand, R. J. Macek, S. J. McKinney, and M. L. Roush, "Probabilistic Risk Assessment for the Worst-Case Design-Basis Accident at the Los Alamos Neutron Scattering Center," Los Alamos National Laboratory document LA-UR-93-3519, in *Proceedings of the Probabilistic Safety Assessment International Topical Meeting*, Clearwater Beach, Florida, January 26-29, 1993.

T. S. Wang, R. Cooper, D. Fitzgerald, S. Frankle, T. Hardek, R. Hutson, R. Macek, C. Chmori, M. Plum, H. Thiessen, C. Wilkinson, E. Colton, D. Neuffer, and G. Rees, "Recent Study of Beam Stability in the PSR," Los Alamos National Laboratory document LA-UR-93-1874, *The 1993 Particle Accelerator Conference*, Washington D. C., May 17-20, 1993.

C. Wilkinson, D. Fitzgerald, S. Frankle, R. Hutson, and R. Macek, "Monte Carlo Based Formula for Radiation Shielding Assessment in the Forward Direction," Los Alamos National Laboratory document LA-UR-93-1925, *The 1993 Particle Accelerator Conference*, Washington D. C., May 17-20, 1993.

R. L. York, D. Tupa, D. R. Swenson, and R. Damjanovich, "Volume H-Ion Source Development at LAMPF," Los Alamos National Laboratory document LA-UR-93-1924, *The 1993 Particle Accelerator Conference*, Washington, D. C., May 17-20, 1993.

Nuclear Physics PRTs

Published Articles

- J. D. Bowman, P. P. J. Delheij, C. M. Frankle, C. R. Gould, D. G. Haase, J. N. Knudson, G. E. Mitchell, S. Penttila, H. Postma, N. R. Roberson, S. J. Seestrom, J. J. Szymanski, J. J. Yeh, S. H. Yoo, V. W. Yuan, and X. Zhu, "Experimental Limit on Parity Violation in Non-Resonant Neutron-Nucleus Scattering," *Physical Review C: Nuclear Physics* **48**, 1116 (1993).
- C. M. Frankle, J. D. Bowman, B. E. Crawford, P. P. J. Delheij, C. R. Gould, D. D. Haase, J. N. Knudson, G. E. Mitchell, S. S. Patterson, S. Penttila, Yu. P. Popov, N. R. Roberson, S. J. Seestrom, E. I. Sharapov, Y. F. Yen, S. H. Yoo, V. W. Yuan, and X. Zhu, "Neutron Resonance Spectroscopy of ^{113}In and ^{115}In ," *Physical Review C: Nuclear Physics* **48**, 1601 (1993).
- C. M. Frankle, J. D. Bowman, J. N. Knudson, S. Penttila, S. J. Seestrom, S. H. Yoo, V. W. Yuan, C. R. Gould, D. G. Haase, G. E. Mitchell, N. R. Roberson, Yu. P. Popov, E. I. Sharapov, H. Postma, and P. P. J. Delheij, "Measurement of Parity Violation in Compound Nuclear Resonances Using Epithermal Polarized Neutrons," *Nuclear Instruments and Methods B* **79**, 306 (1993).
- C. M. Frankle, S. J. Seestrom, N. R. Roberson, Yu. P. Popov, and E. E. Sharapov, "Recent Developments in the Study of Parity Violation in Neutron p-Resonances," *Soviet Journal of Particles and Nuclei* **24**, 939 (1993).
- D. G. Haase, J. D. Bowman, P. P. J. Delheij, C. M. Frankle, C. R. Gould, J. N. Knudson, J. E. Koster, G. E. Mitchell, S. Penttila, H. Postma, N. R. Roberson, S. J. Seestrom, S. H. Yoo, and V. W. Yuan, "Bulk Magnetic Structure Studies Using Polarized Epithermal Neutrons," *Nuclear Instruments and Methods B* **79**, 300 (1993).
- P. E. Koehler, "The $^{14}\text{N}(n,p)^{14}\text{C}$ Cross Section Near Thermal Energy," *Physical Review C: Nuclear Physics* **48**, 439 (1993).
- P. E. Koehler, S. M. Graff, H. A. O'Brien, Yu. M. Gledenov, and Yu. P. Popov, " $^{36}\text{Cl}(n,p)^{36}\text{S}$ Cross Section from 25 meV to 800 keV and the Nucleosynthesis of the Rare Isotope ^{36}S ," *Physical Review C: Nuclear Physics* **47**, 2107 (1993).
- N. R. Roberson, J. D. Bowman, J. E. Bush, P. P. J. Delheij, C. M. Frankle, C. R. Gould, D. G. Haase, J. N. Knudson, G. E. Mitchell, S. Penttila, H. Postma, S. J. Seestrom, J. J. Szymanski, S. H. Yoo, V. W. Yuan, and X. Zhu, "An Apparatus and Technique for Tests of Fundamental Symmetries in Compound Nucleus Scattering with Epithermal Polarized Neutron Beams," *Nuclear Instruments and Methods A* **326**, 549 (1993).
- H. Schatz, F. Kaepfeler, P. E. Koehler, M. Wiescher, and H.-P. Trautvetter, " $^{17}\text{O}(n,a)^{14}\text{C}$ —Bottleneck for Primordial Nucleosynthesis?," in *Nuclei in the Cosmos*, F. Kaepfeler and K. Wisshak, Eds. (Institute of Physics, Bristol, 1993), p. 253.
- H. Schatz, F. Kaepfeler, P. E. Koehler, M. Wiescher, and H.-P. Trautvetter, " $^{17}\text{O}(n,a)^{14}\text{C}$ —Closure of a Primordial CNO Bi-Cycle?," *Astrophysical Journal* **413**, 750 (1993).
- S. A. Wender, S. J. Seestrom, and C. L. Morris, "A Beam-Current Limiting Device," *Nuclear Instruments and Methods A* **334**, 299 (1993).
- J. E. Wise, M. R. Braunstein, S. Hoibraten, M. D. Kohler, B. L. Kriss, J. Ouyang, R. J. Peterson, J. A. McGill, C. L. Morris, S. J. Seestrom, R. M. Whitton, J. D. Zumbro, C. M. Edwards, and A. L. Williams, "Quasi-Free Pion Scattering at 500 MeV," *Physical Review C: Nuclear Physics* **48**, 1840 (1993).

J. D. Zumbro, C. L. Morris, J. A. McGill, S. J. Seestrom, R. M. Whitton, C. M. Edwards, A. L. Williams, M. R. Braunstein, M. D. Kohler, B. J. Kriss, S. Hoibraten, R. J. Peterson, J. Ouyang, J. E. Wise, and W. R. Gibbs, "Inclusive Scattering of 500-MeV Pions from Carbon," *Physical Review Letters* **71**, 1796 (1993).

Publications in Press or Submitted

K. Meggers, H. G. Priesmeyer, W. J. Trela, and M. Dahms, "Investigation of the Austenite-Bainite Transformation in Gray Iron Using Real Time Neutron Transmission," Los Alamos National Laboratory document LA-UR-93-3560 (submitted to *Materials Science and Engineering*).

K. Meggers, H. G. Priesmeyer, and W. J. Trela, "Real Time Neutron Transmission Investigation of the Austenite-Bainite Transformation in Gray Iron," Los Alamos National Laboratory document LA-UR-93-3491 (submitted to *Nuclear Instruments and Methods*).

Contributed Conference Presentations

P. E. Koehler, F. Kaeppler, H. Schatz, Yu. M. Gledenov, Yu. P. Popov, J. A. Harvey, N. W. Hill, M. Wiescher, R. W. Kavanagh, and R. B. Vogelaar, "Recent Results in Explosive and S-process Nucleosynthesis from Measurements on Radioactive and Stable Targets," Los Alamos National Laboratory document LA-UR-93-2418, in *Proceedings of the Eighth International Symposium on Capture Gamma-Ray Spectroscopy and Related Topics*, September 20-24, 1993.

Author Index

<i>Author</i>	<i>Proposal No.</i>	<i>Page</i>	<i>Author</i>	<i>Proposal No.</i>	<i>Page</i>
Albinati, A.	6087	27	Egelstaff, P. A.	6082	151
Allison, J. E.	6058	119	Ezeilo, A. N.	6016	111
	6076	126	Fisk, Z.	6004	109
	6406	136	Fitzsimmons, M. R.	6012	48
Archuleta, J. I.	6405	10		6021	183
Baker, S.	6028	184		6067	123
	6033	186		6068	193
	6040	189		6102	198
	6095	196	Forsman, W. C.	6044	80
Baldwin, J. P.	6103	94	Gallot, Y.	6061	83
Barthes, M.	6086	25	Garner, F. A.	6109	173
Beaucage, G.	6108	96	Glaunsinger, W. S.	6089	29
Benicewicz, B. C.	6074	87	Goldstone, J. A.	6058	119
Benmore, C. J.	6082	151		6059	121
Billinge, S. J. L.	6083	63		6076	126
	6085	23		6077	128
Bish, D. L.	6017	113		6098	130
de Boer, F. R.	6013	159		6406	136
	6032	52	Gottesfeld, S.	6102	198
	6499	65	Gray III, G. T.	6059	121
Bradbury, E. M.	6103	94	Hamilton, W.	6040	189
Bradt, R. C.	6109	173	Hasegawa, T.	6084	21
Browning, J.	6095	196	Havela, L.	6000	42
Bourke, M. A. M.	6058	119		6013	159
	6059	121		6032	52
	6076	126		6499	65
	6077	128	Hayter, J.	6040	189
	6406	136	Hellman, F.	6042	73
Burkel, E.	6021	183	Hellstrom, E. E.	6034	161
Buschow, K. H. J.	6001	107	Hill, M. A.	6059	121
	6003	44	Hjelm, R. P.	6074	87
Butler, P.	6040	189		6075	89
Candler, R. J.	6403	98		6103	94
Canfield, P. C.	6096	169	Hoffer, J. K.	6403	98
	6100	132	Hoffman, P.	6087	27
Chaiko, D. J.	6075	89	Hollenberg, G. W.	6109	173
Cheetham, A. K.	6030	49	Ikeda, S.	6083	63
Cline, J.	5061	41	Imai, B. S.	6103	94
Conant, J. W.	6072	60	James, M. R.	6019	115
Cort, B.	6400	142	Jayasooriya, U. A.	6025	17
Cotton, J. D.	6098	130		6026	19
Craft, S.	6043	75	Kennedy, B. J.	6073	62
Dotson, L.	6089	29	Kent, M. S.	6009	181
Douglas, E. P.	6074	87		6095	196
Dreux, P.	6044	80		6108	96
Dunand, D. C.	6077	128	Kubas, G.	6091	31
Eastman, J. A.	6012	48	Küppers, H.	6107	34
Eckert, J.	6084	21	Kwei, G. H.	6083	63
	6085	23		6096	169
	6086	25	Lager, G. A.	6010	46
	6087	27	Larson, A. C.	6013	159
	6089	29		6034	161
	6091	31		6039	163
	6092	33		6049	165
	6107	34		6063	167

<i>Author</i>	<i>Proposal No.</i>	<i>Page</i>	<i>Author</i>	<i>Proposal No.</i>	<i>Page</i>	
Lawson, A. C.	6096	169	Reeder, R. J.	6049	165	
	6101	171		6042	73	
	6109	173		6000	42	
	6001	107		6001	107	
	6003	44		6003	44	
	6072	60		6004	109	
	6096	169		6013	159	
	6098	130		6032	52	
	6400	142		6042	73	
	6405	100		6082	151	
	6406	136		6100	132	
	Leinenweber, K.	6053		117	6409	153
		Lund, J.		6067	123	6499
	6068			193	Rokop, S.	6071
	Luo, X.-L.	6091		31	Röll, A.	6021
Lynn, J. E.	6400	142	Russell, T. P.	6033	186	
Magid, L.	6040	189		6057	191	
Mari, D.	6077	128		6060	82	
Martin, A.	6092	33		6061	83	
Mattes, B.	6085	23	Schiferl, D.	6054	54	
Mayes, A. M.	6057	191	Schoenborn, B.	6097	91	
	6061	83	Sechovský, V.	6000	42	
Meggers, K.	6400	142		6013	159	
	6402	144		6032	52	
Morgan, J. G.	6030	49		6499	65	
Nakotte, H.	6000	42	Seeger, P. A.	5409	71	
	6003	44		6099	92	
	6013	159		6405	100	
	6032	52	Shapiro, A.	6042	73	
	6499	65	Shi, N.	6076	126	
				6406	136	
Olah, G. A.	6071	85	Sickafus, K. E.	6021	183	
Olivier, B. J.	6082	151		6109	173	
	6409	153	Smith, G. S.	6009	181	
Ong, E.	6089	29		6021	183	
Parise, J. B.	6053	117		6028	184	
	6056	58		6033	186	
Phillips, D. S.	5409	71		6040	189	
	6099	92		6095	196	
Powell, G. L.	6072	60		6102	198	
Priesmeyer, H. G.	6402	144	Smyth, J. R.	6039	163	
Prokes, K.	6032	52	Stride, J. A.	6025	17	
Purwanto, A.	6000	42		6026	19	
	6001	107		6082	151	
	6003	44	Suck, J.-B.	6082	151	
	6004	109	Swope, R. J.	6039	163	
	6013	159	Taube, H.	6084	21	
	6032	52	Thiyagarajan, P.	6075	89	
	6100	132	Todd, R. I.	6104	134	
	6499	65	Toprakcioglu, C.	6028	184	
	Pynn, R.	6021	183	Trela, W. J.	6400	142
		6033	186		6402	144
6040		189	Trewhella, J.	6071	85	
Rabor, J. G.	6091	31	Uribe, F.	6102	198	
Rakovan, J.	6049	165				

<i>Author</i>	<i>Proposal No.</i>	<i>Page</i>
Visser, D.	6063	167
	6101	171
Von Dreele, R. B.	5061	41
	6030	49
	6053	117
	6054	54
	6055	56
	6056	58
Wages, S.	6095	196
Watson, S.	6042	73
Webster, G. A.	6016	111
Webster, P. J.	6016	111
Weidner, D. J.	6053	117
Wilkinson, A. P.	6030	49
Wilcoxon, J.	6043	75
Yau, P. M.	6103	94
Zawodzinski, T.	6102	198
Zocco, T. G.	6405	100

Subject Index

<i>Subject</i>	<i>Proposal No.</i>	<i>Page</i>	<i>Subject</i>	<i>Proposal No.</i>	<i>Page</i>
Acetanilide	6086	25	Garnet	6010	46
Acetic acid	6055	56	Gels	6099	92
Al ₂ O ₃ -SiC	6104	134	Geological hydrogen	6039	163
Al ₂ Si ₂ O ₅ (OH) ₄	6017	113	Grain boundaries	6021	183
Al-SiC	6076	126	Heavy fermions	6100	132
	6406	136	Helium bubbles	6405	100
Al-TiC	6058	119	H-H bonds	6084	21
Alumina	5409	71		6091	31
	6099	92	High-field magnets	6059	121
	6104	134	High-pressure studies	6010	46
Amines	6089	29		6030	49
Amorphous Mg ₇₀ Zn ₃₀	6082	151		6053	117
Amorphous Tb-Fe	6042	73		6054	54
Apatite	6049	165		6055	56
Aqueous biphasic systems	6075	89		6056	58
Austenite-bainite transformation	6402	144	High-T _c superconductors	6034	161
Beta-layering	6403	98		6083	63
Bi ₃ M ₂ SbO ₁₁	6073	62	Homopolymer films	6060	82
Bi ₂ Sr ₂ CaCu ₂ O ₈	6034	161	Hydrogen bonds	6053	117
Boron phosphide	6067	123		6107	34
	6068	193		6409	153
Cationic microemulsions	6043	75	Incommensurate magnetic order	6013	159
Ce _{2-x} Pt ₄ Ga _{8+y}	6096	169	<i>In situ</i> loading	6406	136
Ceramic-ceramic composites	6104	134	<i>In situ</i> compressive loading	6059	121
Ceramic-metal composites	6019	115	<i>In situ</i> shear experiments	6028	184
Clinohumite	6039	163		6040	189
Composites	6019	115		6075	89
Conducting polymers	6085	23	Intercalation	6089	29
	6102	198	Interfaces	6044	80
Cr	6012	48		6095	196
Cristobalite	6056	58	La _{1.875} Sr _{0.125} CuO ₄	6083	63
CsFeBr ₃	6063	167	Kaolin	6017	113
	6101	171	KHF ₂	6409	153
Cu-X alloys	6059	121	Magnetic anisotropy	6042	73
Cyclopropane	6092	33	Magnetic structure	6000	42
Debye-Waller factors	6098	130		6001	107
	6400	142		6003	44
Detector development	6067	123		6012	48
	6068	193		6013	159
Diblock copolymers	6009	181		6021	183
	6061	83		6032	52
	6057	191		6499	65
Diffraction gratings	6033	186	Metal clusters	6026	19
Diffuse scattering	6033	186	Metal complexes	6025	17
	6063	167	Metal-matrix composites	6058	119
	6101	171		6076	126
Dihydrogen complexes	6084	21		6406	136
	6091	31	Metal oxides	6073	62
D-T mixtures	6403	98	MgAl ₂ O ₄	6109	173
Elastic constants	6016	111	Mg(OD) ₂	6053	117
	6098	130	Mg ₇₀ Zn ₃₀	6082	151
Ethylene	6092	33	Molecular composites	6074	87
Ethylene ligands	6087	27	Mo/polyurethane interfaces	6095	196
Fe	6402	144	Muscle protein	6071	85
Filaments	5409	71	Nacrite	6017	113

<i>Subject</i>	<i>Proposal No.</i>	<i>Page</i>	<i>Subject</i>	<i>Proposal No.</i>	<i>Page</i>
Nanocrystals	6012	48	UD ₃	6072	60
Neutron Brillouin scattering	6082	151	UNiGe	6013	159
NiAl	6098	130	UPtSn	6003	44
Nickel	6021	183	Uranium hydride	6072	60
NiTi	6077	128	U ₂ T ₂ X compounds	6032	52
Nitromethane	6054	54	Viscoelasticity	6040	189
Nuclear resonances	6400	142	Voids	5409	71
Nucleosome core	6103	94		6405	100
Oxocentered metal complexes	6025	17	YbBiPt	6100	132
Pair distribution functions	6083	63	Y ₂ In	6004	109
PDMS	6108	96	Zeolites	6092	33
Phase transitions	6004	109	Zn	6098	130
	6056	58	ZrS ₂	6089	29
	6061	83			
Phonon spectra	6400	142			
Plutonium	6400	142			
	6405	100			
Pole figures	6034	161			
Polyaniline	6085	23			
Polymers	6009	181			
	6028	184			
	6044	80			
	6057	191			
	6060	82			
	6061	83			
	6074	87			
	6075	89			
	6108	96			
Polymer blends	6108	96			
Polystyrene	6060	82			
Pb(Zr _{0.7} Ti _{0.3})O ₃	6030	49			
Protein crystallography	6097	91			
Pt-ethylene complex	6087	27			
Quinolinic acid	6107	34			
Radiation damage	6109	173			
Roughness	6033	186			
Shape-memory alloys	6077	128			
Silicon nitride	5061	41			
Si ₃ N ₄	5061	41			
SiO ₂	6056	58			
Solid-liquid interface	6044	80			
Spinel	6109	173			
Standards	5061	41			
Structural distortions	6001	107			
Tb-Fe	6042	73			
Tensile testing	6016	111			
Texture	6034	161			
Ti alloys	6016	111			
TiH ₂	6409	153			
Tritium	6403	98			
Trypsinization	6103	94			
Troponin C	6071	85			
UAuSn	6001	107			
UCoGa	6499	65			
UCuSn	6000	42			